Master's thesis

Auralization of Sound Emitted by an Excited Structure

Acoustics and Audio Technology

Christian Claumarch
August 20, 2018

Supervisor:
Christian Sejer Pedersen

Company Supervisors:
Jan Peter Jensen
Jan Balle Larsen

Aalborg University
Department of electronic systems
Fredrik Bajers vej 7
DK-9220 Aalborg

This report is compiled in LaTeX, originally developed by Leslie Lamport, based on Donald Knuth's TeX. The main text is written in *Computer Modern* pt 12, designed by Donald Knuth. Flowcharts, Graphs and diagrams are made using Tikz, a TeXpackage for generating graphics.

Institute of Electronic Systems
Fredrik Bajers Vej 7
DK-9220 Aalborg Ø

AALBORG UNIVERSITY
STUDENT REPORT

Title:
Auralization of Sound Emitted by an Excited Structure

Theme:
Master's thesis

Project Period:
Spring & summer 2018

Project Group:
AAT10-1065

Participants:
Christian Claumarch

Supervisor:
Christian Sejer Pedersen

Company Supervisors:
Jan Peter Jensen
Jan Balle Larsen

Page Numbers: 140 + 65 p. Appendix

Date of Completion:
August 20, 2018

Abstract:

In development of mechanical products development time and cost are critical factors. In trying to minimize these simulation driven development is a hot topic where the ultimate goal is to be able to design a product solely based on modelling. To do so all aspects of the product will have to be examined before production starts.

The purpose of this master's thesis is to examine if the sound field created by a vibrating structure, a plate, can be predicted by means of modelling. The problem is split in subproblems named vibration, sound generation and listening each contributing their part to the final auralization. A combination of finite elements and acoustical modelling is used to estimate the sound radiation.

The thesis compares data from measurements and analytical work with simulation results to determine if finite elements analysis results are accurate enough to be used for sound generation.

The final outcome of the algorithm is sound which does share some resemblance with the one from the physical object. Still it is concluded that the generated and recorded sounds are not identical, neither objectively nor subjectively.

Preface

This master's thesis in Acoustics and Audio Technology was written during spring and summer 2018 at Aalborg University. The thesis is written in collaboration with the Sound and Vibration Laboratory at Grundfos, who have kindly supported me with equipment, a workstation and guidance. A special thank you to Jan Balle Larsen and Jan Peter Jensen who have been the main supervisors at Grundfos.

Grundfos has influenced the definition of the project, as this is inevitable when the project has been discussed with their employees from the earliest stages of definition of the topic. However at each decision made throughout the project I will try to argue for design choices based on literature or my own reflections rather than simply following someone else's suggestions. That being said my supervisors at Grundfos have a lot more experience in structural mechanics than I do, so their input has influenced my decision making.
The project includes a NDA signed by the student, Grundfos and Aalborg University.

I would also like to thank Wolfgang Kropp from Chalmers Tekniska Högskola, who introduced me to the world of vibration during my exchange semester.

Figures in the report are produced by me unless a source is specified in the caption. Sources are indicated by [author, year] and can be found in the bibliography.

The thesis will begin with an introduction to the overall problem of auralization and a selection of the specific task in this master's thesis, auralization of an aluminium plate. This is the followed by descriptions of and solutions to the five subproblems in the auralization problem; excitation, vibration, radiation, propagation and listening. The results from these five steps are compared to a measured response from the plate and refinements are made to make the algorithm more accurate compared to the measurements. Finally the results are presented to the reader by means of frequency response plots as well as audio.

All computation times from finite elements simulations stated in the thesis are measured on a HP ZBook 15 G3 with an Intel I7-6820HQ CPU and 16 GB memory running Windows 7.1.
All computation times from auralization calculations are based on GPU acceleration using Matlab's Parallel Computing Toolbox. The computer is a desktop computer with an Intel I5-4460 CPU, 8 GB memory, a Nvidia 1070 8 GB 1771 MHz GPU running Windows 10.

Christian Claumarch
cclaum16@student.aau.dk

Aalborg University, August 20, 2018

Contents

Part I

Introduction

1 | Motivation

Imagine the situation; you are sitting at home in your living room where you have a modern metal sculpture. Unfortunately your child enjoys hitting the sculpture with a hammer, which creates an irritating sound. Being a modern parent you never scold the child and therefore it is more convenient to modify the sculpture in such a way that the sound radiated will be less irritating. You only have one shot at modifying the sculpture, so you need to make a simulation that can predict the outcome of different modifications.

The problem above illustrates the task of an engineer working with sound and vibration. In many industries the sound-pollution from a product is a design parameter in terms of either international standards or just end user preference. At the same time development of new products has to happen at an increasing rate. This means that a trial and error based approach to noise minimization, where each trial has to be built and tested, is very inconvenient and too time consuming. During development of a mechanical component it would be beneficial to be able to predict the sound power radiated from a vibrating structure. It would be even more beneficial to be able to listen to a simulation of the radiated sound in a simulated environment. By knowing the sound field up front multiple advantages are achieved, one being that the product can be optimized with respect to sound very early in the design phase saving time and money. Another advantage is being able to demonstrate new technologies to designers and boards, solving the engineering problem of 'explaining how it sounds'.

In many mechanical engineering situations some sort of simulation based tool is used to calculate strains, deformation and other parameters for a product to determine if the product design is strong enough for the intended use. This simulation approach is widely used and many commercial software products intended for this purpose exist. In some cases a by-product of these calculations is a complete discretized description of the deformations of the products surfaces. Therefore the motivation of the project is to develop an algorithm that can transform known structural vibrations of a structure to airborne sound. The airborne sound should be propagated to a 'listening position' and be represented as a binaural recording aiming for a believable representation.

The project will, as mentioned in the Preface, be made in collaboration with Grundfos, who is a top competitor in the industry of water pumps. They have an interest in maintaining their strong market position by being market leading with respect to minimum sound pollution and development time as mentioned above.

2 | Auralization - a definition

The problem outlined above can be reformulated in a shorter way as 'auralization of sound emitted by an excited structure'. Auralization might be used as a slightly vague term in different contexts so a definition will be given here. Furthermore a brief history of approaches taken over the years is included. The definition of auralization used in this project is that originally used by Kleiner et al.

> *"Auralization is the process of rendering audible, by physical or mathematical modelling, the sound field of a source in a space, in such a way as to simulate the binaural listening experience at a given position in the modelled space."* [Kleiner et al., 1993]

The key pointers is that the representation should be binaural, which is also the intended in this project, and that it models a sound field of a source in a space.

The first attempt at auralization was made by Spandöch in the 1930s. He made a scale model of a room and compared a binaural recording of speech made in the scaled room with the real room [Kleiner et al., 1993]. This very early approach based on purely analogue technology is far from the possibilities available using the computational power of a modern computer. Different approaches exist ranging from the analogue scale model option to a fully computed auralization. The computation based algorithms are typically based on a recorded sound signal 'played' by a point source in a room where either ray tracing or mirror source techniques are used to estimate the room impulse response (RIR).

The approach taken in this project is to have fully computed auralization. Instead of computing the RIR and using a simple source, such as a point source, it is desired to model the sound source in a more detailed way. The modelling should include the sources distribution in space as well as the directivity of the structure.

3 | Problem statement

The goal is to develop and validate an algorithm that can take the excitation of an structure as input and yield an accurate auralization of the sound radiated from the structure as output.

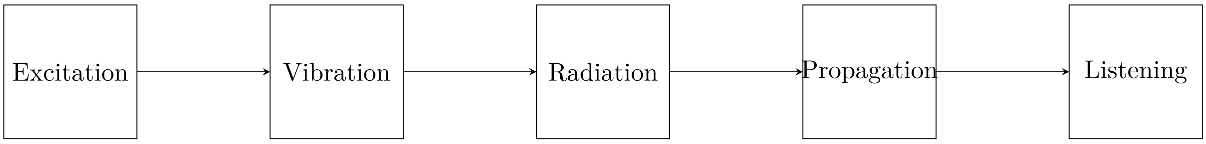

Figure 3.1: The steps required to go from excitation to listening.

While including the steps in figure 3.1 the algorithm should:

- Be sufficiently general that it does not need to be individually adjusted for each new structure.
- Have parameters which are based on physical and quantifiable properties.
- Result in a sound quality that is close to identical compared to a recorded sound from the physical structure.
- Preferably be easy to include in the work flow of product development.

In order to evaluate the performance of the algorithm in terms of quantifiable parameters, numerical results should be compared with analytical solutions and measurements. The parameters of interest are overall noise level, directivity, temporal characteristics and frequency characteristics. If the results seem accurate a listening test should be performed. In order to compare the modelled and measured sound in a listening test both should be represented as binaural recordings. The frequency area of interest is the entire audible range 20 Hz to 20 kHz as the scope of the project is to make the sound believable to the human ear.

3.1 Limitations

As the project is very big and includes many vast areas of research, some limitations are made.

- The only environment considered is an infinite floor with anechoic termination in all other directions (hemi-anechoic).
- Only random vibration is considered[1].
- Sound fields imposed on the structure from other sound sources are not considered.

[1]Random vibration means the structure is exited equally at all frequencies. Opposite is forced vibration where the structure is forced to vibrate at a specific frequency. More on this in section 7.2.

3.2 Workflow

It is desired to develop and validate an algorithm which can simulate sound emission from a vibrating structure. In order to reach this goal the task is fourfold:

1. Determine the theoretical vibration of the structure by means of analytical solutions.
2. Use a numerical method to calculate the vibration of the structure and compare to the analytical solution.
3. Measure the sound radiated from a full scale product including a half power sphere and binaural recording with a HATS.
4. Develop the algorithm for modelling the radiation of airborne sound from the structure and compare with the measured sound.
5. Weak coupling between structure and fluid

Instead of structuring the report to follow the workflow above I have chosen to present it in the order given the block diagram in figure 3.1. This will allow the reader to follow the audio from its origin, the excitation, to the final binaural representation.

4 | Existing methods

4.1 Short literature survey

This section serves the purpose of giving a deeper understanding of some of existing methods. For each method the requirements to the preceding numerical method is listed. In addition to this the possible pitfalls in terms of accuracy are also discussed, such that they can be remedied if the method or parts of it are used later.

The methods are grouped in their respective application areas and then presented in the order they were published.

4.1.1 Methods in engineering

Naturally, prediction of sound from machinery such as cars has been of interest for years. Typically the goal of such a prediction would be to optimize sound parameters such as overall level or maybe even attributes such as harshness or sharpness.

Interior Acoustic Simulation for In-Car Audio Design [Paik et al., 2013]

This paper examines how the performance of a car stereo can be simulated and optimized. In order to do so the numerical methods finite elements method (FEM) and boundary elements method (BEM) are considered. It is concluded that an algorithm based on a variant of BEM called fast-multipoles decreases the computational effort of BEM and thereby allows frequencies up to 4 kHz to be included in the simulation. To include higher frequencies a hybrid approach is used where a ray tracing method calculates the high frequency response. The authors state that the ray tracing is less accurate than FEM or BEM but it enables high frequencies to be included as it is more computationally efficient. The paper includes the car cabin in the simulation and presents the audio as a binaural recording using a KEMAR dummy head.

Requirements to the numerical method
The method requires a combination of a low and mid frequency numerical simulation method and a high frequency ray tracing. An efficient numerical solution is required since frequencies up to 4 kHz are included for the entire volume of the car cabin. The ray tracing method requires that the high frequency source is small and can be modelled as a point source, thereby limiting the application area to small sources such as a tweeter in a car stereo.

Comments on the paper
By using a low and mid frequency FEM or BEM simulation the loudspeaker's excitation of the door that it is mounted in can be included in the low frequency modelling. At higher frequencies

the loudspeaker vibration is assumed not to excite the surroundings, and ray tracing is used for a small source. The latter might not be completely accurate since diffraction will occur from the edges of a finite baffle with a tweeter mounted in it. If a distributed source is to be considered at high frequencies a series of small sources with individual ray tracing could be considered, at the cost of computation time.

The use of a hybrid approach for the audio range in the relatively small volume of a car demonstrates that for large rooms a pure FEM or BEM solution is not feasible.

Engine Sound Weighting using a Psychoacoustic Criterion based on Auralized Numerical Simulations [Duvigneau et al., 2015]

The method proposed in this paper is used to generate audio which can be used in listening tests to ultimately give different stimuli a ranking. The point of this is to be able to design sound quality of a car engine in simulations. Finally they make a model which can predict the result of such a listening test based only on the simulation. An outline of the method is given in figure 4.1

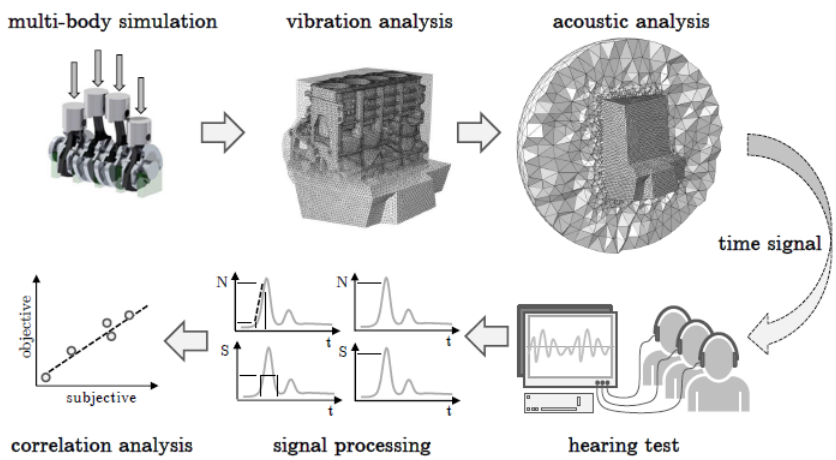

Figure 4.1: Overview of the work done in [Duvigneau et al., 2015].

As shown in figure 4.1 the method uses a numerical method, FEM, to calculate the sound radiated from the source. They claim that at the boundary of the meshed area they use the Sommerfeld radiation condition which means that no reflections are considered. The generated audio is not compared to that of a physical reference.

Requirements to the numerical method

The method requires that the numerical method is capable of determining the vibration caused by movement of the pistons inside the engine. From this the numerical method must be able to determine the radiated sound pressure from the structure to a surrounding enclosure of air.

Comments on the paper

The method calculates the sound pressure at specific frequencies solely based on FEM and uses this information to generate audio. It is likely that this approach is quite accurate but it shows some disadvantages. Firstly you have to mesh the acoustic medium, which is not very efficient especially for large volumes. In a car this might be possible since the enclosure is rather limited but if one considers an environment such as a factory the mesh will be impossibly large. The paper gives no comments on the meshing used but based on figure 4.1 it would seem that the authors mesh the air with a coarse mesh several times bigger that the wavelength of audible sounds.

The paper's definition of auralization differs from the one given in chapter 2 since they do not include neither an environment nor a binaural representation in their audio.

4.1.2 Methods from the computer graphics community

Inspiration for solving the task can be found in video game and virtual reality literature, where the task of producing 'believable' sound solely based on graphics has been examined for many years starting with [O'Brien et al., 2001a][1]. This early paper has brought along a series of newer papers where the algorithm is improved, especially with respect to computational cost which is critical in real time applications such as virtual reality. One way of achieving this is to precompute and store information about the modal behaviour of the structure, which can then be used as a basis for the real time calculations [Li et al., 2015]. For this project however the method is to be used in product development, where real time computational capability is not an issue, but high accuracy is desired. Furthermore the precomputation approaches require that the structure is 'fixed' and that the excitation or listening position changes as is often the case in video games. From a development point of view the 'use case' is likely to be constant while the product is modified in search of some optimal design.

Synthesizing Sounds from Physically Based Motion [O'Brien et al., 2001a]

This paper is one of the founding papers in the field and is typically used as 'baseline' for newer methods in the graphics community. It is not a very efficient algorithm, but it is one of the simplest.

The method is based on a time domain version of FEM to calculate the velocities of each node on a structure. The main equation used is:

$$p = z \cdot v \cdot \hat{n} \tag{4.1}$$

which states that the pressure in front of an element is the impedance of air (ρc) times the velocity of the face of the element times the normal vector of the face of the element. The velocity used is the average velocity of the nodes defining the corners of the face. Not all pressures are used in the final audio. Only pressures from elements with an unobstructed line of sight are included. This also means that reflected sound and diffractions are ignored. The

[1] Video available at http://graphics.berkeley.edu/papers/Obrien-SSF-2001-08/ [O'Brien et al., 2001b]

selected pressures are filtered to avoid aliasing and low frequency movement after which they are stored in an 'accumulation buffer' where the individual contributions are stored at the index corresponding to the travel time to the 'listener location'. Stereo recordings are created by making two separate accumulation buffers. The presented recordings are not binaural and the authors state that this is planned future work.

Requirements to the numerical method

The method requires a time representation of all nodes at sampled times. This time representation of course includes amplitude and phase information in the frequency domain. The method's propagation algorithm includes any non-linearities found by the FEM algorithm, but does not require a non linear analysis method.

Comments on the paper

A few statements are made, which I believe pose a risk in terms of accuracy. Therefore if the method used as inspiration these risks should be eradicated or as a minimum have their impact examined. The statements are not commented by later literature so it is possible that the effect is not catastrophic in reality. The statements are:

1. 'Mesh resolution is approximately 1 cm.'
2. 'To avoid this problem, we add the s^2 values into the buffer by convolving the contribution with a narrow (two samples wide) Gaussian and 'splatting' the result into the accumulation buffer.'

The first statement is in violation with the rule of thumb of 6 elements per wavelength as this requires a maximum element length of one sixth of a wavelength [Schmiechen, 1997]. The wavelength should be determined in both air and the solid and the requirement fulfilled for both. Therefore the meshing should be done at maximum $\frac{1}{6}\lambda = \frac{c_{air}}{6 f_{max}} = \frac{343 m/s}{6 * 20000 Hz} = 2.85 mm$ possibly smaller due to the wavelength in the solid. The authors claim that the inaccuracies at higher frequencies is due to lower SNR at higher frequencies (where vibration levels are much smaller) and discretization. It is however likely that their entire foundation for the simulation is not correct as the mesh is too coarse. The coarse mesh enables the simulation in terms of memory as the number of nodes is increased drastically by a finer mesh.

The second statement is slightly vague in terms of what they actually do. But if the samples of the 'two sample wide Gaussian' are anything but [1 0] they are performing some sort of filtering.[3] It is most likely a low pass filtering similar to moving average as they are attempting to remove a sawtooth artefact in the sound caused by their propagation algorithm. The propagation algorithm is sample based and only delays of $N\frac{1}{fs}$ are valid. A better approach would be to upsample the audio signal and chose an interpolated value.

[2] The pressure p propagated to the receiver adjusted for radiation angle and distance.

[3] If it is [1 0] they are obviously not doing anything.

Synthesizing Sounds from Rigid-Body Simulations [O'Brien et al., 2002]

In this second paper by O'Brien and new co-authors the sound generation is based on the mode shapes and eigenfrequencies of a structure. This is much more efficient and they claim runtime capabilities after a demanding precomputation. The concept is to split the problem in two. A rigid body simulator determining the forces on the structure due to impacts and a second part which determines the mode shapes and eigenfrequencies of the structure.

The majority of the paper describes the FEM algorithm which calculates the required mode shapes and node displacements. A detailed walk-through of this is futile as it would be a copy of that given in the paper and only has relevance for implementing the FEM code.

Instead of explicitly calculating and storing each time step, as in the previous method, a recursive approach is taken. The point is that the modes are treated as individual oscillators with individual frequencies and decays.

The propagation of sound is handled in the same way as the previous article with an accumulation buffer etc. Resulting in the same lack of reflections and diffraction as the previous algorithm.

Requirements to the numerical method

This method requires a FEM modal analysis determining the eigenfrequencies and mode shapes of the structure. A rigid body simulation is also required to allow the sound to differ when the structure is excited in different positions.

Comments on the paper

Again a few worrying decisions were made throughout the paper, which would have to be treated before committing to using the method.

While working on a set of wind chimes the paper adjusts the length of the wind chimes to make the resulting eigenfrequencies fit the intended harmonic scale. They do not examine if the error in fundamental frequency was due to an error in the specification of the wind chime or due to their method. If the first was the case then the tuning was a suitable fix, but if the latter was the case they fitted their algorithm to the exact application. In cases where the correct frequency is not known beforehand this would be impossible.

The authors claim based on a reference to [van den Doel et al., 2001] that not all modes in the audible range need to be retained. High frequencies can be included based on only the first 800 modes. It seems odd to decide on a fixed amount of modes as the eigenfrequencies will depend strongly on the structure. The claim is stated as a suggestion to make the algorithm more efficient. A more accurate approach would be to include all modes in the audible range, which might be less than 800 for some structures.

Again a comment on a coarse mesh creating acceptable sounds is given. In this paper no frequency response plots comparing simulated sounds to actual sounds are given and the high frequency accuracy is not treated.

Precomputed Acoustic Transfer: Output-sensitive, accurate sound generation for geometrically complex vibration sources [James et al., 2006]

The method proposed D. L. James et al. differs from the solutions above in that it includes reflections and diffraction. The method is based on modal decomposition and calculates mode shapes and eigenfrequencies of the structure. From this point it differs drastically from the previous methods in that it computes a set of 'equivalent multipole sources' which create the same pressure at an offset surface as a complete BEM radiation solution. By doing this the method, unlike the previous ones, account for reflections, diffraction and the radiation efficiency of the structure.

Requirements to the numerical method

The method is originally intended for a combination of FEM and BEM, which is more suitable for solving the radiation problem from the structure to the enclosing sphere.

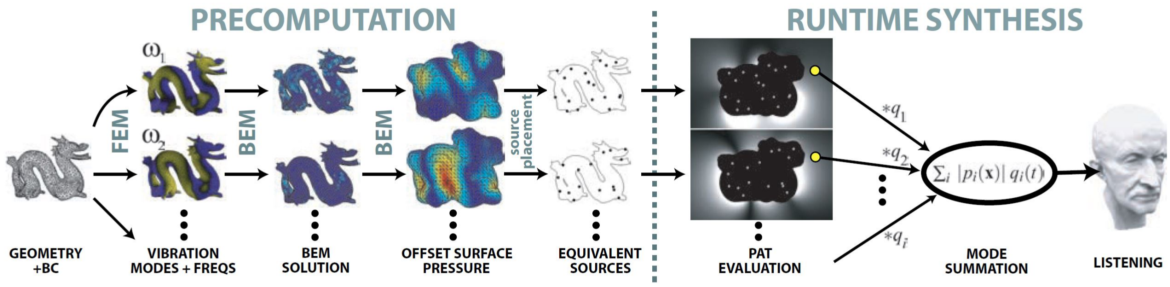

Figure 4.2: Overview of the method proposed by [James et al., 2006].

Figure 4.2 yields an easy overview of the requirements to the numerical method. They are a modal analysis as in the previous method plus a solution of pressures at an offset surface.

Comments on the paper

This method is based on first solving the entire radiation problem at a surface surrounding the source using BEM. Then the solution is approximated using simple sources inside the sphere to recreate the same sound field at the surface. Afterwards the simple sources allows for a faster run time evaluation at arbitrary positions outside the sphere.

One could argue that if the runtime requirement is not of concern the complete solution could just be evaluated for all positions of interest in the first case. However the distance of the offset surface might be much smaller than the distance to the receiver, so if using FEM a lot of meshed air can be saved.

A further advantage of this method is that it decouples the source from the receiving room and represents the source as a set of simpler equivalent sources. In future work it is wanted to be able to auralize structure in different rooms. This method might make it much more simple to integrate the numerical modelling in an existing room simulation software, as simple sources such as monopoles and dipoles should be available in those tools.

4.2 Existing commercial software

Modern simulation based tools include an audio toolbox, which can do some audio prediction based on the existing modelling of the surface. Below a brief introduction to some of the existing software and their claimed capabilities are listed.

Comsol with the 'Acoustic Module' [COMSOL, 2018] is capable of, among many other things, modelling acoustic radiation. Auralization functionality is not included in the software, but can be added as done by HARMAN group. HARMAN has developed 'a playback system that allows for listening, evaluation, and comparison of audio systems (...) all based on simulation results and signal processing' [COMSOL, 2017].

ANSYS with the 'Acoustics ACT' package has roughly the same functionality as Comsol. The acoustical functionality is somewhat new in ANSYS, where it is a cornerstone of Comsol. One disadvantage using ANSYS is that it does not handle unbounded problems well, and the user has to enclose the problem region with 'simulated infinity' called a perfectly matched layer. As with Comsol no auralization is available.

Virtual.Lab is a piece of software from SIEMENS, which is based on a collection of legacy software among which is what was previously known as Sysnoise. Sysnoise was a simulation solution for vibro-acoustic design and as such specialized in the topic of this project. The new version from Virtual.Lab includes 'Ray Acoustics' which claim to be able to give a binaural synthesis of a sound environment. Not much detail is given in how this functionality is achieved, but more details are given for the legacy software RAYNOISE and it follows these steps [LMS International, no date]:

1. All direct and reflected paths from source to receiver calculated. (Up to some order.)
2. Calculate histogram for direct sound and each echo.
3. Multiply with HRTF based on angle of incidence.
4. Inverse FFT for an IR for each echo path.
5. Sum all IRs with time delays corresponding to path length.
6. Convolve the summed IRs with a source signal.

The procedure above is only used at a moderate number of reflection. At higher reflections a diffuse field without HRTF is used instead as angle of incidence is unknown.

Comsol and ANSYS can both calculate the sound pressure created by a complex source, such as a vibrating structure, but no binaural representation is available. Virtual.Lab includes the binary representation, but assumes a simple point source. A feature all the software programs have in common is a large price tag and that they are deeply embedded into their own ecosystems.

5 | Selection of structure

A geometry has to be chosen for the project. It is desired to have a structure where an analytical solution to the problem of determining eigenfrequencies and mode shapes exists. Furthermore it is desired that the structure radiates audible sound and that the radiation pattern is not complicated. A plate in free air fulfils these requirements, if the dimensions and material are chosen correctly ensuring that the radiated sound is audible. Other structures such as a cylinder also fulfils these requirements but as a plate can be seen as a 2 dimensional structure it is a more simple structure. The selection of a plate has the further advantage that in can be directly mounted on an excitation source in its centre, resulting in a simple and balanced experimental setup. To select plate material and dimensions a prestudy is made. After the prestudy a plate of the chosen dimensions and material was ordered from the workshop at Grundfos.

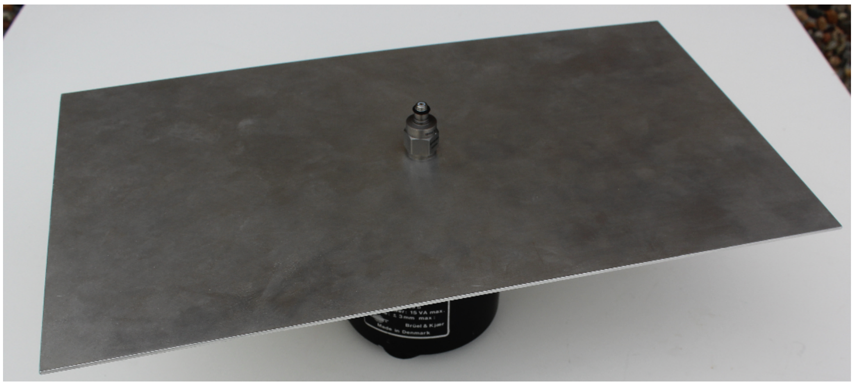

Figure 5.1: Picture of the plate used in this thesis.

5.1 Plate prestudy

The purpose of this prestudy is twofold. First a practical reason was the need for a decision on plate dimensions in order to have one made in a workshop. Different dimensions where selected by trial and error until a satisfactory result was obtained. The requirements were that:

- the plate should have a thickness of minimum 1.5 mm on order to not deform permanently during handling.
- the aspect ratio of the plate should be an irrational number e.g. $\sqrt{\pi}$ in order to avoid that multiple modes will have the same frequency. A counterexample is if the width is chosen to be equal to the length, i.e. a square plate, then mode (3,1) and (1,3) will have the same eigenfrequency, but different mode shapes.
- the lowest eigenfrequency of the plate not to low to be reliably measured, so above 80 Hz.
- distinct eigenfrequencies exist the frequency range of typical interest to Grundfos, 100 Hz to 2 kHz.

By trial and error the following dimensions and material parameters were selected, where the material parameters correspond to those of aluminium, AW-6060.

Parameter	Symbol and value
Density	ρ=2700 $\frac{Kg}{m^3}$
Poisson's ratio	ν=0.33
Young's modulus	$E = 7.1 \cdot 10^{10} \frac{N}{m^2}$
Length	a=0.3 m
Width	b=$\frac{0.3}{\sqrt{\pi}}$ m
Height	h=0.0015 m

Table 5.1: Material parameters and dimensions of the plate in AW-6060 aluminium. All edges of the plate are free.

The second reason for the prestudy was to examine the accuracy of numerical methods. The final algorithm will rely on this accuracy as complex structures are unlikely to have a known analytical solution. Therefore the study examines the eigenfrequencies of a thin plate using an analytical solution and solutions found using FEM. The reason for only examining FEM is that it is that the software which was available to me[1] early in the project is FEM based.

5.2 Analytical solution prestudy

The analytical solution is found in [Blevins, 1995] which states that the resonance frequency in Hz is given by (accurate within 5%):

$$f_{ij} = \frac{pi}{2}\left[\frac{G_i^4}{a^4} + \frac{G_j^4}{b^4} + \frac{2J_iJ_j + 2\nu(H_iH_j - J_iJ_j)}{a^2b^2}\right]^{1/2}\left[\frac{Eh^3}{12\rho h(1-\nu^2)}\right]^{1/2} \tag{5.1}$$

where i, j is the order of the mode in x and y direction respectively. In the case of free ends on all sides G, H and J are given by:

[1]SOLIDWORKS student license

$$G_n = \begin{cases} 0, & \textbf{if } n = 1,2 \\ 1.506, & \textbf{if } n = 3 \\ n - \frac{3}{2}, & \textbf{if } n > 3 \end{cases}, \; H_n = \begin{cases} 0, & \textbf{if } n = 1,2 \\ 1.248, & \textbf{if } n = 3 \\ (n - \frac{3}{2})\left[1 - \frac{2}{(n-\frac{3}{2}\pi}\right], & \textbf{if } n > 3 \end{cases} \quad \textbf{and} \tag{5.2}$$

$$J_n = \begin{cases} 0, & \textbf{if } n = 1 \\ 1.216, & \textbf{if } n = 2 \\ 5.017, & \textbf{if } n = 3 \\ (n - \frac{3}{2})^2\left[1 - \frac{6}{(n-\frac{3}{2}\pi}\right], & \textbf{if } n > 3 \end{cases} \tag{5.3}$$

Using eq. 5.1 the following eigenfrequencies for the mode (i,j) have been found. Frequencies which are probably above the validity of the calculation are included since the resonances will be very closely spaced and a 5% error turns to quite a few hertz at higher frequencies.

i \ j	1	2	3	4	5	6
1	-	-	293	806	1580	2612
2	-	102	359	863	1631	2659
3	93	228	528	1029	1786	2806
4	257	401	743	1261	2015	3028
5	503	645	1012	1550	2307	3315
6	831	970	1349	1903	2665	3670
7	1242	1376	1761	2326	3092	4095
8	1735	1866	2251	2824	3593	4593
9	2309	2438	2821	3398	4169	5166
10	2966	3092	3474	4052	4823	5817

Table 5.2: Eigenfrequencies of mode (i,j) in Hz. (1,1), (2,1) & (2,1) are rigid body modes meaning that the plate moves or rotates with no deformation and constant speed.

5.3 Finite elements method prestudy

In order to evaluate the accuracy of FEM a free plate with the dimensions and material characteristics mentioned above was drawn in SOLIDWORKS 2016 [SOLIDWORKS, no date]. The simulation toolbox was used to do a 'frequency study', which determines resonant frequencies and mode shapes. Two simulation results are plotted: one where the mesh of the structure was 'standard' and one where it was 'fine'. This demonstrates that the meshing is an important parameter, where a finer mesh is required the higher the upper frequency of interest is.

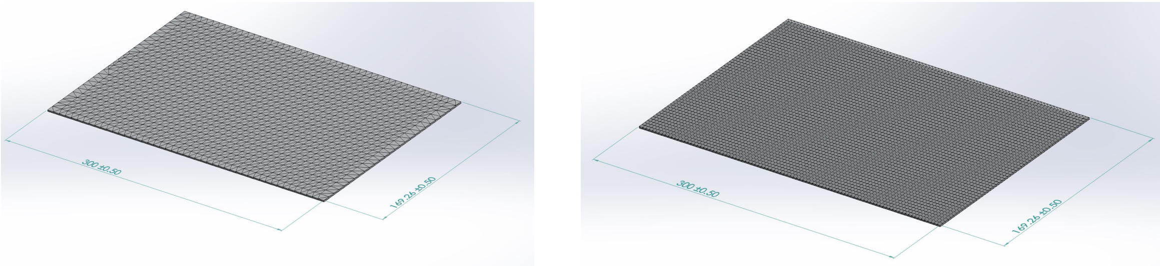

(a) Plate with standard mesh.
(Element size 6.4 mm, 8180 elements.)

(b) Plate with fine mesh.
(Element size 3.2 mm, 66167 elements.)

Figure 5.2: The plate under study with different meshes.

Below the calculated eigenfrequencies from table 5.2 and tolerances are plotted together with the result from a FEM simulation in SOLIDWORKS 2016.

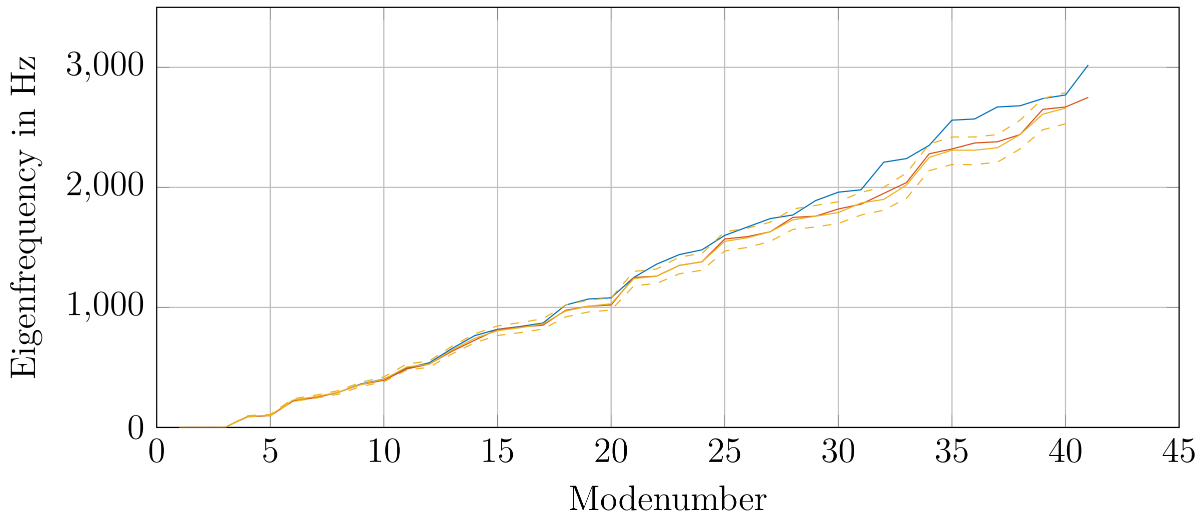

Figure 5.3: Estimated eigenfrequency as a function of modenumber. Normal resolution (—), high resolution (—), analytical solution (—) and analytical solution tolerances (- -).

The accuracy of the analytical approach is only 5%. Any deviation smaller than this must be acceptable for simulation also. From figure 5.3 it is clear that the FEM is capable of estimating the deformations of a plate to the same degree of accuracy as the analytical approach, if the meshing is done correctly. On the note of meshing if one assumes that 6 elements are required per wavelength [Schmiechen, 1997] the upper frequency, on this plate with an elements size of 6.4 mm is 485 Hz and 1940 Hz with an element size of 3.2 mm[2].

[2]Bending waves in solids are dispersive so the wavelength in the solid does not scale with the same ratio as the frequency as described later by eq. 8.2.

Part II

Auralization of a vibrating structure

6 | Overview of the auralization algorithm

The development of the auralization algorithm has to consider the five blocks in figure 3.1. For each block a theory section, a list of possible methods, a choice and an implementation has to be shown. To further complicate things the algorithm does not strictly follow figure 3.1 as, for instance, it proves convenient to compute the influence of the propagation before the radiation.

To better be able to read this part, an overview of the final auralization algorithm is given here. The arguments for the choices made will be presented as the thesis progresses.

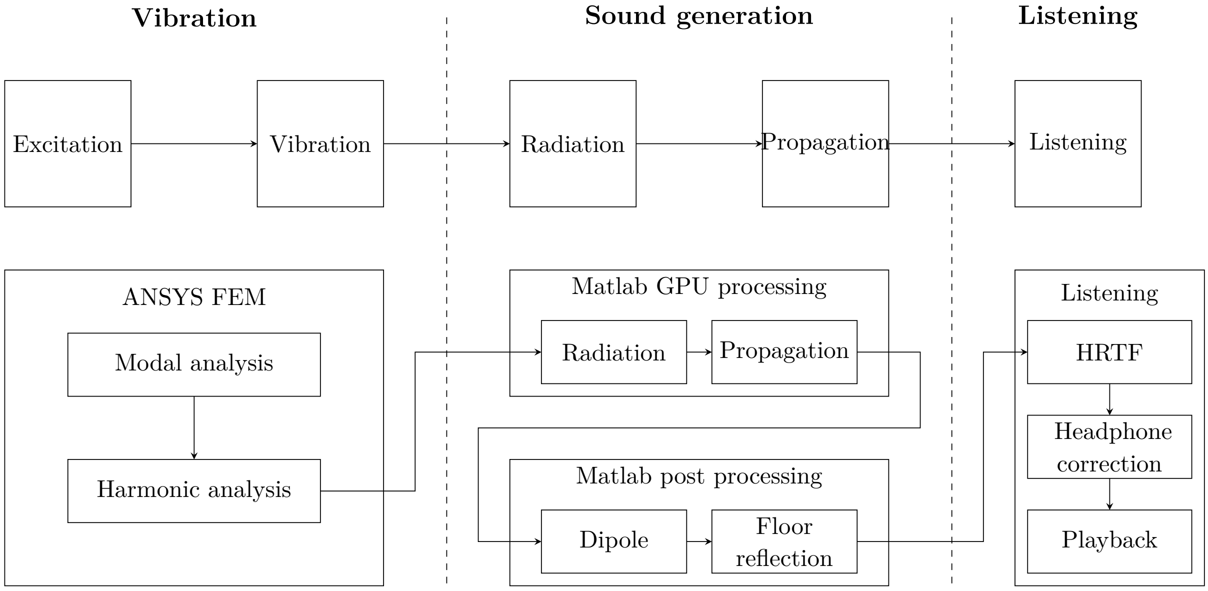

Figure 6.1: An overview of the auralization algorithm presented in this part. Figure 3.1 is included in the figure to make it clear where the different parts belong. When crossing the first dotted line the vibration of the structure is known. When crossing the second dotted line the sound pressure in a position in an environment is known. The last part is responsible for presenting the audio binaurally.

7 | Excitation

7.1 Theory

In order to have a vibrating structure some energy must first be put into the structure to excite it. This chapter describes the methods which can be used to do so, mainly focusing on how to do so in practice. A reader completely new to vibration should skip ahead and read section 8.1 before reading this chapter. This will give an understanding of bending waves which is beneficial to understanding how they are excited.

One way of seeing excitation of an object is that you apply a force to it in some position. This will according to Newtons second law result in the object moving since $F = m \cdot a$. Then if the excitation force is oscillating on the form $F = Ae^{j\omega t}$, where A is some amplitude and ω the angular frequency of the oscillation, then the acceleration will also be oscillating meaning that the object vibrates [Cremer et al., 2005].

In analytical work it is convenient to work with a point excitation meaning that the applied force is put into the structure at an infinitely small position. In practice it is not quite as simple since the source will be distributed over some area.

7.1.1 Real world sources

In machinery the main cause of vibration is often a moving part, for instance the pistons in an engine moving up and down at high speed. A person walking on a bridge will excite the bridge. A source might also be a rotating part which is not perfectly balanced. Think of the vibration of a bicycle with a skewed tire. Sound waves can even excite structures if the level is sufficient. In short excitation of vibrations happens everywhere and all the time in the real world. The issue in engineering is to use an excitation which can be controlled and thereby replicated.

7.2 Methods

In order to examine vibration on a physical structure the structure naturally has to receive energy in some way. Different methods allow for excitation of a structure and the choice of method depends on the kind of excitation wanted as well as practical considerations.

7.2.1 Forced vibration

A shaker can be mounted to the object and made to vibrate at a single frequency (or a set of frequencies). This excitation method is called forced vibration, because it forces the object to vibrate at a given frequency. This method is convenient if it is desired to determine how an object vibrates if connected to something operating at a fixed set of frequencies.

(a) A shaker, Brüel & Kjær type 4809. [Brüel & Kjær, no date a]

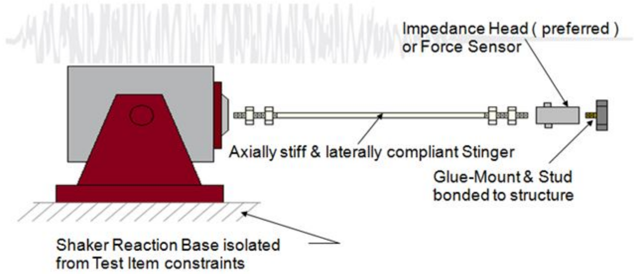

(b) A setup with a shaker including a stinger. [SignalNews, no date]

Figure 7.1: A shaker and a schematic of a typical setup.

A drawback of the shaker is that it is slightly bulky and requires some effort during setup. For instance a 'stinger' might be required to ensure that only forces normal to the structure are transferred . Also mass loading of the structure is an issue since the shaker is in constant contact with the object under study.

7.2.2 Impact excitation

Another way of exciting a structure is impact excitation, which can be achieved by hitting the object with a hammer. Impact excitation will, in the case of a perfect impulse, excite the structure with all frequencies. This will result in the structure vibrating at all frequencies, but the vibration will be dominated by the eigenfrequencies. Therefore this is an 'easy' way to excite all modes of the structure. A drawback however is, that it is impossible to judge the power of the impact if using a regular hammer. Impact hammers serve the purpose of measuring the input force applied at each impact. This however does not solve the issue of repeatability in terms of hitting the same point with the same force multiple times. A further downside of hitting an object with a hammer is that you have to hit the object with a hammer. Imagine examining the vibrational pattern of a wall; the applied force has to be so large that it excites the wall yet not so large that it damages the wall.

Figure 7.2: An impact hammer, B&K 8207 [Brüel & Kjær, no date d].

7.2.3 Additional concepts

A third way to excite a structure also uses a shaker, but excites all frequencies, rather than single tones, by using coloured noise, sweeps or other types of broadband noise with a known distribution. This overcomes the issues of the impact hammer since the energy can be continuously applied to the system, distributing the same energy as from a single hit with an impact hammer over more time.

An additional important note is that a mode cannot be excited in a node of the mode shape regardless of the input type. This is analogous to attempting to excite the 2-0-0 mode of a room with a loudspeaker in the middle of the room.

7.3 Choices

It is desired to have an experimental setup which is as stationary and repeatable as possible. For such a setup an impact hammer is not suitable since the location and force of impacts will vary on each hit. The remaining instrument, and therefore the chosen one, is a shaker which is rigidly mounted on the plate in its centre position. This allows for both forced vibration at single frequencies as well as shaking the plate with a broadband signal such as white noise. By doing the latter the steady state response of the plate can be examined. Mounting the shaker in the middle of the plate ensures that only doubly symmetric mode shapes can be excited since the plate must have the derivative of the bending at the excitation position equal zero. The drawback of using a shaker rigidly mounted on the plate is that it might affect the plate's vibrational behaviour more than an impact hammer would have done.

In the analytical and simulated work the excitation is made as a point excitation in the exact centre of the plate.

8 | Vibration

8.1 Theory

Having determined how a structure is made to vibrate it is appropriate to examine how it vibrates. To that end this theory section contains the basics of bending waves as well as the most simple vibrating structure, a single degree of freedom oscillator. After this the vibration of the plate is determined by means of an analytical as well as a numerical method.

The information in this section is a resume of knowledge obtained in the textbook 'Structure-Borne Sound' [Cremer et al., 2005].

8.1.1 Single degree of freedom oscillator

The most simple oscillating system one can consider is the single degree of freedom system consisting of a mass and a spring. It consists of a simple mass connected to a spring which is connected to ground. In such a system the mass can vibrate at any frequency, but it is especially willing to move at a specific frequency, the eigenfrequency. At resonance the mass of this undamped system would, theoretically, move to infinity when a small force is applied. In reality the system will always include some amount of damping, which will make the resonant peak less steep as shown in figure 8.1b.

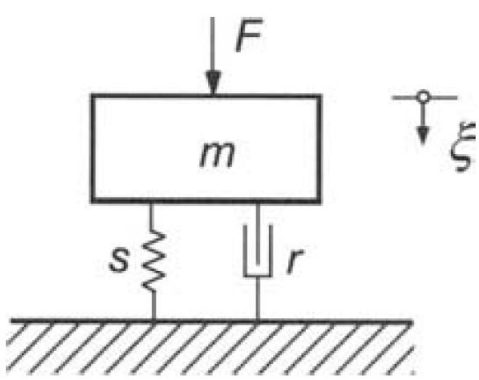

(a) Single degree of freedom system. m is a mass, s is a spring and r is a damper.

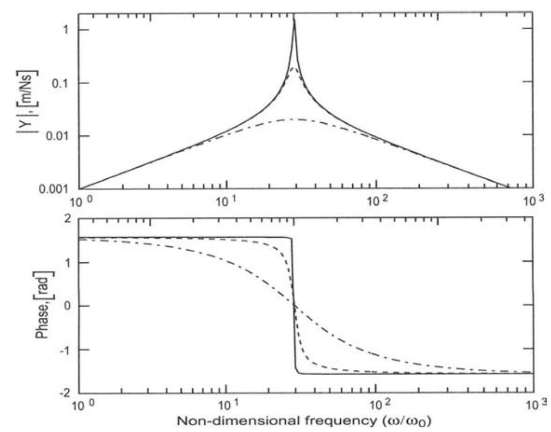

(b) Frequency response of a single degree of freedom system. The dashed lines show the response when damping is increased.

Figure 8.1: A single degree of freedom system. Both figures are from [Cremer et al., 2005].

The resonance frequency of such as system is given by

$$f_0 = \frac{1}{2\pi}\sqrt{\frac{s}{m}} \tag{8.1}$$

Transferring this knowledge to a more complex structure would correspond to a series of these simple structures connected to each other resulting in a system response. In fact a continuous beam might be discretized as a a series of mass spring systems as discussed by [Kropp, 2015].

8.1.2 Wave types in solids

In solids different wave types exist. Some of the fundamental wave types are longitudinal waves, transverse waves, torsional waves and bending waves. In figure 8.2 an illustration is given of the first two types.

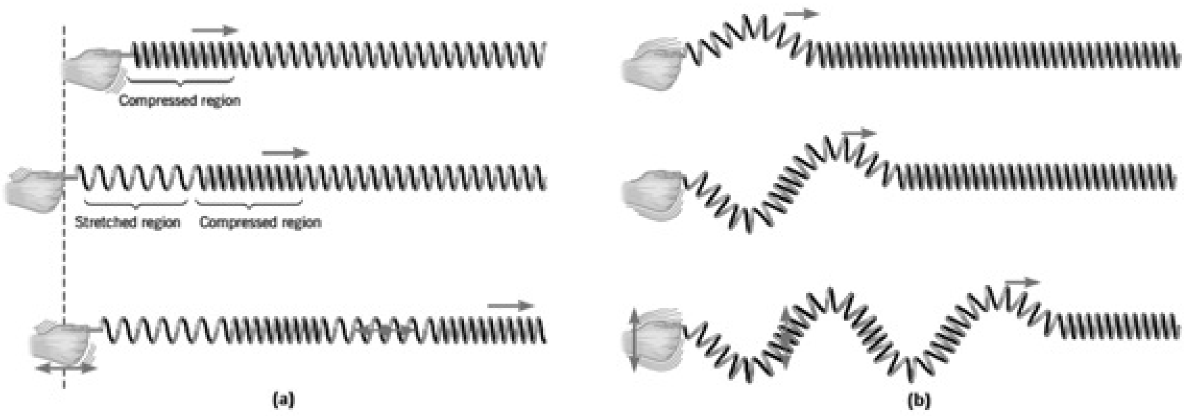

Figure 8.2: Example of a longitudinal wave (a) and a transverse wave (b). Torsional waves would be if the hand rotated back and forth. [Johnson and Cutnell, 2012]

The reason for only considering bending waves in this thesis is that it is the wave type that couples significantly more with airborne sound waves than the other wave types. That being said the other wave types are not irrelevant since coupling between different wave types will exist in any finite structure. For instance two beams meeting in a 90° angle where one beam is excited with a longitudinal wave will primarily show bending waves on the second beam.

8.1.3 Characteristics of bending waves in solids

A bending wave will cause bending of a structure such as a plate or a beam. One might think how does that differ from a transverse wave? That question might be best answered graphically with a 'zoom' on a part of a beam where a transverse or a bending wave is propagating. In figure 8.3 it is clear that the transversal wave merely change the shape of the beam, not the volume. In the case of a bending wave the volume is also changed as the material is compressed and elongated.

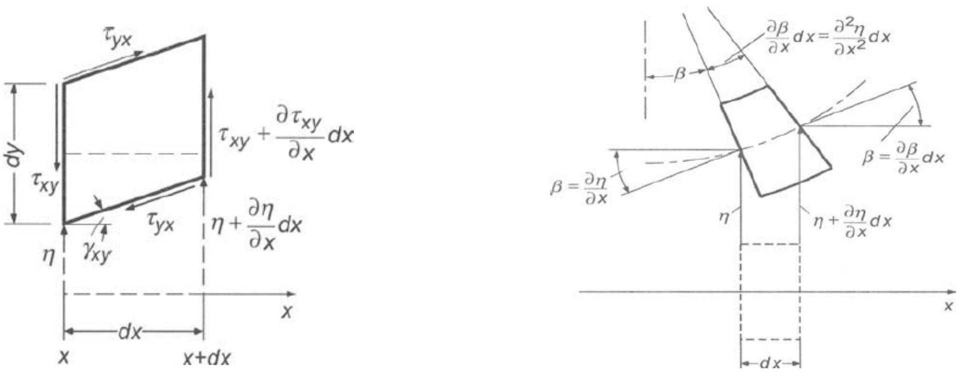

(a) A transverse wave

(b) A bending wave

Figure 8.3: Zoom on bending and transverse wave on a beam. Note here Cremer uses η as displacement where this thesis uses ξ to avoid confusion with the loss factor. [Cremer et al., 2005]

If an infinite beam is excited with an oscillating force on the form $Ae^{j\omega t}$ at some position x=0 a bending wave will propagate from the excitation position in two directions. The bending waves will be a propagating sine on the form $\xi(x,t) = Ae^{\pm jkx}e^{jkt}$. So the displacement of the beam will depend on where and when you look. In addition to the propagating wave an important characteristic of bending waves is the existence of near fields. In the example above where the beam was excited in a single point and two waves propagate in opposite directions from the excitation position a problem occurs at the excitation position. The transition between the two waves will be infinitely small and (at most times) non-continuous - this will result in a non-continuous bending of the beam. This defies physics and instead a bending near field will ensure that the derivative of the bending at the excitation point is 0. The bending near field decreases with distance from the excitation point and does not contribute with or remove any power - it simply stores it for a brief period of time and gives it back during the same cycle.

One of the main differences between airborne sound and structure borne sound is that bending waves in solids are dispersive. This means that different frequencies travel at different velocities in the solid. The speed of bending waves in a solid is given by $C_b = \sqrt[4]{\frac{B}{m'}} \cdot \sqrt{\omega}$, where m' is the mass per unit length, ω is the angular frequency and B is the bending stiffness defined by: $B = EI$, where E is Young's modulus and I is the second moment of area[1]. So in short the wave speed depends on frequency, material and dimensions of the structure. From this follows

[1]For a plate this is $B = EI = \frac{Eh^3}{12(1-poissonRatio^2)}$

that the wavelength also depends on the same parameters since:

$$\begin{aligned}\lambda_b &= \frac{2\pi C_b}{\omega}\\ &= \frac{2\pi\sqrt[4]{\frac{B}{m'}}\cdot\sqrt{\omega}}{\omega}\\ &= \frac{2\pi\sqrt[4]{\frac{B}{m'}}}{\sqrt{\omega}}\end{aligned} \tag{8.2}$$

8.1.4 Representing bending waves

When working with bending waves two approaches can be adopted based on preference or convenience, namely a modal approach or a wave approach.

The modal approach uses modal amplitudes and modal shapes to describe the displacement of the object. The concept is similar to that of Fourier theory, that a time signal can be recreated by a series of sine waves. Normally in signal processing the Fourier transform is done with respect to time, but there is no reason to not use it with respect to distance. This allows for the definition of eigenfunctions (or mode shapes), which depend on the length of the object, the boundary conditions and the order of the mode. Each mode will be linked to a single frequency called the eigenfrequency. All the modes contribute to the displacement and the total displacement can be found as a superposition of modes because the modes are orthogonal. This method works very well for resonant systems, i.e. systems with little damping, as almost all energy is stored at the eigenfrequencies. Modal decomposition also proves useful in the sense that the model is accurate up to the eigenfrequency of the highest mode. With that knowledge the question; 'How many modes do I need to include?' can be answered up front[2]. Computationally it is convenient as you only have to store the mode number (and thereby know the modal shape and eigenfrequency) and the modal amplitude. To calculate the wave field you do a summation of weighted sine functions. A disadvantage is that at higher frequencies the eigenfrequencies might be so close to each other that they are no longer separable in practice.

The wave approach is based on superposition of propagating waves. This means that for each wave in the structure a wave, i.e. an amplitude and a direction of propagation, has to be stored. Each time a propagating wave meets an impedance change such as an ending of a beam, a change of cross-section or a corner, other waves are created as reflections or transmissions. This means that when structures grow in complexity the amount of waves to include becomes arbitrarily large. The benefit is that this method also works well for damped structures.

[2]If considering the behaviour below the first mode or anti-resonances this does not hold, more modes are needed for accurate results.

8.1.5 Boundary conditions

Before discussing boundary conditions it is worth noting that these must hold regardless of which of the two approaches above is selected. Where the above is a way of describing wave fields at all positions and at all times, the boundary conditions can be used to solve sets of equations to determine the amplitudes of the mode or propagating waves by providing a known value or relation at one position, the boundary, for all times. For bending waves in plates or beams the parameters defined by the boundary conditions are:

ξ Displacement

β Bending angle

M Bending moment

F Shear force

Different boundaries will result in different boundary conditions as described in table 8.1.

Boundary condition	Description of boundary	Implication
Free end	End terminated in free air	$M = F = 0$
Simply supported	End supported at infinitely small point at boundary	$\xi = M = 0$
Clamped	The end of the beam rigidly connected to baffle/structure	$\xi = \beta = 0$
Guided	The end of the beam can move but not rotate	$F = \beta = 0$

Table 8.1: Boundary conditions for bending waves and their implications when invoked at one end of a semi-infinite beam.

Obviously when solving the amplitudes of the modes or propagating waves, the same amount of boundaries has to be known (equations) as the number of amplitudes (unknowns).

8.1.6 Losses in bending waves

In airborne sound the losses due to viscous friction in the medium is typically ignored and the only loss of level is due to the propagation in three dimensions, spreading the energy over a larger and larger surface. For bending waves the area does not increase in three dimensions but one in the case of a beam or two in the case of a plate, allowing waves to propagate over much larger distances than known from airborne sound.

Furthermore solids cannot be seen as a lossless medium and a loss factor, η, is introduced to describe how much energy is lost per period of a propagating wave. One way of handling losses in bending waves is to introduce a complex Young's modulus as:

$$E_c = E(1 + j\eta) \tag{8.3}$$

which in turn will result in a complex bending stiffness, B. For further knowledge on this topic the reader is referred to literature: [Cremer et al., 2005].

This concludes a very brief general introduction to bending waves in solids. Further theory will be provided when needed as the report progresses.

8.2 Methods - analytical

To determine the mode shapes of the plate under study, and preferably also the eigenfrequencies with a higher accuracy than that achieved in table 5.2, two approaches have been examined in order to chose the better one. They are called Rayleigh-Ritz and Gorman Superposition and will be presented below.

8.2.1 Rayleigh-Ritz

The Rayleigh-Ritz method is the basis for the equations used in determining approximate eigenfrequencies in table 5.2. This method can be further expanded upon to also include mode shapes [Blevins, 1995]:

$$z_{ij}(x,y) = \sum_m \sum_n a_{mn}^{ij} z_m(x) z_n(y) \tag{8.4}$$

where $z_{ij}(x,y)$ is the plate mode shape and $z_m(x)$ and $z_n(y)$ are mode shapes of free beams with the boundary conditions of two opposite sides on the plate. a_{mn}^{ij} are a set of constants, which are determined by the Rayleigh-Ritz procedure. This method can yield good results if two opposite sides are simply supported, but in the case where all sides are free the method is not applicable [Blevins, 1995]. Even the estimation of the eigenfrequency is wrong as the method in fact calculates an upper bound for the eigenfrequency [Leissa, 1969]. In spite of this clear downside the Rayleigh-Ritz method seems to be the go-to solution for finding eigenfrequencies and mode shapes of plates.

8.2.2 Gorman superposition

A newer alternative is the superposition method proposed by Daniel J. Gorman, which attempts to remedy the downsides of the Rayleigh-Ritz method. The method was first summarized in the Journal of Sound and Vibration in 1976 [Gorman, 1976] and later published for a completely free plate in the same journal in 1978 [Gorman, 1978]. The method is rather elaborate, but in short it splits the problem of a plate into four sub-problems of smaller plates. The split is made through the middle of the plate along the x and y direction. Hereby boundaries inwards of the subproblems are then not free but depend on the symmetry of the mode; fully symmetric, symmetric antisymmetric or fully antisymmetric[3]. Each edge of the subproblems are then treated individually in sub-subproblems and finally the sub-subproblems are combined to form an eigenvalue matrix. The major benefit of this method, apart from being accurate for any type

[3]The two symmetries are around the centre of the plate around the x/y axis. So 'fully symmetric' is read as 'symmetric around the x-axis and y-axis.'

of boundary condition, is that the algorithm is based on a summation of terms of higher and higher order. This means that by increasing the order, and thereby the computational effort, the algorithm converges towards the true solution. It is therefore possible to select the right amount of terms for any desired degree of accuracy.

8.3 Choices - analytical

Based on the brief study of the two methods, the Gorman superposition is chosen as reference analytical solution because:

- this project does not include simply supported plates where the Rayleigh-Ritz yields a good solution.
- for use in auralization a highly accurate description of the surface movement of the plate is required - hence the analytical reference should be highly accurate.
- the fact that accuracy can be achieved to a specific number of decimal points at the cost of additional computation need is seen as a nice feature.

8.4 Analytical solution

An analytical solution to the eigenfrequencies of the plate were determined in table 5.2. Later it was determined that a more accurate method, developed by Gorman, exists. A brief outline of the idea behind Gorman superposition is given in section 8.2. This chapter aims to document an implementation of the Gorman superposition algorithm used to determine analytical solutions to the eigenfrequencies and mode shapes of the plate.

8.4.1 Plate physical dimensions

The plate considered in this project is a thin rectangular plate with the length and the width along the x and z axis respectively. Displacement due to bending waves are in the y direction. The plate is, in all cases, excited in its centre, which in the analytical and simulated solution is handled as a point excitation. On the physical structure this kind of excitation is not realizable so some inaccuracy is to be expected from the distributed excitation.

The Specifications of the physical plate from table 5.1 are used at their specified values and tolerances in the production of the plate are listed below:

- Length = 300 mm $\pm 0.1mm$
- Width = 169.256 mm $\pm 0.1mm$
- Thickness = 1.5 mm $\pm 0.1mm$

8.4.2 Overall concept of Gorman superposition

As mentioned in section 8.2 the method splits the solution into 3 categories based on symmetry of the mode shape; fully symmetric, symmetric antisymmetric or fully antisymmetric. The mathematical background for the method is not replicated here, instead the reader is referred to the book on the topic [Gorman, 1999], where it is described in detail in chapter 1.

In order to quickly understand the concept of the Gorman superposition method an outline is given below:

1. The plate problem is split in 4 subproblems and all calculations are performed on only a quarter plate. The rest of the plate is then created based on the chosen symmetry properties. In the case of double symmetric mode shapes the edges toward the other quarter-plates a slip-shear boundary condition is imposed meaning 'no vertical edge reaction along the edge and that slope taken normal to the edge is everywhere zero.' Gorman [1999].
2. The quarter plate subproblem is then split in 2 sub-subproblems called 'building blocks'. Each building block is then treated separately in the following way.
   (a) One of the free sides is imposed with the slip-shear boundary condition.
   (b) The other free side is imposed with a harmonic edge rotation.
   (c) Combining this excitation and the reactions caused by the boundary condition half the eigenvalue matrix, A, is set up.
3. Having performed the steps above for both building blocks the determinant of the eigenvalue matrix, A, is calculated. The result will be 0 at resonance.

The steps 'a' through 'c' above are performed for K terms. The number of terms determines how many components the solutions have. The higher the amount of terms the better the accuracy. The eigenvalue matrix, A, will be be a 2K by 2K square matrix.

8.4.3 Implementing Gorman superposition

The entire code for finding the eigenfrequencies and mode shapes of the plate is available digitally. Pseudocode showing the structure of the code is available in Listing D.2 in Appendix D. Having calculated the determinant of the A matrix as described above the eigenvalues are determined by reading where the determinant of A as a function of trial eigenvalue crosses through zero. Having determined the eigenvalues in this way the mode shapes can be calculated afterwards. An outline og the code determining mode shapes is given in Listing D.2

The two listings in Appendix D compose the standard Gorman superposition algorithm on top of which some modifications have been made. The modifications allows the algorithm to run with varying frequency steps. This is beneficial as the methods searches for eigenvalues by trial and error, requiring a very fine step for an accurate solution. The algorithm has been modified to do an initial search with relatively large steps after which it refines the resolution around possible solutions. This process is controlled in a 'refinementLoop', which can be controlled in the setup of the script. In that way the search is first performed with a step in guessed eigenvalue of 0.1 corresponding to 5 Hz on the plate. After this the refinement is a factor 10 per refinementLoop with a final resolution 0f 0.05 Hz near the zero cross.

```
refinementLoops=number of refinements
refinement=scale of refinement
for j=1:refinementLoops
    do the code in listing D.1
    % find zerocross as two adjacent Y values with opposite sign.
    zeroIndex=find(Y(1:end-1)*Y(2:end)<0)
    % refine searchrange
    if j!=refinementLoops
        refinements=searchrange(zeroIndex):step/refinements^j:searchrange(
            zeroIndex+1)
        searchrange=[searchrange(1:zeroIndex) refinements  searchrange(
            zeroIndex+1:end)]
    end
end
```

Listing 8.1: Pseudocode for the refinement loops.

The algorithms in its initial form also yields false eigenvalues at points where the determinant of A jumps from minus infinity to positive infinity. In a sampled version this jump will appear to go through zero on the y-axis indicating an eigenvalue. These jumps are handled by checking if the value two steps before crossing zero is smaller than value one step before. This would indicate that the eigenvalue was headed for infinity rather than zero. This sorting of potential eigenvalues is solved by visual inspection in the original works but a newer paper comparing Gorman superposition to Rayleigh-Ritz method uses the same selection of correct eigenvalues[Mochida and Ilanko, 2010]. The procedure is done after the refinement to ensure a high degree of certainty that a false value has been found.

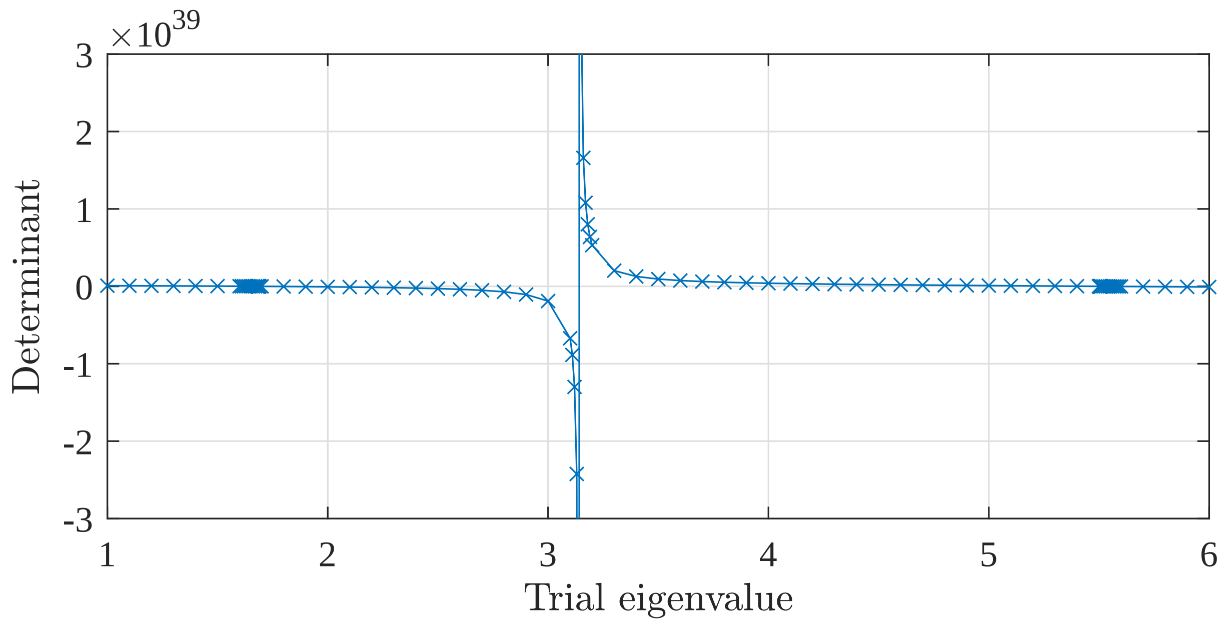

Figure 8.4: Search for actual eigenvalues. 'x' indicates a calculated point. It is clear that around 3 the determinant is wrapping from minus infinity to infinity, whereas around the true eigenvalues the algorithm refines the search.

```
%this code is at the end of the program after refinement
for i=zeroIndex
    if (|Y(i)|-|Y(i-1)|>0) % check if Y was moving away from 0
        delete zeroIndex(i)
    end
end
```

Listing 8.2: Deletion of false eigenvalues.

After the refinement and deletion of false eigenvalues the two values around the zero crossing are known. These do not represent the actual eigenvalue which will lie somewhere between the two. To account for this a linear interpolation is performed between the two points to get closer to the actual eigenfrequency. It should be noted that this interpolated value cannot be used in calculating the mode shape as the trial eigenvalue and its corresponding A matrix are used in calculating the mode shape. The A matrix is not set up for the interpolated value. Instead the trial eigenvalue just before the zero crossing is used, which should be sufficiently accurate as the resolution is about 0.05 Hz after three refinement loops.

As this project is working on a plate that is excited in its centre, only the fully symmetric modes are relevant. This is another convenience of the Gorman superposition method, which makes it so that the selection of these symmetric modes is inherent in the method. For this reason only the relevant modes are examined and modes with any kind of antisymmetry are not included in the analytical solution.

8.4.4 Results

The following results are obtained using the parameters given below as well as the plate dimensions given in table 5.1:

- Number of terms; K=15
- Lower limit of search; ALMDS_init=0.1
- Initial step-size; DEL=0.1
- Upper limit of search; DLIM=40
- Number of refinement loops; refinementLoops=3
- Factor of refinement per loop; refinement=10

Using these parameters the following eigenfrequencies have been determined; 88 Hz, 288 Hz, 479 Hz, 519 Hz, 991 Hz, 1226 Hz, 1568 Hz, 1728 Hz and 1786 Hz.

As the mode shapes do not say anything about absolute amplitudes they are shown as normalized. Furthermore the viewing angle is set to directly above and the absolute value of the displacement is used. This resembles the way I will later show mode shapes from the simulation so easy comparison is possible. The scale goes from dark blue, no displacement to bright yellow, most displacement.

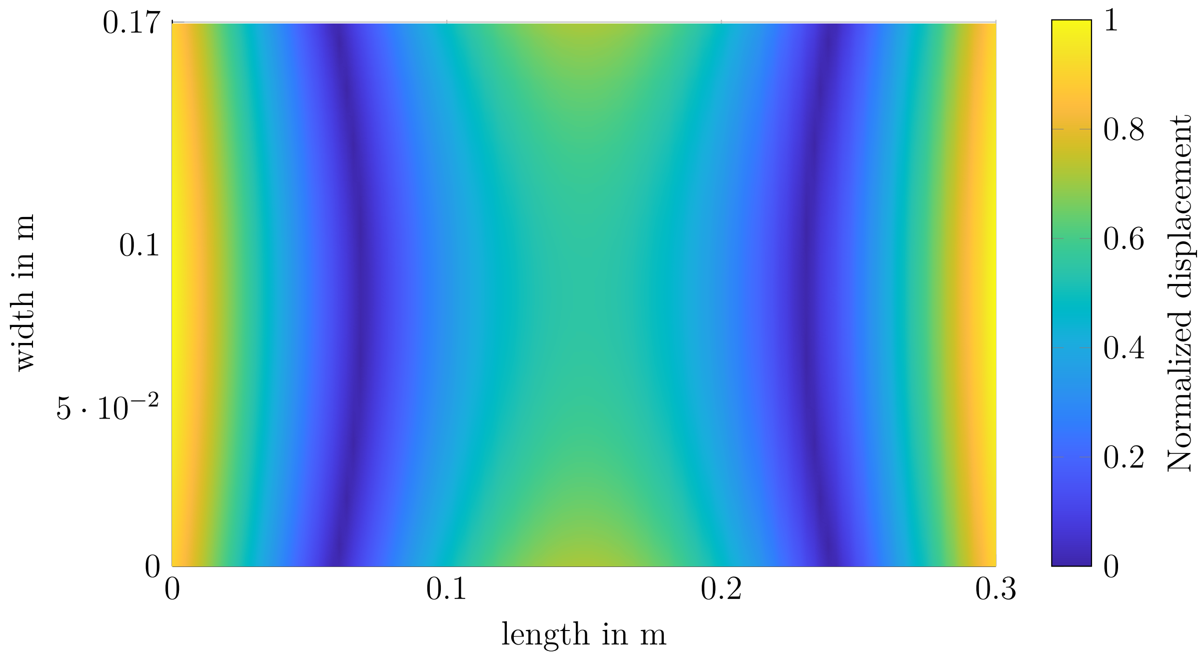

Figure 8.5: Mode shape of eigenfrequency 88 Hz.

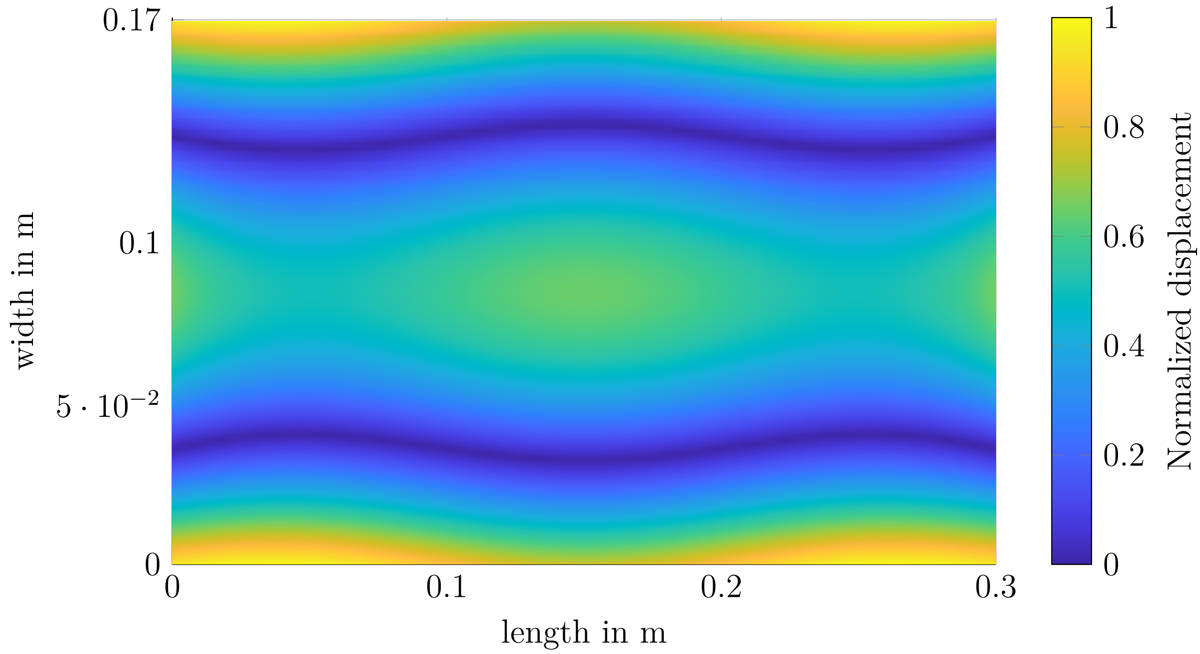

Figure 8.6: Mode shape of eigenfrequency 288 Hz.

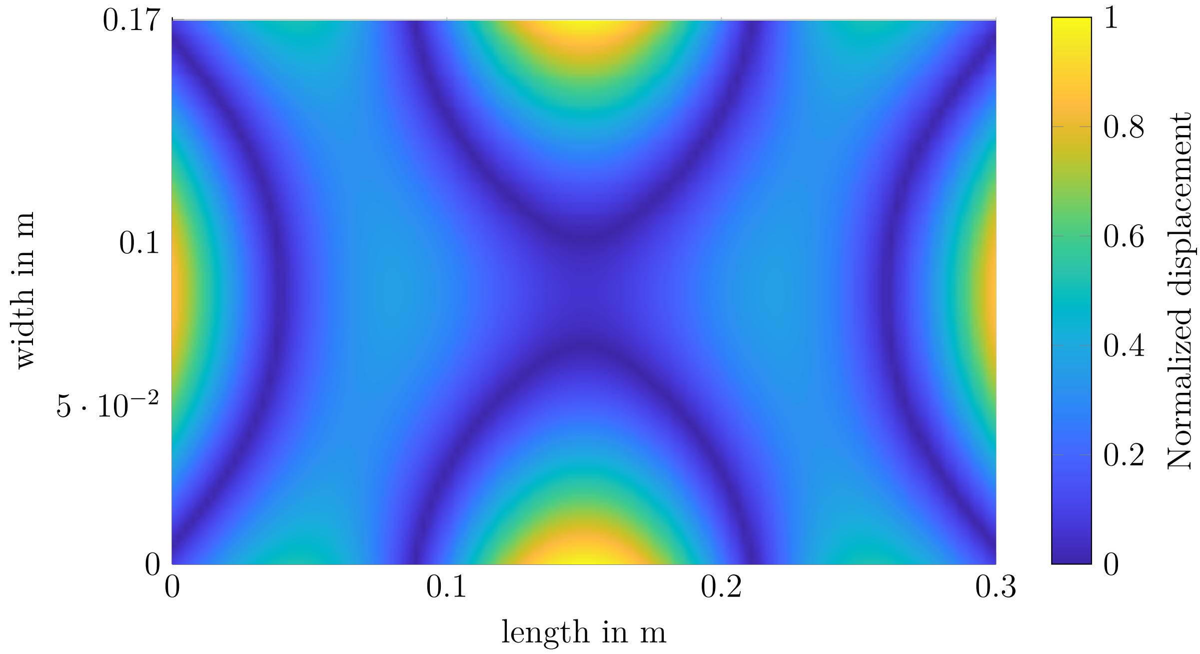

Figure 8.7: Mode shape of eigenfrequency 479 Hz.

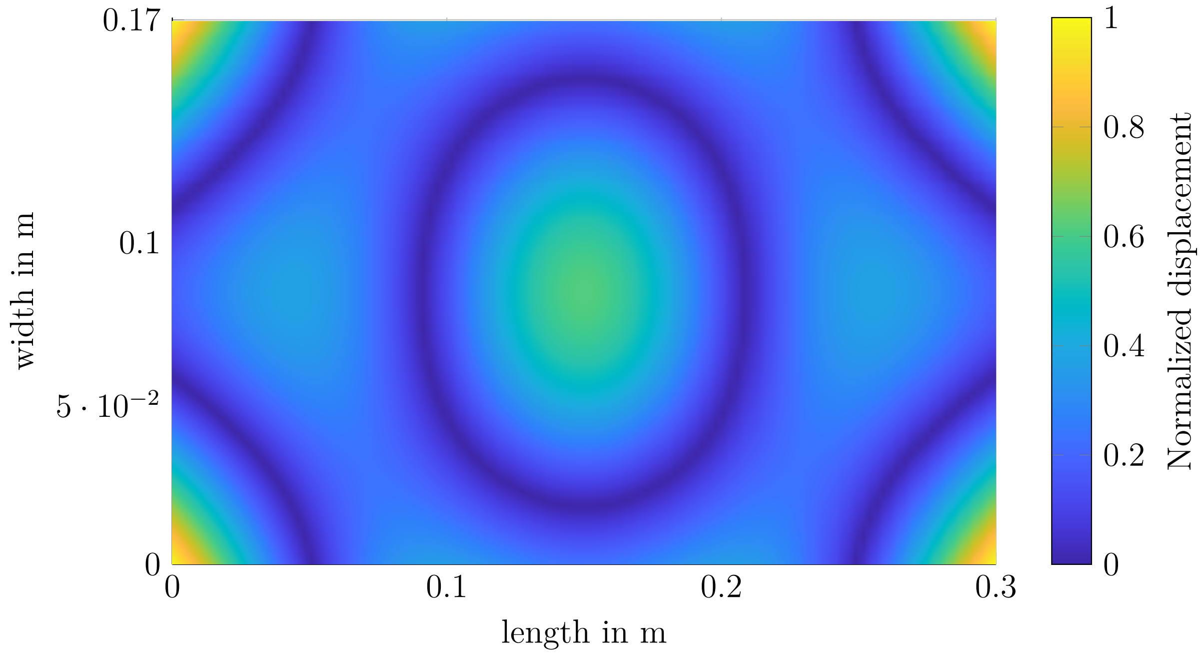

Figure 8.8: Mode shape of eigenfrequency 519 Hz.

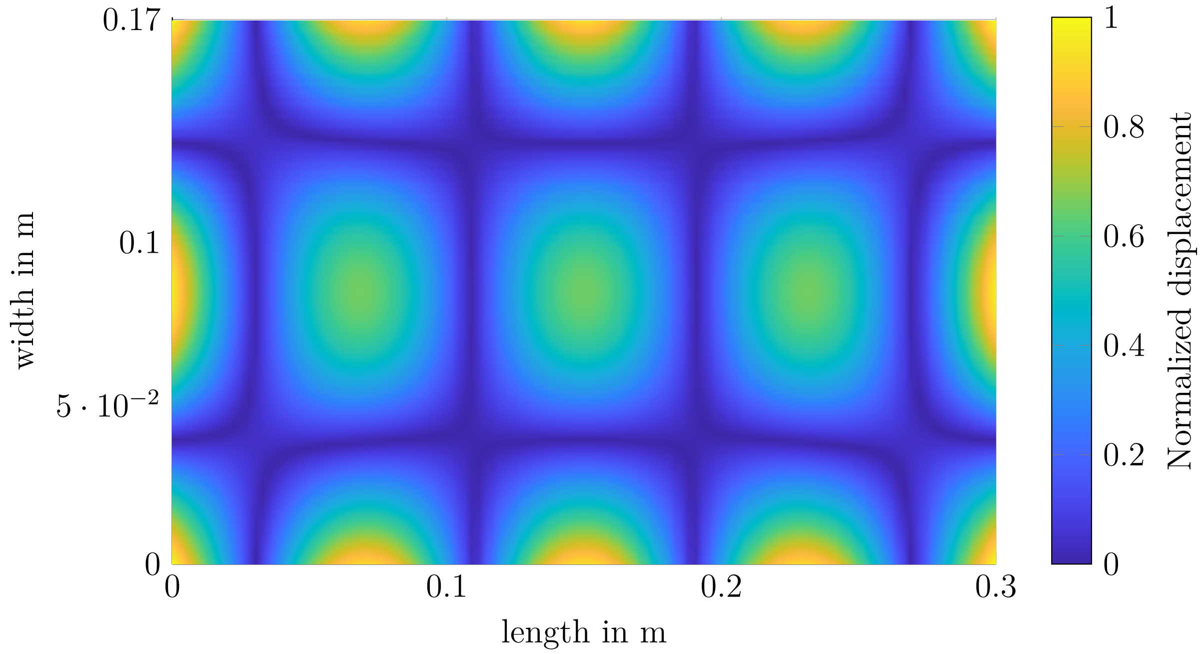

Figure 8.9: Mode shape of eigenfrequency 991 Hz.

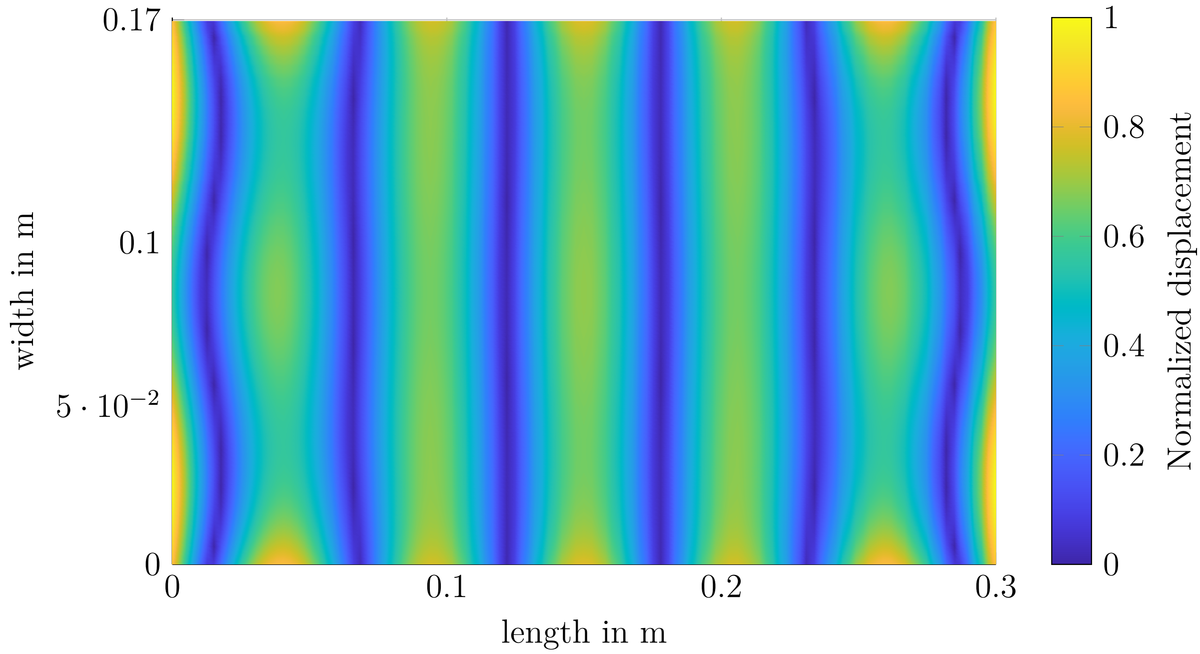

Figure 8.10: Mode shape of eigenfrequency 1226 Hz.

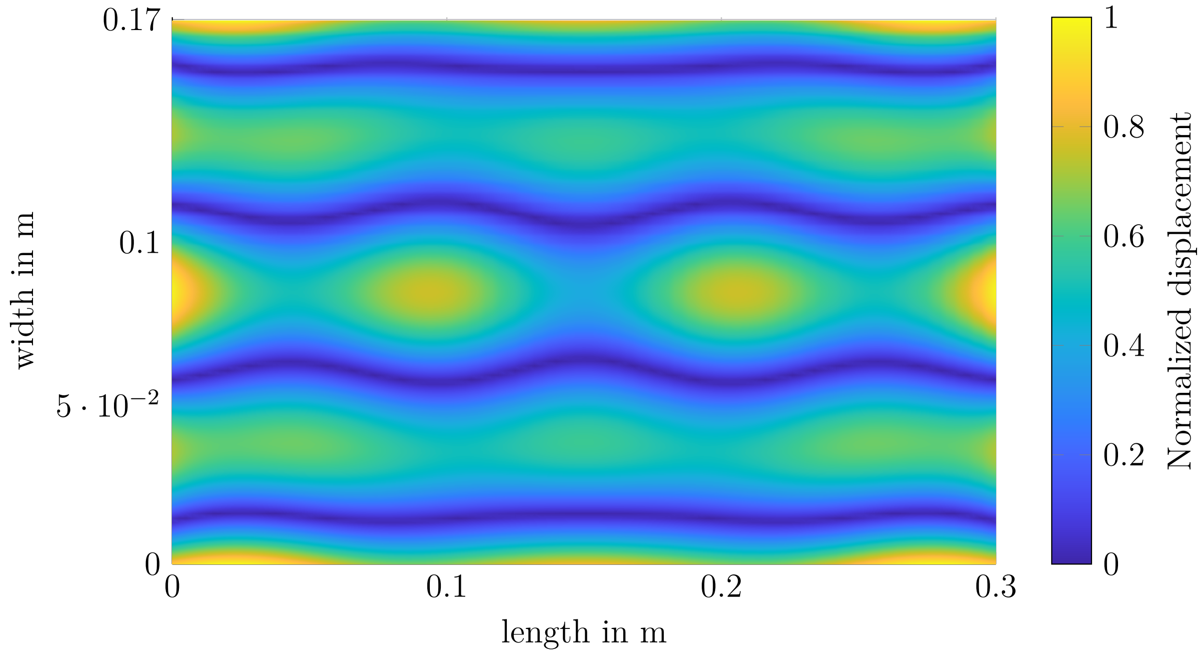

Figure 8.11: Mode shape of eigenfrequency 1568 Hz.

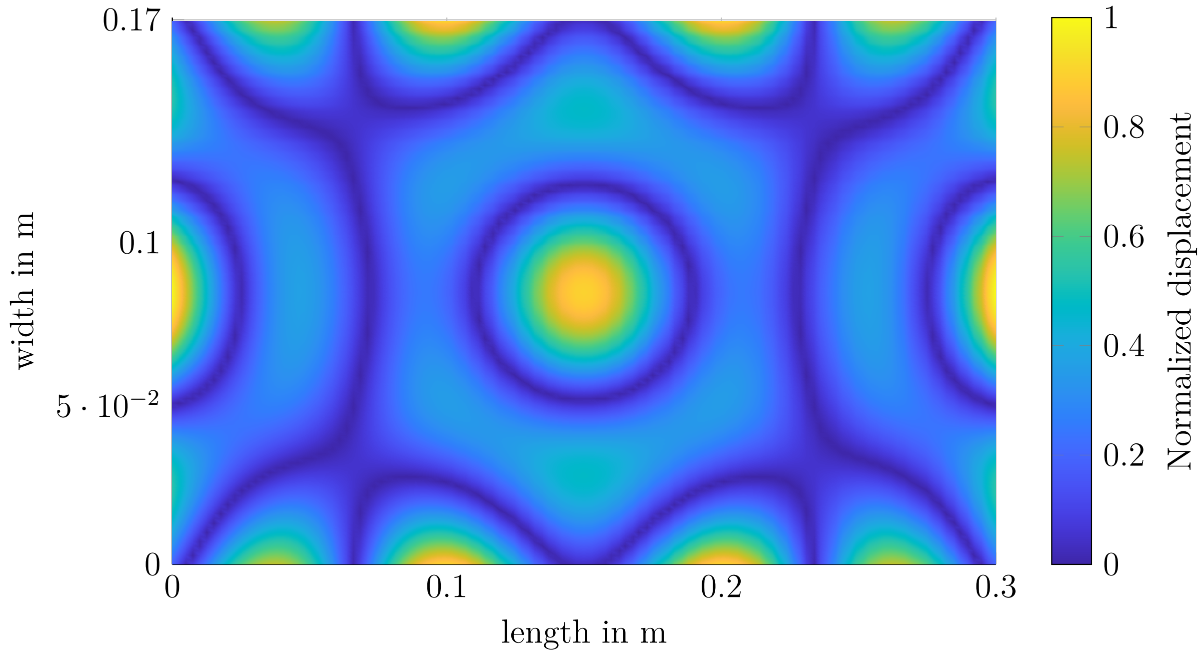

Figure 8.12: Mode shape of eigenfrequency 1728 Hz.

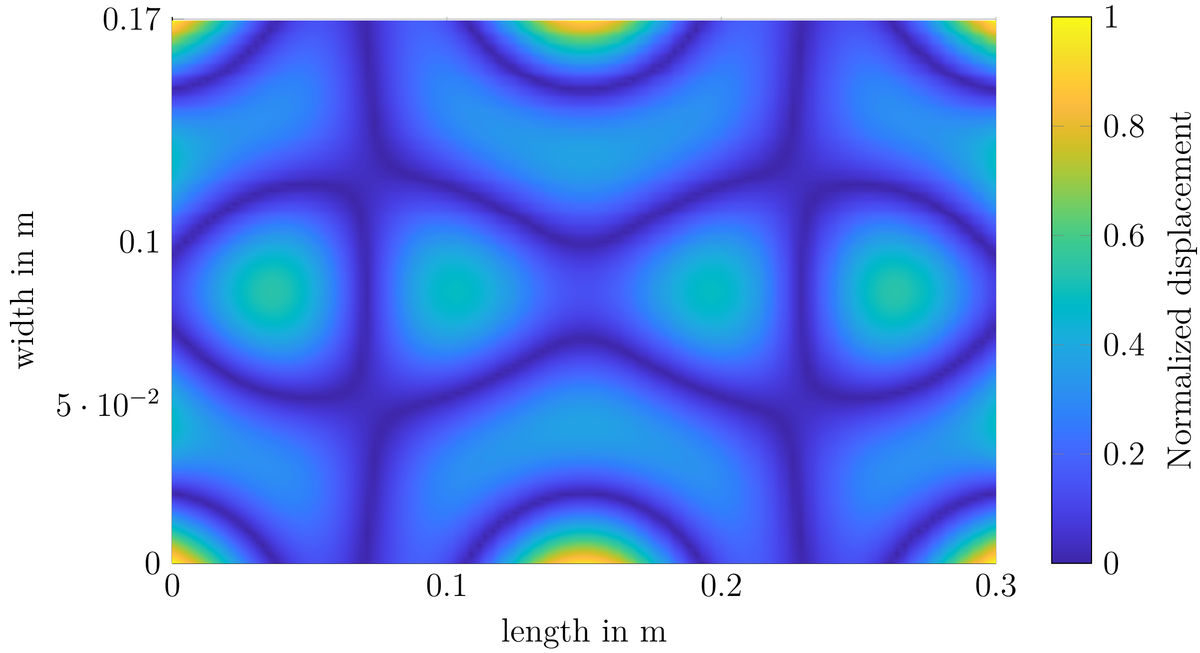

Figure 8.13: Mode shape of eigenfrequency 1786 Hz.

From the figures 8.5 through 8.13 a series of eigenfrequencies and mode shapes have been determined. They will be compared to the results from the simulation and the measurement in subsection 12.3.2.

8.5 Methods - numerical

In order to make an auralization of the sound radiated from a structure the surface movement of the structure has to be determined. As it is desired to be able to determine the surface movement of any structure, only numerical simulation methods are considered. The possible candidates for the input to the sound generation algorithm are finite elements method, boundary elements method and finite difference method. The hope is that any of these is sufficiently accurate to be used as input to the sound generation algorithm, and the choice of vibration computation method can be left to the end user. This will be a major benefit since this type of simulation software is typically very expensive and users might only have one of them available. Below a brief introduction to the three methods is given together with an overview of what aid they can provide in terms of acoustics.

In mechanical engineering finite elements method (FEM) is widely used to simulate the strains and vibrations in a structure [Raamachandran, 2000]. FEM can calculate the vibration at discrete points on and within the structure. FEM deviates from other methods by meshing the inside of the object. This means that it is capable of modelling internal strains in the object. The drawback is that the entire volume of interest has to be meshed. This means that it is not useful when analysing unbounded problems such as acoustic radiation in a free field.

Boundary elements method (BEM) is a less computationally heavy alternative to FEM. BEM only models the boundaries of the object, losing information about internal strains. It has a large advantage over FEM when solving unbounded problems since the unbounded area does not need meshing [Raamachandran, 2000]. An example might be sound radiation in an unbounded volume, where it does not have to mesh the entire volume of the unbounded area but only the boundary between the object and the surroundings. Therefore BEM is considered a 'first choice' in solving acoustical sound radiation problems [Sorokin, no date].

Finite difference method (FDM) is similar to FEM in the sense that the entire volume is meshed [Sakuma et al., 2014]. It differs from FEM in that the shapes are, at least in its simplest form, cubic. This makes the method less suited for structures of arbitrary shape as fitting the boundaries is tricky. The meshing has to be as fine as FEM making it unsuitable for high frequency problems. As with FEM the unbounded problems are not handled well. In acoustics a special case of FDM called finite difference time-domain method (FDTD) has its merits. It is easily formulated and rooms tend to be more or less regular in shape compared to mechanical parts. The major benefit is that a sampled history of pressures and particle velocities at different times is obtained. Furthermore the idea of pressure changing as volume moves from one cube to a neighbour at time steps is intuitive to the user.

In both FEM and FDM a 'perfectly matched layer' (PML) can be used to emulate an infinite surrounding by enclosing the object of interest in a medium with same input impedance as the object [Sakuma et al., 2014]. Inside the PML the damping is large, thus little energy is reflected off the outer boundary of the PML back into the acoustic medium.

8.6 Choices - numerical

In a case of light fluid loading, where the medium surrounding the object is assumed to not influence the movement of the object, any of the above methods can be used to model the displacements of the boundaries. Hereafter the radiation to the surrounding medium can be modelled separately. For this project the fluid loading is always that of air, and the radiation problem will not be solved by either of the above mentioned solutions[4]. Instead the approach will be to use any of the above to calculate the vibration of the object after which an algorithm similar to that used in the video game and virtual reality community can be used to calculate the sound radiation as mentioned in section 4.1.

In section 5.3 it was determined that FEM could find the eigenfrequencies of a plate with an acceptable accuracy. Other methods such as BEM or FDM might prove to be as good as, or possibly better than, FEM for the purpose or modelling surface movement. I have still not been able to acquire a license to a commercial program for this type of simulation and I believe it would be too time consuming to implement my own simple version, which would probably give far worse results than top of the line commercial software. Therefore it is seen as sufficient to conclude that FEM serves the needs of this project, even if other methods might be used instead. From this point onward it will be implicit that FEM is the method used when modelling vibrational patterns.

8.7 Methods - finite elements method

This chapter serves the purpose of examining different ways of computing the vibration of the plate using FEM. This knowledge combined with knowledge about the possible radiation algorithms is required in order to select a 'pair' forming a total solution from simulated excitation to airborne sound.

In the initial FEM prestudy SOLIDWORKS was used under the AAU student license. At Grundfos ANSYS is the software of choice and it provides much more functionality. I was given the chance to work at the office of the 'FEA-group'[5] at Grundfos, which supported me to quickly master the basics of FEM in ANSYS. I have completed a 10 lesson tutorial and gone over the documentation for the analysis systems before proceeding with the objects from the project, to ensure that fewer mistakes would be made due to lack of knowledge about lack of knowledge.

8.7.1 Introduction to finite elements method

Before proceeding with the discussion of FEM on the plate two simpler situations will be considered. This should allow the reader to understand how FEM works and what it can do. The two cases considered are a 2D structure affected by a static load and a mass spring system solved by FEM.

[4] This decision is made in section 9.3. It is a bit of a 'the hen and the egg' situation where the selection of vibration, radiation and propagation algorithm must be made simultaneously.

[5] Finite Elements Analysis group

2D structure - static load

A 2D rectangular structure is considered. The rectangle is fixed on the rightmost edge and a diagonal force is applied to the bottom left corner. The meshing of the rectangle is made so it consists of two elements of identical size and shape.

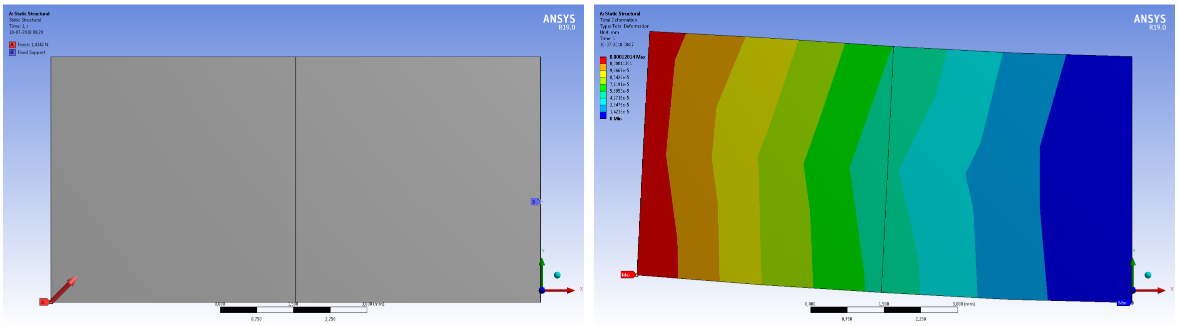

(a) Meshed structure. **(b)** Deformation result.

Figure 8.14: Simulation on 2D plate.

From the results one can read the displacement at any node position. On top of that ANSYS has implemented some interpolation scheme so a value can be read at any point on the surface. A key point is that the leftmost element is pushing and thereby deforming the rightmost element. In a larger problem the rightmost element would again push its neighbour and the deformation of all elements can be determined.

Mass spring system

The second topic of interest is how vibrations are described as resonances. To examine this a simple mass spring system is considered. The mass is made as a single element with a density of $7.85 \cdot 10^{-3}$ kg. The spring is connected to the top of the mass and fixed in space with the other end. The spring is defined with a stiffness of 5 N/m. From these values the theoretical resonance is, as given in eq. 8.1, $f_0 = \frac{1}{2\pi}\sqrt{\frac{s}{m}} = \frac{1}{2\pi Rad/s}\sqrt{\frac{5N/m}{7.85 \cdot 10^{-3} Kg}} = 4016.7$ Hz. ANSYS determines the resonance frequency to be 4016.6 Hz.

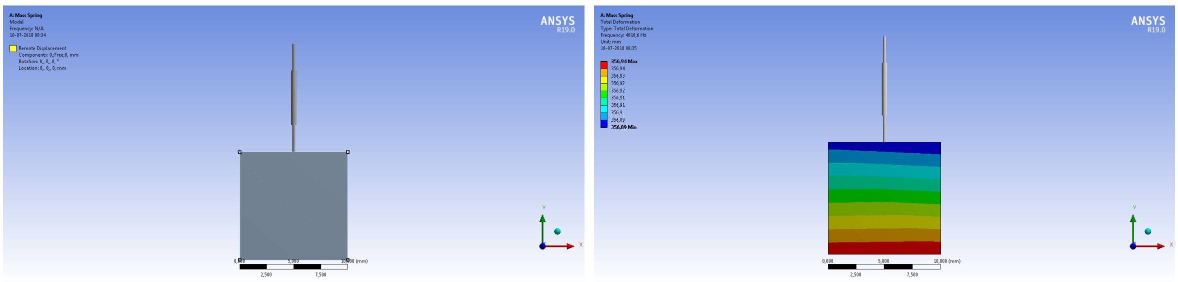

(a) Mass spring. **(b)** Deformation result.

Figure 8.15: Simulation on mass spring system.

8.7.2 Summary of analysis system

Different types of analysis are available in ANSYS and are called 'analysis systems'. They include among others modal analysis, random vibration, harmonic response and transient structural. The before mentioned analysis systems are the ones deemed possibly relevant for this project and a description of each and their possible use in this project is given in Appendix G. Here only a few key points are included as the results are not directly included in the auralization algorithm.

The mesh has to be created sufficiently fine to model frequencies of 20 kHz. Using the rule of 6 elements per wavelength [Schmiechen, 1997]. This requirement is with regards to the wavelength in the solid medium, however it should also be fulfilled for the wavelength in air to make the sound generation accurate. Therefore the element size is chosen as the smallest of the two requirements thereby fulfilling both. The element size required due to the material is calculated using eq. 8.2 and dividing by 6:

$$\frac{1}{6}\lambda_{plate} = \frac{1}{6}\frac{2\pi\sqrt[4]{\frac{B}{m'}}}{\sqrt{\omega}} = \frac{1}{6}\frac{2\pi\sqrt[4]{\frac{7.5\cdot 10^{10}N/m^2\cdot(0.0015m)^3\cdot 0.1693m/12}{2770kg/m^3\cdot 0.0015m}}}{\sqrt{20000Hz\cdot 2\cdot pi}} = 2.86mm \tag{8.5}$$

The element size required due to air is $\lambda_{air} = \frac{c}{6f_{max}} = \frac{343m/s}{6*20000Hz} = 2.85mm$. The two values are almost identical but the requirement in air is dominating with a maximum element size of 2.85mm. This new meshing results in a total of 84456 nodes for the plate. On a side note, the fact that the wavelength on the plate is longer than that on the medium means that 20 kHz is below the critical frequency - so sound radiation should only be generated at the edges as discussed later in subsection 9.1.3.

A summary of the capabilities of the different analysis systems are given below.

<table>
<tr><th>Type:</th><th>Random</th><th>Harmonic</th><th>Modal Transient</th><th>Pure Transient</th></tr>
<tr><td>Magnitude:</td><td>✓</td><td>✓</td><td>✓</td><td>✓</td></tr>
<tr><td>Phase:</td><td>X</td><td>✓</td><td>✓</td><td>✓</td></tr>
<tr><td>Computation time:</td><td><1 min</td><td>1 min</td><td>9 min</td><td>70 min</td></tr>
<tr><td>Storage requirement</td><td>Minimal</td><td colspan="3">Large</td></tr>
<tr><td>Impact/continious:</td><td colspan="2">Continious</td><td colspan="2">Impact</td></tr>
<tr><td>Nonlinearities:</td><td>X</td><td>X</td><td>X</td><td>✓</td></tr>
<tr><td>Upper Frequency determined by:</td><td colspan="3">Highest mode included</td><td>Mesh size</td></tr>
</table>

Table 8.2: Comparison of analysis systems.

8.8 Choices - finite elements method

The objective for the FEM analysis is to acquire the vibrational pattern and frequencies of vibration of the plate. The data should naturally be calculated in as accurate a way as possible.

8.8.1 Random analysis system

Let us first treat the random analysis system, which does not include phase information, so it would be impossible to ensure that the timing between the modes is correct. The applicability of this method therefore depends on the perceptional ability of the human auditory system with respect to phase errors. No study has been found on the difference in annoyance caused by randomizing phase in harmonic signals. A study examining the perceived difference of random phase compared to magnitude level changes can be found in [Laitinen et al., 2013]. The study is made comparing a triangular waveform to a random phase signal with the same magnitude at all frequencies and it is concluded based on listening tests that:

> *"Formal listening tests were arranged and synthetic harmonic complex signals were used as test signals. The results of the tests confirm that humans are not 'phase deaf', the perceived difference due to randomization of the phase spectrum can be larger than the difference due to randomization of the magnitude spectrum with a standard deviation of 4 dB"* [Laitinen et al., 2013].

Based on this if the perceived difference is larger than 4 dB level difference the effect of randomizing phase will be audible. Most likely this experiment resembles a worst case scenario as all frequencies are related to a fundamental by integer values. In the case of a vibrating structure this will not happen due to the dispersive nature of bending waves in solids.

8.8.2 Harmonic analysis system

The harmonic analysis system does include phase information as stated previously. If an evenly sampled response is needed with high resolution for each node then the storage requirement is rather high, but not impossibly high. Points that might further reduce this is that ANSYS can be made to increase the density of points around eigenfrequencies and decrease the density everywhere else. This would require a sound generation algorithm that does not require an evenly sampled spectrum or work in the time domain. This could be based on modal superposition and then the storage requirements would be similar to that of the random system. This would limit the algorithm to work on resonant structures only. Another approach would be to solve the problem at a very high resolution and then transform back to the time domain. The resolution would have to be high as the resonant peaks are narrow and possibly closely spaced.

8.8.3 Transient analysis systems

The transient analysis systems have phase information but can only model impacts. For the purpose of this project it is desired to be able to auralize a continuously vibrating structure. The use of these systems would therefore require that all the computations from vibrating field to propagating sound are linear. If that is the case the vibrational impulse response might be used to calculate a 'structure to binaural' transfer function that can then be used as a filter for any input vibration. This has the limitation that the non-linearities calculated in the full transient analysis would be lost.

Another disadvantage is that the vibrational impulse response does not include the time decay of the impact as only the first period of 50 Hz is currently included in the simulation. In order to include the decay the simulation would have to be run until a certain decay in level is achieved. If one assumes a loss factor, η, of 0.002 and want to achieve a decay of 20 dB the simulation would have to run for:

$$\frac{-20dB}{20log_{10}(1-0.002)} \approx 1500 \text{ periods} \tag{8.6}$$

which at 50 Hz would take 23 seconds. In Appendix G it was found that the storage requirement was 972 MB for 0.02 seconds. The resulting data from 23 seconds would be 1117 GB which is obviously not feasible.

Two possible ways of overcoming these difficulties would be to either make a multi-rate system or to predict the decay of the impulse response. A multi-rate system could use a much less refined mesh at a lower temporal resolution for low frequencies and an increasingly finer mesh and high temporal resolution for higher frequencies. At the transaction frequencies digital filtering could be used to transaction from one solution to the next. Another possibility would be to use the loss factor to create an algorithm which calculates the tail of the impulse response.

8.8.4 Choice

The random analysis system is immediately disregarded since the lack of phase information is likely to be critical to the listening experience. Secondly the transient system can be discarded since the storage requirement will be impossibly large when data is to be moved from ANSYS to Matlab. The storage issue might be overcome by predicting the tail of the impulse response or by using a multi-rate system, but these solutions will increase the complexity of the algorithm significantly. This leaves the harmonic system, which includes the information needed assuming that the structure is rather undamped so that modal decomposition is valid. This will be the case for a structure such as the used aluminium plate. The storage requirement scales with 2 times the amount of frequencies included in the analysis - so the number of included frequencies should be kept as low as possible. This is be done by only considering the resonance frequencies and then creating time domain oscillators with the found frequency, amplitude and phase information.

8.9 Numerical solution

8.9.1 Design goal numerical solution

The purpose of the simulation on the plate is to determine a numerical solution to the vibration of the plate. That means determining a set of eigenfrequencies and mode shapes that are excited in the middle of the plate.

The plate dimensions and material given in table 5.1 are used.

8.9.2 The simulation setup

The simulation setup is very similar to the ones used in Appendix G. The two analysis systems used are the modal and the harmonic.

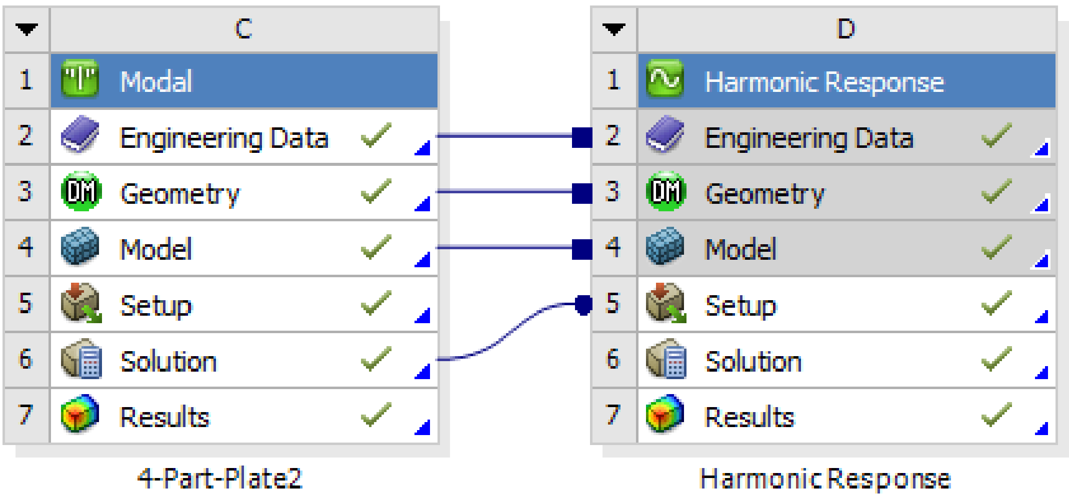

Figure 8.16: The simulation environment used. The blue lines from the modal analysis system to the harmonic analysis system indicates that information is shared between the two. For instance the solution from the modal analysis is used in the setup of the harmonic analysis.

The geometry is identical to the plate used in Appendix G, where the plate is split in four rigidly connected parts. This split ensures that a node is positioned exactly at the centre of the plate. The meshing is done according to the requirement in section 8.7 where the element size is set as 2.85 mm and the mesh method used is quadratic tetrahedrons. The choice of quadratic tetrahedrons is based on flexibility hoping to allow many different structure to be modelled accurately using the same mesh-type. In the case of a thin plate a sensible finite elements analysis would utilize the thin dimension to solve a 2D problem using plate elements. If one insists on doing 3D simulation a hexahedron mesh would be preferred as the plate edges are bending at 90°. However at a later stage the method should be applied to more irregular objects where the flexibility of quadratic tetrahedrons will be required.

The parameters that have been changed since the study of analysis systems in Appendix G is that it is no longer an acceleration that is applied to the plate. Instead a point force is used as this carries a better physical meaning since you push stuff with a force to achieve an acceleration. This has the further advantage that no fixed support in the middle position has to be defined, so the plate is truly free in the simulation as it will be in the measurement setup.

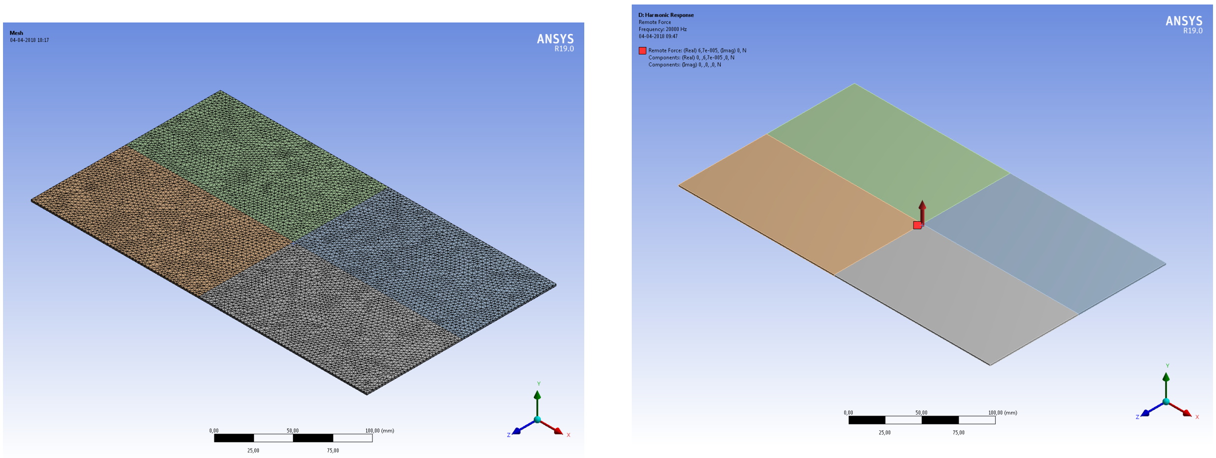

(a) The mesh used in the simulation.

(b) The plate split in four parts with a force exciting the centre position.

Figure 8.17: The plate used in the simulation.

8.9.3 Determining eigenfrequencies and mode shapes

The modal analysis is set to only determine eigenfrequencies in the range 20 Hz to 20 kHz. Resulting in 249 eigenfrequencies. Of these the first 16 are shown below.

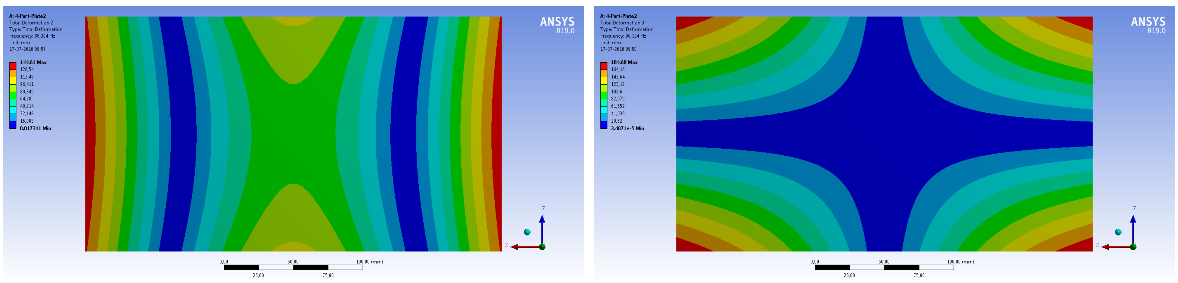

(a) Mode 1 at 88 Hz.

(b) Mode 2 at 96 Hz.

Figure 8.18: Mode shape 1 & 2. Mode 1 shape and frequency correspond well with the analytical solution.

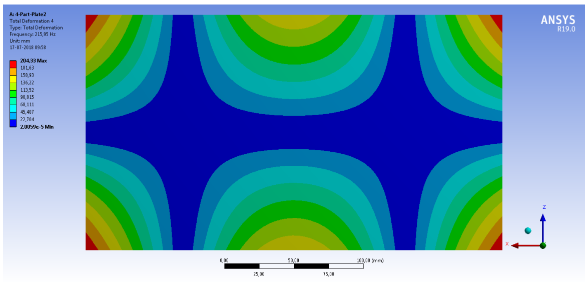

(a) Mode 3 at 216 Hz.

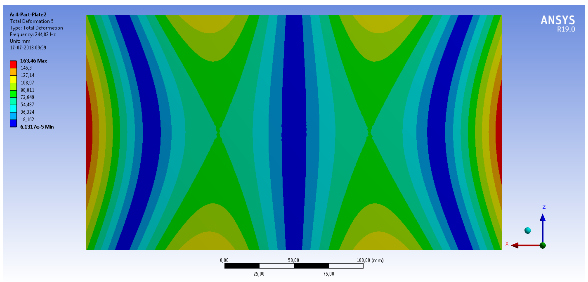

(b) Mode 4 at 245 Hz.

Figure 8.19: Mode shape 3 & 4.

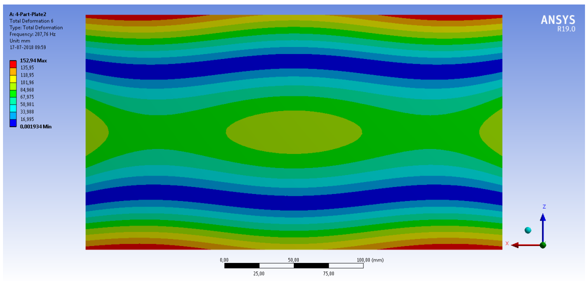

(a) Mode 5 at 288 Hz.

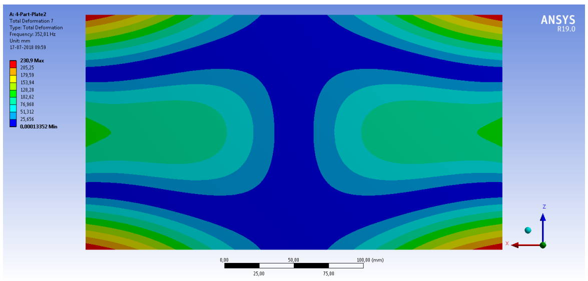

(b) Mode 6 at 352 Hz.

Figure 8.20: Mode shape 5 & 6. Mode 5 shape and frequency correspond well with the analytical solution.

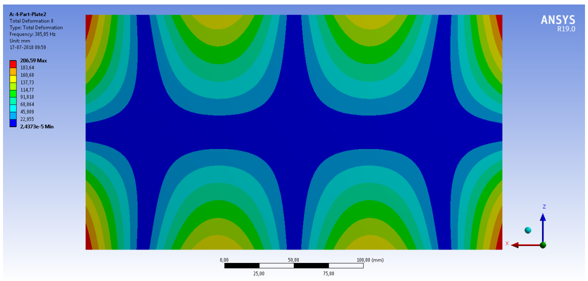

(a) Mode 7 at 386 Hz.

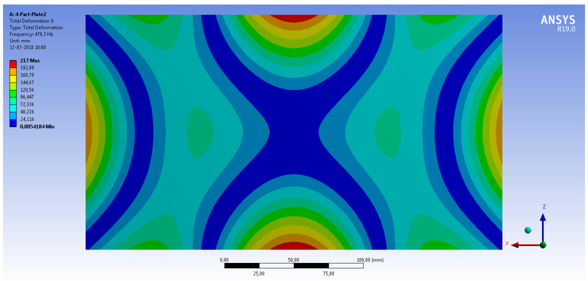

(b) Mode 8 at 478 Hz.

Figure 8.21: Mode shape 7 & 8. Mode 8 shape and frequency correspond well with the analytical solution.

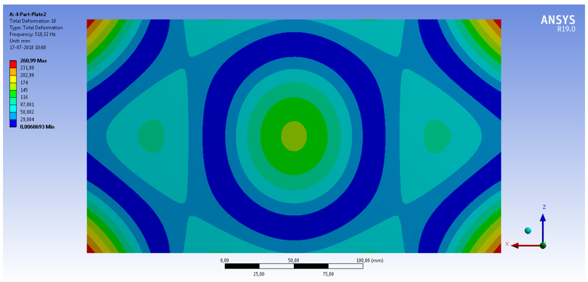

(a) Mode 9 at 518 Hz.

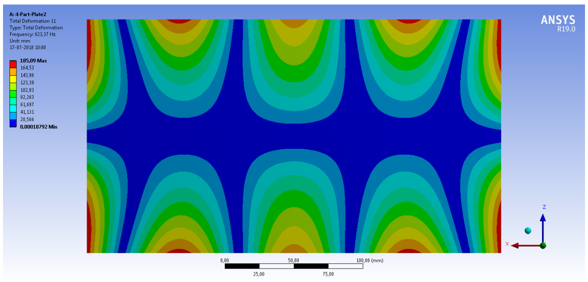

(b) Mode 10 at 623 Hz.

Figure 8.22: Mode shape 9 & 10. Mode 9 shape and frequency correspond well with the analytical solution.

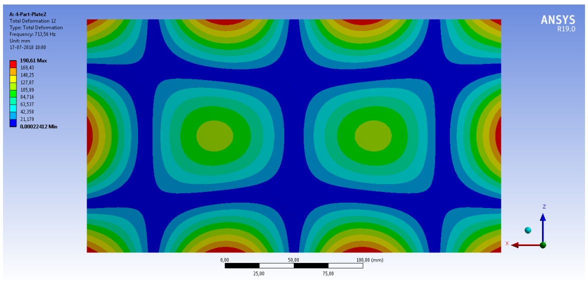

(a) Mode 11 at 714 Hz.

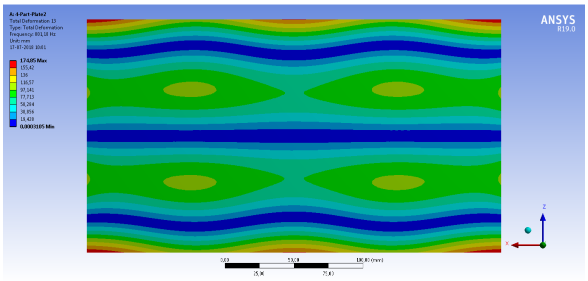

(b) Mode 12 at 801 Hz.

Figure 8.23: Mode shape 11 & 12.

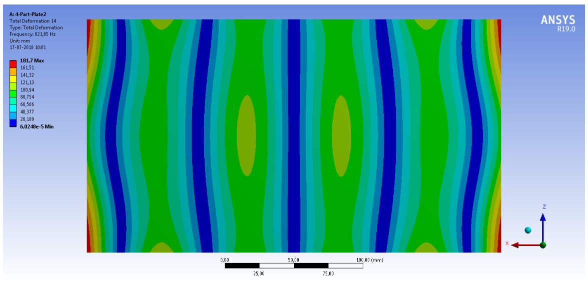

(a) Mode 13 at 822 Hz.

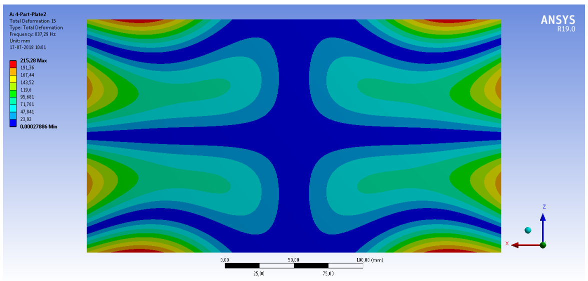

(b) Mode 14 at 837 Hz.

Figure 8.24: Mode shape 13 & 14.

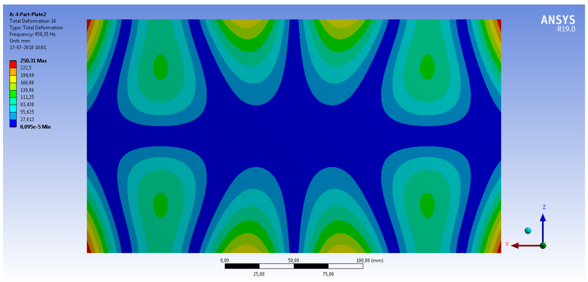

(a) Mode 15 at 958 Hz.

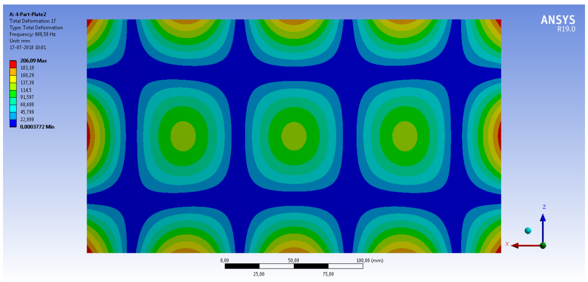

(b) Mode 16 at 989 Hz.

Figure 8.25: Mode shape 15 & 16. Mode 16 shape and frequency correspond well with the analytical solution.

In order to show a few more of the simulated mode shapes without showing all intermediate non-symmetrical mode shapes some modes are skipped between the symmetrical mode shapes shown below.

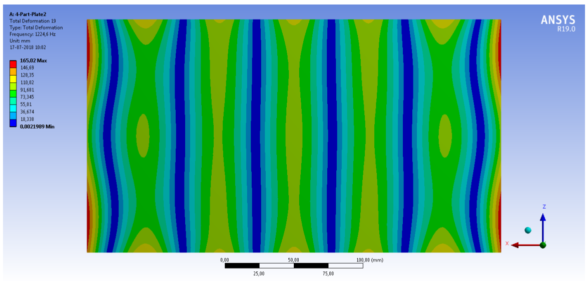

(a) Mode 18 at 1225 Hz.

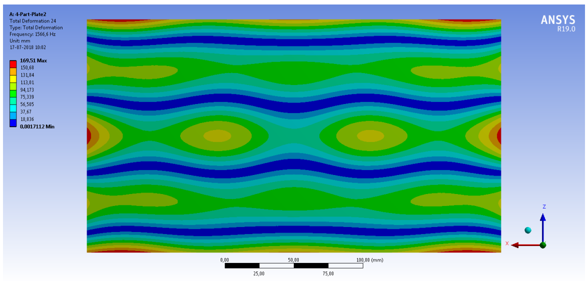

(b) Mode 23 at 1567 Hz.

Figure 8.26: Mode shape 18 & 23. Mode 18 & 23 shape and frequency correspond well with the analytical solution.

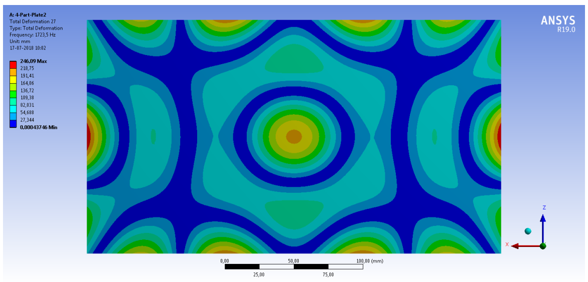

(a) Mode 26 at 1724 Hz.

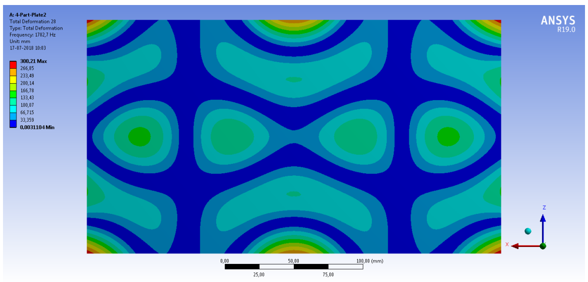

(b) Mode 27 at 1783 Hz.

Figure 8.27: Mode shape 26 & 27. Mode 26 & 27 have shape and frequency correspond well with the analytical solution.

The numerical solution corresponds very well with the analytical solution in subsection 8.4.4. The largest percentage diversion in resonance frequency is at mode 26 with an error of about 0.2% referenced to the analytical solution.

Additional mode shape when centre position is fixed

It was discovered while working with the version of the plate with a fixed support in the centre position in subsection 12.3.2 that an unexpected eigenfrequency appeared. This unexpected eigenfrequency was later also observed in the plate measurements, so it is included here. The eigenfrequency is at 56 Hz and has a mode shape as shown in figure 8.28.

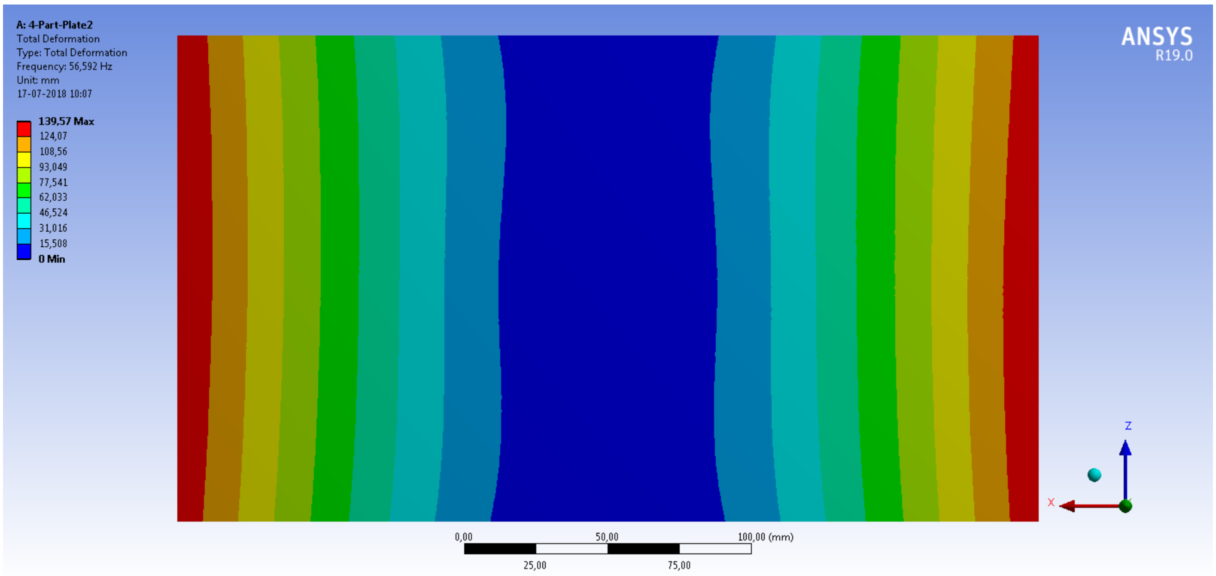

Figure 8.28: The mode shape at 56 Hz with a fixed support at the centre position.

In the simulation with an additional boundary condition the mode shape shown in figure 8.18a is not found. It will later be shown in subsection 12.3.2, that both mode shapes exists on the real plate.

8.9.4 Determining amplitudes of modes

The harmonic response is calculated for the eigenfrequencies determined by the modal analysis. This is done by specifying 'user defined frequencies' as the frequencies found in the modal analysis. This ensures that all modes are included without redundant frequencies which would add to computational demands. The harmonic response analysis is carried out with a damping ratio $\zeta = \eta/2 = 5 \cdot 10^{-5}$ corresponding to aluminium [Irvine, 2004]. The input force was defined as 1 Newton in positive y-direction.

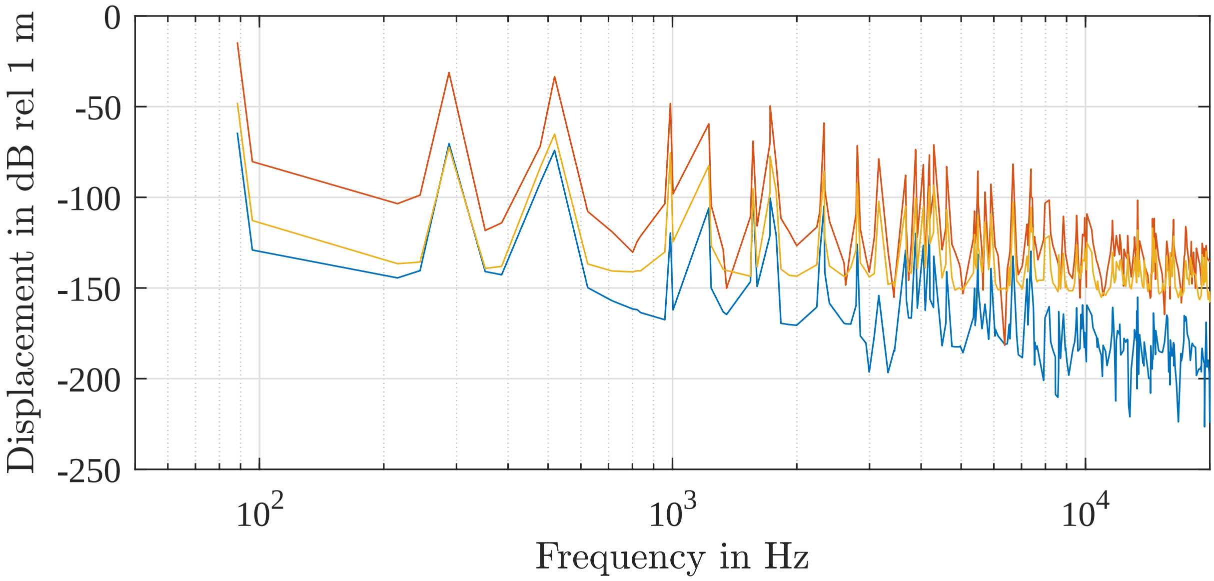

Figure 8.29: The simulated frequency response of the plate. An average of the top surface calculated by ANSYS (—), the maximum displacement at each frequency over all nodes (—) and the displacement of the centre top node (—).

From figure 8.29 it is clear that only some eigenfrequencies are excited and others not. By further inspection it is noted that the first few eigenfrequencies that are exited are at 88, 288, 478, 518, 989, 1225, 1567, 1724 and 1783 Hz. Looking back in subsection 8.9.3 these corresponds to mode 1, 5, 8, 9, 16, 18, 23, 26 and 27 which are all the mode shapes where there is movement in the centre. In three dimensional plots it is also visible that these are the ones that have doubly symmetric mode shapes. From this it is concluded that FEM can determine which modes have a contribution when the structure is excited in a specific position. The tendency of smaller displacement at higher frequencies seen in figure 8.29 is also believable, as the input impedance of an infinite plate is independent of frequency[6]. The input impedance is defined as $Z_{in} = Force/velocity = Force/(j\omega \cdot Displacement)$. So as the force is kept at unity in the simulation displacement should decrease with frequency.

It is still left to be verified if the mode shapes found through the numerical approach are related to the analytical solution and even more importantly the actual response of the plate. This will be done under one in subsection 12.3.2.

8.9.5 Extracting data from ANSYS

To implement an sound generation in Matlab the first task at hand is to extract data from ANSYS. The required data is the vibrational level and phase of each node at each frequency in the simulation. The data is extracted such that for each node a result similar to that found in figure 8.29 is determined. This is the reason for trying to have as few frequency points included

[6]This will be discussed in subsection 12.2.3

in the analysis as possible since the amount of nodes cannot be changed due to the mesh sizing requirement.

The data could be extracted for each node manually using the graphical user interface in ANSYS, but seeing as the structure has more than 70000 nodes this is not manageable. Instead the APDL coding environment is used to print the data to a file. The APDL environment is the old interface to the FEM solver from before the guided user interface was launched, and the language is specific to ANSYS. No course on APDL is given here but a few comments might help the reader to better understand the code:

- APDL is not case sensitive.
- different ANSYS processors have different instruction sets, here only /post1 is used.
- Exclamation marks (!) denote the beginning of a comment.
- Stars (*) indicate a function name. (however not all functions have a star - for instance 'set' and '*set' are two completely different function calls.)
- 'set' controls the currently selected dataset.
- '*set' defines a variable.
- functions such as *vwrite and *vget controls a vector of data points.
- *mwrite writes a matrix of data to a file.

```
/post1
set,last !no * as this is a different function.
allsel
set,list

*get,AnalysisPoints,active,,set,sbst ! Get the number of AnalysisPoints
*get,mxnd,node,,num,max ! Get the max node number
*get,lastFreq,active,,set,freq ! Get the Frequency of the last mode

!predefine and zerofill array
*set,temp1
*dim,temp1,array,mxnd,AnalysisPoints

*set,temp2
*dim,temp2,array,mxnd,AnalysisPoints

!Get frequency vector
*set,freqz
*dim,freqz,array,AnalysisPoints,1
*do,j,1,AnalysisPoints  !loop on frequencies
set,1,j,1,3 ! get amplitude
*get,currentFreq,active,,set,freq ! Get the frequency
freqz(j,1)= currentFreq
*enddo

/output,C:\910546Ansys\modal_harmonic\VExtractorFreq2,txt,,!append
*mwrite,freqz(1,1),,,,ijk,
(F10.2)
/output


*do,j,1,AnalysisPoints  !loop on frequencies
set,1,j,1,3 ! get amplitude
*vget,temp1(1,j),NODE,i,U,Y, ! gets the nodes at this single frequency

set,1,j,1,4 ! change to get phase
*vget,temp2(1,j),NODE,i,U,Y
*enddo
!!!!!!!!!!!!!!!!!set here number of nodes here in case more than 100000
/output,C:\910546Ansys\modal_harmonic\VExtractorDisp,txt,,!append
*mwrite,temp1(1,1),,,,ijk,
(100000E13.6)
/output

/output,C:\910546Ansys\modal_harmonic\VExtractorPhas,txt,,!append
*mwrite,temp2(1,1),,,,ijk,
(100000F10.2)
/output
```

Listing 8.3: APDL code to extract amplitude and phase at each frequency for each node. The data is stored in seperate files that can be read into Matlab. In the final version with three harmonic analysis studies the outputs are given different paths.

Apart from the data extracted using Listing 8.3 the position of each node and their connections (forming faces) have to be known. This is easily done in the guided user interface using named selections and the export option. The named selection for the nodes is made by using the scoping method 'worksheet' and selecting all nodes with an ID larger than 0.

Node Number	X Location (mm)	Y Location (mm)	Z Location (mm)
1	150,	0,	0,
2	150,	1,5	0,
3	150,	0,	-84,628
4	150,	0,	-2,8209
⋮	⋮	⋮	⋮

Table 8.3: Example of node positions extracted.

The elements are stored by selecting all 'mesh elements' with an ID larger than 0. This yields the type of the element, in this project all quadratic tetrahedrons, as well as the ID corresponding to table 8.3 for the four nodes forming the corners of the element plus the six intermediate points, which are ignored.

Element Number	Element Type	Node 1	Node 2	Node 3	Node 4	...
1	Tet10	900	2450	2000	1038	...
2	Tet10	900	2354	2000	2450	...
3	Tet10	450	2000	1038	900	...
4	Tet10	900	1210	2450	1038	...
⋮	⋮	⋮	⋮	⋮	⋮	⋱

Table 8.4: Example of element connections extracted. The table continues to Node 10, but the 6 nodes skipped here are always the intermediate points of the quadratic elements.

From the data in table 8.4 the four faces of an element can be determined by combining the corners in all unordered unique selections of three. Now the positions and vibration patterns of the individual nodes are known as well as the connection between the nodes in the mesh.

9 | Radiation

9.1 Theory

A fundamental equation in acoustics is that $p = zV$ where p is the pressure in front of a surface of size S, z is the impedance of air ($\rho_0 c$) and V is the particle velocity, from eq. 10.9.1 in [Kinsler et al., 2000]. This can be used at a boundary between a source and air where the particle velocity has to be equal to the surface velocity. This is one of the simplest acoustical models and it does not account for all phenomena that might exist. For instance it does not include directivity and diffraction. Therefore more advanced radiation models as well as some radiation phenomena will be presented in this chapter.

9.1.1 The Rayleigh integral

The Rayleigh integral is a way to split a baffled plate in a series of point sources. The formulation is based on mounting a series of point sources in an infinite and rigid baffle. The point sources are monopoles by definition and their physical shape is irrelevant. Due to the baffle the volume velocity is half that of a free source. The integral is formulated as follows [Cremer et al., 2005]:

$$p = \frac{j\omega\rho_0}{2\pi} \int \frac{v(s)}{r} e^{-jk_0 r} dS \tag{9.1}$$

Which means that each point source has an infinitely small surface and some velocity. The integral can be sampled in space. The sampling points are given a source strength depending on the area they cover and velocity $q_i = v_i \cdot S_i$. Then the sampled version looks like:

$$p = \frac{j\omega\rho_0}{2\pi} \sum_i \frac{q_i}{r_i} e^{-jk_0 r_i} \tag{9.2}$$

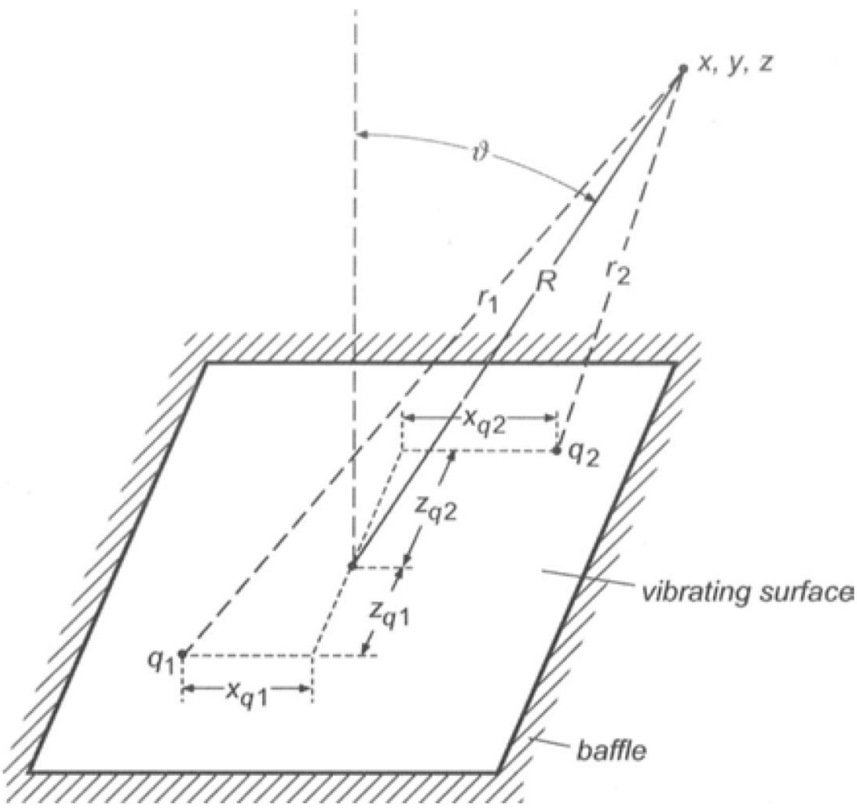

Figure 9.1: Schematic illustration of the contribution from a set of point sources. [Cremer et al., 2005]

9.1.2 Dipole sources

It is assumed that the reader is already familiar with the terms monopole source and dipole source. In this project the structure mainly resembles dipole sources as is is not infinite and oscillate back and forth rather than breathe. The issue is that most methods such as the Rayleigh integral is based on monopole sources and therefore the approach does not capture dipole characteristics. To account for the dipole radiation of the structures a transfer function from a monopole breathing sphere to a dipole oscillating sphere is used. It is calculated as the difference between the pressure at a position generated by a monopole and a dipole directly in front of the spheres as described by [Cremer et al., 2005]:

$$P_{monopole} = \frac{j\omega\rho a^2}{r(1+jka)}\hat{v}e^{-jk(r-a)} \tag{9.3}$$

$$P_{dipole} = \frac{j\omega\rho\hat{v}a^3}{2+2jka-k^2a^2}\cdot(\frac{1}{r^2}+\frac{jk}{r})\cdot cos(\theta)\cdot e^{-jk(r-a)} \tag{9.4}$$

where a is the source radii and r is the distance to the receiver. To determine the difference between the two $P_{Dipole}/P_{monopole}$ is calculated below. The values a=0.084, $\theta = 0$ and r=2.8 have been used for this example.

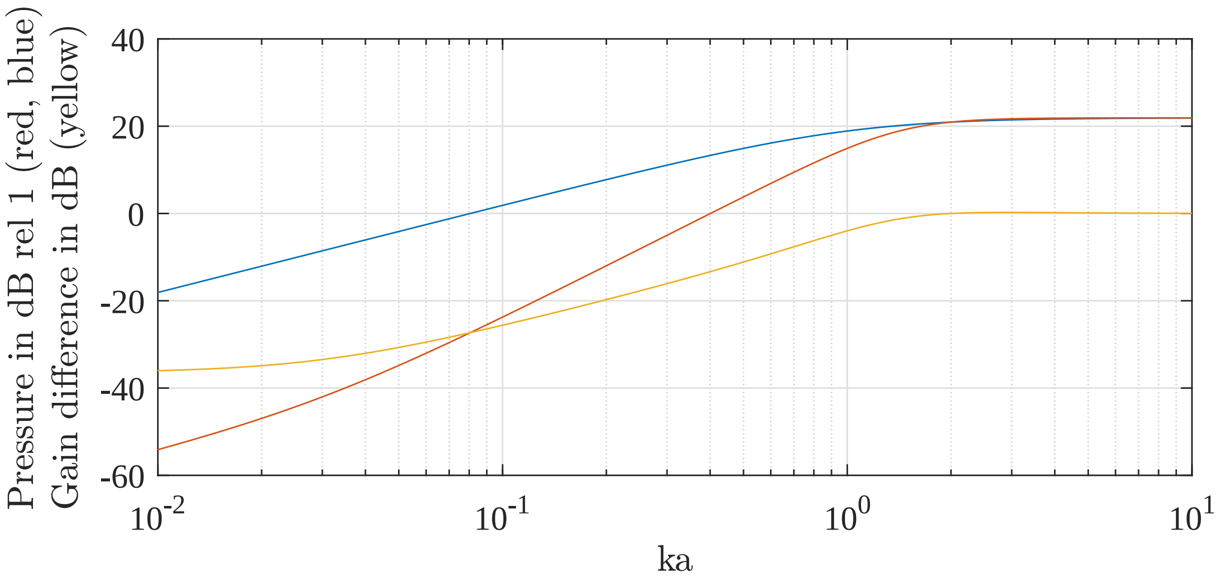

Figure 9.2: Pressure from a monopole (—) and a dipole (—) with same source strength. The difference between the two (—).

In reality the structures under study are neither pulsating nor oscillating spheres, but plates or in the future more complex structures. Still the filter can be applied to correct for the dipole characteristic of the plate since this is better than doing no correction, even if it is a simplification. If the plate is seen as a pure monopole the low frequency response will be unbelievably high.

9.1.3 Critical frequency

On top of the correction for a dipole source attention has to be paid to the critical frequency of the structure. The critical frequency is described in [Cremer et al., 2005] and its definition is made on an infinite plate in (x,y) direction with bending waves propagating in one direction, say x. The dispersive nature of bending waves makes the speed of sound a function of frequency as shown in eq. 8.2. From this follows that the wavelength is not a linear function of frequency. This means that at some frequencies the wave-speed on the plate is larger than the wave-speed in air at the same frequency, which is constant c_0. At other frequencies the wave-speed is lower than c_0. The frequency where c_b=c_0 is called the critical frequency and the radiation from a structure depends strongly on this.

Below the critical frequency the wavelength of a bending wave is shorter than the wavelength in air. This means that no power transfer between the two waves can exist[1]. One might ask; what happens with the air in front of the plate when it is not pushed away from the plate as a propagating wave. The answer is that a short circuit between rises and dips on the structure causes air to move back and forth between the two as they oscillate. This can happen over the entire plate surface which in this discussion goes to infinity.

[1]near-fields can exist but they do not transmit power.

At the critical frequency the wavelength of the structure wave and air wave are identical. This will cause a, theoretically infinite, plane wave propagating along the plate.

At frequencies above the critical frequency the wavelength in air is shorter than that on the bending wave. Then a projection of the air wave onto the plate can be created at a single angle. This angle is then the radiation angle for this specific frequency.

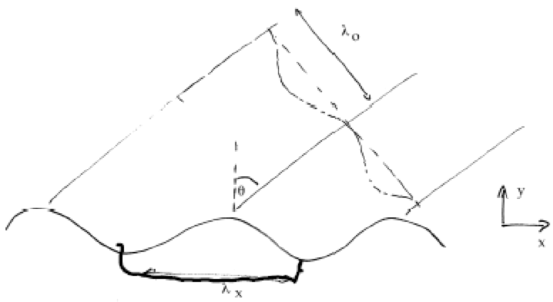

Figure 9.3: Radiation at an angle above the critical frequency. [Kropp, 2015]

The angle of radiation, ϕ can be determined geometrically from figure 9.3 as $sin(\phi) = \frac{k_b}{k_0}$

Finite structures

When the structure considered is no longer infinite but finite the matter gets more complicated as described in [Kropp, 2015]. If the plate is baffled at the ends a phenomena similar to that of a applying a rectangular window on a sampled sine wave arises, namely lobes in frequency domain. Here the window is made in the space domain with resulting lobes in the wave number domain. This topic continues far into the wave number domain and is beyond the scope of this project. Instead the result from the boundary is considered in a more intuitive way.

As discussed previously for an infinite structure no radiation occurs below the critical frequency due to short circuits. The short circuits happen between rises and dips oscillating in opposite phase. In a 1D case one could say that half the air pushed by a part going outwards is sucked by the right hand neighbour going backwards. The other half by the left hand neighbour. Applying this line of thinking to a 2D plate one could imagine this phenomena happening in both directions over the entire surface at the plate. Then what happens at the edges where no neighbour is present on one side - this boundary will cause sound radiation.

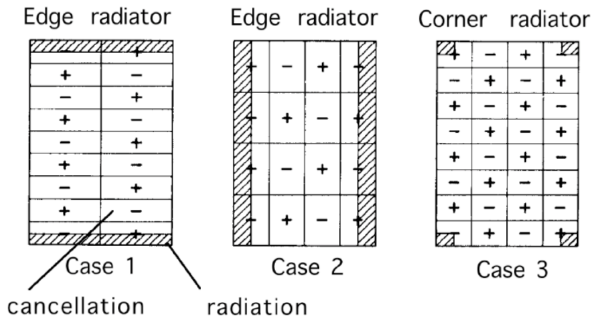

Figure 9.4: 2D cases of short circuits for different mode shapes with radiation areas indicated. [Kropp, 2015]

The point of figure 9.4 is that in case 1 and 2 the wavelength of the bending is short compared to air in one direction and radiation occurs at the edges. In case 3 the wavelength of the bending wave is shorter than the wavelength in air in both directions and radiation occurs at the corner only. This phenomena can be expected to be directly observable on the plate if somehow the sound contribution from the edges of the plate can be separated from the contribution from the rest of the plate.

9.2 Methods

In the methods introduced in the literature in section 4.1 two overall directions for solving the radiation problem are considered.

9.2.1 Numerical method

One way of calculating the radiation is by using a numerical methods such as BEM[2] as proposed in [Duvigneau et al., 2015], Paik et al. [2013] and [James et al., 2006] to calculate the radiated sound. These method can be expected to be accurate as it includes all phenomena discussed in chapter 9. These methods are based on putting the vibrating structure into a simulated environment and includes the propagation of sound to the listener position.

9.2.2 Approximate method

A simpler solution is to use that the pressure in front of a face with an area S can be described by $p = zV$. This does, as discussed in section 9.1, not account for complex radiation phenomena. The benefit of this method is that it decouples the radiation problem from the propagation problem. This approach is the same as that used in [O'Brien et al., 2001a] introduced in subsubsection 4.1.2.

[2]ANSYS provides the same functionality using FEM in the acoustics toolbox.

9.3 Choices

Ideally the radiation problem would be solved by an analytical solution such as the Rayleigh integral in subsection 9.1.1. The issue with using an analytical solution is that it is specific to a single case. For the Rayleigh integral that case is a baffled plate. This leaves us with approximate and numerical methods.

9.3.1 Numerical methods

Numerical methods such as FEM or BEM are likely to be the most accurate and general methods as they include directivity characteristics such as the dipole radiation pattern expected for a vibrating free plate. They do have a major disadvantage in that they tightly couple the vibration problem via the radiation problem to the propagation problem. This means that if a new room is to be considered as listening environment the entire algorithm would have to be rerun. In the case of FEM it is unlikely that a large room can be meshed according to the meshing requirements for the entire audible range. Furthermore these numerical methods do not separate where the pressure contributions are coming from, so it would be impossible to use different head related transfer functions (HRTF) in the binaural representation for direct sound and reflected sound.

9.3.2 Approximate methods

Approximate methods such as the one used by [O'Brien et al., 2001a] $p = zV$, will allow the radiation and the following propagation to be modelled separately from the vibration analysis. The method is general enough to be used to auralize sound for a vibrating structure of any shape and it utilizes the fact that the structure has already been discretized in the FEM study. Some of the missing characteristics such as the dipole radiation efficiency in figure 9.2 can be added in post-processing as a digital filter. The critical frequency is more difficult to incorporate and if left out, it might cause large errors in the final result.

9.3.3 Choice

The approximate method using that the pressure in front of a surface of size S is $p = zV$ used. The monopole to dipole transfer function in figure 9.2 is used to correct for the frequency dependent radiation efficiency. The radiation from the dipole also depends on the radiation angle θ as shown in eq. 9.4. The $cos(\theta)$ term is a scaling which is 1 if the receiver is normal to the surface and 0 if the receiver is in the surface plane. This is similar to what is done in [O'Brien et al., 2001a] based on the directivity of a plate described in [Kinsler et al., 2000]. In [O'Brien et al., 2001a] the surfaces considered might be larger than a wavelength making this approximation inaccurate. In this project the faces are always at least six times smaller than the wavelength so the approximation is better suited here.

9.4 Implementation

9.4.1 Importing data from ANSYS

The first task of the radiation algorithm is to import the data from ANSYS. This is done using the Matlab command 'textread' to read the node positions, connections, frequencies of vibration as well as phase and amplitude for each node.

9.4.2 Calculating pressure in front of plate

The radiation is calculated for each face individually. Each face is attributed a number of single oscillators, one for each eigenfrequency found in the numerical vibration analysis in subsection 8.9.3. The oscillators are then created with the amplitude and phase determined in subsection 8.9.4. Lastly the radiated pressure in front of the face is calculated as $p = zV = \rho c \cdot \xi \cdot j\omega$. This pressure is then scaled with the radiation angle by $cos(\theta)$ as well as the area of the face, S.

9.4.3 Dipole radiation efficiency

The dipole correction is made as the simplification discussed in subsection 9.1.2 by designing a 1025 tap symmetric FIR filter to fit the yellow curve in figure 9.2 using Matlab's built in function FIRLS. The resulting filters magnitude response is identical for all frequencies of interest. The value used as source size is 0.0846 m corresponding to half the width of the plate. The equation for the pressure from a dipole, eq. 9.4, contains a dependency on the radiation angle. This dependency is already included in subsection 9.4.2 so only the frequency dependency is accounted for here.

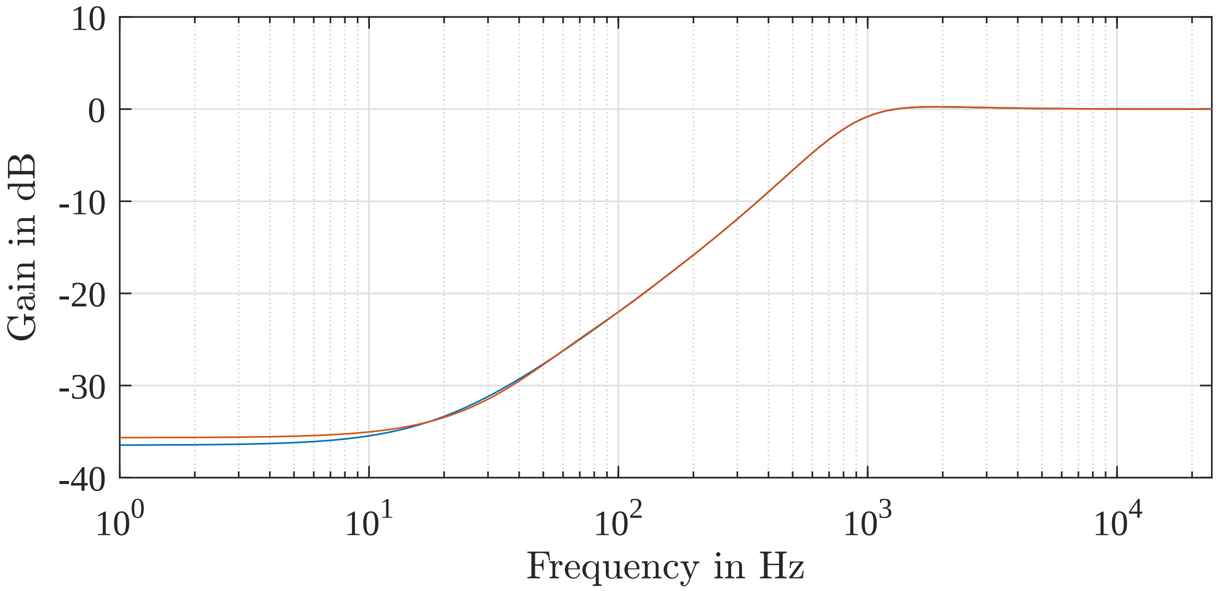

Figure 9.5: The magnitude response found infigure 9.2 (—) and its approximation (—).

9.4.4 Results

The pressure directly in front of a single face calculates using the method above and assuming a radiation angle of 0° is shown below.

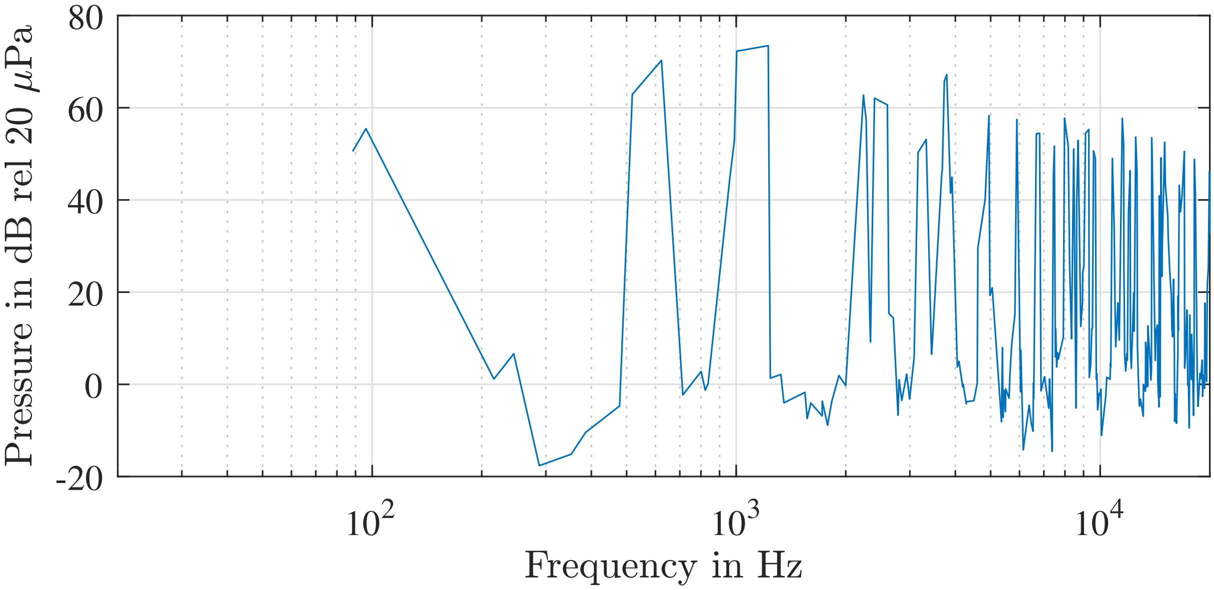

Figure 9.6: Pressure directly in front of a single face. The radiation angle 0° is used.

10 | Propagation

10.1 Theory

This chapter will give a brief introduction to propagating sound waves in air. First let us consider the sound pressure at a position generated by a breathing sphere as described in [Kinsler et al., 2000]:

$$P(r,t) = (A/r)e^{j(\omega t - kr)} \tag{10.1}$$

From this it is clear that the distance to the receiver r causes both a delay in time and a decay in amplitude.

10.1.1 Propagation delay

Propagation of sound waves happens at finite speed, the speed of sound $c = 343m/s^2$. This means that a sound generated at a position, Loc1, will be received at another position, Loc2, after a time delay. The delay will depend on the distance between the two points as.

$$\Delta t = \frac{|Loc1 - Loc2|}{c} \tag{10.2}$$

This is described in eq. 10.1 by e^{-jkr}.

10.1.2 Propagation decay

Two sources of decay can be considered when sound is propagating. The viscous friction and the distribution of energy over a larger and larger surface. The latter happens as pressure propagates in three dimensions. It turns out that the viscous friction is negligible in terms of decay [Kinsler et al., 2000] and it is often ignored, as it also is in eq. 10.1. The decay is then described as $1/r$ in eq. 10.1, meaning that at double the distance half the sound pressure is present.

10.1.3 Reflections in rooms

When a sound source is put an environment, which is not free field, reflections will occur. This means that a source will be received by a listener multiple times. The first sound to arrive at the listener is called the direct sound. Early reflections are the ones arriving shortly after low order reflections from floor, ceiling or walls. Later the sound will be diffuse as the reflections come from all directions.

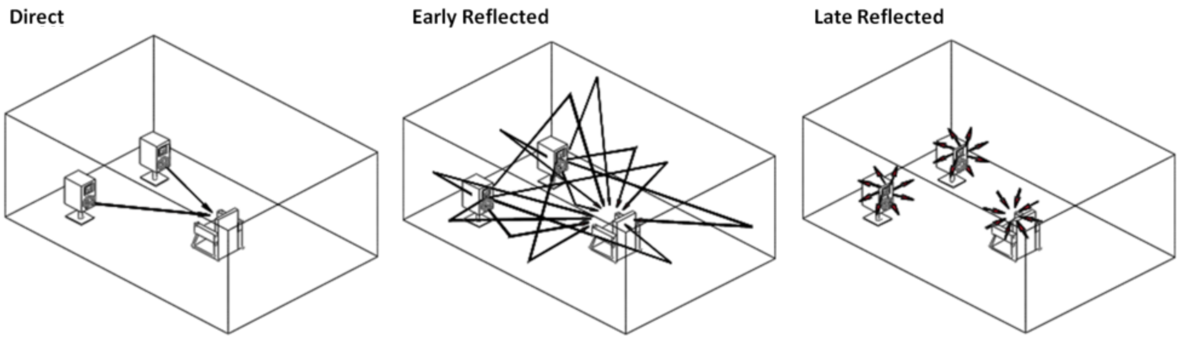

Figure 10.1: Overview of direct sound, early reflections and the diffuse sound field. [frontiers, 2015]

This phenomena plays an important role in how sound is perceived. Imagine the sound of a clap in a cathedral compared to a clap on a corn field.

10.2 Methods

10.2.1 Propagation delay and decay

The theoretical way of describing propagation allows any propagation delay and thereby any distance between sender and receiver. The issue is that digital signal processing of sound is performed on sampled sound.

In a sampled domain a propagation buffer can be used to store generated sound pressures moving them one sample closer to the receiver each time a sample is presented to the receiver and a new one is generated. This approach is taken by [O'Brien et al., 2001a]. The issue is that in a sampled domain only time steps of $T = 1/fs$ are valid. One approach would be to change the propagation delay to the nearest valid time step. This introduces artifacts in the sound as discussed by [O'Brien et al., 2001a] where they propose distributing the pressure over multiple samples. In subsubsection 4.1.2 a better approach is proposed stating that the signal could be up-sampled and an interpolated value chosen.

10.2.2 Sources to include

If it been had chosen to use BEM or another numerical method for calculating the radiation and propagation under one the question of 'which parts of the structure influences the sound' would be solved by those methods. Having chosen to separate the propagation from the radiation this is not the case so an approximation must be made.

In [O'Brien et al., 2001a] the faces to include are chosen based on 'line of sight', meaning faces that the listener can see are included in generation of the audio. This is the reason that the method does not capture dipole characteristics of an object, where the pressure on the backside short circuits with the pressure on the front.

10.2.3 Room simulation

Again if it had been chosen to use a numerical method the room simulation could be included in this method. The listening environment would then be included in the model and meshed before computing the resulting sound pressure at a chosen position. As mentioned in subsection 9.3.1 this might be not so practical since the information about where sound is coming from is lost. It is possible that finite difference time domain (FDTD) introduced in section 8.5 could overcome this issue since it is a time domain method where the direction of waves is known by their particle velocity in three dimensions.

Having chosen to not use a numerical method for the radiation problem an alternative solution must be found for the inclusion of a room in the propagation problem.

Mirror source

The mirror source method is based on that the reflection from a flat wall can be seen as an identical source mirrored around the wall. The contribution from the mirrored source is scaled with a frequency dependant reflection coefficient of that wall [Kuttruff, 1991]. For a perfectly reflective surface this value would be 1 at all frequencies. This method is rather simple to implement for the first reflection, the issue arrives when higher order reflections are to be considered as image sources of image sources and so forth. The problem size grows exponentially with the amount of reflections.

Ray tracing

The Ray tracing method was first introduced by [Krokstad et al., 1968] and it follows sound particles propagating in all directions from a certain position at a certain time. At boundaries the particle is reflected and attenuated according to the characteristics of the wall. Whenever a particle crosses the receiving position the time and energy of the particle is stored [Kuttruff, 1991]. Based on this a room impulse response from a sender position to a receiver position can be calculated. In [Kuttruff, 1991] it is proposed to used the ray tracing method for the early reflections only and let the late reflections be modelled by a statistical method. The paper examines if this ray tracing method is accurate enough to be used for auralization and it concludes that it is.

10.3 Choices

10.3.1 Propagation delay and decay

In this project the vibration of the plate is modelled by a set of simple oscillators. The most intuitive way to generate audio is to compute the pressure in front of the plate and then propagate it to the listener. In this project it is chosen to generate the sound pressure directly at the listening position. This allows the exact propagation delay and attenuation to be used as described in subsection 10.1.1.

10.3.2 Sources to include

As it has already been decided to not use a numerical method such as BEM for the radiation problem the 'line of sight' approach is the only remaining option. One of the downsides of this method, that it does not include the dipole characteristics of the plate. This is already compensated for in by using the dipole transfer function as described in subsection 9.4.3.

10.3.3 Room simulation

In this project the room is limited to a hemi-anechoic room where only one reflective surface exists. The ray tracing method is then over complicated as most particles will newer hit the reflective surface and then the receiver. In fact only two particles would be included - the one propagating directly to the listener and the one reflecting off the floor to the receiver. This situation is modelled perfectly well by the mirror source method which is chosen for its simplicity. The floor is seen as a perfectly reflective surface as per the definition of a hemi-anechoic room.

Ideally the floor reflection would be included for each face individually. It should include some method to include a high frequency standing wave field between the plate and the floor. It should account for the fact that low frequencies radiated downwards will bounce back and 'ignore' the plate on the path to the receiver. Possibly even the reflected sound should be included in the finite elements analysis since it will excite the plate. On top of this the floor in the measurement environment is not perfectly reflective and has some slots in the it for mounting equipment.

As including all the physical phenomena above will be very cumbersome in terms of computation and workload a simplification is used instead. A single mirror source located at the negative coordinates (below the floor) is used.

10.4 Implementation

10.4.1 Selection of faces of vibration

The first task of the sound propagator is to establish which faces contribute to the radiated sound. The 'line of sight' method has been chosen for this. The selection is done using the fact that any considered position will be above the plate, so all the nodes of the faces in line of sight will have y-coordinates at 1.5 mm in the plate's coordinate system.

```
% loop over all elements. Each element can have maximum 1 face at the top
    of the plate.
for i=1:length(Elements)
    % check if node 1, 2 and 3 are all on Y=1.5mm
    if nodepositionY(Element(i,[1,2,3]))==1.5
        faces=[faces Element(i,[1,3,3])] % Append face to list
    % check if node 1, 3 and 4 are all on Y=1.5mm
    elseif nodepositionY(Element(i,[1,3,4]))==1.5
        faces=[faces Element(i,[1,3,4])] % Append face to list
    % check if node 1, 2 and 4 are all on Y=1.5mm
    elseif nodepositionY(Element(i,[1,2,4]))==1.5
        faces=[faces Element(i,[1,2,4])]  % Append face to list
    % check if node 2, 3 and 4 are all on Y=1.5mm
    elseif nodepositionY(Element(i,[2,3,4]))==1.5
        faces=[faces Element(i,[2,3,4])]  % Append face to list
    end
end
```

Listing 10.1: Pseudo code of the selection of faces relevant to sound generation.

From Listing 10.1 it is known which faces contribute to the sound pressure at the listening position. The plate can now be moved to any position in space by adding an offset to the node locations.

10.4.2 The floor reflection

The mirror source is chosen to have opposite sign compared to the original source since when a top element is pushing particles upwards the underside is pulling particles so top and bottom have opposite phase. A schematic of the mirror source is given in figure 10.2.

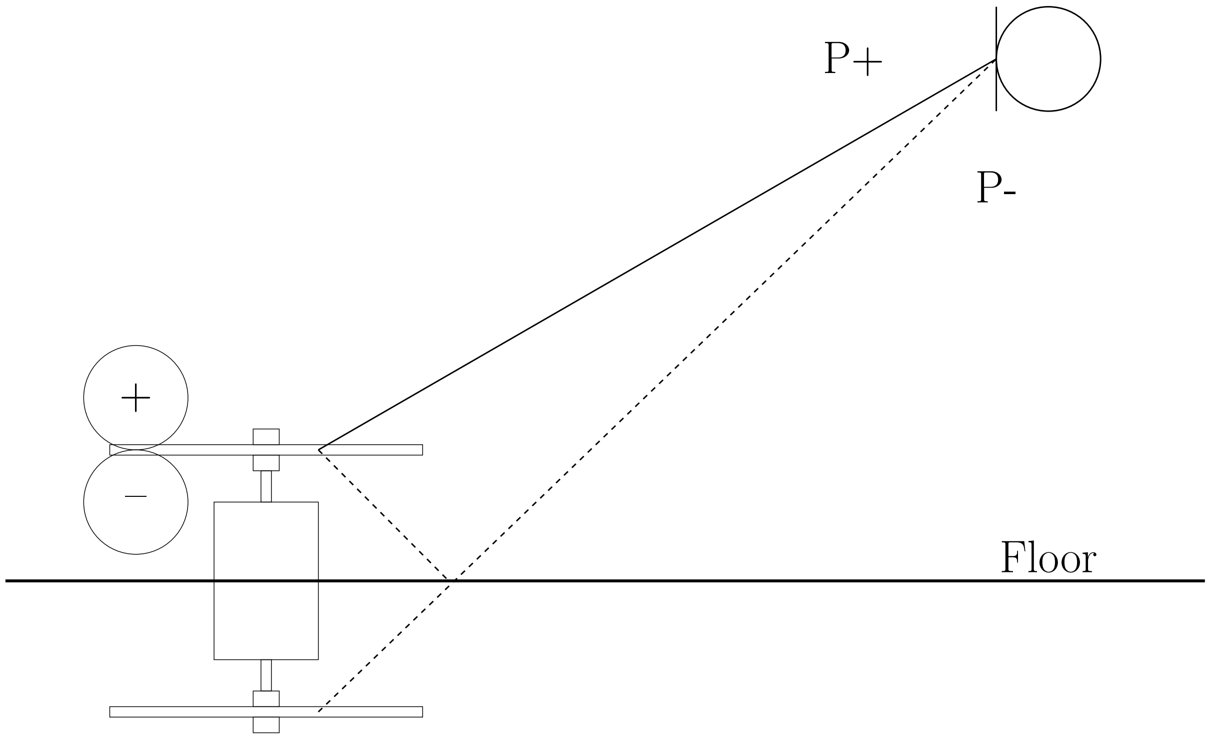

Figure 10.2: Schematic of the mirror source accounting for the floor reflection. P+ is the direct sound pressure and P- is a delayed, phase inverted and attenuated version of P+. The figure shows the plate mounted on a shaker as it will later be used in the measurements in chapter 12 as well as the dipole radiation pattern of a free plate.

The simplification is implemented as a sum of the generated sound and a delayed, phase inverted and attenuated version of itself.

First the additional propagation distance is calculated as:

$$\Delta Dist = \|receiverPos - MirrorSourcePos\|^2 - \|receiverPos - SourcePos\|^2 \tag{10.3}$$

this will result in a delay of $\Delta Dist/fs$ samples which is rounded to an integer number - for this setup with M20 as 'receiverPos', the centre of the plate as 'SourcePos' and 'MirrorSourcePos' equal 'SourcePos' with inverted y-coordinate this is 26 samples[1].

The gain caused by the additional propagation distance is calculated as:

$$Gain = 1 + \left(\frac{1}{\|receiverPos - MirrorSourcePos\|^2} - \frac{1}{\|receiverPos - SourcePos\|^2} \right) \tag{10.4}$$

For this setup with M20 as 'receiverPos' this will be 0.98. This will yield the comb filter which can be described as a FIR-filter with 26 taps. The first tap is 1 and the last -0.98; the rest are zero. The comb filter's magnitude response is shown in figure 10.3

[1]These positions are the ones used in the measurement in chapter 12.

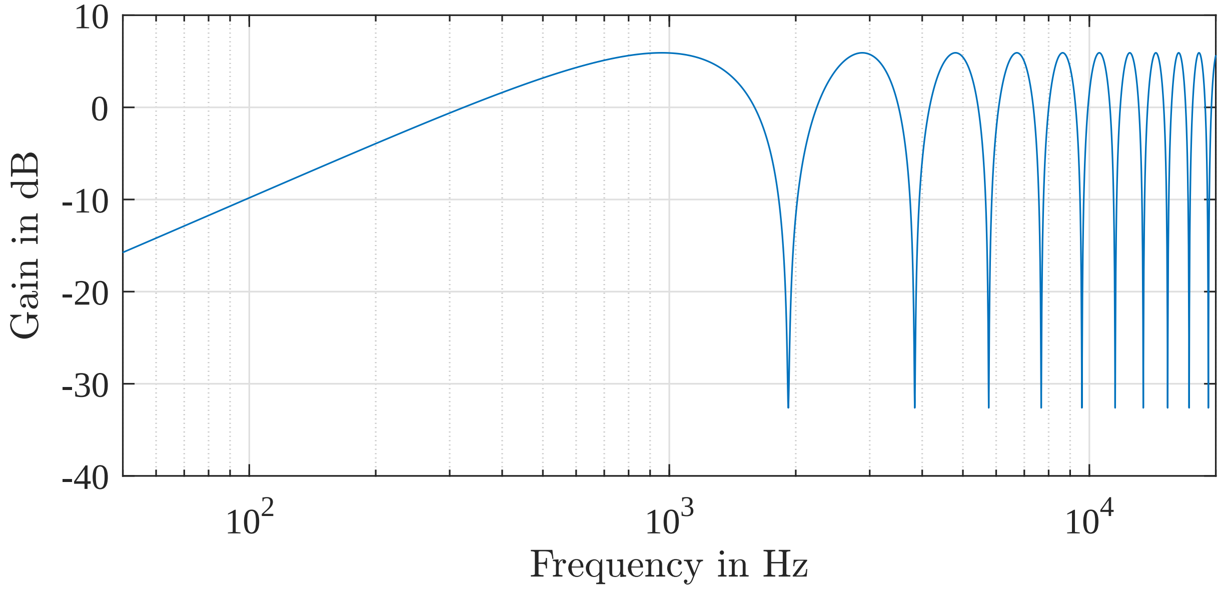

Figure 10.3: The magnitude response of the comb filter from the floor reflection.

10.4.3 Results

Here the result at a listening position accounting for sound propagation and floor reflection is shown.

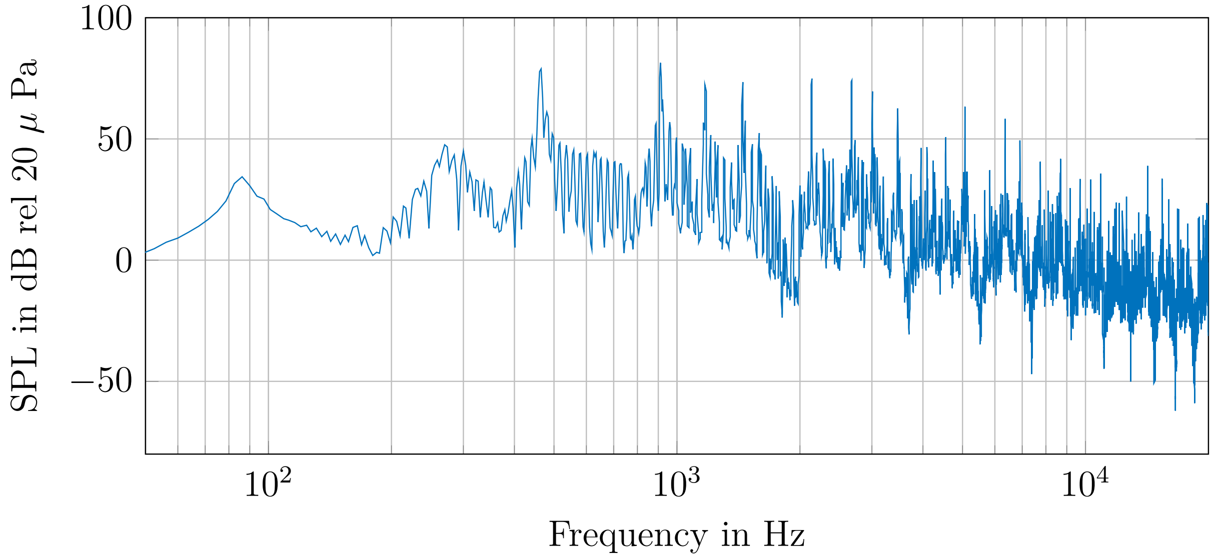

Figure 10.4: The sound pressure level at a listening position after propagation.

11 | Listening

11.1 Theory

This section will give brief description of what is required to give a binaural presentation of audio.

11.1.1 Head related transfer functions

The definition of auralization in chapter 2 states that a 'binaural listening experience' should be presented. This means that the perceptual characteristics of the sound should be as if the listener had been in the simulated environment. To achieve this goal the sound pressure at a given position should be converted to the sound pressure at two eardrums inside an ear canal accounting for reflections from the listener. It should also include the temporal difference meaning the time delay between the sound pressure arriving at one ear compared to the other.

In practice the binaural representation can be recorded using a person with small microphones in the ear canal. Alternatively a dummy head a so called head and torso simulator (HATS) can be used. This will yield what is called a binaural recording.

It is also possible to make a digital filter converting a single sound pressure in a position to a binaural representation. This type of transfer function is called a head related transfer function (HRTF) and is described in detail in [Møller, 1992]. Here only a brief overview is given. The HRTF is created by recording a reference signal, e.g. a sine sweep or MLS sequence played by a loudspeaker, in a reference position. Then a person or a HATS is placed with the centre of their head in the reference position and the sound pressure in the ear canal is recorded using the same reference source. The two responses can then be used to form two transfer functions, one for each ear.

A HRTF is dependent on angle of incidence both vertically and horizontally (elevation and azimuth). Sound coming from the right hand side of a listener will arrive at the right ear first and later a lowpass filtered version will arrive at the left ear. This is used by the auditory system to determine where the sound came from. The vertical localization is dominated by reflections from the outer ear and shoulders into the ear canal. The importance of the HRTF to the perception of sound is not treated further here and the reader is referred to [Møller, 1992] for further information.

The HRTF is an independent feature for each person. One persons HRTF cannot be used for another person and averaging over people carries no meaning [Hammershøi and Møller, 2005].

11.1.2 Reproduction system

When using a HRTF to present a binaural recording it is important that the listener is exposed to the exact sound pressure which would be at their eardrum if the source had been external in an environment. This requires a headphone which has a flat frequency response at the eardrum. This essential feature is not readily available in off the shelf headphones, since headphone designers have a different target curve [Olive et al., 2018]. On top of this the frequency response of a headphone will depend on the person wearing the headphone as well as the positioning of the headphone.

In order to give an accurate binaural representation the headphone characteristics should be removed by means of an inverse filter. This means that like the HRTF the headphone transfer function should be measured on the person whom the binaural representation is intended for. Preferably it should even be measured each time the headphones are remounted. Then the inverse filter should be computed and applied to the HRTF filtered audio which then becomes a binaural representation.

11.2 Methods

11.2.1 Binaural representation

In this project the audio signal is generated through simulation. This means that the binaural representation must be added digitally. Two methods for arriving at a binaural representation can be considered.

In situation HRTF

The HRTF could be measured in situation meaning in the room which is to be used in the auralization. This would require that a loudspeaker playing a reference signal is put in the position of an intended source. The reference position is then chosen as the listening position. This approach has the benefit that the room characteristics are included in the HRTF so the reflection from the floor calculated in subsection 10.4.2 is redundant. This does also mean that the acquired HRTF is specific to one single sender and receiver position in one specific room.

Anechoic HRTF

The HRTF can also be measured in an anechoic environment. From this the HRTF can be acquired independently of the environment. The HRTF will still show a dependency on angle and distance. For this reason multiple measurements are typically performed yielding a database of HRTFs for different azimuth and elevation. If multiple distances are wanted then this can naturally also be varied in the measurement. The anechoic method will require that the room response is added separately for instance as done in subsection 10.4.2.

11.3 Choices

11.3.1 HRTF

A setup in an anechoic environment measuring a complete HRTF database is quite complicated and time consuming to make. For this reason it was first intended to do an in situation measurement of the HRTF which would then limit the possible listening positions to a few predefined positions. An experiment doing this is presented in an Appendix A in section A.3. This measurement had multiple issues in signal quality which makes it so that it should be reperformed if the results were to be used.

By chance another student at my master's programme was working on his master's thesis including measurements of HRTFs on live subjects [Hauen, 2018]. Sigurd Van Hauen offered me that I could use his setup to acquire a HRTF database in an anechoic environment. This solution is much more general than the in situation measurement and could be used for many listening positions in many environments. For this reason it was chosen to not reperform the original experiment and instead use a database acquired in anechoic conditions.

11.3.2 Listener

Both the headphone frequency response and the HRTF should be measured on the individual to whom the binaural listening experience will be presented. For this reason a listener must be chosen at this point. For convenience the HATS owned by Grundfos is used. It is a Brüel & Kjær 4100D which is made to approximate 'the average human listener'. This naturally makes it so that the representation is not accurate for any human listener, but this allows the methodology for creating a binaural reproduction system to be presented. It is chosen to acquire a HRTF database for this HATS and do a headphone compensation on that same HATS.

11.4 Implementation

11.4.1 Measuring HRTF

The complete works for measuring the HRTF of the HATS is presented in Appendix B. All credit for the setup and performing the experiment (which is automated) should be credited to Sigurd Van Hauen [Hauen, 2018]. The post processing required in going from the impulse response of the loudspeakers at the reference position and at the HATS microphone positions to filters that can be used in the binaural representation is made by me.

The setup

The reader is referred to Appendix B for a description as well as a diagram and pictures of the setup. For an even more thorough description of the setup the reader is referred to [Hauen, 2018].

Here only a very brief description of the essential knowledge is given. The setup is made to acquire the HRTFs of the HATS at a distance of 1.7 meters. The resolution in azimuth is 1° and in elevation it is 8° from −40° to 40°. 11 loudspeakers at different positions on an arch are used to get the elevation responses. The HATS is mounted on a turntable which automatically turns the HATS around the reference position to vary the azimuth.

Post processing

Again the reader is referred to Appendix B for a more detailed explanation of what has been done. Here only the concepts of what is done are presented.

Removing reflections

In the data given by the work of Sigurd Van Hauen reflections from the setup are included in the impulse responses. This causes a ripple in the frequency response due to the comb filter created by the reflection. To remove this a time gating technique is used. The impulse responses are cut using a Hamming filter with an order of 512 samples. This removes reflections from reflectors far away from the reference position.

Spectral division

The data supplied by the measurement system by Sigurd Van Hauen is impulse responses of the loudspeakers in the reference position as well as at the microphones of the HATS. From this the HRTF can be calculated as

$$HRTF = IFFT(\frac{FFT(ImpulseResponseEar)}{FFT(ImpulseResponseReference)}) \tag{11.1}$$

This process is what is also known as a cyclic deconvolution [Müller and Massarani, 2001], which has the effect that sound arriving at a HATS microphone before it arrives at the reference position ends up in the end of the acquired impulse response instead of in 'negative time'. This is solved by shifting the response 28 samples to the right. This might cause part of the reverberant tail to be included in the beginning of the response, but this is better than having the onset of the impulse response after the rest of the response.

Removing pre-ringing

As the three microphones used are connected to different channels in the analogue to digital converter the anti-aliasing filters are not completely identical. When performing the spectral division this causes what is known as pre-ringing. That is a tone at fs/2 starting before the impulse response. This is removed by means of a low pass filter at 23 kHz.

Removing DC component

As the HATS is small compared to the wavelength of sound at low frequencies the HRTF should not contain a gain at low frequencies. A DC offset is present in the measurements and it is removed by setting the value of the first bin in frequency domain equal unity as proposed by [Hammershøi and Møller, 2005].

Result

Here the frequency response curves found in Appendix B are shown.

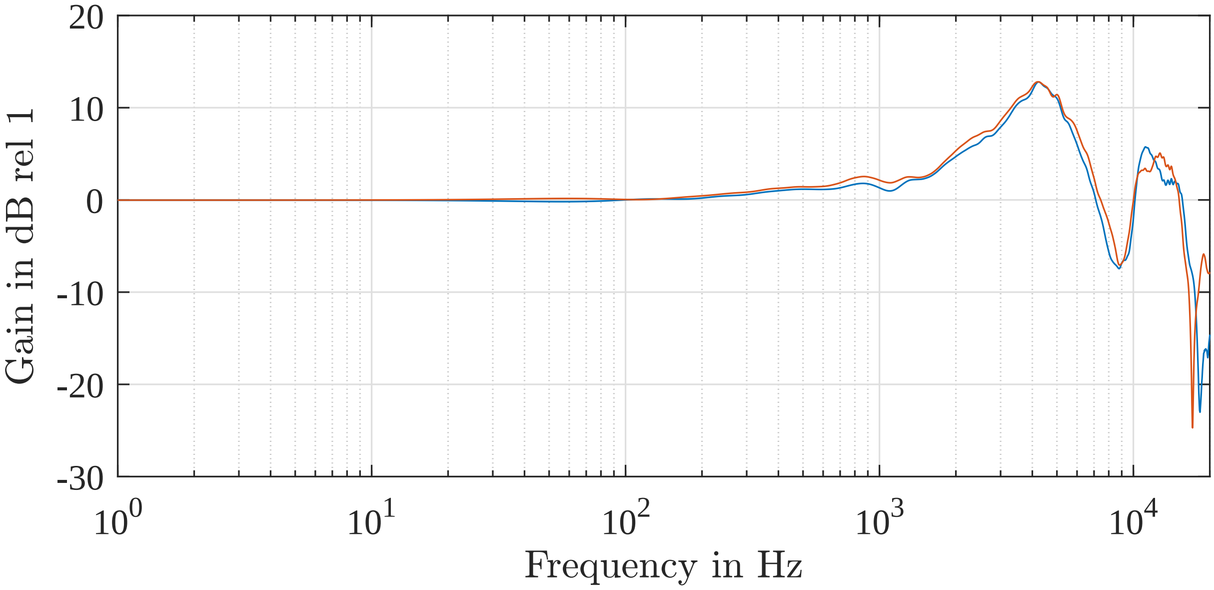

Figure 11.1: The The HRTF of the HATS facing forwards left ear (—) and right ear (—).

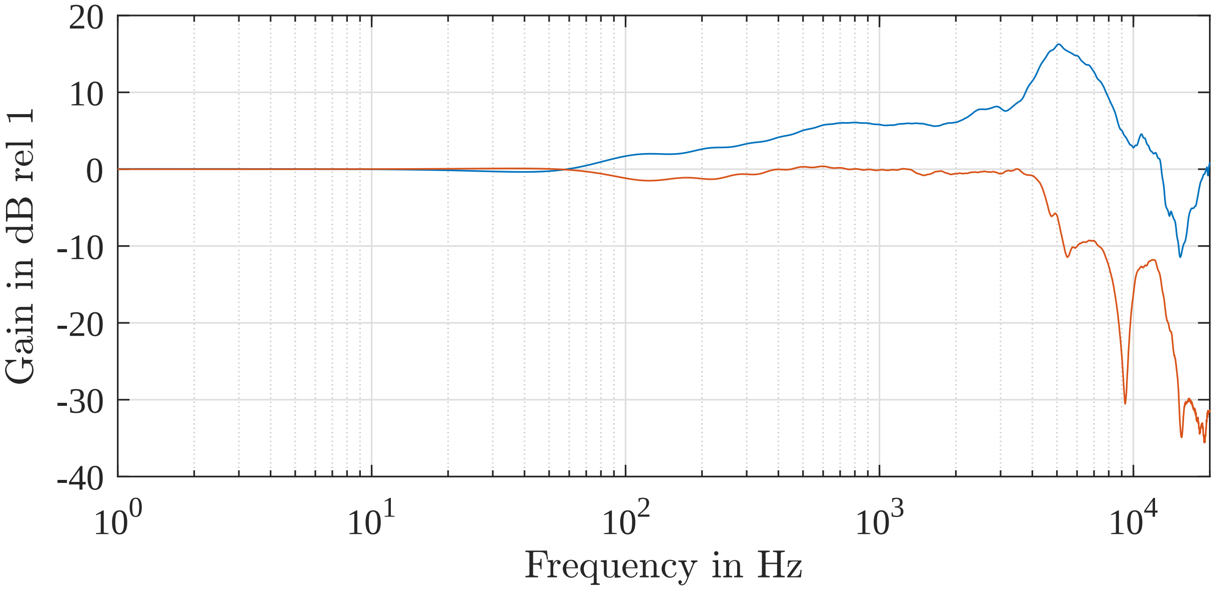

Figure 11.2: The The HRTF of the HATS turned 90° clockwise, left ear (—) and right ear (—).

The frequency responses shown above have a corresponding 512 samples long impulse response.

This impulse response can be used directly as a FIR-filter to convert the sound pressure at a reference position to that at the ear microphones of the HATS.

11.4.2 Measuring frequency response of a headphone

The complete procedure for measuring the transfer function of a headphone is given in Appendix C.

Setup

The experiments uses a Steinberg sound card, the HATS used in the HRTF measurements as well as a pair of headphones. The stimuli used is a logarithmic sine sweep generated in frequency domain as proposed by [Müller and Massarani, 2001].

The setup is not calibrated to measure specific sound pressures, only the shape of the magnitude response is of interest.

Processing

Since a sweep is used as reference signal it is possible to separate the linear response of the headphone from the harmonic distortion as proposed by [Müller and Massarani, 2001] and shown in figure 11.3

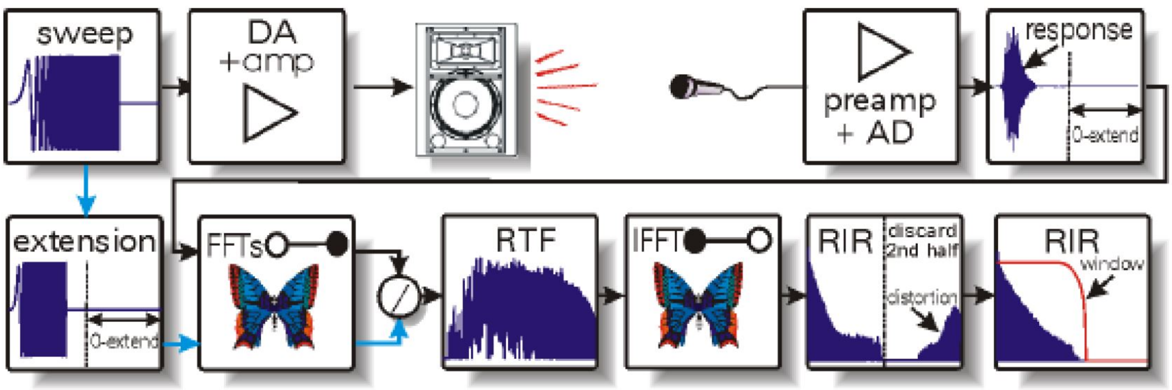

Figure 11.3: Non-cyclic deconvolution as given in [Müller and Massarani, 2001].

Result

The magnitude response of a pair of headphones is given below.

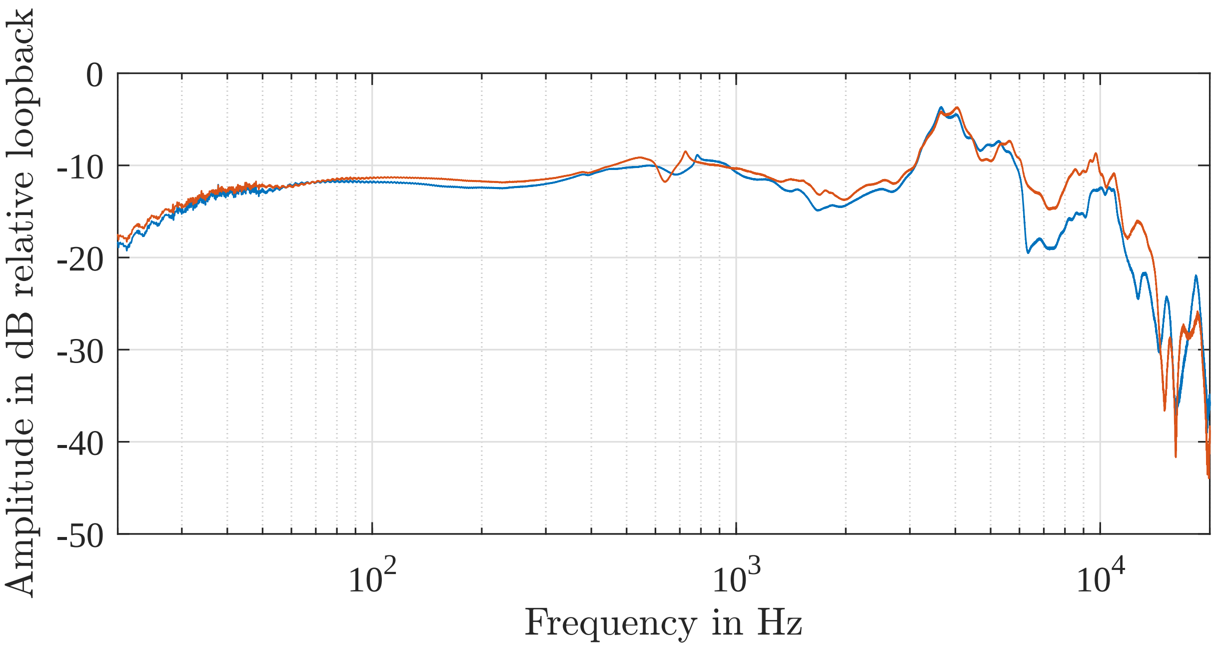

Figure 11.4: Magnitude response of left channel (—) and right channel (—) of a pair of Beyerdynamic T90 headphones.

11.4.3 Assembling a binaural listening system

A block diagram showing the connection of the components used in a binaural synthesis is shown in figure 11.5.

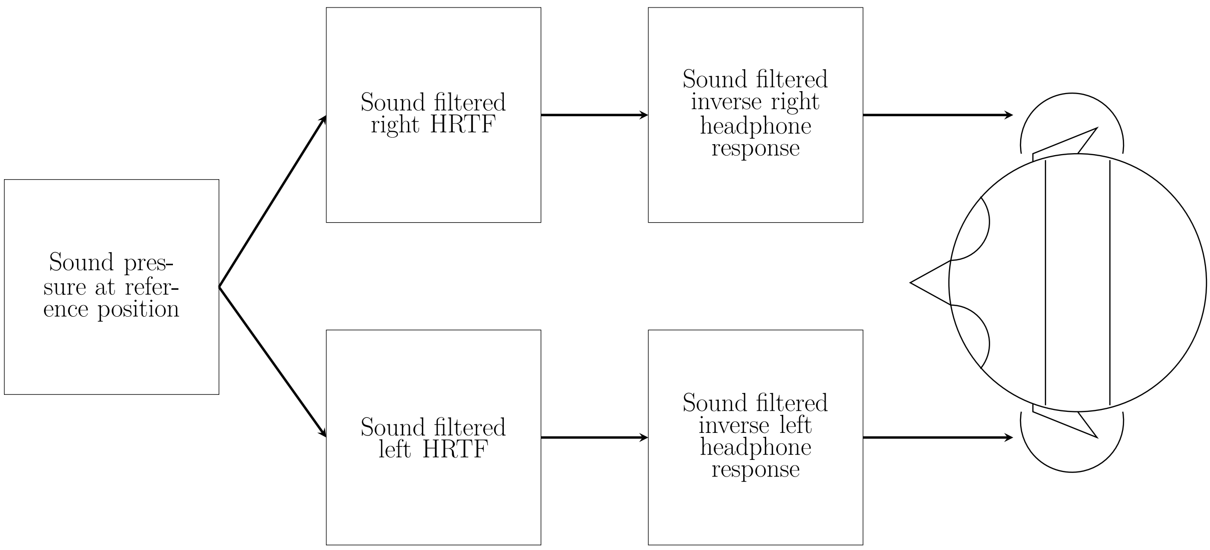

Figure 11.5: Block diagram of binaural listening system.

Applying the HRTF

The HRTFs found in subsection 11.4.1 can be used direcly as a FIR filter by means of a convolution of the mono signal with the filter for each ear. From this two time representations are found, one for each ear.

An issue might arise if the angle of incidence is not included in the HRTF database. The interpolation methods such as the one proposed in [Sandvad, 1996] could be considered. Alternatively the nearest known HRTF could be used. In this project the HATS is chosen to face the plate so the HRTF at 0° azimuth and elevation can be used.

Correcting for the headphone

The frequency response of the headphone in figure 11.4 could be used to form a minimum phase filter with the opposite magnitude response. This filter could be chosen less sharp than the measured response to avoid fitting it to steep dips, which are likely to be change with to placement of the headphone. Here a more simple approach is used, namely that the acquired impulse responses are zero padded to the same length as the audio signal. Then it can be used to deconvolve the headphone frequency response from the stimuli as follows:

$$AudioSignalFiltered = IFFT(\frac{FFT(AudioSignal)}{FFT(ImpulseResponseZeroPadded)}) \tag{11.2}$$

11.4.4 Results

The response with the headphone response deconvolved represents the electrical signal passed to the headphone. This is then filtered by the headphone and ear canal to give the sound pressure at the ear drum. Therefore the sound pressure a the eardrum is shown as that filtered by the HRTF only since the other transfer function is first removed and then added again.

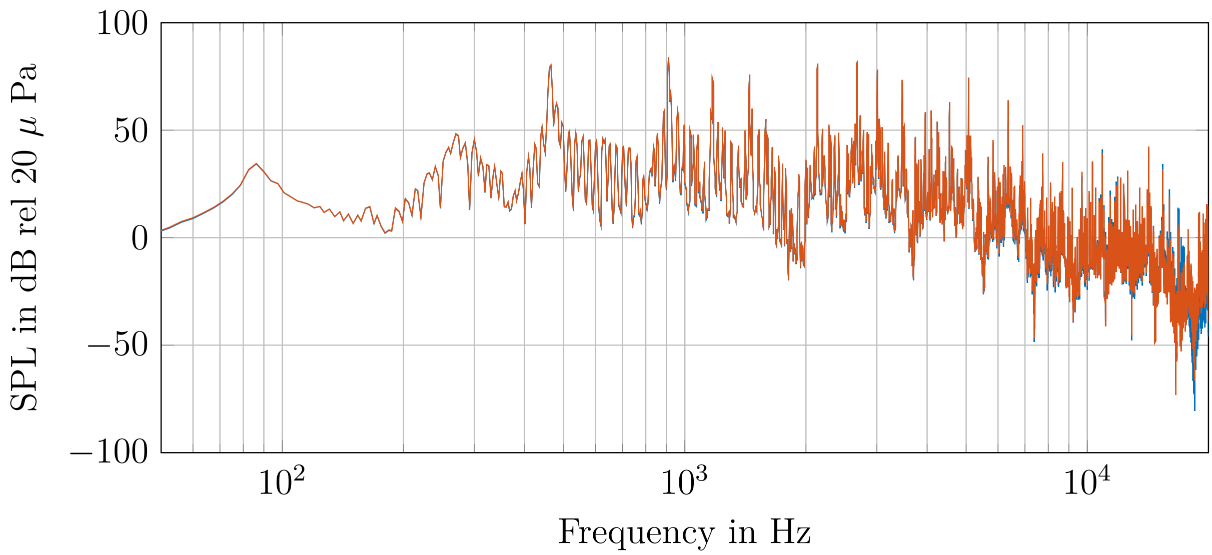

Figure 11.6: The sound pressure level at the left (—) and right (—) ear of the listener.

In figure 11.6 the frequency content of the sound pressure at the left and right eardrum of the HATS is shown.

This concludes the chapter on the auralization algorithm. It has been shown that an audio signal can be generated and processed to replicate a listening situation. How this simulated audio relates to an audio recording of the actual structure remains to be seen, this will be treated in subsection 12.3.2.

Part III

Measurements

12 | Plate measured response

12.1 Design goal measurements

The purpose of the measurement is to acquire real world data for comparison with the simulated data. Therefore the measurement should try to mimic the simulation as best as possible[1]. The measurement is split in three parts, one measuring the steady state audio response at multiple positions plus multiple binaural recordings with a HATS. During this part the loading on the plate is kept at a minimum. The second part determines the mode shapes of the plate and the impact on sound is not crucial. In both measurements large deformations should be avoided to limit non-linear behaviour of the plate, which are not included in the simulation work. The third measurement measures the in situation HRTF of the HATS using a small loudspeaker. As discussed in subsection 11.3.1 the signal quality in this measurement was low and the HRTF database is acquired in anechoic conditions in subsection 11.4.1. The experiment measuring the in situation HRTF is therefore only included in Appendix A and not discussed further in the main report.

First a brief walk through of the environment and equipment used in the measurement is given, so that the reader understands the conditions under which the measurements are performed. All the more detailed tables and figures needed for reproduction are given in Appendix A, everything related to the conceptual understanding and choices is presented in this chapter.

12.1.1 The measurement environment

The measurement environment is designed to comply with ISO 3745, which is a precision grade standard specifying how to measure sound power levels for machinery. The room is hemi-anechoic with a concrete floor. The room is certified down to 50 Hz with the ventilation turned off[2]. There are 20 fixed microphones placed on a half-sphere at a distance r=2.8 m.

[1] In reality the simulation is trying to emulate the real world as best as possible

[2] It is only turned on when heat developing machinery runs for prolonged periods. Never in this project.

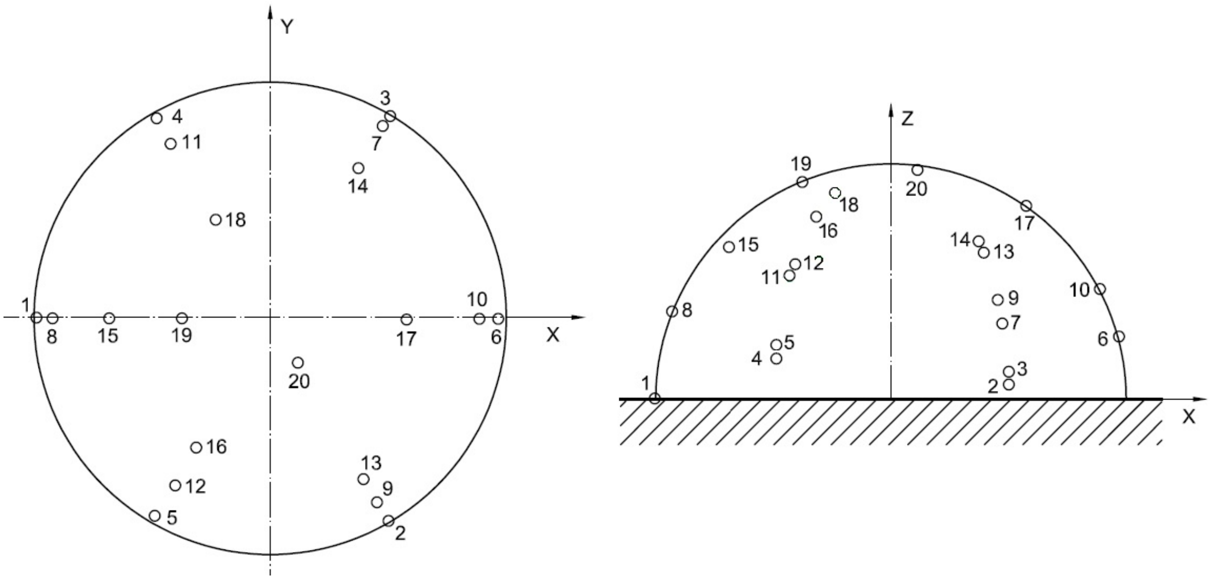

Figure 12.1: Microphone positions as given in the ISO 3745. In this project the orientation of the coordinate system is different corresponding to swapping the y and z value. [DEWESoft, no date]

The room is mounted on sylomer to isolate it from vibrations originating outside the measurement environment. The room is also equipped with a floating concrete block in the middle of the room. The block serves the purpose of further isolating the device under test from the building. The concrete block is constantly adjusting it's position, which produces a small amount of sound. To stop this the it can be 'locked', but in that case it is moving slowly downwards as air leeks from the system. In this project where the vibrational levels and weight of objects is very small compared to the objects this block was designed for it is always deflated. This ensures that distances to microphones are constant.

12.1.2 Measurement equipment

A brief overview on the used equipment is given.

Shaker

The shaker used in this experiment is chosen as the B&K 4810, which is the smallest stationary shaker available at Grundfos. The reason for choosing the shaker as small as possible is that the shaker itself will produce sound. A larger shaker such as B&K 4809 produces more unwanted sound. The small B&K 4810 is capable of delivering a maximum displacement of 4 mm peak-peak corresponding to 49 m/s^2 with a payload of 186 grammes [Brüel & Kjær, no date b]. The plate weighs around 200 grammes.

Impedance head

Instead of using an actual impedance head the same functionality is achieved by combining a accelerometer, B&K 4514, and a force transducer, B&K 8200. This setup will allow the force and acceleration actually applied to the structure to be measured. A further advantage is that they can be screwed together around the plate, fixating it in the process. The force transducer can operate up to vibration levels of 9807 m/s^2, well above the requirements here and has a frequency response depending on the load. The lower limit is 0 Hz and the upper limit is determined by the load[3]. It has a mass of 21 grammes whereof 3 grammes are rigidly connected to the top screw making that the only mass loading. The accelerometer can operate up to vibration levels of 98 m/s^2, again more than the shaker can produce and has a frequency response ±2 dB from 10 Hz to 10 kHz. It has a mass of 8.7 grammes.

Microphones

The microphones used in the array are B&K 4955. They have a frequency range of 10 Hz to 16 kHz and a maximum SPL level of 110 dBSPL. Their internally generated noise floor is 6.5 dB(A).

Data acquisition hardware

The acquisition hardware used at Grundfos is B&K 3050-B, which are 6 channel A/D converters that can be chained and synced using Ethernet. A variant the 3060A has 4 A/D channels and 2 D/A channels, which can be used to drive a shaker. They both have built in charge amplifiers for accelerometers and power supply for microphones.

Data acquisition software

Using B&K acquisition hardware necessitates the use of B&K software in this case Pulse LabShop 22, in short Pulse. From Pulse it is possible to acquire .wav files with normalized data plus a normalization factor, which enables the user to go back to the original calibrated levels. Alternatively data extraction can be done using ASCII files. The software is also capable of enhancing and presenting the data in multiple ways like averaging, filtering, re-sampling, plotting or playing recordings.

12.2 Audio measurement summary

For the audio measurement the 20 microphone positions given in the ISO-3745 standard are used, this will give the sound pressure at 20 positions on a sphere above the plate. Furthermore a HATS, B&K 4100D, is used in two positions, one directly above the plate and another at an angle to the side. The second position is chosen so the HATS is not blocking line of sight from any microphones to the plate so a measurement of the array and the HATS can be performed simultaneously. The position with the HATS directly over the plate is deemed disturbing to the rest of the sound field, so here the 20 microphone signals are discarded.

[3] As shown in eq. 12.1

12.2.1 Setup

Below illustrations give an overview of the setup. figure 12.2 illustrates the setup specific to this measurement. figure 12.3 illustrates the setup always available in the hemi-anechoic room.

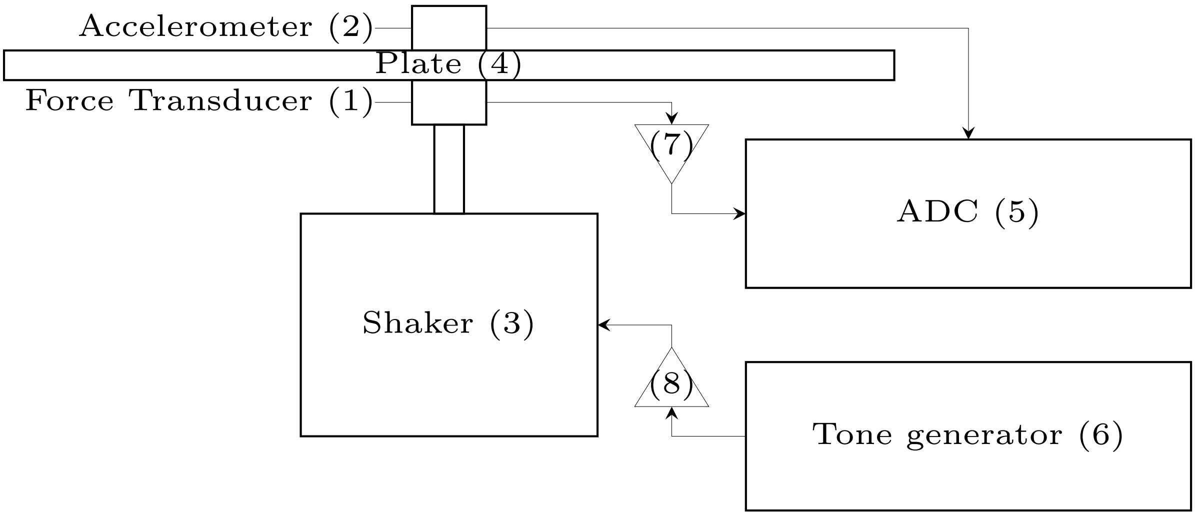

Figure 12.2: Experimental setup for plate. Zoom on the local setup around the plate. Numbers correspond to item numbers in table A.2.

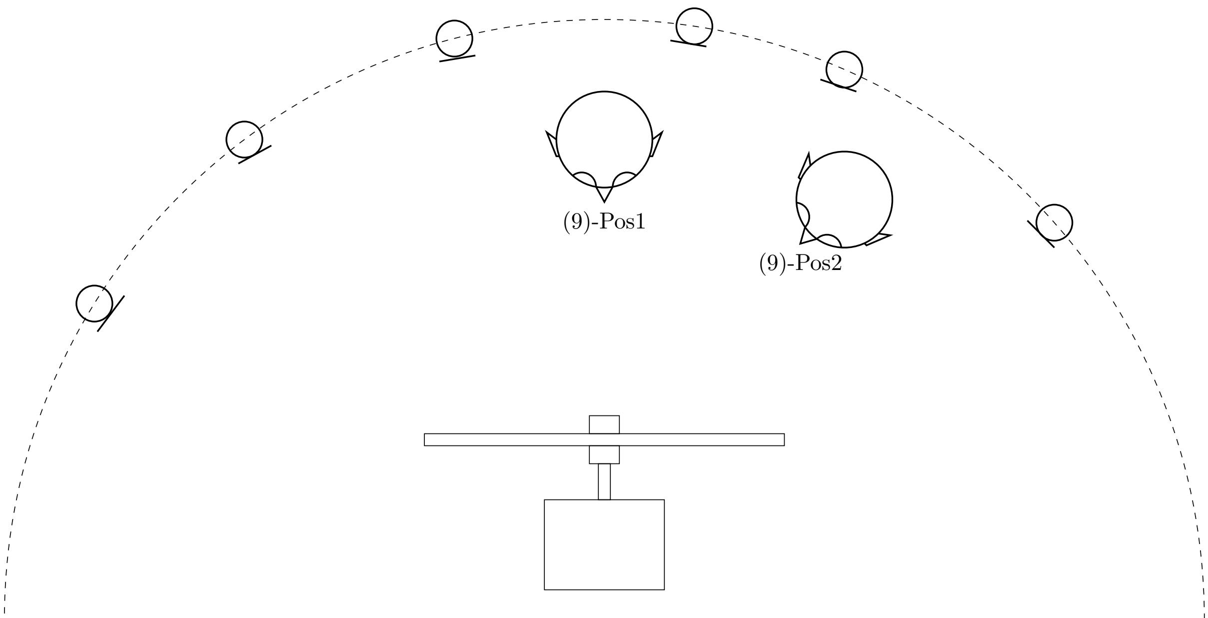

Figure 12.3: Experimental setup for plate. The global setup around the plate. The microphone placement is arbitrary, the actual 3D locations of all 20 microphones are given in table A.4. The electrical connections are left out here but can bee found in table A.6. The items around the plate are connected as in figure A.1 and all the microphones are connected to an ADC.

12.2.2 Results

In order to determine the resonance frequencies that are excited in the middle position of the plate the output from the 20 microphones is used in combination with the output from the 'home-made' impedance head. The microphone output is a suitable way to determine eigenfrequencies in the frequency area where the plate is an efficient radiator. For frequencies below sound radiation the impedance head can be used to measure the input impedance and find resonances.

Only the 20$^{\text{th}}$ microphone signal is plotted in time domain.

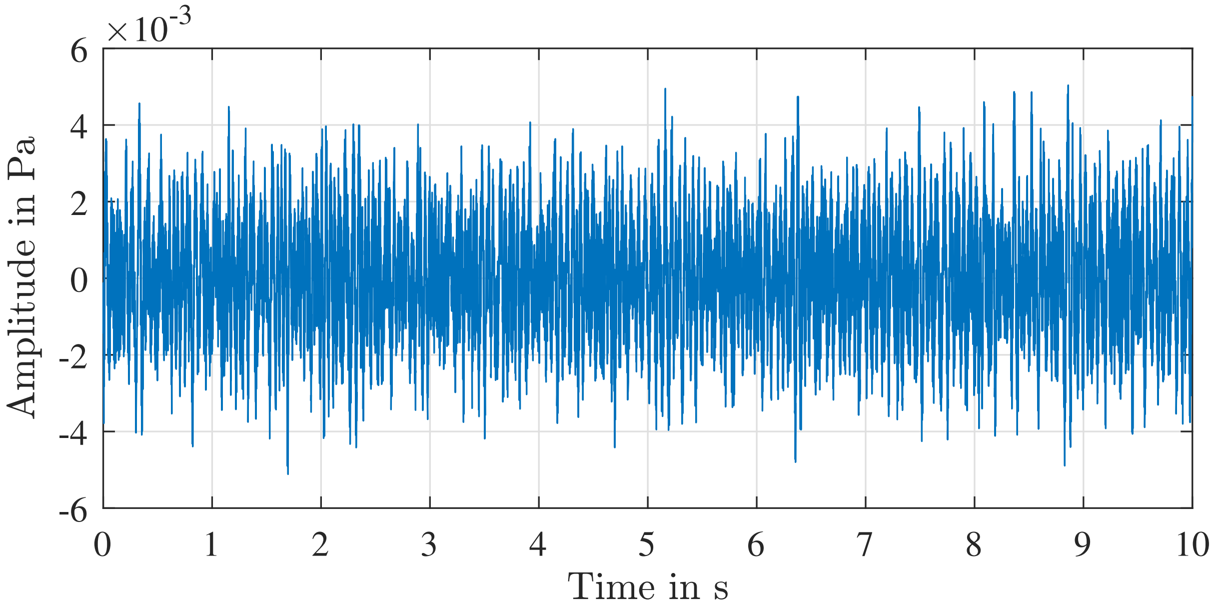

Figure 12.4: The time signal at the M20 microphone position.

All 20 microphones as well as the background level with and without the shaker running is shown in figure 12.5.

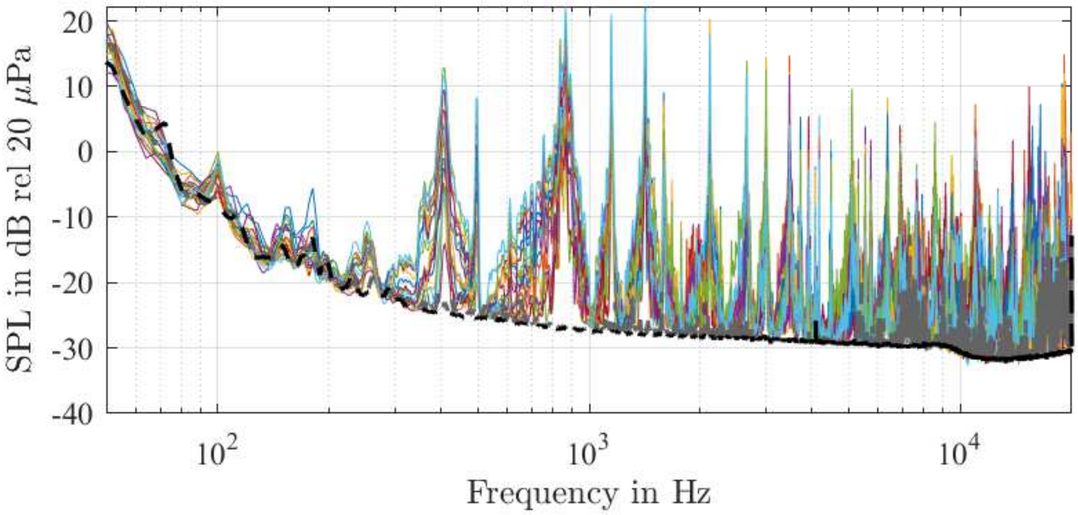

Figure 12.5: The sound pressure level at the 20 microphone positions. Background noise at microphone 10 (– –) and noise from shaker without plate and same driving voltage at microphone 10 (– –).

Some selected eigenfrequencies of the plate are given below. A complete list would be pointless, but a few frequencies allows for later comparison with the analytical and simulated results. Resonances occur at: 400, 496, 864, 1148, 1416 and 1588 Hz.

It can be seen in figure 12.5 that the plate is an inefficient radiator of sound below 400 Hz. Therefore the eigenfrequencies below this have to be determined using the impedance head.

The input impedance can be calculated from the time series of the acceleration and force. The input impedance is calculated as $Z(\omega)_{in} = \frac{Force(\omega)\cdot j\omega}{Acceleration(\omega)}$ in a spectral division including phase. As can be seen in Appendix A the SNR is not high enough to directly calculate the input impedance. Instead it is calculated from acceleration and force in frames and averaged which is also described in the appendix.

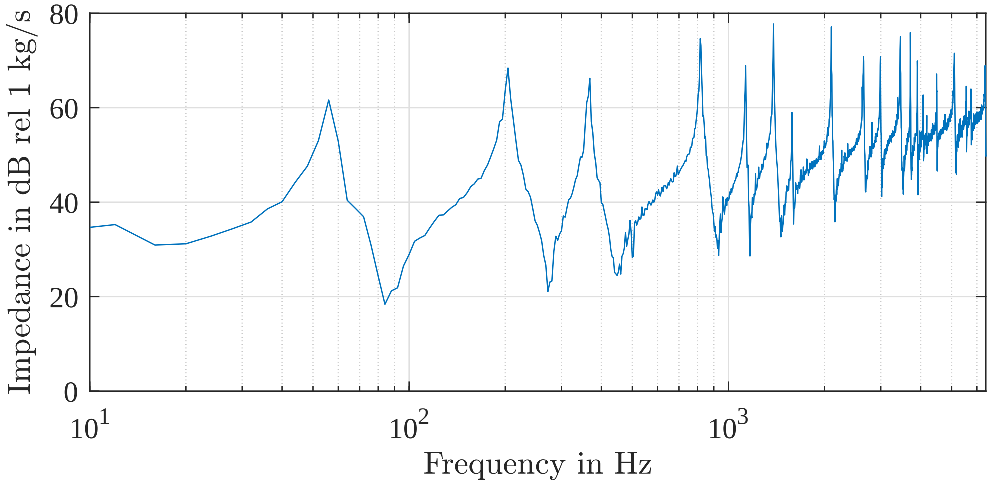

Figure 12.6: The averaged input impedance.

From figure 12.6 it can be seen that resonances occur at frequencies below those that are clearly visible in the audio spectra. For example resonances exist at 87 Hz and 274 Hz.

12.2.3 The measurement systems influence on the plate

The analytical and simulated work assumes no measurement setup is attached to the plate. In the measurements this is obviously not the case. Therefore the influence of the measurement setup should be discussed

When recording audio from the vibrating plate the recording is a result of a system response and not purely the plate. Two factors are considered, namely:

1. The shaker has a spring and mass characteristics which is rigidly connected to the bottom of the force transducer.
2. The accelerometer and top of the force transducer are rigidly connected to the plate causing a mass loading.

This explains why Sound is radiated at 400 Hz even though no impedance drop can be seen in figure 12.6. The impedance is calculated as the force input to the plate, accelerometer and the top of the force transducer divided by the velocity of these. The input impedance measurement does therefore not consider the influence of the shaker and the other things in item 1 above. The microphone signals will pick up the complete system response including the shaker. In short the microphone signals and the input impedance are not measuring the same thing.

The influence from item 2 can be seen as a mass, which has the impedance $j\omega M$. In Appendix A the removal of this is described in better detail and the result is shown in figure 12.7.

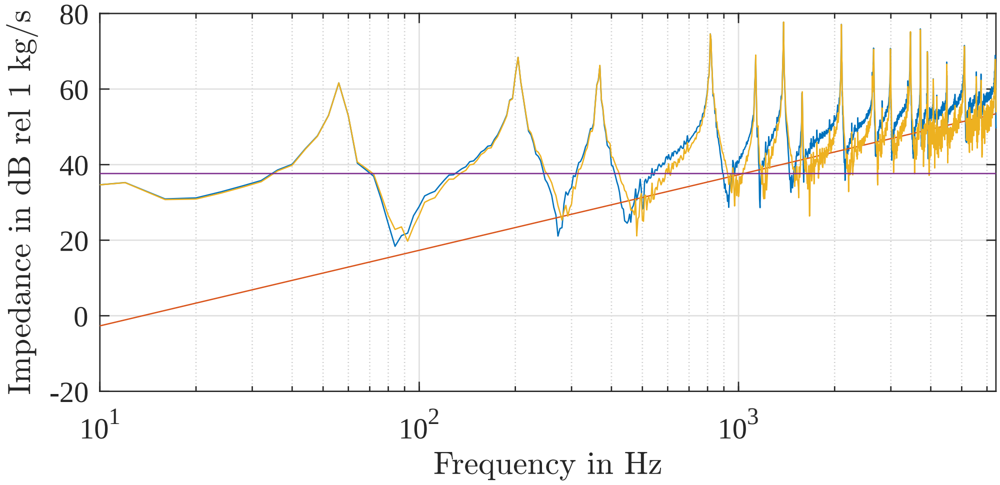

Figure 12.7: The averaged input impedance. Measured input impedance (—). Impedance of mass 11.7 grammes (—). Input impedance of plate alone (—). Theoretical input impedance of an infinite plate of same material and thickness (—).

From this it is clear that the additional mass loading due to item 2 shifts the resonance frequencies slightly downwards compared to an unloaded plate.

To summarize the yellow line in figure 12.7 is comparable to the analytical solution as well as the simulation in section 8.9. The audio measurement as well as the input impedance in figure 12.6 are not directly comparable to the previous works.

Force transducer

From figure 12.7 it is clear that the impedance of the plate increase unexpectedly with frequency. The upper limit of the accelerometer is 10 kHz which is above the range shown here. The upper limit of the force transducer is dependent on the load and so it is examined further here. One issue arise in that the dependency is on the impedance of the load as described by [Brüel & Kjær, 1994]:

$$\frac{F_{measured}}{F_{applied}} = 1 + \frac{j\omega m_{top}}{Z} \tag{12.1}$$

This means that the impedance of the object has to be known to calculate the transfer function and thereby the upper limit of the force transducer. Seeing as the force transducer is used to measure the impedance of the object this causes an unfortunate loop. In an attempt to remedy this the impedance of the infinite plate is used to estimate the upper limit .

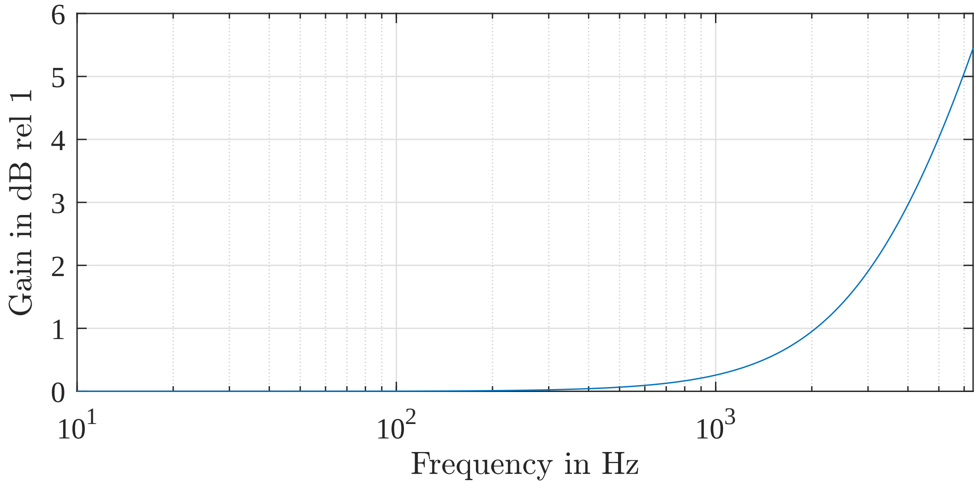

Figure 12.8: Magnitude response of force transducer when connected to an infinite plate.

From figure 12.8 the 1 dB upper limit of the force transducer is 2050 Hz. On the physical plate this can be expected to be even lower since the input impedance of the plate will have large dips at resonances below this frequency. No compensation is made to account for the error introduced by the force transducer as this would require a more detailed knowledge of the error that the approximation in figure 12.8.

Three measurement situations

Three different sets of resonant frequencies can be found from the acquired data. One for a completely free plate, from the yellow line in figure 12.7. One from a plate with mass loading (item 2), from figure 12.6. And finally one from a plate with a mass loading mounted on a spring (item 1+2), from figure 12.5.

Here some of the resonant frequencies in the three cases are listed.

Analytical	Plate alone	Plate+2	Plate+1+2
88 Hz	92 Hz	87 Hz	unknown
288 Hz	288 Hz	274 Hz	256 Hz ✿
479 Hz	480 Hz ❧	450 Hz ❧	400 Hz
519 Hz			496 Hz
991 Hz	972 Hz	932 Hz	864 Hz
1226 Hz	1208 Hz	1168 Hz	1148 Hz
unknown	1544 Hz ❧	1460 Hz ❧	1416 Hz
1568 Hz			1588 Hz

Table 12.1: The measured resonance frequencies of the different systems. '1' and '2' refers to the two factors on page 86. 'Plate alone' data is from yellow line in figure 12.7. 'Plate+2' data is from figure 12.6. 'Plate+1+2' is from figure 12.5.

✿ Read from large acceleration in figure A.11.

❧ Which it is not clear from the impedance measurements if two eigenfrequencies exist close to each other. Mode shapes are not available so checking is impossible.

.

12.3 Vibration measurement summary

To examine the mode shapes the frequencies from table 12.1 column 'Plate+1+2' are considered as these are the ones corresponding to the setup that is used. Two approaches were considered for the vibration measurement namely:

1. Measuring mode shapes using accelerometers.
2. Examining mode shapes using sugar [Chladni, 2015][4].

The first approach is by far the most accurate as it will yield results on the level of vibration in addition to making it possible to measure at high frequencies. The drawback is that it requires multiple accelerometers mounted on the plate. To capture the mode shape of the (3,1) mode two Accelerometer is sufficient. For the (2,2) mode three are needed[5]. For higher mode shapes many accelerometers are needed, unfortunately due to the small thickness of the plate this will cause a

[4]A method first introduced by Ernst Chladni in the 18th century although he used sand.
[5]In reality 4 to avoid uneven loading

non negligible mass loading. The mode shapes might be close to identical if the accelerometers are evenly spaced but the eigenfrequencies will move, making it hard to track which mode shapes belong at which eigenfrequency.

The second approach is simple, but only yields a visual impression of the mode shape. By pouring sugar on the vibrating plate the nodal lines of the mode shapes are made visible as the sugar will collect in the non-moving areas. This will cause a mass loading much smaller than the accelerometer based method.

For the purpose of verifying that the FEM analysis is indeed finding the correct mode shapes for the eigenfrequencies and more importantly determining which modes can be excited in the centre of the plate the second approach is chosen. This puts an upper frequency limit on modes that can be examined, as the deformation, which moves the sugar, decreases with frequency. In the case of this plate and the used shaker this limit is somewhere above 496 Hz. Above this limit it was found that by substituting the sugar with fine salt mode shapes for eigenfrequencies up to 1588 Hz could be visualized.

12.3.1 Setup

The setup is simple and utilizes part of the setup used in the audio measurement. She shaker and plate are connected as before (figure 12.2), but now the tone generator is set to vibrate sinusoidally at a single frequency.

12.3.2 Results

It has already been determined that FEM is in alignment with the analytical solution when it comes to determining the mode shape of a free plate. Now it is desired to examine whether they are in alignment with the actual response of the plate under study mounted on a shaker.

Before continuing with the resonance frequencies determined in the audio measurement an additional frequency is added. The reason for this being included is that something was present at 57 Hz frequency in the HATS measurement in figure A.7 and figure A.8. The slight peak is not present at the 20 microphone positions further away, indicating a possible near field. Still in order to produce a near field at 57 Hz some resonance must exist in the system. It has been possible to recreate its mode shape and approximate frequency by applying a fixed support in the centre position in the finite element analysis. The conclusion therefore is that the mounting at the centre of the plate influence the vibration at this frequency.

Sugar is distributed on the plate as carelessly as possible, however it is difficult to ensure that the concentration of sugar is even over the entire plate. To give the reader and idea of the inaccuracy the distribution was done with figure 12.9 shows sugar as placed initially before measurements. The sugar is clustering, so the approach is only valid when the sugar clearly moves to new positions to create clear patterns.

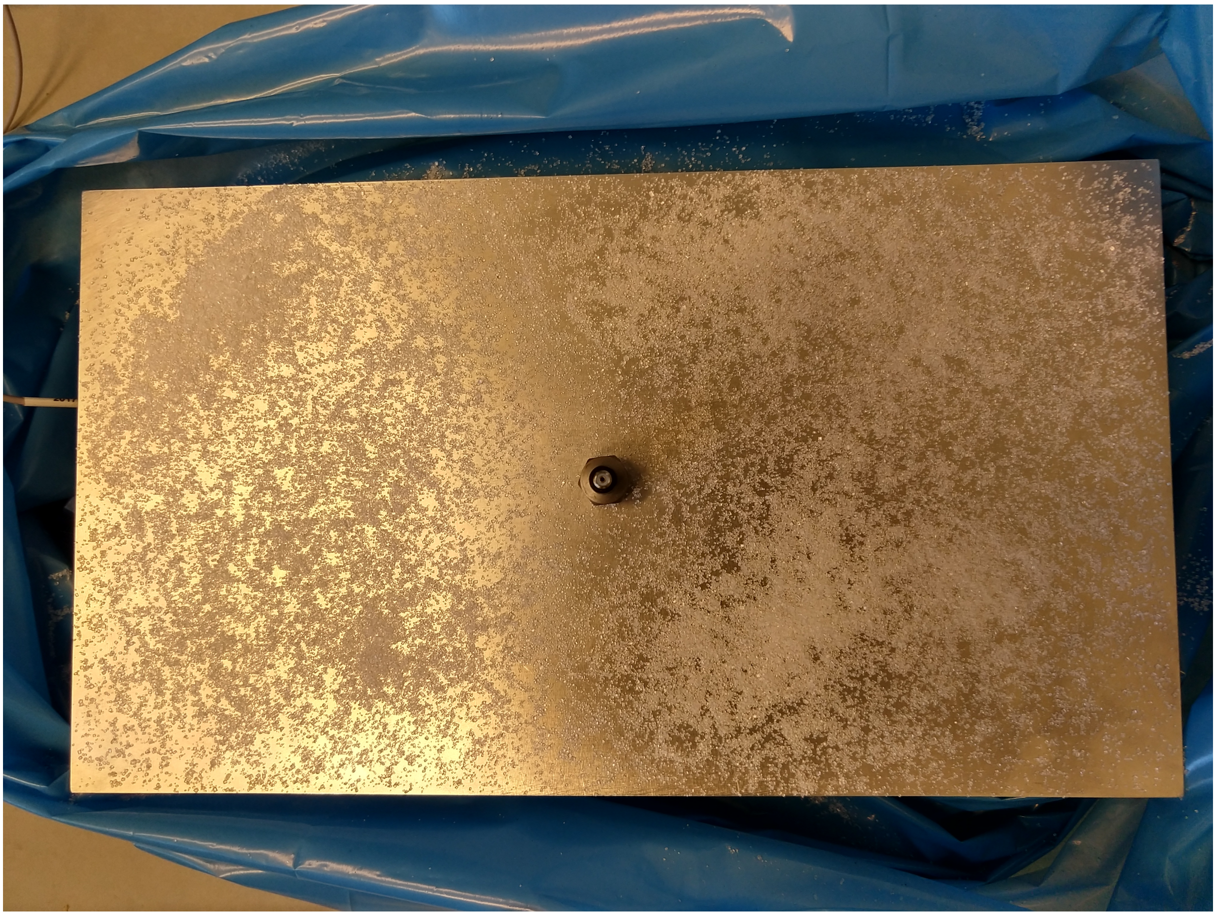

Figure 12.9: Example of sugar position before shaking.

(a) Analytical result unknown.

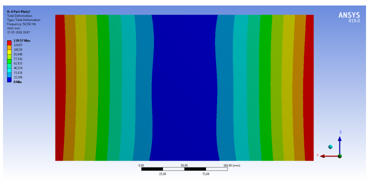

(b) Simulated 56 Hz.

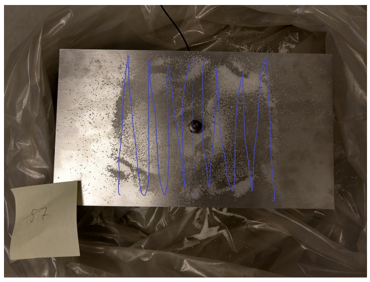

(c) Measured 57 Hz.

Figure 12.10: The mode shapes determined for the additional mode found in measurements. No analytical solution is known. The FEM eigenfrequency is 56 Hz with a fixed support in the centre. The pattern appears slightly more circular in the realization than in the simulation because all sugar from the edges are stored at the edge of the non vibrating zone.

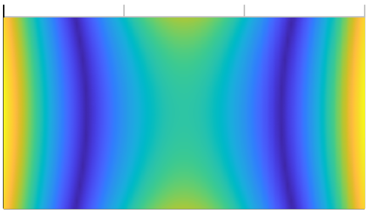

(a) Analytical 88 Hz.

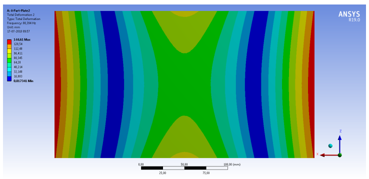

(b) Simulated 88 Hz.

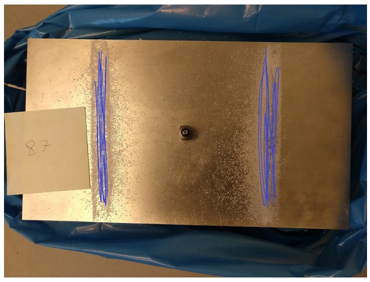

(c) Measured 87 Hz.

Figure 12.11: The mode shapes determined for the 88 Hz mode. FEM determines the eigenfrequency to be 88 Hz. The plate measurement determined the eigenfrequency to be 87 Hz (from the input impedance figure 12.6). The use of the input impedance to select frequency is not correct as it does not account for the shaker as previously discussed. However no alternative is available and the sugar is moving easily so the 87 Hz is close to the resonance.

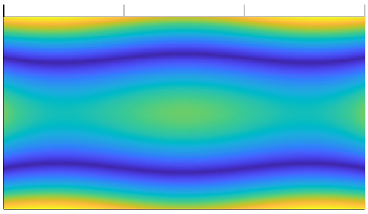

(a) Analytical 288 Hz.

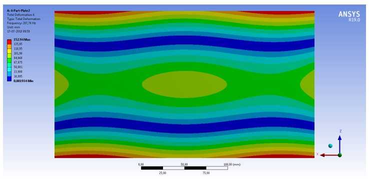

(b) Simulated 288 Hz.

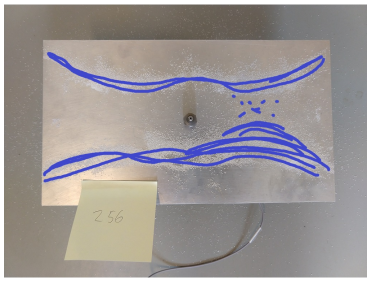

(c) Measured 256 Hz.

Figure 12.12: The mode shapes determined for the 288 Hz mode. FEM determines the eigenfrequency to be 288 Hz. The plate measurement determined the eigenfrequency to be 256 Hz (from the acceleration figure A.11). The dotted blue lines on the measured indicate that a possible node line might be present.

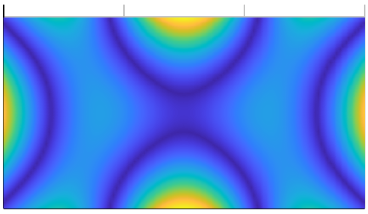

(a) Analytical 479 Hz.

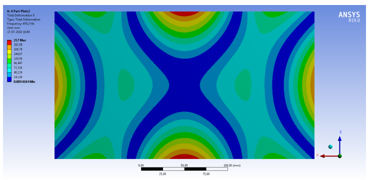

(b) Simulated 478 Hz.

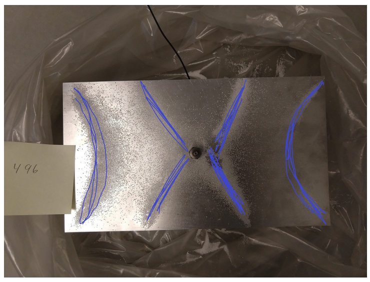

(c) Measured 496 Hz.

Figure 12.13: The mode shapes determined for the 479 Hz mode. FEM determines the eigenfrequency to be 487 Hz. The plate measurement determined the eigenfrequency to be 496 Hz (from the radiated sound figure 12.5).

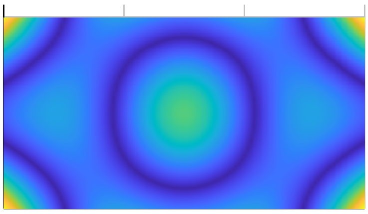

(a) Analytical 519 Hz.

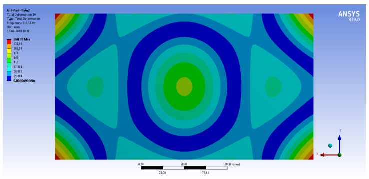

(b) Simulated 518 Hz.

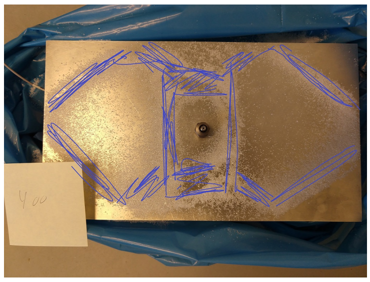

(c) Measured 400 Hz.

Figure 12.14: The mode shapes determined for the 519 Hz mode. FEM determines the eigenfrequency to be 528 Hz. The plate measurement determined the eigenfrequency to be 400 Hz (from the radiated sound figure 12.5).

As the sugar method does not work for higher frequencies the sugar is substituted with fine salt allowing for higher frequencies to be visualized. The pictures of the measured response are rotated 180 degrees to show the same orientation as the previous pictures as the plate was rotated by mistake when remounted.

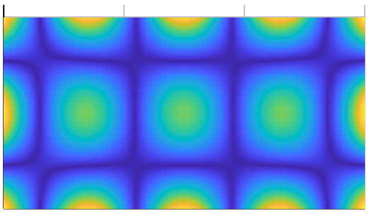

(a) Analytical 991 Hz.

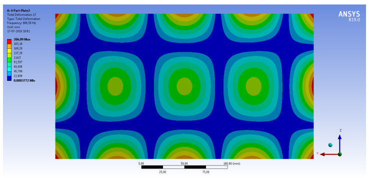

(b) Simulated 989 Hz.

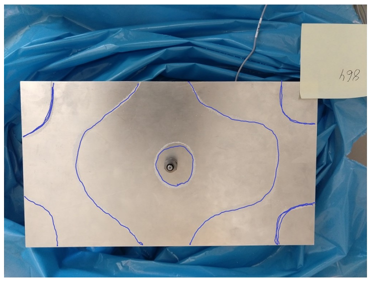

(c) Measured 864 Hz.

Figure 12.15: The mode shapes determined for the 991 Hz mode. FEM determines the eigenfrequency to be 989 Hz. The plate measurement determined the eigenfrequency to be 864 Hz (from the radiated sound figure 12.5).

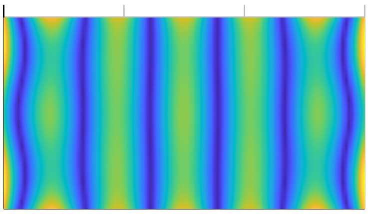

(a) Analytical 1226 Hz.

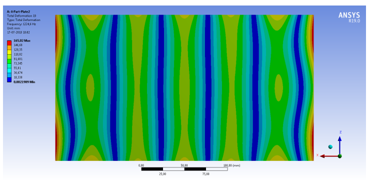

(b) Simulated 1225 Hz.

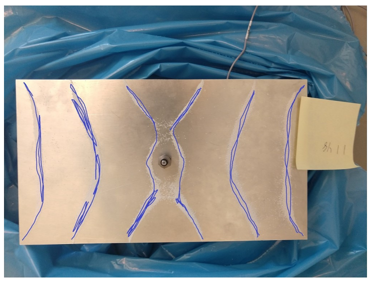

(c) Measured 1148 Hz.

Figure 12.16: The mode shapes determined for the 1226 Hz mode. FEM determines the eigenfrequency to be 1225 Hz. The plate measurement determined the eigenfrequency to be 1148 Hz (from the radiated sound figure 12.5).

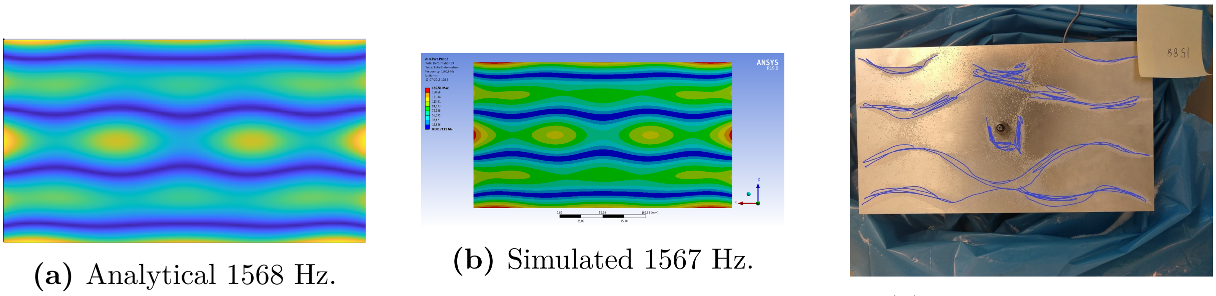

(a) Analytical 1568 Hz.

(b) Simulated 1567 Hz.

(c) Measured 1588 Hz.

Figure 12.17: The mode shapes determined for the 1568 Hz mode. FEM determines the eigenfrequency to be 1567 Hz. The plate measurement determined the eigenfrequency to be 1588 Hz (from the radiated sound figure 12.5).

The measured mode shape at 1416 Hz is not similar to any of the mode shapes found in analytical or simulated work.

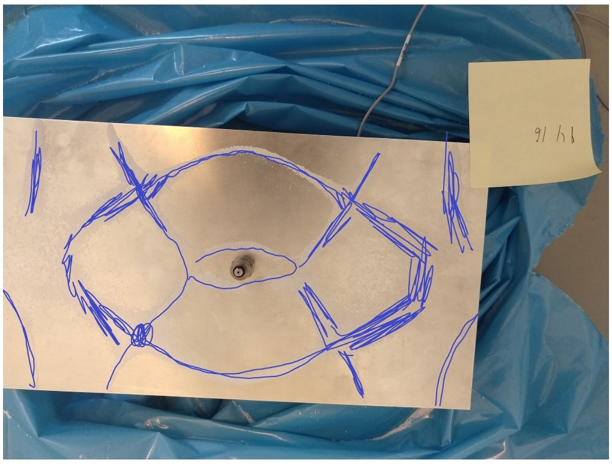

Figure 12.18: Measured 1416 Hz.

The simulated mode shapes are overall in alignment with the actual mode shapes on the plate. At higher frequencies the hole and the mounting seems to influence the mode shape by pulling nodal lines towards the centre. The fact that the frequencies are not aligned is explained in subsection 12.2.3.

12.4 Relating measurement results to simulation results

It is clear from the comparison of measured mode shapes and results from FEM that the simulation need some refinement to capture the influence of the measurement setup. It is also clear that directly comparing result from simulation on a perfect plate and the measurement results in terms of frequency and mode shape is pointless.

A choice is left to be made; should the measured data be processed to fit the analytical solution by removing the influence of the force transducer, accelerometer and shaker? Or should the simulation be expanded to include more of the measurement system? Naturally auralization of the situation without a measurement setup would have the largest value. Removing the effect of the mass loading on the plate from the reference recording is unlikely to be accurate as it affects the mode shapes of the plate. Therefore only the two other situations are considered. Which of the two methods is superior in terms of sound quality is unknown. For this reason both cases are included in the further work in chapter 13.

It is required to remodel the plate in such a way as to make the simulation setup fit the measurement setup better. At this point simulation and analytical solutions show a good agreement verifying the validity of using FEM. For complex structures finding analytical solutions will be more complicated or impossible, which is the argument for using numerical simulation tools in the first place. For this reason I will not attempt to find an analytical solution to an imperfect plate.

12.4.1 Asymmetries in mode shapes

The assumption that the measurement setup is completely symmetric around the centre does not hold. This can be seen as asymmetries in some of the measured mode shapes at 256 Hz figure 12.12 and 864 Hz figure 12.15. The asymmetry is likely due to the location of the centre hole, will be modelled in a more detailed way in chapter 13.

12.4.2 Time varying sound

When listening to the sound which is recorded at the microphone positions it seems to vary with time. This will be examined further in section 14.1.

Part IV

Refinement

13 | Vibration version 2

13.1 Design goal numerical solution

Recognizing that there is a difference between the eigenfrequencies determined through simulation in section 8.9 and those measured on the plate chapter 12 it is desired to examine how to make simulations fit reality better. To that end modifications are made to the model of the plate to include the asymmetry of the centre hole. Then the measurement system is included in the simulation to mirror the measurement situation better.

13.2 Remodelling the plate

The physical plate was measured using a ruler and callipers, which introduces tolerances is terms of accuracy in the order of 1 mm for the ruler and 0.1 mm for the callipers. The measurement of the plate yielded the following dimensions[1]:

- Length = 299.3 mm $\pm 1mm$
- Width = 169.3 mm $\pm 1mm$
- Thickness = 1.5 mm $\pm 0.1mm$
- Centre hole Ø = 4.8 mm $\pm 0.1mm$
- Centre hole location L=149.9 mm, W=84.4 mm $\pm 1mm$

[1]The dimensions used in the previous simulation can be seen in table 5.1.

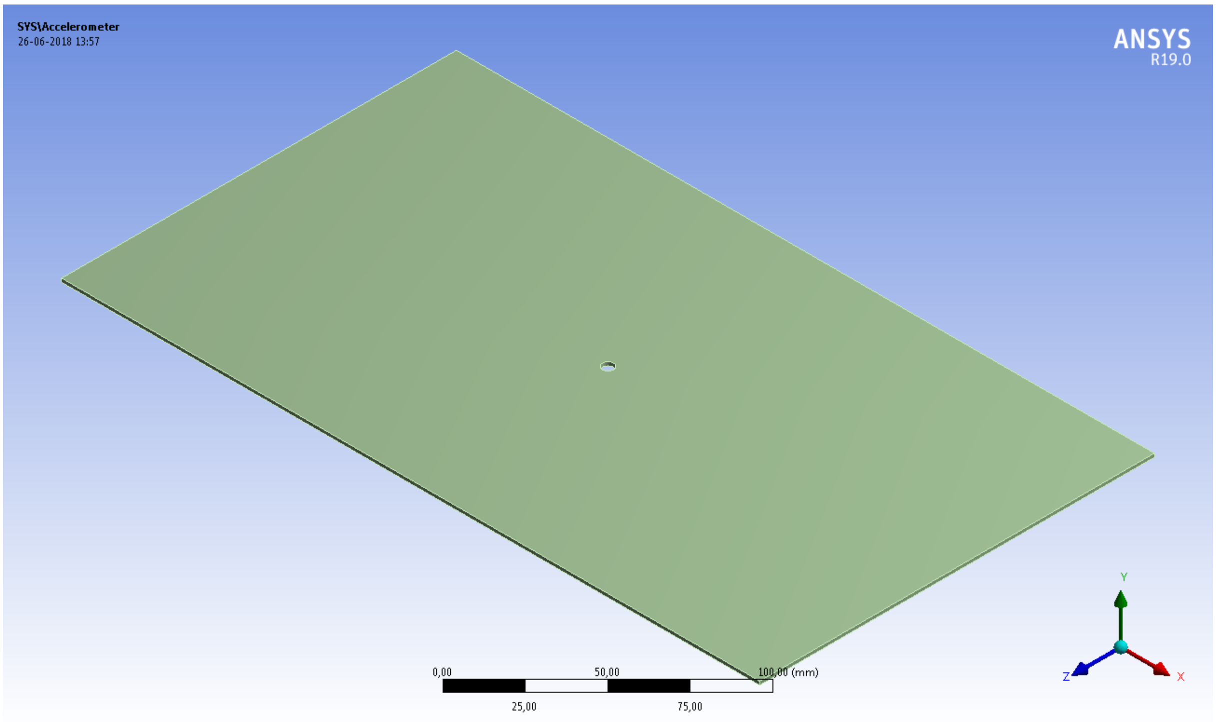

Figure 13.1: The redesigned plate with hole slightly off centre.

13.2.1 Including force transducer and accelerometer

It is also desired to examine the influence that the excitation setup might have on the eigenfrequencies of the plate. The setup is first seen as a simple mass loading of 11.7 grammes at the edge of the centre hole. This mass corresponds to 3 grammes from the top of the force transducer and 8.7 grammes from the accelerometer. This situation is referred to as **11.7g**.

Secondly the geometry of the fitting of the accelerometer and force transducer might affect the solution, so two cylindrical geometries are added to the simulation setup. The cylinders are chosen to have a diameter corresponding to the contact edge towards the plate of the part they model, 9.6 mm for the force transducer and 12 mm for the accelerometer. Their length is chosen to result in the correct mass for the component using a density of 2750 kg/m^3. The two components are rigidly connected[2] via a 3.7 mm cylinder which is a part of the force transducer. The plate is defined with no separation to either component. This situation is referred to as **Acc+FT**.

[2]In ANSYS 'Bonded'.

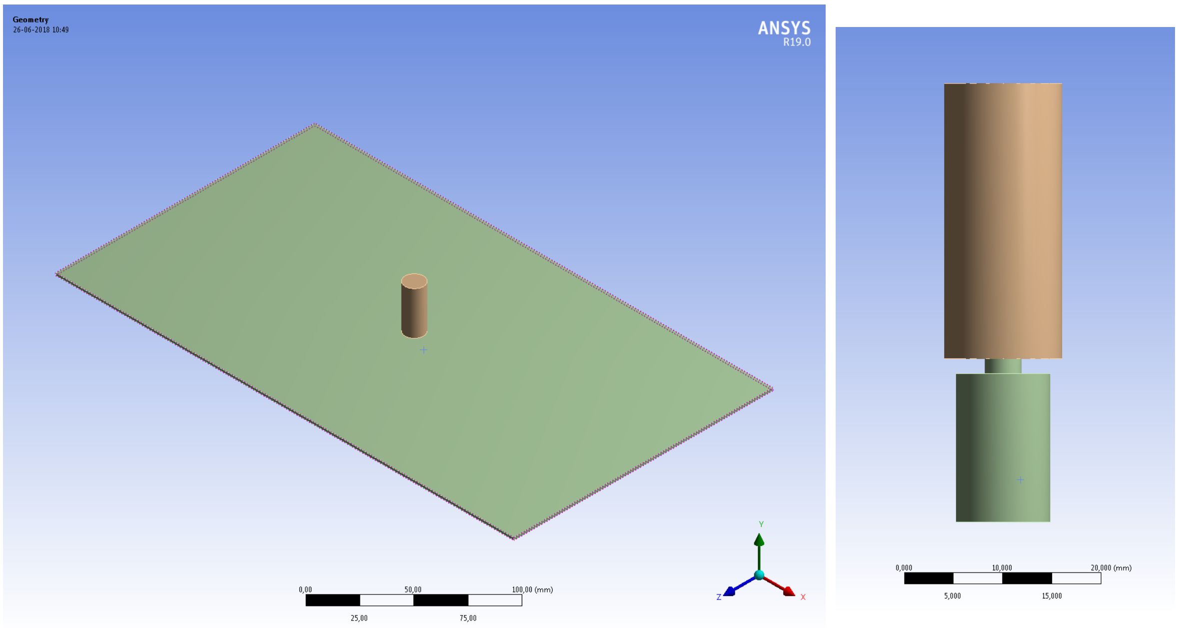

(a) Entire setup.

(b) Plate hidden.

Figure 13.2: New simulation setup including geometry of force transducer and accelerometer called 'Acc+FT'.

To examine if the centre hole mounting needs additional refinement a face sizing in a sphere of influence with a radius of 10 mm centred at the hole centre has been used. The refinement was to 0.5 mm mesh size which is about 5 times finer than the original mesh. This situation is referred to as **mesh refined**.

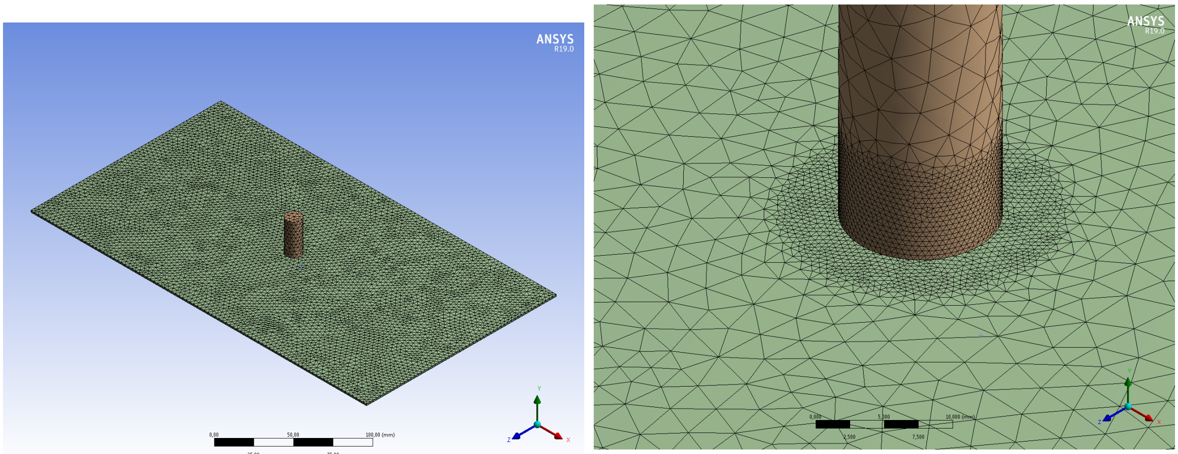

(a) Normal mesh for setup 'Acc+FT.

(b) Zoom on refined mesh in setup 'mesh refined'.

Figure 13.3: Meshing of the new geometry in two cases.

13.2.2 Including shaker

Theoretically the force transducer decouples the shaker from the structure, here it will be examined what would happen if this is not the case. The implication of including the shaker would be an additional mass loading of 18 + 18 grammes from the shaker moving mass and force transducer bottom. On top of this the two masses of the force transducer are connected with a spring with stiffness $5 \cdot 10^8$ N/m. The shaker acts like a spring connecting the force transducer to ground with a stiffness of 2000 N/m. This situation is referred to as **complete**.

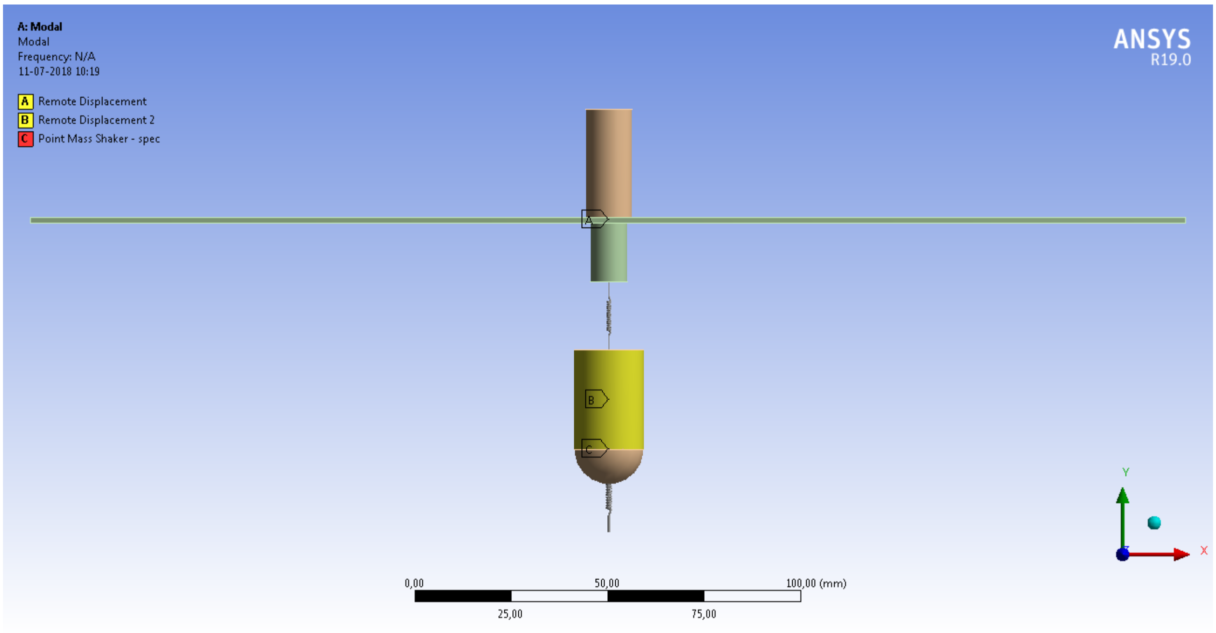

Figure 13.4: Setup when considering measurement system geometries. The shaker moving mass is considered a point mass on the force transducer bottom. The 'Remote displacement' boundary conditions serve the purpose of fixing the objects in x and z direction to prevent them from drifting away. This setup is referred to as 'complete'.

The above setup might also be simplified by acknowledging that the force transducers stiffness is very large and that the force transducer top and bottom must move as a single unit except at very high frequencies. This would allow the entire force transducer mass and shaker moving mass to be included as a point mass on the plate as for the accelerometer and force transducer top before. The centre of the plate can then be connected to ground via a spring of stiffness 2000 N/m. This situation is shown in figure 13.5a

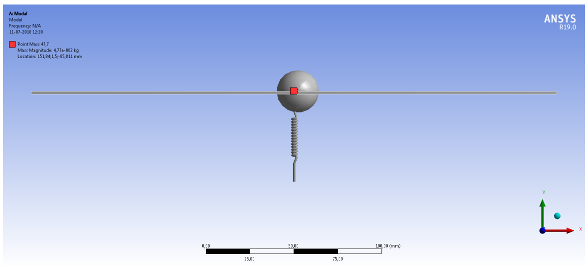

(a) Setup when considering measurement system as an additional mass plus a spring.

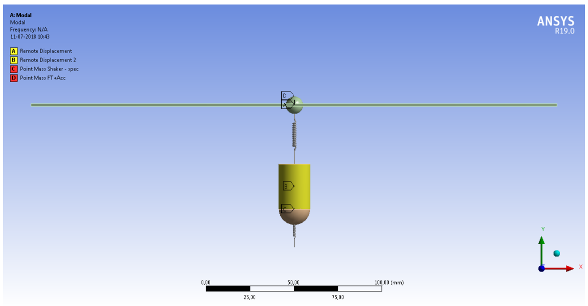

(b) Setup when considering measurement system as a point mass on the plate connected via a spring to the shaker setup. This setup is referred to as 'complete simplified'.

Figure 13.5: Two approaches at simplifying the setup including spring.

The setup used in figure 13.5a turned out to deform some mode shapes significantly. Instead the hybrid solution in figure 13.5b is considered as the simplification. Here the accelerometer and force transducer top are considered point masses and the excitation system is modelled fully as in figure 13.4. This situation is reffed to as **complete simplified**.

13.3 Improvements in modal analysis

The results from the improvements is given in the table below. First only the eigenfrequencies are considered as the mode shapes are similar in most cases.

Mode	Original	11.7g	Acc+FT	Mesh refined	Complete	Complete simplified	Measured
1 figure 8.18a	88 Hz	86 Hz	87 Hz	87 Hz	81 Hz	81 Hz	87 Hz❋
5 figure 8.20a	288 Hz	273 Hz	276 Hz	276 Hz	248/249 Hz†	245 Hz	256 Hz
8 figure 8.21b	478 Hz	482 Hz	485 Hz	485 Hz	483 Hz	482 Hz	496 Hz
9 figure 8.22a	518 Hz	463 Hz	471 Hz	471 Hz	415 Hz	415 Hz	400 Hz
16 figure 8.25b✪	989 Hz	911 Hz	934 Hz	933 Hz	860 Hz	860 Hz	864 Hz
18 figure 8.26a✪	1225 Hz	1175 Hz	1194 Hz	1193 Hz	1168 Hz	1166 Hz	1148 Hz
23 figure 8.26b✪	1567 Hz	1588 Hz	1603 Hz	1603 Hz	1624 Hz	1624 Hz	1588 Hz

Table 13.1: Results from simulation in different configurations.

❋ Only found by mode shape, might be inaccurate.

✪ Refined simulation finds different mode shapes than the original simulation. The simulations including mass loading have a mode shape more similar to the measured one.

† Splits the mode shape in two deformed mode shapes.

From table 13.1 it is clear that the modifications made to the simulation setup moves the results closer to the measured audio. Refining the mesh was found to not affect results significantly so this modification is discarded. Without commenting on every single entry in the table a few trends are pointed out - which are further validated through an informal fiddling with the parameters below.

- Increasing the point mass on the plate moves all resonance frequencies (as expected). But some are more sensitive to mass than others (mode 9 and 16).
- Including the 2000 N/m spring changes all resonance frequencies, but only mode 1 and 5 seem to be sensitive to it's value.
- Including the geometry of the force transducer and accelerometer has a tendency to 'distort' some mode shapes - this is documented further below.

13.3.1 Improved mode shapes

As discussed above some of the simulated mode shapes improve, compared to the measured ones, when the centre geometry is added. Below some of the mode shapes affected by the mass loading are shown for five simulated results and the measured result.

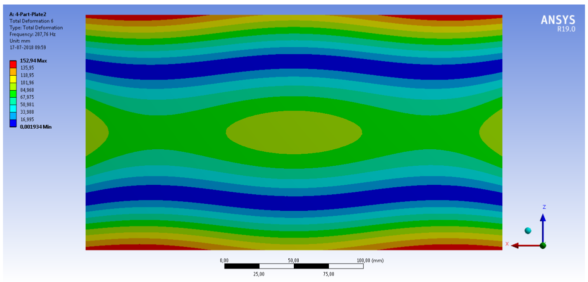

(a) Original - 288 Hz.

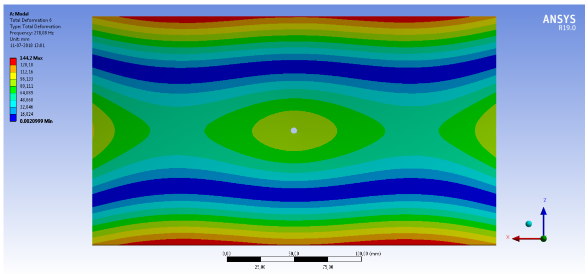

(b) 11.7g - 273 Hz.

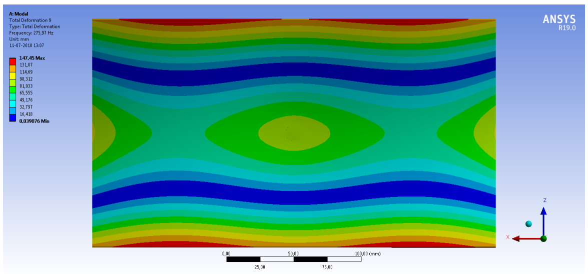

(c) Acc+FT - 276 Hz.

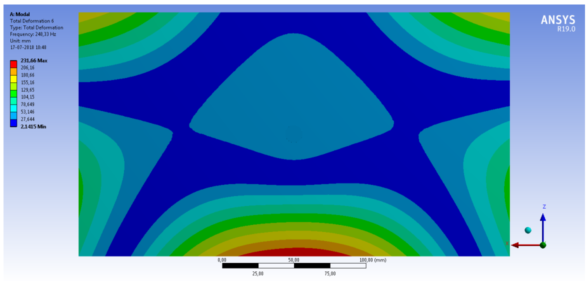

(d) Complete - 248/249 Hz.

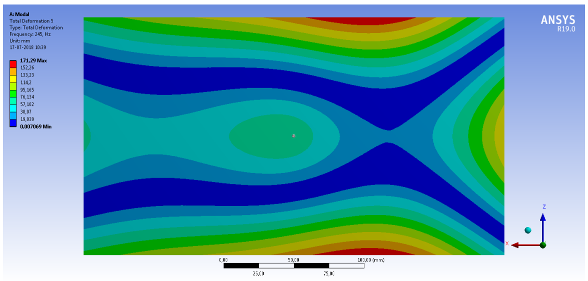

(e) Complete simplified - 245 Hz.

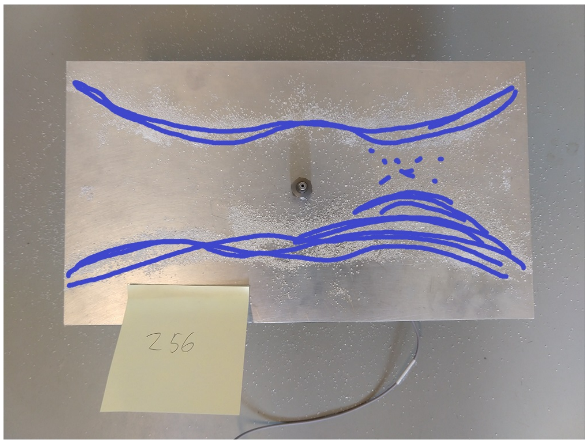

(f) Measured - 256 Hz.

Figure 13.6: Five simulated mode shapes for mode 5 compared to the measured result. The dotted blue lines on the measured indicate that a possible node line might be present. The 'Complete' simulation also resulted in mode shape as shown above flipped upside down at 249 Hz.

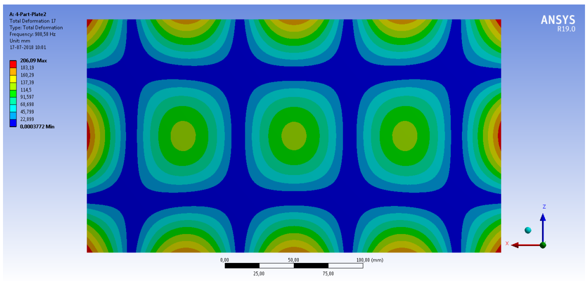

(a) Original - 989 Hz.

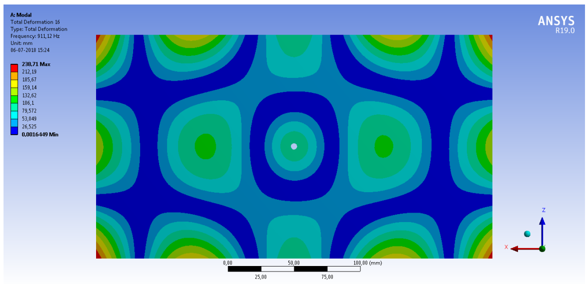

(b) 11.7g - 911 Hz.

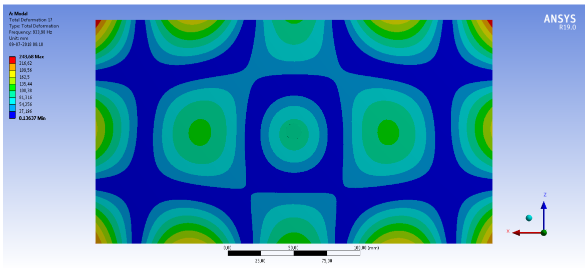

(c) Acc+FT - 934 Hz.

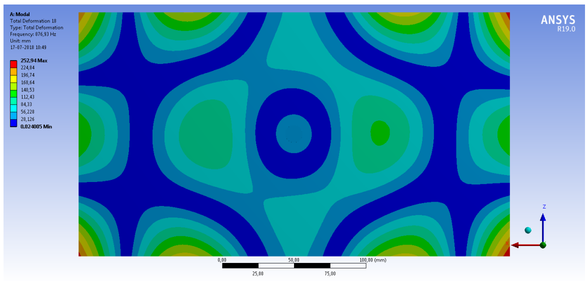

(d) Complete - 860 Hz.

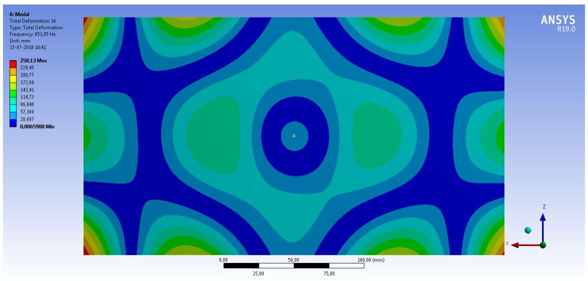

(e) Complete simplified - 860 Hz.

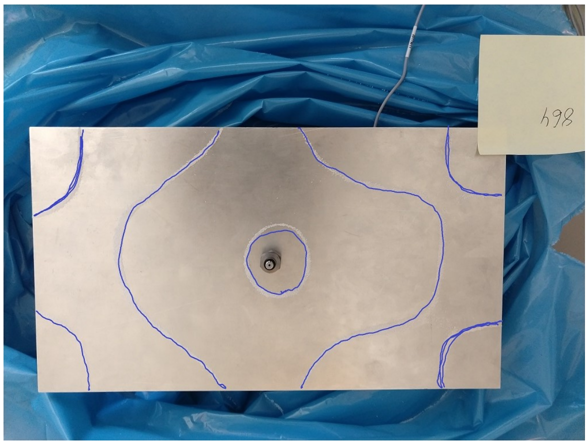

(f) Measured - 864 Hz.

Figure 13.7: Five simulated mode shapes for mode 16 compared to the measured result.

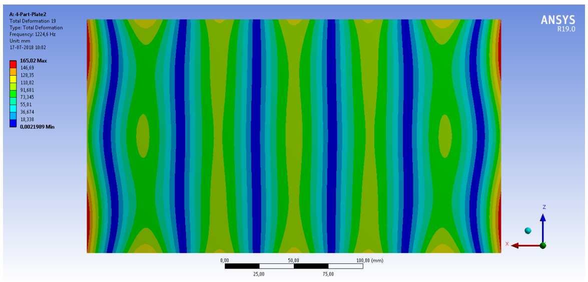

(a) Original - 1225 Hz.

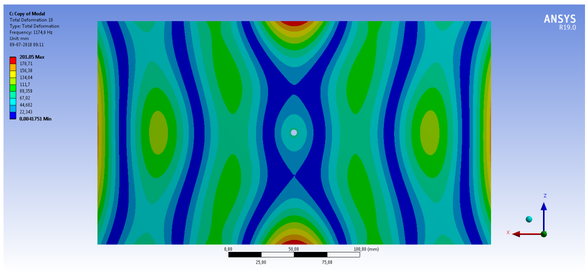

(b) 11.7g - 1175 Hz.

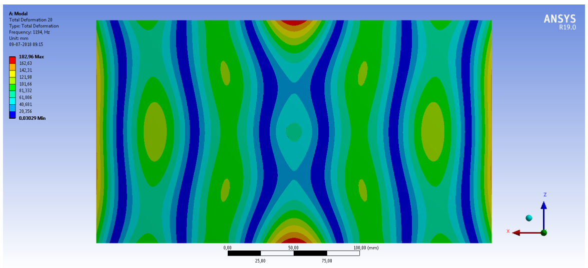

(c) Acc+FT - 1194 Hz.

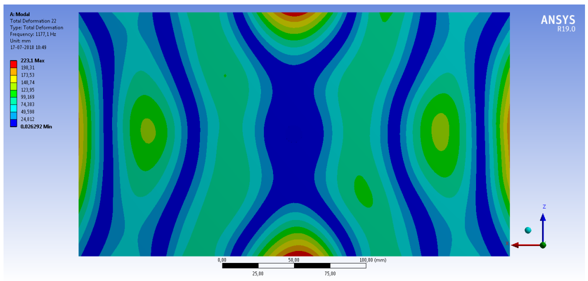

(d) Complete - 1168 Hz.

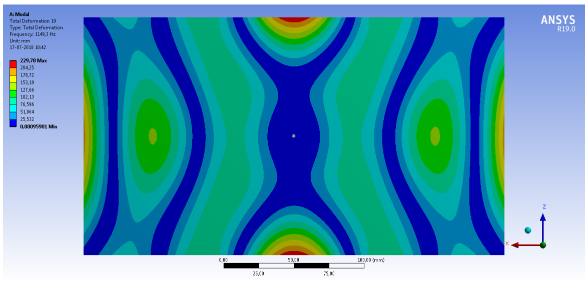

(e) Complete simplified - 1166 Hz.

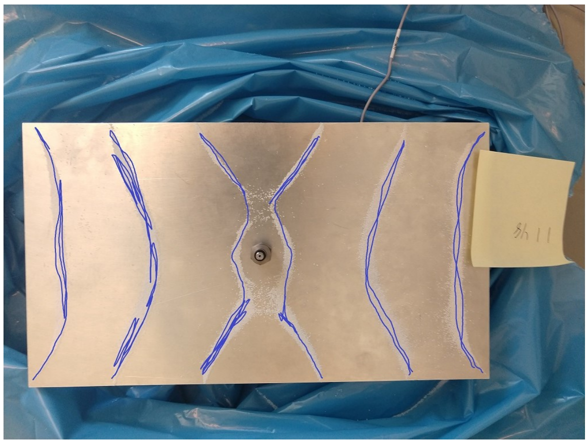

(f) Measured - 1148 Hz.

Figure 13.8: Five simulated mode shapes for mode 18 compared to the measured result.

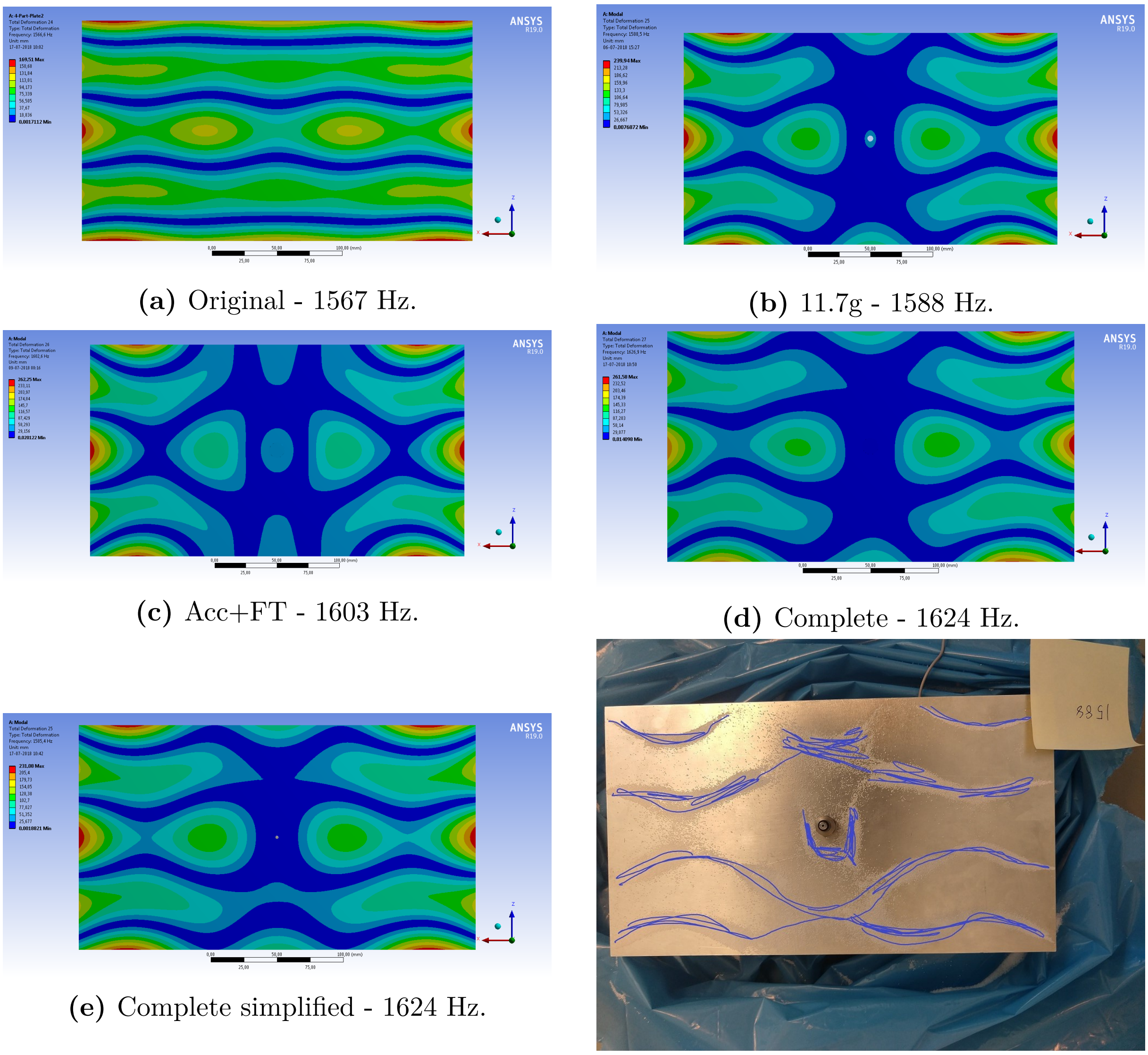

(a) Original - 1567 Hz.

(b) 11.7g - 1588 Hz.

(c) Acc+FT - 1603 Hz.

(d) Complete - 1624 Hz.

(e) Complete simplified - 1624 Hz.

(f) Measured - 1588 Hz.

Figure 13.9: Five simulated mode shapes for mode 23 compared to the measured result.

In the measurement sound was radiated at 1416 Hz and a mode shape was found using fine salt. In the previous analytical and simulated work this mode shape did not appear. In the simulation including a mass loading in the centre a it did.

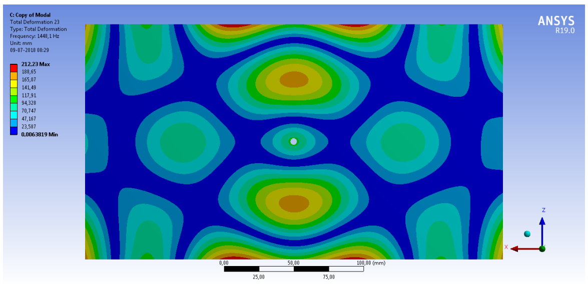

(a) 11.7g - 1448 Hz.

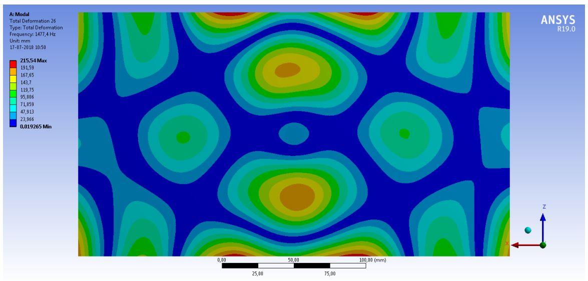

(b) Complete - 1477 Hz.

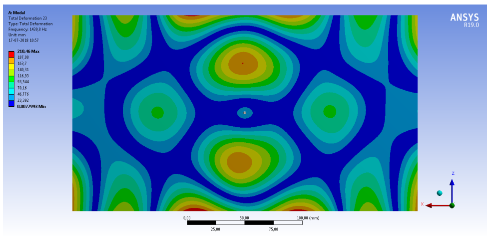

(c) Complete simplified - 1440 Hz.

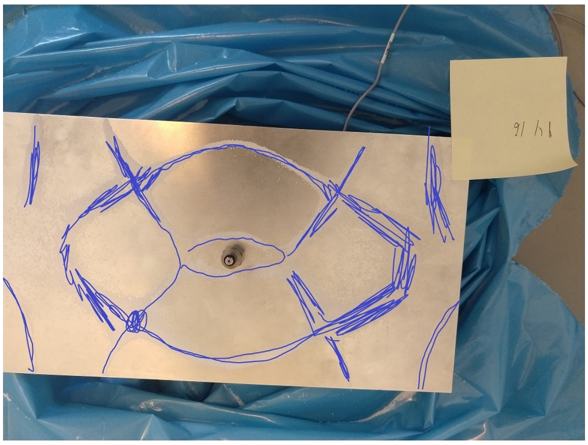

(d) Measured 1416 Hz.

Figure 13.10: Measured compared to simulated mode shape including mass loading.

13.3.2 Summary modal analysis

The increased level of detail in the simulated structure has improved not only the found eigenfrequencies but also the determination of mode shapes compared to measurements. Adding a point mass to the excitation position in combination with accounting for the spring characteristics of the shaker yields good results in determining eigenfrequencies and mode shapes. By also including the geometry of the force transducer and accelerometer some mode shapes where 'distorted'. For this reason the possible candidates 'Acc+FT' and 'complete' are not considered.

Two systems remain. They do not model the same situation and should be compared to different measurement results. The system '11.7g' should be compared to the column 'Plate+2' in table 12.1 whereas 'complete simplified' should be compared to the column 'Plate+1+2'. The two sets of measured data comes from the input impedance and the microphone signals respectively.

Plate+2	11.7g	error in Hz	error in %	Plate+1+2	Complete simplified	error in Hz	error in %
87 Hz	86 Hz	1	1	unknown	81 Hz	NaN	NaN
274 Hz	273 Hz	1	0	256 Hz	245 Hz	11	4
450 Hz	482 Hz	32	7	496 Hz	482 Hz	14	3
	463 Hz	13	3	400 Hz	415 Hz	15	4
932 Hz	911 Hz	21	2	864 Hz	860 Hz	4	0
1168 Hz	1175 Hz	7	2	1148 Hz	1166 Hz	18	2
1460 Hz	1588 Hz	128	9	1588 Hz	1624 Hz	36	2
	1448 Hz	12	1	1416 Hz	1440 Hz	24	2

Table 13.2: The errors for the two possible simulation system candidates. The column names refer to the setups described in section 13.2 and the percentage errors are calculated with the measurement as reference.

From the table above it is seen that both simulation systems are close to their respective measured results. In the case of '11.7g' large errors arise at the points where the two resonance frequencies could not be clearly separated in the measurement. Therefore it is likely that the simulation is in fact more accurate than the measurement.

Both systems seem to be suitable in terms of determining a correct frequency but the complete simplified is slightly better at including the asymmetries of the plate mounting in the mode shape results.

13.3.3 Persistent errors

Some degree of error in the determination of eigenfrequency is to be expected. In an unpublished Grundfos study where a vibration measurement engineer and a finite elements expert collaborate in a project examining how to mount a structure in measurements to allow for direct comparison with Finite Elements analysis they found that errors of 2-3% are the least one can expect - and that this would require detailed fitting of the simulation to the measurement. The accuracy of eigenvalue determination using FEM is examined in [Fried, 1971] in an attempt to predict the errors using a model. In this study results from studies performing measurements are compared to FEM results and the errors are discussed. In this case the errors for simple plate like structures are about 1% for high eigenvalues. In a study by [Duvigneau et al., 2016] the differences are much larger, in the order of 10%.

A few additional factors have been considered to see if they would influence the results:

- Using a static structural analysis before the modal analysis to simulate the strain on the plate caused by the tight screw fit of accelerometer and force transducer. No large difference in results followed.

- Including gravitational acceleration in the simulation. No large difference in results followed. The outermost edges of the plate deformed about 0.1 mm due to this static load.

13.4 Parameter sensitivity study

In Appendix E a parameter study examining the modal analysis's sensitivity to variation in plate dimensions and material properties is presented. The width, length, thickness, Young's modulus and centre hole location are varied within tolerances and the resulting changes in resonant frequencies listed. In general the variations in resonant frequencies due to this are of the same magnitude, or larger, than the errors listed in table 13.2.

The parameter to which the simulation is the most sensitive is the plate thickness. Fortunately this parameter is quite well defined as the plate is rolled with an accuracy much better than the callipers used in determining thickness. The Young's modulus also influence the results drastically - this parameter is part of the defining material properties and as such the specifications should be somewhat accurate.

13.5 Improved harmonic analysis

Two improvements on the harmonic analysis are considered, namely including additional frequencies and changing the damping ratio of the system.

13.5.1 Additional frequencies

In the original harmonic analysis only the resonance frequencies were included in the study. By cheating and running this data trough the auralization algorithm that will later be discussed it was found that this approach resulted in a sound which was much to tonal. The assumption that all vibration happens at resonance frequencies is based on undamped structures, which as the next subsection will show might not be as much the case as expected. To account for this additional frequencies are included to model the decrease in amplitude as a frequency moves away from resonance.

The new harmonic analysis is made so that it includes all eigenfrequencies found in the preceding modal analysis plus 150 additional frequencies chosen by ANSYS. The 150 points are logarithmically distributed in the frequency range 20 Hz to 20 kHz. The choice off 150 points is made as a trade-off in terms of sound quality and computational load in both ANSYS and the following sound generation algorithm. To give context the modal analysis results in about 250 eigenfrequencies, so 150 additional analysis points yields a significant increase in computational load and storage requirements.

13.5.2 New damping ratio

It can be realized from the audio measurements that the plate is probably not so undamped as originally though. In subsection 8.9.4 a damping ratio of $\zeta = \eta/2 = 5 \cdot 10^{-5}$ was used corresponding to that expected for aluminium. What was not accounted for is the fact that the mounting significantly increases the damping of the system. From the measurements it is possible to determine the damping at each resonance based on the 3 dB bandwidth of the acceleration [Cremer et al., 2005]. Below B&K Pulse LabShop 22 is used to determine the 3 dB bandwidth at three of the clearest resonances on the acceleration. This is done using the 3 dB bandwidth cursor from the cursor menu.

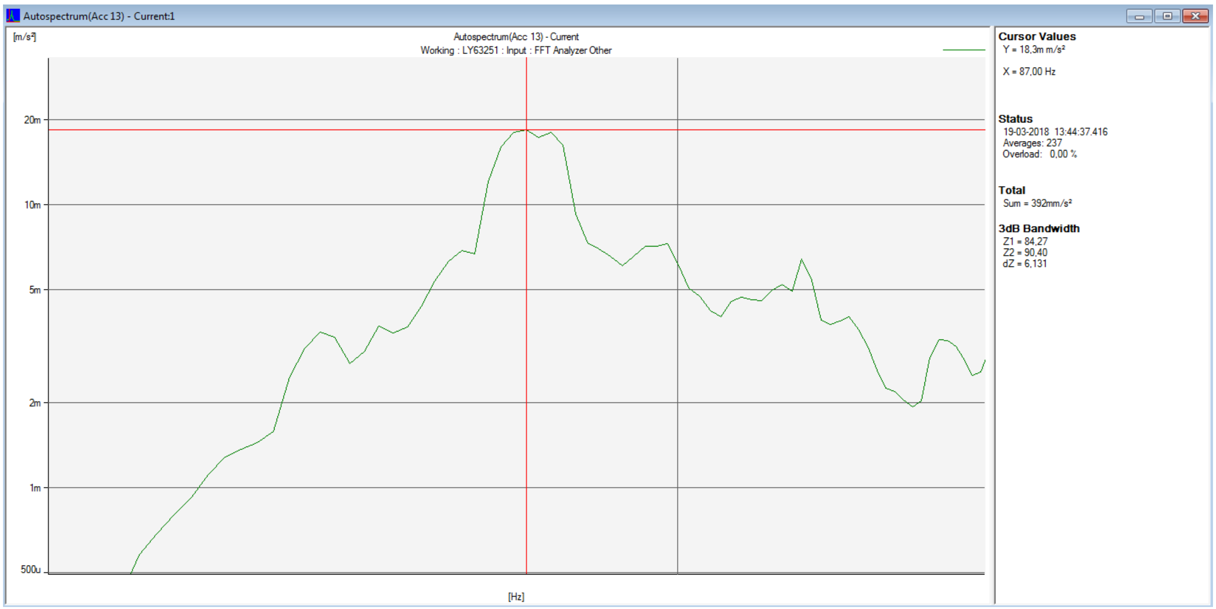

Figure 13.11: Zoom on acceleration at 87 Hz.

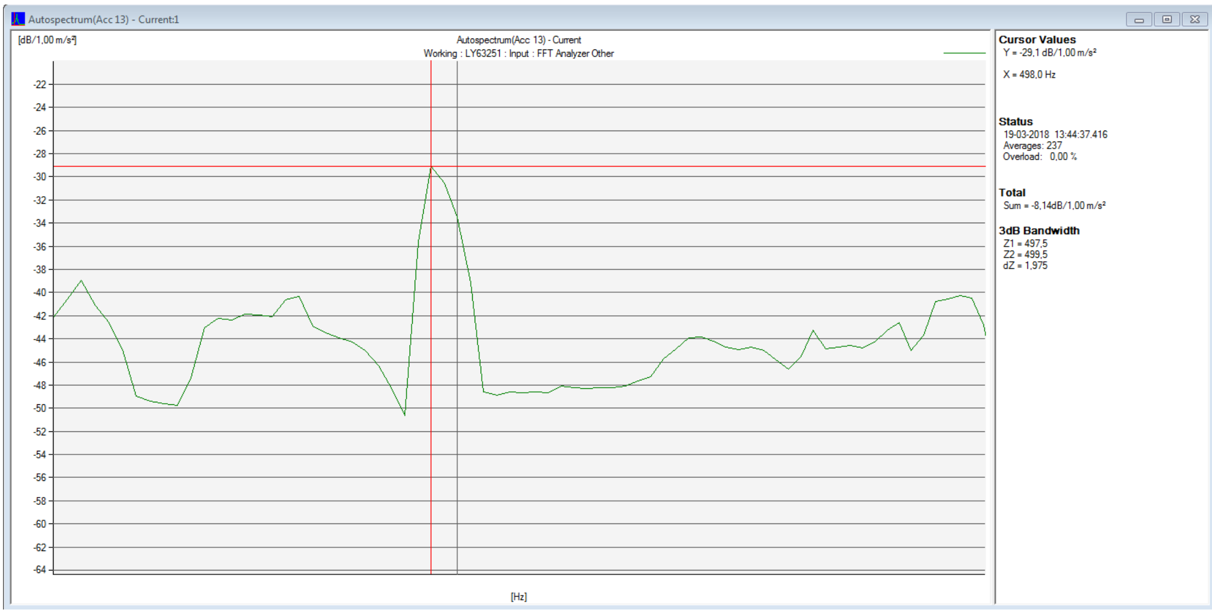

Figure 13.12: Zoom on acceleration at 498 Hz.

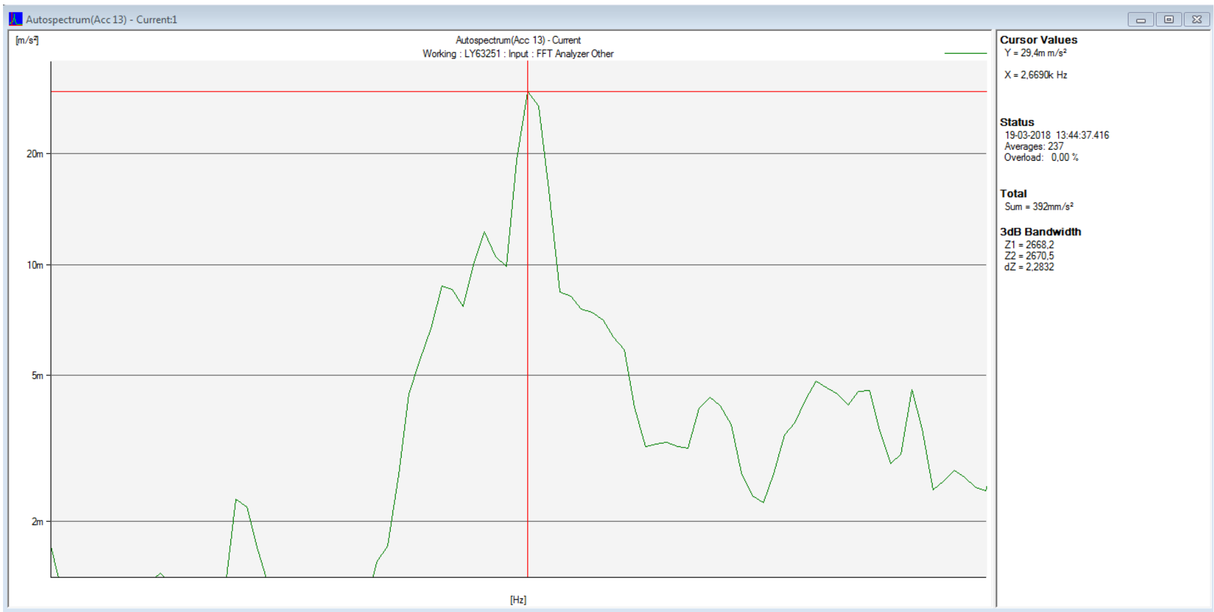

Figure 13.13: Zoom on acceleration at 2669 Hz.

The damping ratio is calculated as $\zeta = \eta/2 = \Delta f/(2 \cdot f_0)$:

Frequency	Δf	η	ζ
87 Hz	6.1 Hz	0.070	0.035
498 Hz	2.0 Hz	0.004	0.002
2669 Hz	2.3 Hz	$8.6\ 10^{-4}$	$4.3\ 10^{-4}$

Table 13.3: Measured loss factors/damping ratios for three frequencies.

Based on table 13.3 it is clear that the original value for damping was underestimated. Unfortunately the damping ratio cannot be measured at very high frequencies, since the acceleration spectra is not 'clean' enough - even after averaging. The affect of using the different damping ratio candidates is examined below.

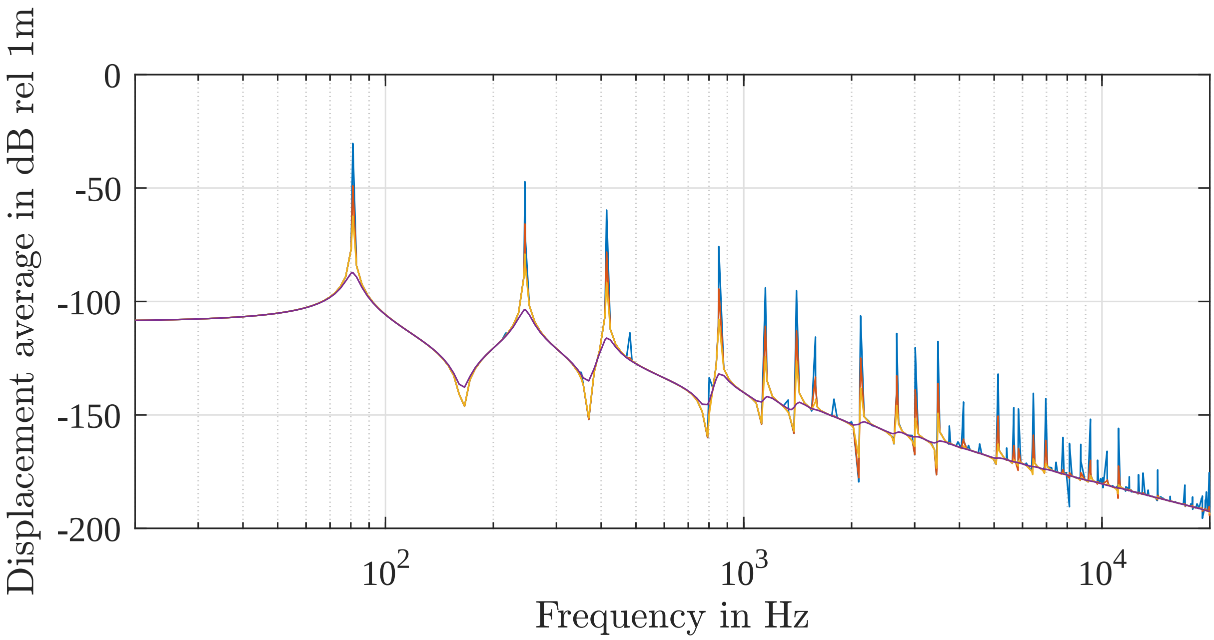

Figure 13.14: The magnitude response for the plate using four different damping ratios. $\zeta = 5 \cdot 10^{-5}$(—), $\zeta = 4.3 \cdot 10^{-4}$(—), $\zeta = 0.002$(—) and $\zeta = 0.035$(—). The values are exported from frequency responses of the entire top face of the plate to avoid hitting a node at a single position. In the final algorithm a frequency response is extracted per node.

From figure 13.14 it is clear that the damping ratio drastically affect the amplitude of the vibration. E.g. the first peak where the difference between using the measured damping ratio and the original is about 50 dB. Unfortunately ANSYS does only allow a single damping ratio to be used for each study. Therefore the analysis is split in several smaller frequency bands and vary damping with frequency. The frequency bands are selected as the three decades from 20 Hz to 20 kHz, except the first which is extended to 300 Hz, since the second mode has a measured damping ratio closer to 0.035 than 0.002 that being 0.031.

13.5.3 Summary harmonic analysis

The new harmonic analysis will be performed in frequency bands with additional frequency points included in the study. On top of this a frequency varying damping ratio is used.

Frequency Range	Additional points	ζ
20-300 Hz	50	0.035
300-2000 Hz	50	0.002
2-20 kHz	50	$4.3\ 10^{-4}$

Table 13.4: Loss factors/damping ratios and additional logarithmically spaced analysis point for three frequency bands.

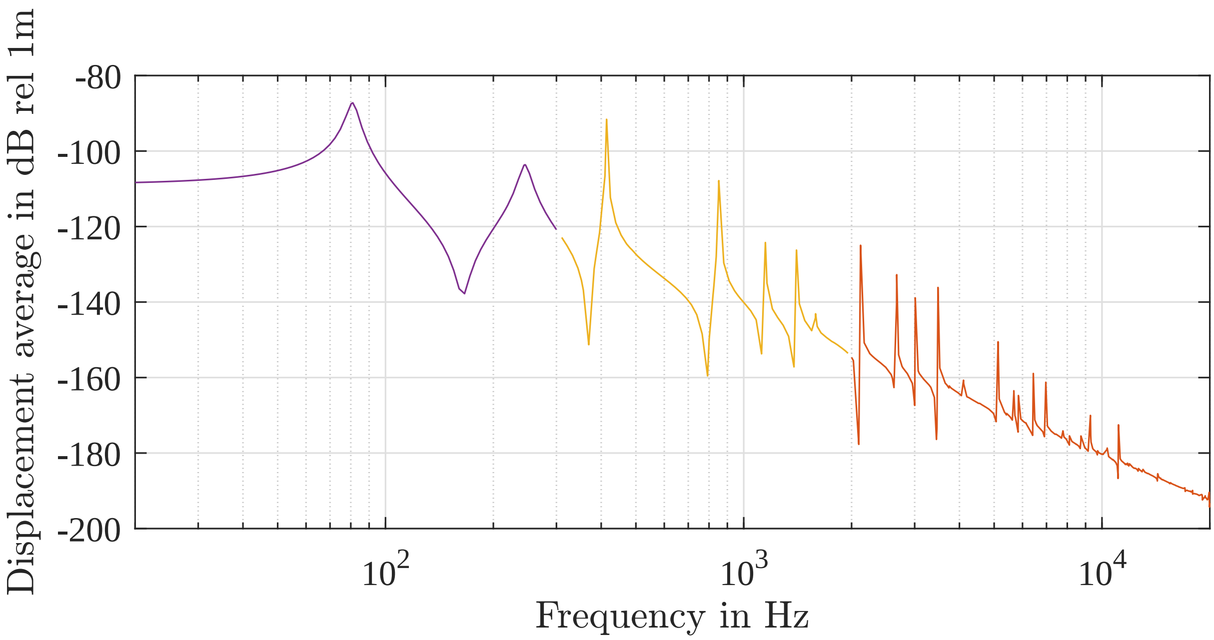

Figure 13.15: The magnitude response for the plate combining three different damping ratios. $\zeta = 4.3 \cdot 10^{-4}$(—), $\zeta = 0.002$(—) and $\zeta = 0.035$(—). The values are exported from frequency responses of the entire top face of the plate to avoid hitting a node at a single position. In the final algorithm a frequency response is extracted per node.

14 | Time varying signal

14.1 Examining the problem

Through the measurements it has been determined, by listening, that the sound recorded at the microphones seems to be time varying. This is examined further by means of a spectrogram.

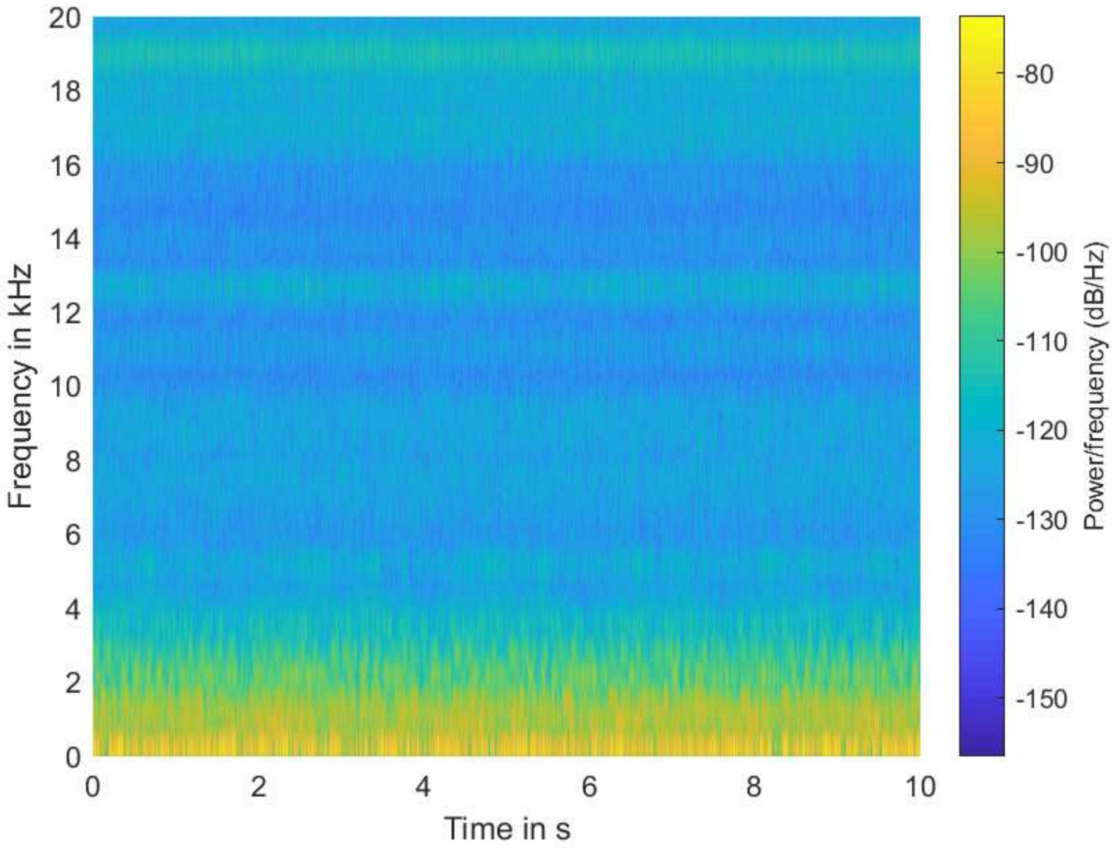

Figure 14.1: A spectrogram of the recording at M20. The Matlab function 'spectrogram' has been used with a hamming window with a length of 128 an overlap of 120 and an FFT order of 1024.

From figure 14.1 it is clear that some time variance is present and as this is audible and changes the sound feel a lot the auralization algorithm should account for this. To do so the phenomena causing it should first be understood. The hypothesis is that the displacement of the plate is so large that the time varying propagation distance is not negligible. The displacement is naturally caused by the bending of the plate. Also the shaker which moves the plate up and down might also play a part.

A simple case is studied to examine if the displacement of an oscillator is audible. A single

950 Hz oscillator is moved back and forth with an amplitude of 1 cm and a frequency of 100 Hz. The 950 Hz tone is propagated from the sender position at (0,0,0) m plus the displacement caused by the 100 Hz movement to a reviver 2 meters away (0,2,0) m. Both the amplitude and phase changes are accounted for even though the phase is expected to be the dominating cause. A Matlab script calculating the sound caused by a stationary source and a moving source is supplied called 'MovingSource.m'. Here a link to the audio is given so that the reader can hear the difference themselves.

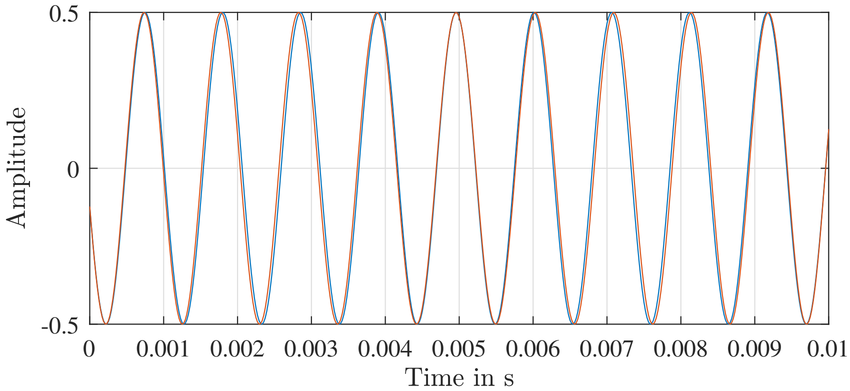

(a) Time plot of the two tones. Pure 950 tone (—) and osculating tone (—).

(b) A pure 950 Hz tone followed by a 950 Hz tone oscillating at 100 Hz - Link.

Figure 14.2: Results from small experiment with a osculating sound source. The fact that the oscillating source sometimes arrive at the receiving position before the stationary source and sometimes after can be seen using a sufficient zoom-level.

To further study if time dependant propagation might be the cause of the variation over time seen in figure 14.1 a zoom on the spectrogram of the recorded sound and the sine from figure 14.2 is shown. The reader should note that the recorded sound naturally does not only contain a single frequency as the system has damping. The generated single tone has a single frequency of oscillation at a high amplitude; the recording naturally has many frequencies of oscillation at lower amplitude. Furthermore the plots are made at different sample frequencies. Even though the two zooms on the spectrograms are made under different conditions and at different zoom levels the similarity of the phenomenon is clear in figure 14.3.

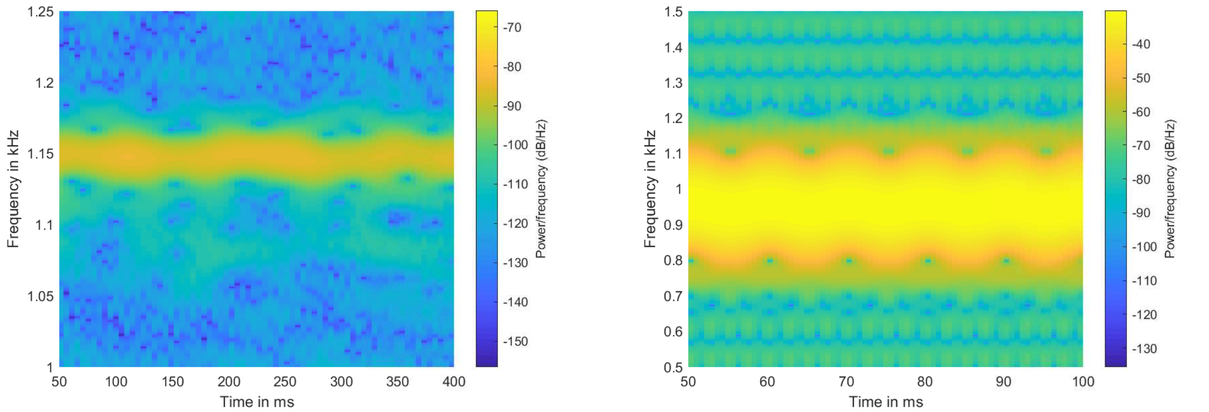

(a) Spectrogram of plate recording. fs=6553.6 Hz, frame size=512, overlap 480 samples, FFT order 2^{15}.

(b) Spectrogram of oscillating sine. fs=48000 Hz, frame size=512, overlap 480 samples, FFT order 2^{15}.

Figure 14.3: Zoom on the spectrograms of the recording as well as the generated oscillating sine.

As the effect of a single source oscillating is audible it is likely that the effect of thousands of oscillators moving is also audible. Therefore the time varying propagation distance should be included in the auralization of the plate.

14.2 Implementation

To include the time dependency in the sound propagation the position of each face in time and space is first calculated based on the results from the vibration analysis. Remember that only bending in the y-direction is considered. First the displacement of each node on the face at all frequencies as a function of time is calculated as a combination of amplitude and phase for that node. Then the contributions from each frequency is summed giving the displacement of each node as a function of time. Then the displacement of the face is calculated as the average of the displacement of the three nodes. The displacement is added to the equilibrium position of the face. From this the propagation delay and propagation decay can be calculated as a function of time using the relations described in subsection 10.1.1. Pseudocode for the implementation can be seen in Appendix F.

14.3 A note on time variant systems

A major drawback of the selection of a plate as 'object under study' is that it easily deforms a lot and therefore the setup is not linear time invariant (LTI). Due to this the traditional property of scalability from input to output does not hold. In LTI systems doubling the amplitude of the input will only double the amplitude of the output. In this system the displacements will be bigger which will affect the temporal part of the response. That being said no alternative to scaling is readily available so some scaling will be performed in the post processing.

Part V

Results

15 | Results

In this chapter the required post processing of the generated audio is applied so that recoded and simulated results can be compared. As a reference the measurement position M20 is used. The available microphone positions are listed in table A.4 and the one for M20 is (x,z,y)=(0.5376, 0.3108, 2.7300) m. The plate is turned with its length along the x-axis in both measurements and auralization and in both cases the centre of the plate is located at (x,z,y)=(0,0,0.094) m. The reason for mainly considering M20 is that it is the microphone position which is closest to directly above the plate. This will make the approximation to of the directivity of the faces in subsection 9.4.2, have the smallest error.

The frequency content of the sound recorded at M20 is displayed again below for easier readability:

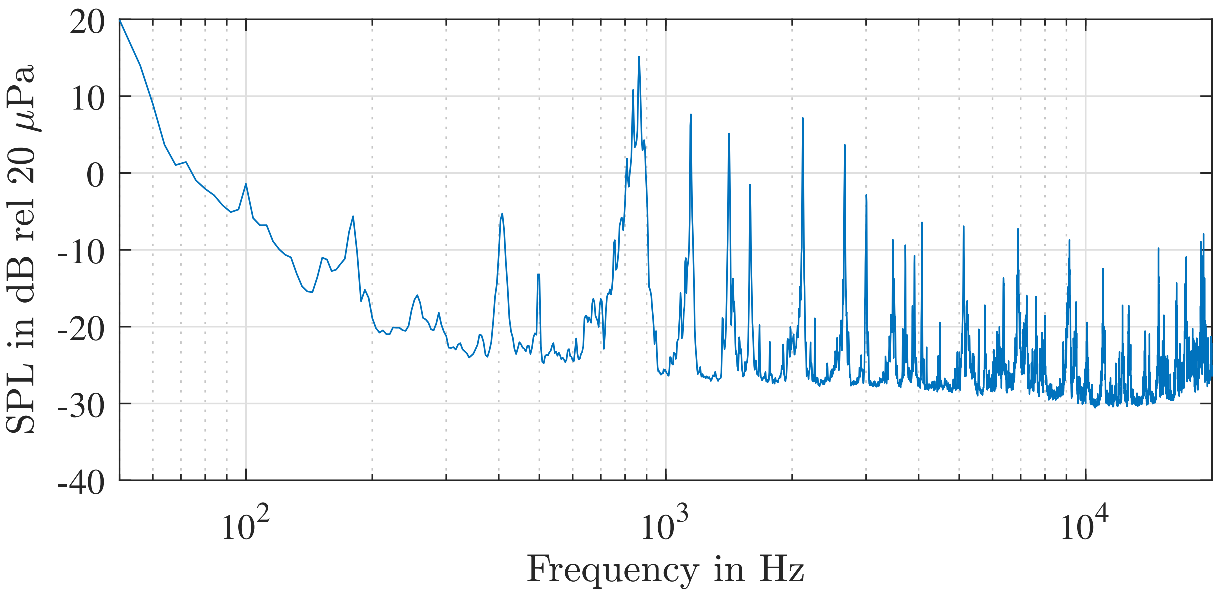

Figure 15.1: The sound pressure level at M20 microphone position.

As hinted previously some post processing is required to make the measurement data and the simulated data comparable. This chapter describes what has to be done in the two cases where:

1. The auralization is desired to replicate the measurement situation directly making the responses from the microphones the target.
2. The auralization is desired to replicate an idealized measurement situation by correcting the microphone recordings to what would have been if unit force was applied to the plate.

Therefore this chapter will show how to post process the gathered data for comparison in the two cases. An overview is given in figure 15.2.

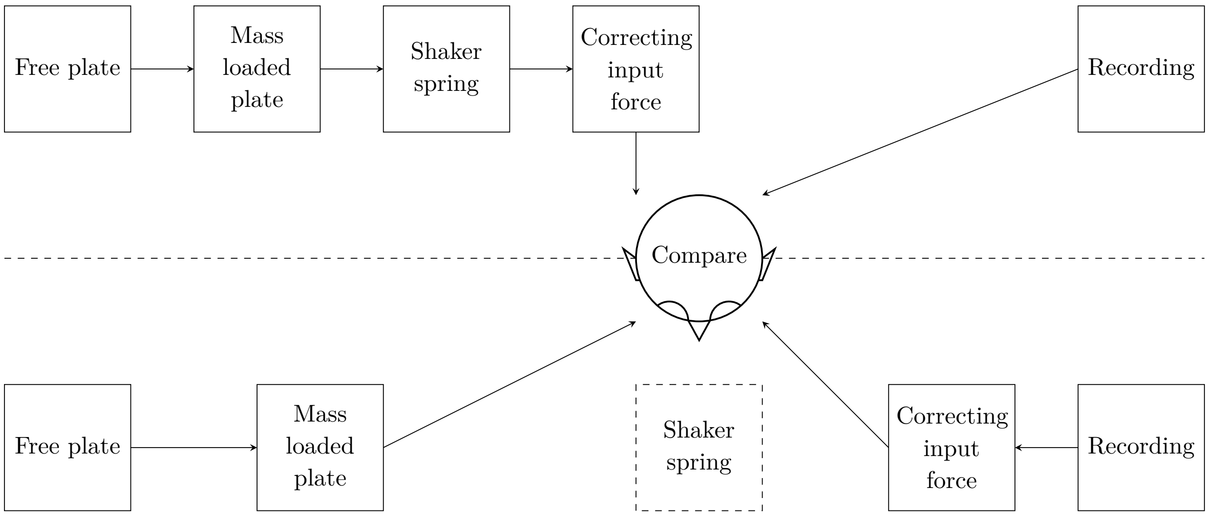

Figure 15.2: Schematic of the two listening cases. Top Situation 1. Bottom situation 2. The dashed box 'shaker spring' is not accounted for in situation 2.

15.1 Using 'complete simplified'

This subsection contains the results from the setup 'complete simplified' and should be compared to the microphone recordings. The reader is reminded that the input in the simulation is made using unit force as input, which result in large SPL. The items to account for in the post processing in this case are:

- The force input to the plate.
- The dipole characteristics of the plate.
- The first reflection from the floor.

Below the output from the Matlab simulation is shown before post processing:

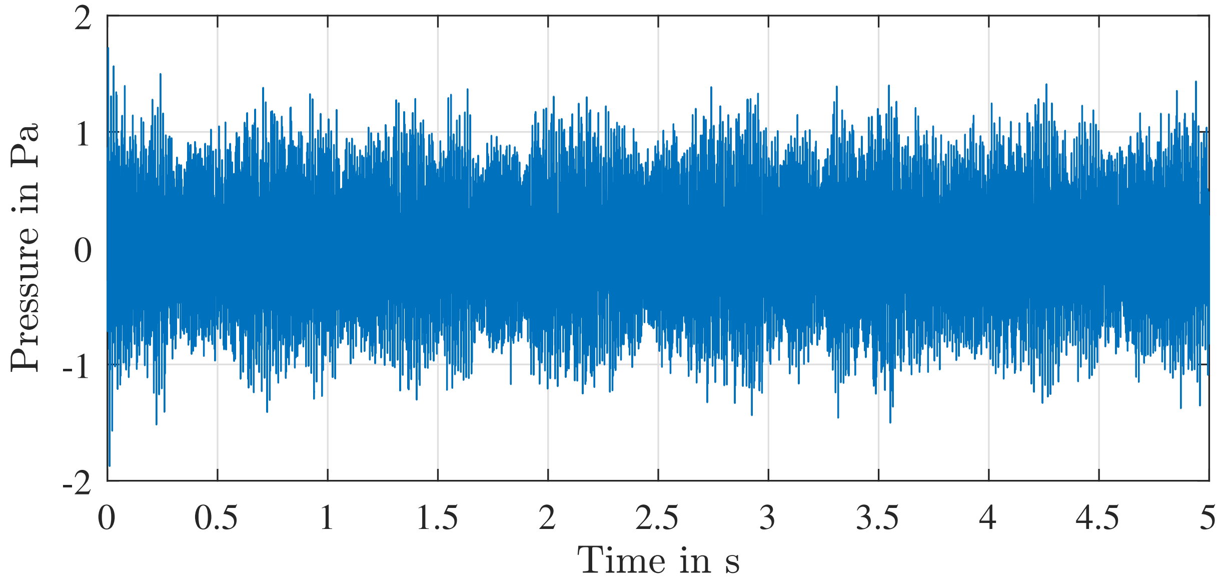

Figure 15.3: Time signal from sound generation algorithm using the results from FEM 'complete simplified' as input.

In figure 15.3 it is clear that the result has some time variance. This is due to the displacement of the plate being included in the sound generation.

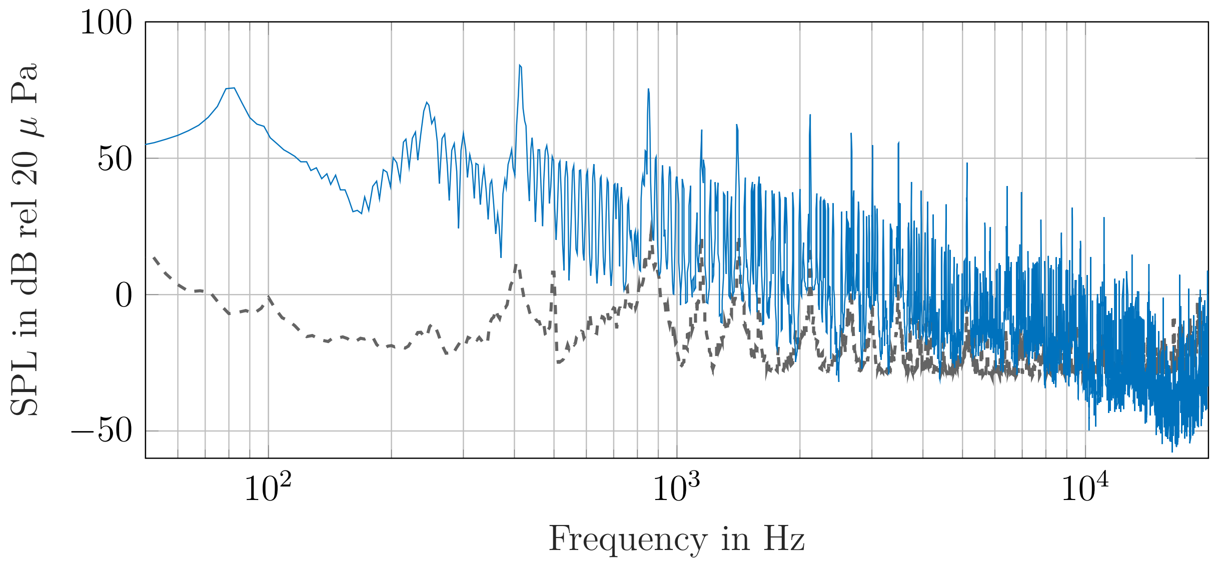

Figure 15.4: Frequency spectra from sound generation algorithm using the results from FEM 'complete simplified' as input. Reference response from figure 15.1 (– –).

The frequency content of the generated sound has a tonal behaviour as expected and the frequencies with the highest amplitude are those determined to be symmetric eigenfrequencies in table 13.2. The two lowest frequency modes at 87 Hz and 245 are included in the sound as expected since the dipole characteristics has not been handled by sound generation but will be added later. The SPL is very large as the input force has not yet been accounted for. Also the tonal balance seems a bit off since the recording figure 15.1 has the levels decreasing up to about 4 kHz after which they seem to stabilize. For the simulated sound the level is continuously decreasing with frequency.

15.1.1 Force input to plate

The force put into the plate has been measured and it is tempting to directly correct for this by filtering the simulated unit force response with the measured one. Two issues arise with this approach. Firstly the resonant peaks in the simulation are at different frequencies than in the measurement - so the corrections would be done at shifted frequencies. Secondly the measurement system and the simulation is running at different sample rates, 65.5 kHz and 48 kHz respectively the force cannot be used directly.

Instead an approximating symmetric FIR filter generated using Matlab's FIRLS function is used. The filter is designed to fit the response up to 24 kHz using 1025 taps yielding a lowest included frequency of 47 Hz. Only using 1025 taps makes the filter less 'jumpy' compared to the force measurement while still following the trends. The measured force and the approximating FIR-filter can be seen in figure 15.5.

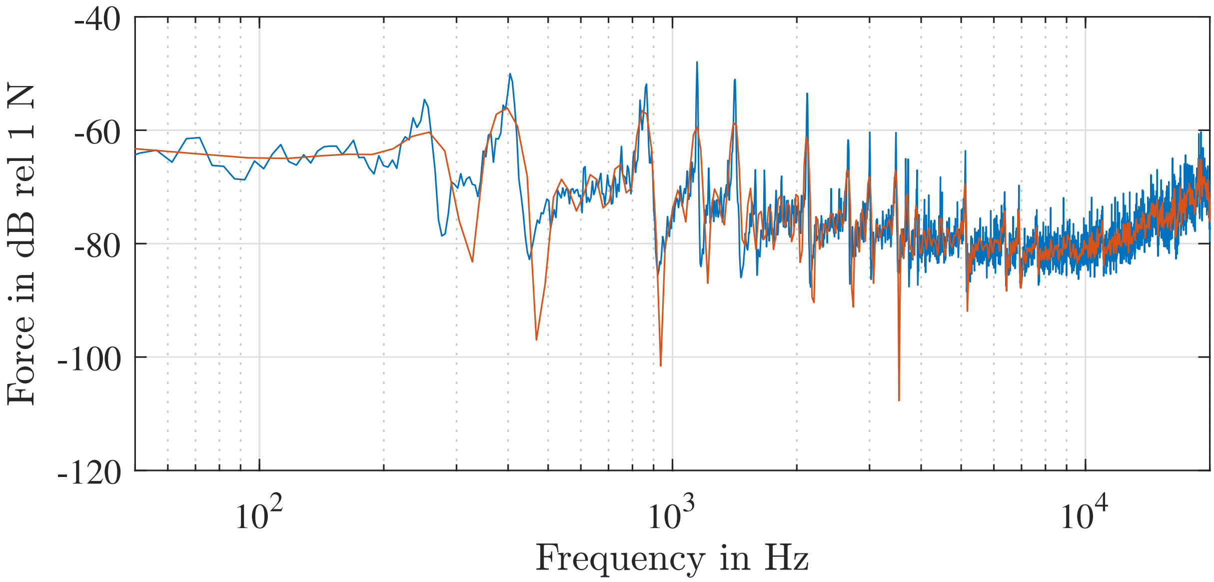

Figure 15.5: The measured input force (—) and the approximating filter (—).

The simulated sound before and after the filtering is shown in figure 15.6

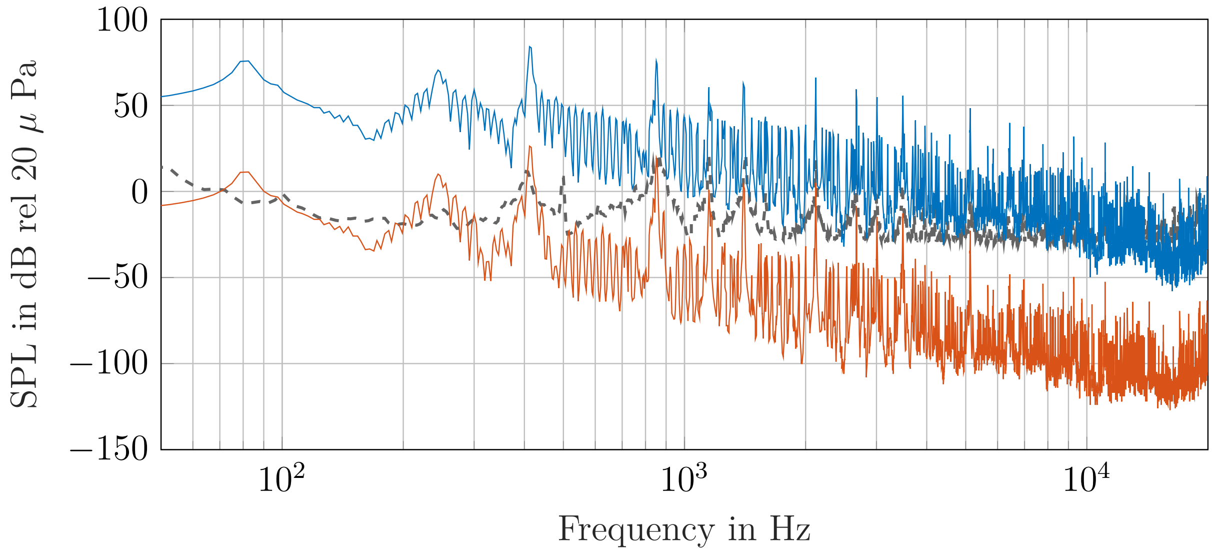

Figure 15.6: The frequency spectra from sound generation algorithm before (—) and after (—) correcting for the input force. Reference response from figure 15.1 (– –).

Correcting for the input force has moved the level to roughly the same order of magnitude as the recording in figure 15.1.

15.1.2 The dipole correction

Here the dipole filter described in subsection 9.4.3 is applied to the audio.

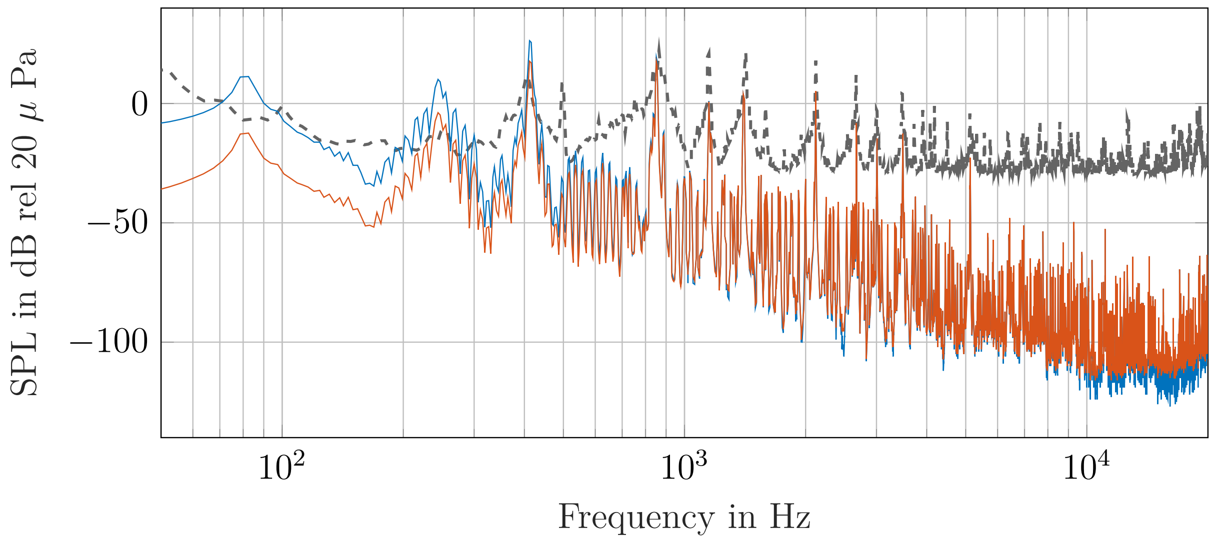

Figure 15.7: The frequency spectra from sound generation algorithm before (—) and after (—) correcting for the dipole characteristics of the plate. Reference response from figure 15.1 (– –).

Correcting for the dipole characteristics of the plate the low frequency output has been reduced. The dipole filter has a small gain at high frequencies, 0.02 dB at 10 kHz, but the level at high frequencies is increased much more than this - this could be due to numerical issues since the values are very small.

15.1.3 Floor reflection

The reflection from the floor is calculated as described in subsection 10.4.2. Filtering the simulated sound with this comb filter yields the following response:

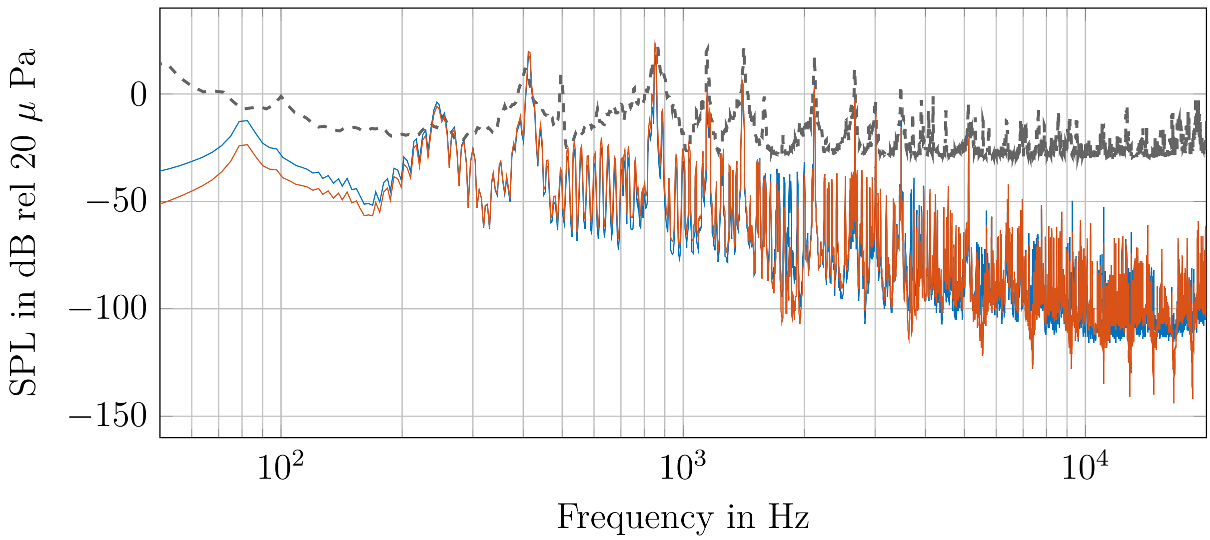

Figure 15.8: The frequency spectra from sound generation algorithm before (—) and after (—) including the comb filter. Reference response from figure 15.1 (– –).

15.1.4 Results

Finally the recorded sound and the simulated sound at M20 can be plotted together.

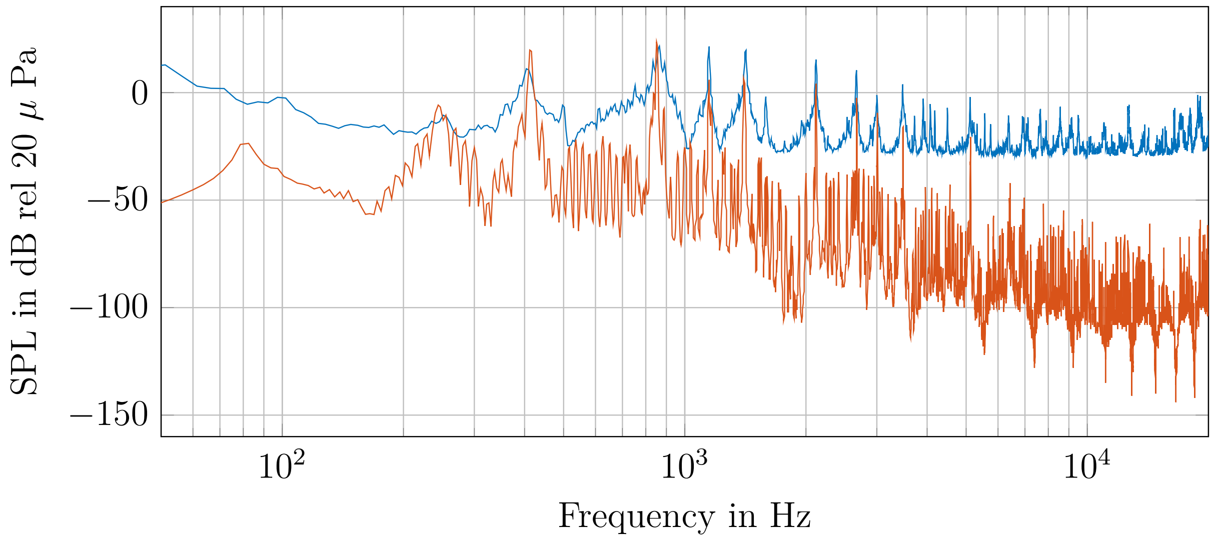

Figure 15.9: The frequency spectra from the recording at M20 (—) and the output from Sound generation algorithm (—).

As an alternative representation the recorded and simulated sound is plotted in 1/3 octave bands. This is done directly from the recorded sound so no averaging has been performed. The Matlab function 'octaveFilter' is used with a filter order of 8 and one of the octave bands has 1000 Hz as centre frequency.

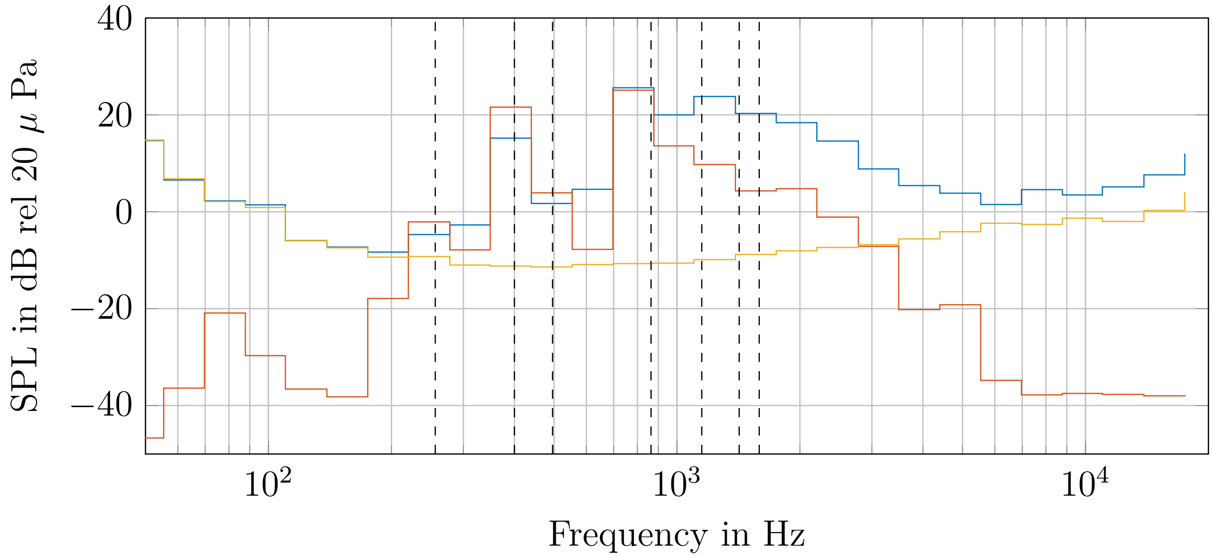

Figure 15.10: The 1/3 octave band filtered sound from the recording at M20 (—) and the output from sound generation algorithm (—). The output from the recording at M20 with the plate removed and the shaker exciting the force transducer and accelerometer only (—). Black lines (**- -**) indicate where measured resonances where found in table 13.2 column 'Plate+1+2'.

The results from the sound generation algorithm which tries to replicate the measurement situation are not all to promising. The phenomena which are observed are:

1. The level is underestimated in the sound generation compared to the measurement.
2. The low and high frequency responses are further from the measurement than the mid frequencies.
3. The resonant peaks are narrower in the sound generation compared to the measurement.

The low frequency deviation is a result of the measurement environment, which has an increasing noise level at lower frequencies. The sound recorded at very low frequencies can only be created by the background noise and not the plate, since it cannot radiate low frequency sound. The yellow line in figure 15.10 also shows shows the sound emitted from the setup without the plate - at low frequencies it follows the background noise level of the room as specified in the certification. At higher frequencies the shaker rises the noise floor slightly above the values in the certification.

The high frequency error might be due to one of three things. Firstly it was not possible to measure a damping ratio for very high frequencies in subsection 13.5.2, so the one measured at 2669 Hz is used all the way to 20 kHz. It is likely that this overestimates the damping, which would decrease the sound level at high frequencies. The second issue is the frequency response of the force transducer. If the force transducer over estimates the force above 2 kHz as described in subsection 12.2.3 then the filtering correcting for the input force will result in an underestimated sound pressure level. On top of these two the sound radiated from the shaker itself might be a factor as it is predominantly high frequency as shown in the dotted grey line in figure 12.5.

The fact that the overall level is underestimated can in part also be credited to the background noise, which in the measurement adds with the noise from the plate. This is primarily visible in the unaveraged data in figure 15.10 as the averaging puts the noise floor at least 20 dB below the resonant peaks as shown in figure 12.5. In fact the peaks of the generated sound in figure 15.9 are almost at the same level as those recorded for mid frequencies. This leads to the issue that the width of the peaks in the simulated sound is narrower than the recording. The with of the peaks are determined by the damping ratio which is included in the simulation. However each resonance is only modelled with a single oscillator. In order to give the single oscillator a width multiple lower amplitude oscillators should be included around the resonance. Unfortunately doing so will result in closely spaced tones which cause amplitude modulation, which in turn ruins the sound quality.

Lastly some error, possibly large, will be introduced by filtering of the generated sound with the output from the force transducer in subsection 15.1.1. To avoid filtering the generated sound with something from the measurements another approach is considered below.

15.2 Using '11.7g'

This subsection contains the results from the setup '11.7g' and cannot be directly compared to the microphone recordings since the shaker is not included in the simulation. The items to account for in the simulation in this case are:

- The dipole characteristics of the plate.
- first reflection from the floor.

whereas the force input to the plate should be accounted for by processing the recorded sound. This is shown in figure 15.11 where the recording at M20 has been scaled with the frequency dependent input force as:

$$ModifiedRecording = \mathrm{IFFT}\left(\frac{\mathrm{FFT}(Recording)}{|\mathrm{FFT}(InputForce)|}\right) \tag{15.1}$$

Doing the above directly will include the measurement noise from the force transducer in the sound - which ruins the sound quality completely. To avoid this the averaging method is again used to average out the noise. To maintain the same frequency resolution, allowing for the spectral division, the time frames are zero padded to the same length as the full recording, 10 seconds. The averaging uses a hamming window with a length of 12802 samples and 75% overlap.

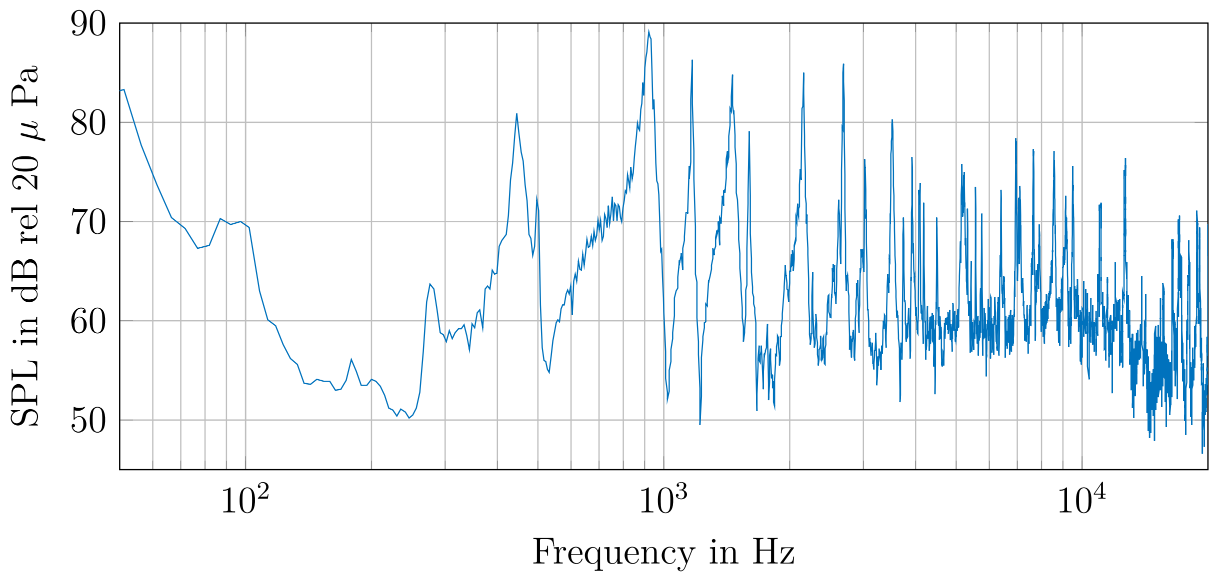

Figure 15.11: Frequency spectra from recording at M20 corrected to unit input force.

Below the output from the Matlab sound generation is shown before post processing:

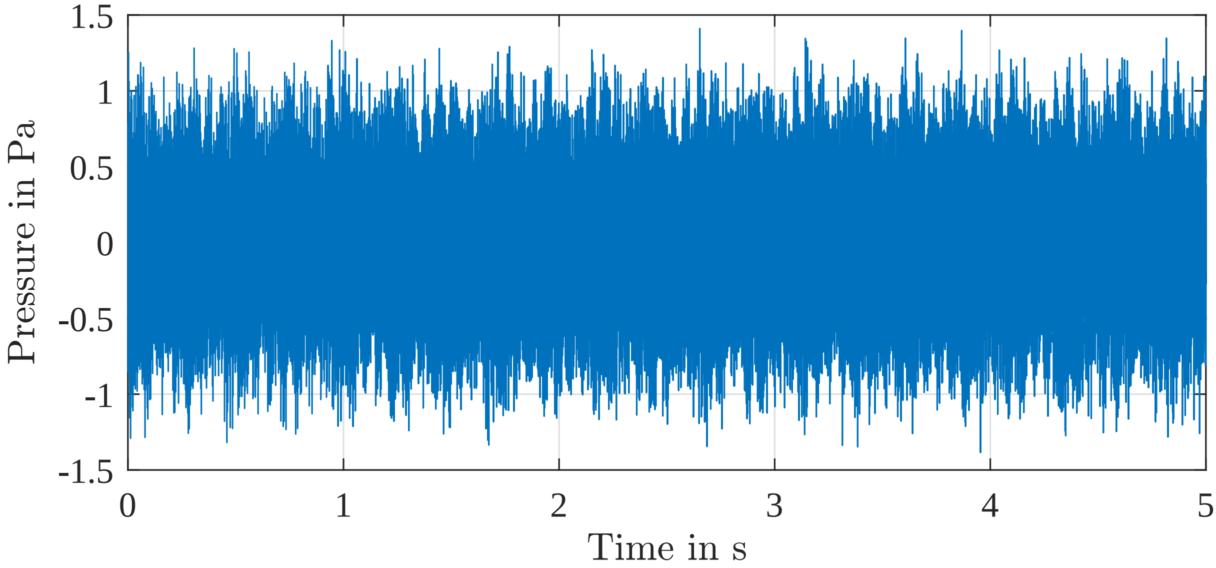

Figure 15.12: Time signal from sound generation algorithm using the results from FEM '11.7g' as input.

In figure 15.12 the time variance has decreased compared to figure 15.3 because here the plate is not allowed to be 'bouncing up and down' on the spring. The effect of including the displacement of the plate in the sound generation is still audible.

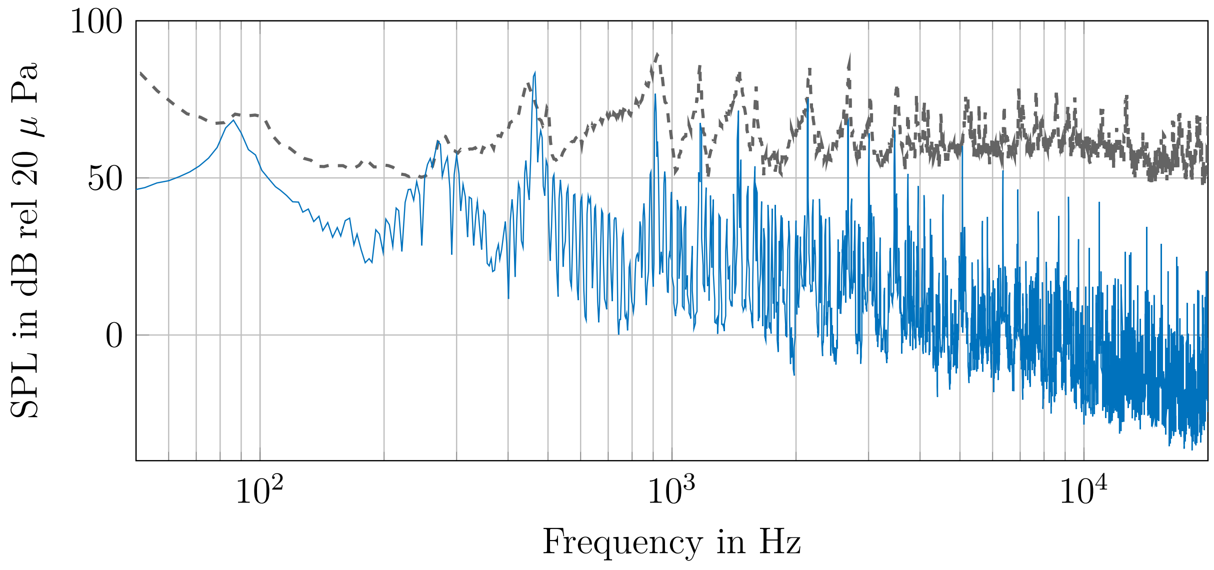

Figure 15.13: Frequency spectra from sound generation algorithm using the results from FEM '11.7g' as input. Reference response from figure 15.11 (– –).

As in section 15.1 the result is tonal and includes the low frequency vibration. The dipole characteristics and the input force have not been accounted for and the tonal balance seems to be off.

Comparing figure 15.11 to figure 15.13 it is noted that the order of magnitude is comparable as they both correspond to an input force of 1 Newton. It is also noted that correcting for the frequency dependent input force in the measurement changes the resonance frequencies in the recording to better align with the values in table 13.2 column 'Plate+2', and thereby also in terms of the resonant frequencies found in the simulation '11.7g'. The resonances are at 276 Hz, 455 Hz, 926 Hz, 1167 Hz, 1459 Hz and 1602 Hz.

15.2.1 The dipole correction

The dipole correction is done in the same way as in the other case using the filter designed in subsection 9.4.3.

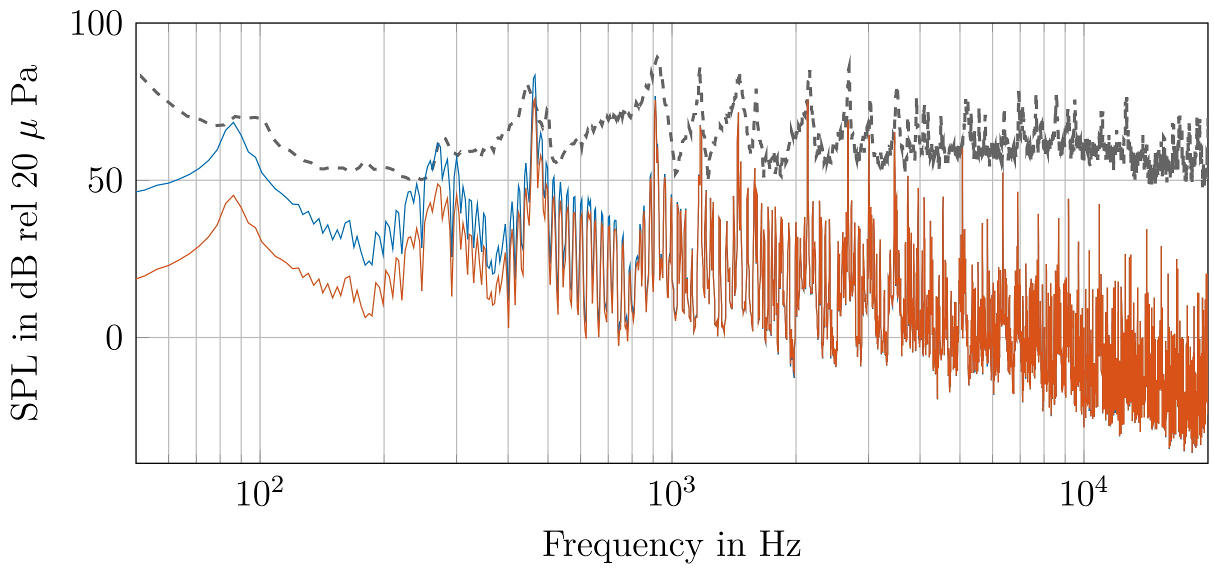

Figure 15.14: The frequency spectra from sound generation algorithm before (—) and after (—) correcting for the dipole characteristics of the plate. Reference response from figure 15.11 (– –).

15.2.2 Floor reflection

The reflection from the floor is again calculated as described in subsection 10.4.2. Filtering the simulated sound with this comb filter yields the following response:

 Christian Claumarch

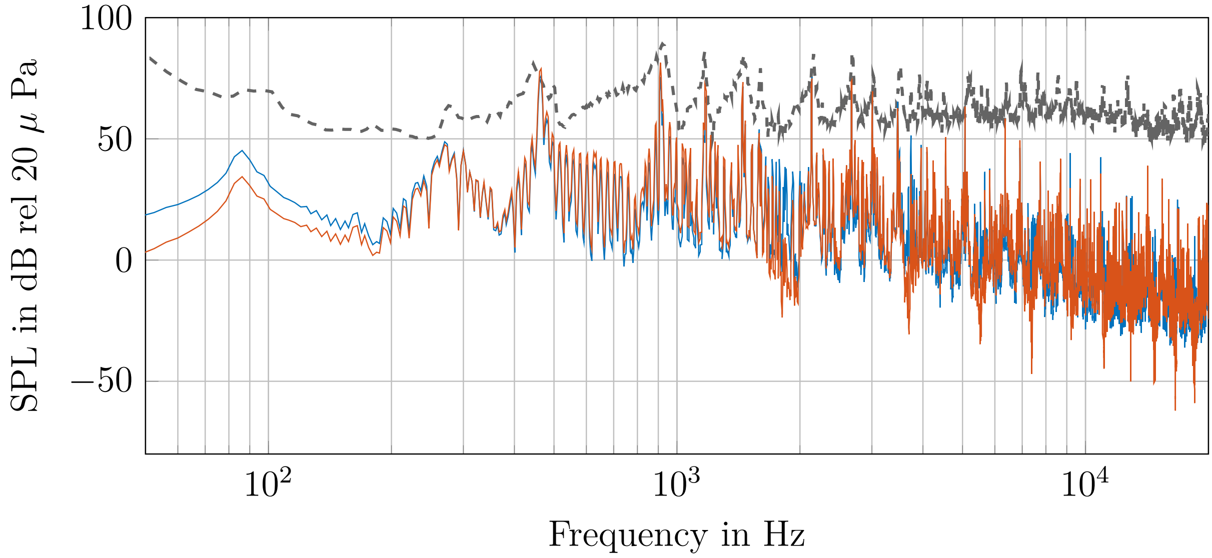

Figure 15.15: The frequency spectra from sound generation algorithm before (—) and after (—) including the comb filter. Reference response from figure 15.11 (– –).

15.2.3 Result

Finally the recorded sound and the simulated sound at M20 can be plotted together.

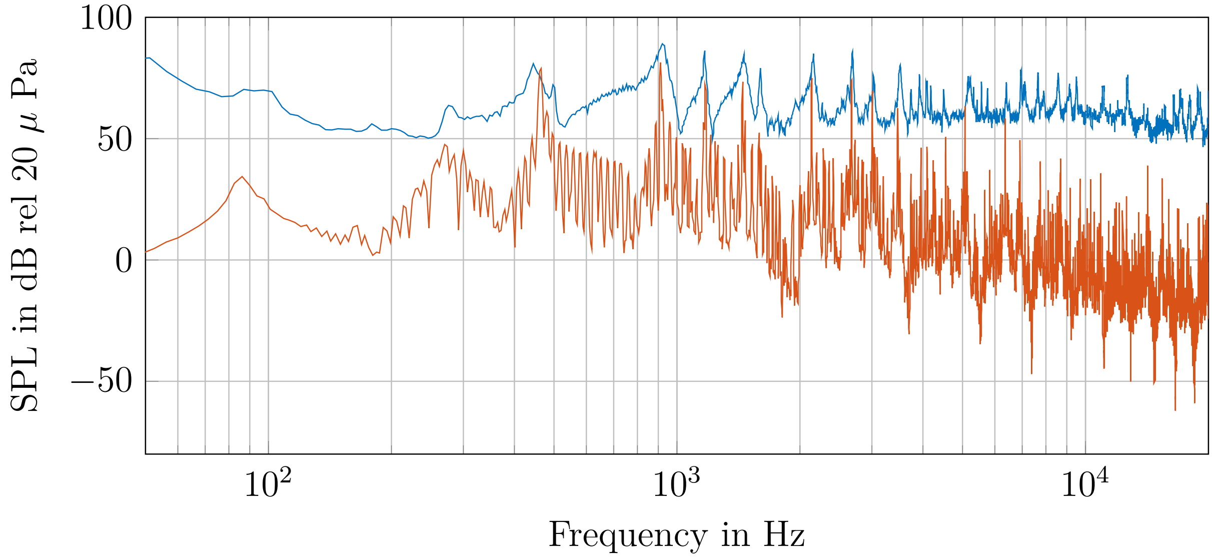

Figure 15.16: The frequency spectra from the recording at M20 corrected to unit input force from (—) and the output from sound generation algorithm (—).

Again 1/3 octave filtering as described above figure 15.10 has been applied to the data and the result is shown in figure 15.17.

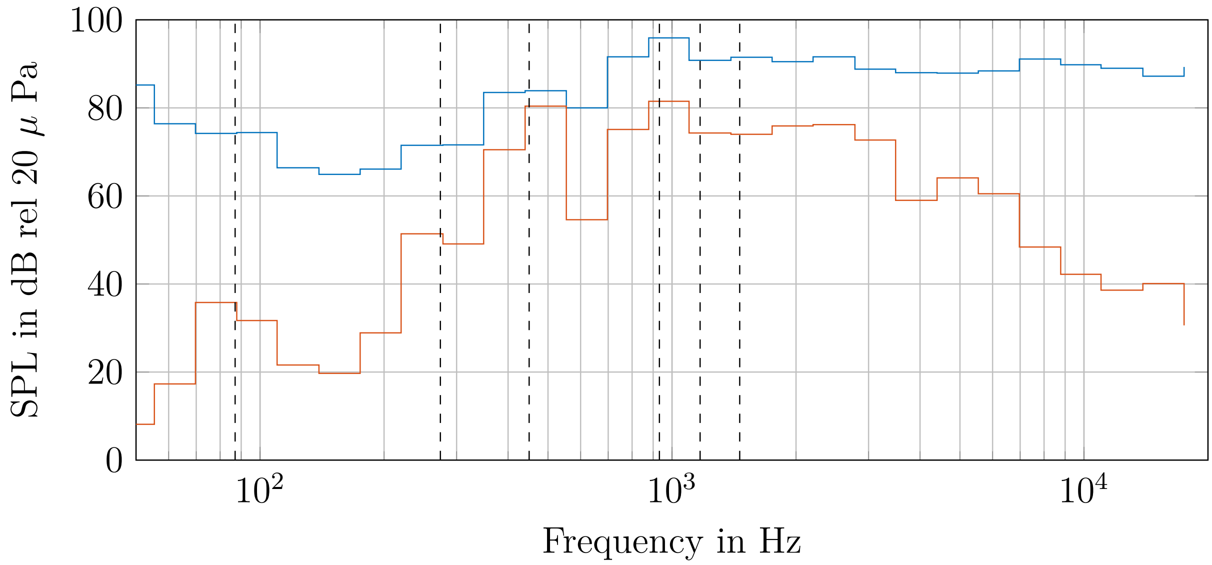

Figure 15.17: The 1/3 octave band filtered sound from the recording at M20 corrected to unit input force (—) and the output from sound generation algorithm (—). Black lines (- -) indicate where measured resonances where found in table 13.2 column 'Plate+2'.

Basically the same description of the errors from the sound generation as that given in subsection 15.1.4 applies here, so it will not be repeated. In this solution the overall level is even further off. The background noise is not plotted as it would require a scaling with the input force. Two sources are present in the background measurement. First the low frequency background noise of the room itself, which does not scale with the force put into the plate. Secondly at higher frequencies the primary noise source is the shaker. Here scaling would require that the shaker makes the same sound if forced to drive 1 N into an object - no matter the object. This is not the case thus a scaling does not make sense.

15.3 Listening test

Originally it was intended to perform a listening test to examine if the recorded and simulated sound could be distinguished from each other by a method such as three alternative forced choice. The listening test would take the sound generated above and present it binaurally as described in subsection 11.4.3. In case the auralization did not leave any doubt that this experiment would fail the algorithm a study of 'credibility' compared to the reference could be considered instead. As the sound quality is so low that even this study is be expected to yield poor results this experiment has not been performed either. For the same reasons it does not make sense to show plots of audio filtered with the HRTFs since the input is wrong.

To allow the reader to make their own opinion on the sound quality in the different cases audio-snippets are made available via the QR-codes/links below. The representation is not binaural as this requires a calibrated setup where the HRTF of the individual listener as well as the frequency response of the headphone is accounted for. Instead it is directly as measured or generated at the position of M20. All audio files are normalized since the level differences are so significant that they make comparison of anything but level impossible. The measured responses are, in the here presented audio files, resampled to 48 kHz to allow any media player to be able to play it.

(a) Reference section 15.1 - Link.

(b) Sound generated in section 15.1 - Link.

(c) Reference section 15.2 - Link.

(d) Sound generated in section 15.2 - Link.

Figure 15.18: QR-codes/links to sound files. The QR-codes can be scanned using a smart-phone on a printed copy. In a digital version 'Link' is a clickable hyperlink. The audio from measurements has been resampled from 65563 Hz to 48 kHz to allow the online player to play it. All the audio files have been normalized to have a maximum amplitude of 1, so the level difference cannot be heard.

15.3.1 Additional audio

This section includes a few additional situations considered. Only a brief description of what has been done to arrive at this audio is given below each QR-code. As such these sounds are mainly for the benefit of the reader and does not contribute much to the scientific value of the report.

(a) Sound generated in section 15.1 with the addition of the recorded noise from the shaker - Link.

(b) Sound generated in section 15.2 Without the additional 150 frequencies introduced in section 13.5 - Link.

(c) Reference section 15.2 low-pass filtered at 2 kHz - Link.

(d) Sound generated in section 15.2 low-pass filtered at 2 kHz - Link.

(e) Sound generated in section 15.2 with the floor reflection created by a complete plate 'below' the floor i.e. a distributed mirror source - Link.

(f) HATS recording at 'HATS position 2' corrected to unit input force. HATS facing plate. No headphone correction is applied - Link.

(g) Auralization of sound generated in section 15.2 at 0° elevation and azimuth using HRTF from HATS. No headphone correction is applied - Link.

(h) Auralization of sound generated in section 15.2 at 90° elevation and azimuth using HRTF from HATS. No headphone correction is applied - Link.

Figure 15.19: QR-codes/links to sound files. The QR-codes can be scanned using a smart-phone on a printed copy. In a digital version 'Link' is a clickable hyperlink. All the audio files have been normalized to have a maximum amplitude of 1, so the level difference cannot be heard.

Part VI

Discussion & Conclusion

16 | Discussion

Previous papers have shown that audio can be generated solely based on numerical simulation methods. Some methods are based on a complete FEM or BEM solution of an environment by which they lose the angle of incidence of reflected sound making a binaural representation impossible. Other methods use ray tracing methods to maintain this information but then the capability of modelling a distributed source is lost in the process. In addition to this the researched literature does not provide meticulous comparison to measured sound - in fact most papers never compare the simulation to the sound field of a physical object at all.

This study examined if the methods could be combined in such a way as to be used in engineering to achieve accurate binaural results. The method was developed to allow for a distributed source and it separates the vibration problem from the sound generation problem. This allows the two problems to be solved by separate methods well suited for their part of the complete auralization problem. The accuracy was examined by comparing the audio generated via computer simulation to measurements on a physical model.

Through a simulation it was possible to calculate the frequencies and shapes of vibration of the studied plate with an accuracy which was acceptable, yet not perfect. A listener will be able to hear a difference between for example the recorded 932 Hz and the generated 911 Hz tone, but whether the annoyance is different is another topic and probably dependent on the rest of the audio spectra. For computing an overall dB(A) weighted noise level or an octave band representation the accuracy in terms of frequency is adequate.

In this project three measured damping ratios were used, which is not ideal. Either the damping ratio should be measured at all relevant frequencies or some prediction model should be used. Measuring at all relevant frequencies naturally defeats the purpose of the algorithm as this requires a physical structure. An alternative solution is to use Rayleigh damping as proposed in [O'Brien et al., 2002]. This estimator calculates damping based on the stiffness and mass matrices. The final sound will be very sensitive to the accuracy of this estimator. An estimator which also includes the damping due to mounting is probably required.

In summary, a multitude of parameters influence the auralization such as the before mentioned damping ratio, the deformation as a function of time as well as the accuracy which one can achieve in a simulation without fitting it to a physical measurement. The combination of all these factors make a high precision output hard to achieve in practice. That being said by applying closer attention to topics such as radiation efficiency, acoustic short circuits, diffraction and the coupling between the structure surface and air, one should be able to achieve better results in terms of level and tonal balance. It is possible that this could be achieved using a tool intended for acoustics, such as the acoustics toolbox in ANSYS, which natively include these phenomena in their solutions, instead of the simplification used in this thesis. Such an algorithm would require a way of decoupling the sound propagation from the sound radiation to allow for separate modelling of the listening environment.

17 | Conclusion

The purpose of this project was to examine if the sound field created by a vibrating structure could be predicted by means of mathematical modelling. It was intended to arrive at a solution which was general and accurate enough to be used in product development and based solely on physical parameters of the structure. To that end methods originating from scientific papers in general engineering and in the video game community were considered. The methods share the feature that they all utilize some sort of physical modelling, mostly finite elements analysis.

A detailed study on the accuracy of finite elements analysis was performed by comparing analytical solutions as well as measured data with numerical results from a finite elements analysis. It was found that there was almost no difference between analytical and numerical results when considering an idealized geometry. In order to make the numerical results fit the measurement results the measurement system had to be included in the simulation. After including these modifications the difference in eigenfrequency between measurements and numerical results was in the order of 4%. This deviation is likely to be due to a combination of errors in both simulation and measurement. A major issue was the upper frequency limit of the force transducer used in measurements which is about 2 kHz at best. This prevents verification of the algorithm at higher frequencies.

The studied structure was a thin plate which was chosen as an analytical solution is available and it has a simple radiating surface. It turned out that the deformations caused by the vibration were so significant that they influenced the perceived sound demanding a more complex algorithm which included a time-varying propagation distance.

Despite of this increase in complexity the algorithm is, as intended, solely based on quantifiable physical parameters, the method makes no assumption of the shape of the structure and the total man hours required to setup the algorithm is less than an hour. Computation time is about 4 hours for 5 seconds of sound. The assumptions that the algorithm does make are that the structure considered is a resonant structure and that vibration is dominated by oscillations rather than breathing. If the latter is not the case a dipole correction filter can be left out.

The final sound was highly dependant on the frequency dependant damping ratio of the vibrating structure. Even though it is a physically explained property which can be estimated it is, to the author's knowledge, normally measured for more accurate results. This puts a spoke in the project's wheel as the intention was to predict the sound without having the physical structure at hand. Even after fitting the simulation with the measured damping ratios the generated sound was not sufficiently close to the reference measurement. The level was underestimated and the sound quality artificial. For this reason work on a binaural representation in listening tests as well as calculating overall noise level and directivity is omitted, as the foundation for doing so is wrong. As the deviation from measurements is large it is not, at this point, possible to confirm that a simulation driven auralization can achieve highly accurate results.

18 | Future work

As this thesis completely disregards the effect of the critical frequency, yet still achieves results which are not so far off as could be expected, it should be examined further how this phenomenon affects the radiation pattern of the plate. This might be done using an acoustic camera.

The only considered listening environment is a hemi-anechoic room which allows for the use of a single mirror source for room modelling. For more complex environments this method is likely to pose too large computational demands and more advanced room modelling is required.

The influence of deformation of an object on sound quality should be mapped in greater detail. If it is critical to the perception it is likely that a time domain solution is required despite the computation cost. If the time dependency is only important in the case of a plate with relatively large displacements, then the method of substituting the object's many faces with much fewer simple sources as proposed by [James et al., 2006] would be very interesting in combination with a room simulation algorithm. To show how this might be done in ANSYS a 'recipe' is given below. The objective is to obtain sound pressures at an offset surface from the plate.

Simulation tool for [James et al., 2006]

The analysis system 'harmonic acoustics' can be used. It is a special analysis system for acoustic problems and includes functionality related to sound. As previously discussed the issue with using FEM for acoustic problems is the need to mesh the entire volume of interest. The proposed method only requires meshing for a small subspace which is terminated anechoically. This is in alignment with the use of the 'harmonic acoustics' analysis system where an object can be placed in some media which is enclosed by a PML[1].

From the ANSYS course material on the use of the acoustic extension it can be found that the use of acoustic media and PML sets the following requirements on the model:

- Acoustical domain thickness of an integer of the mesh size e.g. 2.
- Meshing size of acoustical domain of 12 linear elements per wavelength.
- PML layer thickness of minimum $\lambda/4$.
- Minimum 3 elements across the PML (12 elements per wavelength).

The demand on thickness related to the wavelength will require large distances for low frequencies. The demands on number of elements per wavelength will yield a high amount of elements for large distances at high frequencies. Fortunately the proposed method splits the problem into single frequency subproblems; they are not required to share the same radiation boundary. This allows the FEM solution to split the problem in multiple subproblems where the minimum requirements above are adhered to only for the single frequency under study. This can be done using the parameter functionality in ANSYS. The results from a modal analysis of the plate can be taken as input to the calculations. Generation of the acoustic region and PML region for each considered frequency can then be automated.

[1] Perfectly matched layer briefly introduced in section 8.5; in short it is an anechoic termination.

Bibliography

Robert D. Blevins. *Formulas for natural frequency and mode shape*. Krieger Publishing Company, 1995. ISBN 0-89464-894-2.

Brüel & Kjær. Technical documentation - force transducers 8200 and 8201, 1994.

Brüel & Kjær. Microphone handbook vol. 1, 1996. URL https://www.bksv.com/media/doc/be1447.pdf. Downloaded 25/07-2018.

Brüel & Kjær. Vibration exciter type 4809, no date a. URL https://www.bksv.com/en/products/shakers-and-exciters/measurement-exciters/vibration-exciter-type-4809. Downloaded 09/02-2018.

Brüel & Kjær. Vibration exciter type 4810, no date b. URL https://www.bksv.com/-/media/literature/Product-Data/bp0232.ashx. Downloaded 16/03-2018.

Brüel & Kjær. ½' low-noise free-field teds microphones type 4955 and 4955-a, no date c. URL https://www.bksv.com/-/media/literature/Product-Data/bp2148.ashx. Downloaded 19/07-2018.

Brüel & Kjær. Modal sledge hammer type 8207, no date d. URL https://www.bksv.com/en/products/transducers/vibration/Vibration-transducers/impact-hammers/8207. Downloaded 09/02-2018.

Brüel & Kjær. Condenser microphone cartridges — types 4133 to 4181, no date e. URL https://www.bksv.com/media/doc/Bp0100.pdf. Downloaded 15/06-2018.

E. F. F. Chladni. *Treatise on Acoustics*. 2015. ISBN 3-319-20360-6. doi: 10.1007/978-3-319-20361-4.

COMSOL. Comsol news - special edition acoustics, 2017. URL http://cdn.comsol.com/comsolnews/COMSOL_News_2017_Special_Edition_Acoustics_low-res.pdf. Downloaded 07/02-2018.

COMSOL. Analyze acoustics and vibrations with the acoustics module, 2018. URL https://www.comsol.com/acoustics-module. Seen 07/02-2018.

L. Cremer, M. Heckl, and B.A.T. Petersson. *Structure-Borne Sound*. Springer, 3rd edition, 2005. ISBN 3-540-22696-6.

DEWESoft. Microphone position iso 3745, no date . URL https://https://dewesoft.pro/online/course/sound-power-measurement/page/microphone-position-iso-3745. Downloaded 21/06-2018.

F. Duvigneau, S. Koch, R. Orszulik, E. Woschke, and U. Gabbert. About the vibration modes of square plate-like structures. *TECHNISCHE MECHANIK*, 36(3):180–180, 2016. URL http://www.uni-magdeburg.de/ifme/zeitschrift_tm/2016_Heft3/03_Duvigneal_et_al.pdf.

Fabian Duvigneau, Steffen Liefold, Ulrich Gabbert, Marius Höchstetter, and Jesko Verhey. Engine sound weighting using a psychoacoustic criterion based on auralized numerical simulations. 05 2015.

I. Fried. Accuracy of finite element eigenproblems. *Journal of Sound and Vibration*, 18(2):289 – 295, 1971. ISSN 0022-460X. doi: https://doi.org/10.1016/0022-460X(71)90351-8.

Acoustic frontiers. Early reflections 101, 2015. URL http://www.acousticfrontiers.com/early-reflections-101/. Downloaded 10/08-2018.

Daniel J. Gorman. A comprehensive approach to the free vibration analysis of rectangular plates by the use of the method of superposition. *Journal of Sound and Vibration*, 47(1), 1976.

Daniel J. Gorman. Free vibration analysis of the completely free rectangular plate by the method of superposition. *Journal of Sound and Vibration*, 57(3), 1978.

Daniel J. Gorman. *Vibration Analysis of Plates by the Superposition Method*. World Scientific, 1st edition, 5 1999. ISBN 981-02-3682-6.

D. Hammershøi and H. Møller. Binaural technique: Basic methods for recording, synthesis, and reproduction. *Communication Acoustics*, 2005.

Sigurd Van Hauen. *Pinna Reconstruction Filter for Behind the Ear Hearing Aids*. Unpublished master's thesis, Aalborg University, Aalborg, Denmark, 2018. URL https://projekter.aau.dk/projekter/da/studentthesis/pinna-reconstruction-filter-for-behind-the-ear-hearing-aids(8cea1d9d-6632-4113-bc11-25709a7a70ed).html.

Tom Irvine. Damping properties of materials revision c, 2004. URL https://syont.files.wordpress.com/2007/05/damping-properties-of-materials.pdf. Downloaded 10/07-2018.

Doug L. James, Jernej Barbič, and Dinesh K. Pai. Precomputed acoustic transfer: Output-sensitive, accurate sound generation for geometrically complex vibration sources. *ACM Transactions on Graphics (SIGGRAPH)*, pages 987–995, 2006.

K. W. Johnson and J. D. Cutnell. *Physics*. Wiley, 9th edition, 2012.

Lawrence E. Kinsler, Austin R. Frey, Alan B. Coppens, and James V. Sanders. *Fundamentals of Acoustics*. Wiley, 4th edition, 2000. ISBN 978-0-471-84789-2.

Mendel Kleiner, Bengt-Inge Dalenbäck, and Peter Svensson. Auralization-an overview. *J. Audio Eng. Soc*, 41(11):861–875, 1993. URL http://www.aes.org/e-lib/browse.cfm?elib=6976.

A. Krokstad, S. Strom, and S. Sørsdal. Calculating the acoustical room response by the use of a ray tracing technique. *Journal of Sound and Vibration*, 8(1):118 – 125, 1968. ISSN 0022-460X. doi: https://doi.org/10.1016/0022-460X(68)90198-3.

Wolfgang Kropp. *Technical Acoustics 1*. Unpublished manuscript, Chalmers, Göteborg, Sweden, 2015.

K. Heinrich Kuttruff. Auralization of impulse responses modeled on the basis of ray-tracing results. Oct 1991. URL http://www.aes.org/e-lib/browse.cfm?elib=5594.

Mikko-Ville Laitinen, Sascha Disch, and Ville Pulkki. Sensitivity of human hearing to changes in phase spectrum. *J. Audio Eng. Soc*, 61(11):860–877, 2013. URL http://www.aes.org/e-lib/browse.cfm?elib=17068.

Arthur W. Leissa. *Vibration of Plates.* national Aeronautics and Space Administration, 1st edition, 1969.

Dingzeyu Li, Yun Fei, and Changxi Zheng. Interactive acoustic transfer approximation for modal sound. *ACM Trans. Graph.*, 35(1), 2015. doi: 10.1145/2820612.

LMS International. Raynoise revision 3.1 users manual, no date. URL http://sunileng.biz/pic/etcdata/rn31.pdf. Downloaded 13/02-2018.

Henrik Møller. Fundamentals of binaural technology. *Applied Acoustics*, 36(3/4):171–218, 1992. ISSN 0003-682X.

Swen Müller and Paulo Massarani. Transfer-function measurement with sweeps. *J. Audio Eng. Soc*, 49(6):443–471, 2001. URL http://www.aes.org/e-lib/browse.cfm?elib=10189.

Y. Mochida and S. Ilanko. Transient vibration analysis of a completely free plate using modes obtained by gorman's superposition method. *Journal of Sound and Vibration*, 329:1890–1900, 2010. ISSN 0022-460X. doi: 10.1016/j.jsv.2009.11.029.

James F. O'Brien, Perry R. Cook, and Georg Essl. Synthesizing sounds from physically based motion. *Proceedings of ACM SIGGRAPH 2001*, pages 529–536, 2001a.

James F. O'Brien, Perry R. Cook, and Georg Essl. Sounds from physically based motion (siggraph 2001), 2001b. URL http://graphics.berkeley.edu/papers/Obrien-SSF-2001-08/. Seen 05/07-2018.

James F. O'Brien, Chen Shen, and Christine M. Gatchalian. Synthesizing sounds from rigid-body simulations. *Proceedings of ACM SIGGRAPH 2002*, pages 175–181, 2002.

Sean Olive, Todd Welti, and Omid Khonsaripour. A statistical model that predicts listeners' preference ratings of around-ear and on-ear headphones. In *Audio Engineering Society Convention 144*, May 2018. URL http://www.aes.org/e-lib/browse.cfm?elib=19436.

Soonkwon Paik, Manu De Geest, and Koen Vansant. Interior acoustic simulation for in-car audio design. *Sound and Vibration*, 47(1):10–17, 01 2013. URL https://search-proquest-com.zorac.aub.aau.dk/docview/1314355905?accountid=8144.

J. Raamachandran. *Boundary and Finite Elemements: theory and problems.* Alpha Science, 1st edition, 2000. ISBN 1-84265-013-0.

Tetsuya Sakuma, Shinichi Sakamoto, and Toru Otsuru. *Computational Simulation in Architectural and Environmental Acoustics bibtex.* Springer, 2014. ISBN 9784431544548.

J. Sandvad. Dynamic aspects of auditory virtual environments. May 1996. URL http://www.aes.org/e-lib/browse.cfm?elib=7547.

Philipp Schmiechen. *Travelling wave speed coincidence*. Unpublished doctorate, doctorate, London, England, 1997. URL http://www3.imperial.ac.uk/pls/portallive/docs/1/40375703.PDF.

SignalNews. Modal testing with shaker excitation, no date. URL http://blog.dataphysics.com/modal-testing-with-shaker-excitation/. Downloaded 14/02-2018.

SOLIDWORKS. Finite element analysis, no date. URL http://www.solidworks.com/sw/products/simulation/finite-element-analysis.htm. Seen 21/01-2018.

Sergey V. Sorokin. *Lecture notes on Machine Acoustics*. Unpublished manuscript, Aalborg University, Aalborg, Denmark, no date.

Kees van den Doel, Paul G. Kry, and Dinesh K. Pai. Physically-based sound effects for interactive simulation and animation. *ACM SIGGRAPH 2001*, pages 537–544, 2001.

John Vanderkooy. Aspects of mls measuring systems. *J. Audio Eng. Soc*, 42(4):219–231, 1994. URL http://www.aes.org/e-lib/browse.cfm?elib=6951.

P. Welch. The use of fast fourier transform for the estimation of power spectra: A method based on time averaging over short, modified periodograms. *IEEE Transactions on Audio and Electroacoustics*, 15(2):70–73, Jun 1967. ISSN 0018-9278. doi: 10.1109/TAU.1967.1161901.

Part VII

Appendix

A | Measuring plate

This appendix is split in 3 sections called audio measurement, vibration measurement and in situation HRTF measurement. The audio measurement seeks to determine the eigenfrequencies of the plate by a combination of audio measurements and an input impedance measurement. The vibration measurement seeks to determine the mode shapes of the plate. The third measurement acquires the HRTF in the hemi-anechoic environment.

A.1 | Audio measurement

The wanted outcome from this measurement is to provide data which can be used to verify the validity of the auralization. Two key points are of interest the first being the sound pressure over time at discrete positions, where the auralization and measurements can be compared. The second is gathering a set of binaural recording to enable verification in a listening test. To that end the following measurements are required:

- Microphone measurements on a half sphere.
- HATS measurement at two positions.

The measurements should be performed over as much as the audio band as possible. This will put a lower limit due to the hemi-anechoic room of 50 Hz and an upper limit of 16000 Hz due to the microphones.

A.1.1 Setup

For a list of equipment see table A.2. The plate is mounted through a 4.8 mm hole in the middle with a force transducer on the bottom side and an accelerometer on the top side[1]. The plate is placed parallel to the ground plane and the shaker excites in the direction normal to the plate.

[1] Yielding an impedance head.

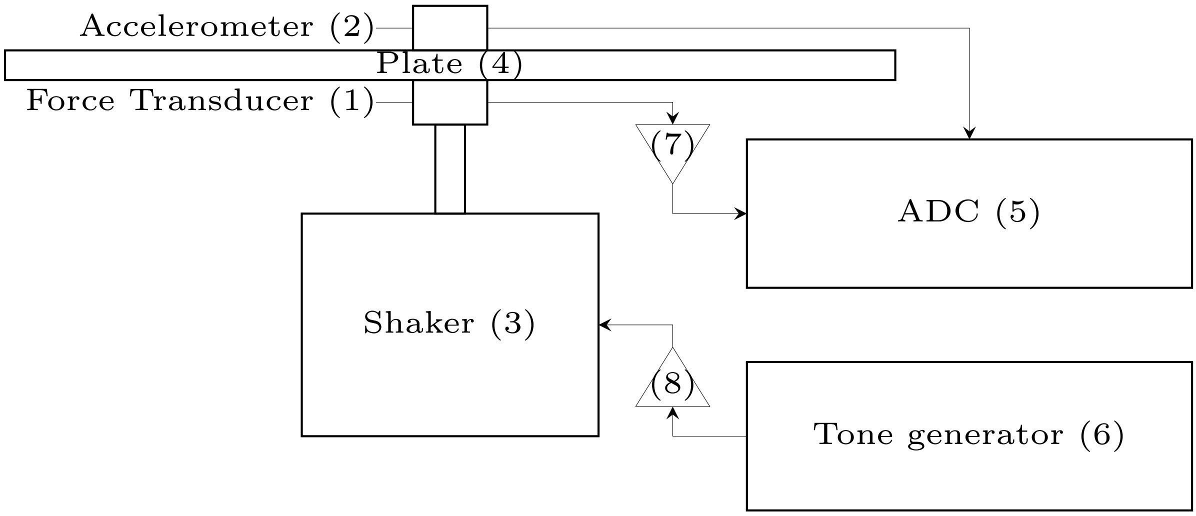

Figure A.1: Experimental setup for plate. Zoom on the local setup around the plate. Numbers correspond to item numbers in table A.2.

In figure A.2 a 2 dimensional overview of the setup is given. The plate is placed so that its centre position is at the position (x,y,z) (0,0.094,0) m. The length of the plate is turned along the x-axis as in the simulation. The HATS is turned to be facing the centre of the plate for both measurement positions.

Object	Position	x-coordinate/m	y-coordinate/m	z-coordinate/m
Plate	Centre point	0	0.094	0
HATS Position 1	Mid between ears, facing plate.	0	1.097	0
HATS Position 2	Mid between ears, facing plate.	1.04	1.60	0.76
Microphones M1-M20	Centre of membrane		See table A.4.	

Table A.1: Positions in the measurement environment.

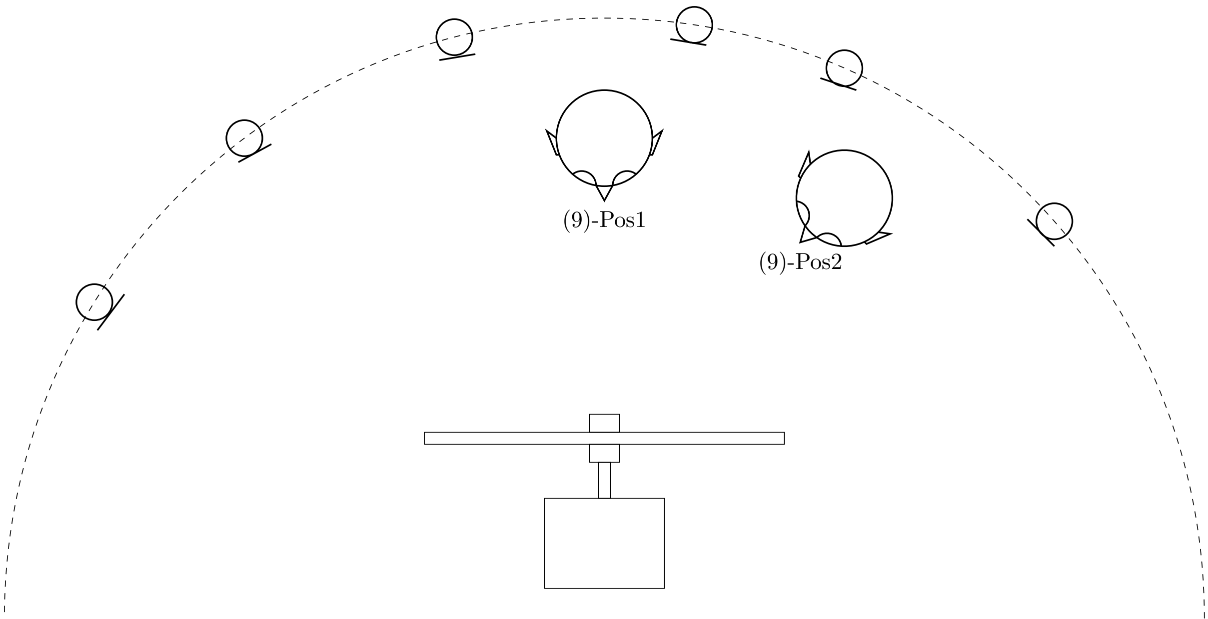

Figure A.2: Experimental setup for plate. The global setup around the plate. The microphone placement is arbitrary, the actual coordinates of all 20 microphones are given in table A.4. The electrical connections are left out here but can bee found in table A.6. The items around the plate are connected as in figure A.1 and all the microphones are connected to an ADC.

Function	Model	Serial number	Number in setup
Force transducer	B&K 8200	2190752	1
Accelerometer	B&K 4514-B-001	52030	2
Shaker	B&K 4810	1128303	3
Plate	NaN	NaN	4
ADC	B&K 3050-B	101343	5
Tone generator	Agilent 33220A	MY44004996	6
Charge amplifier FT	B&K 2646	2178390	7
Power amplifier	B&K 2706	1113510	8
HATS	B&K 4100D	2209464	9
20 microphones	B&K 4955	See table A.3	M1-M20
4 ADCs	B&K 3050-B	See table A.5	A1-A4

Table A.2: Model and serial numbers of the items used in the setup.

Microphone number	Model	Serial number
M1	B&K 4955	2703788
M2	B&K 4955	2863786
M3	B&K 4955	2707482
M4	B&K 4955	2716184
M5	B&K 4955	2760307
M6	B&K 4955	2856041
M7	B&K 4955	2846186
M8	B&K 4955	2760310
M9	B&K 4955	2760311
M10	B&K 4955	2760312
M11	B&K 4955	2774589
M12	B&K 4955	2774590
M13	B&K 4955	2783591
M14	B&K 4955	2783592
M15	B&K 4955	2783593
M16	B&K 4955	2793992
M17	B&K 4955	2792993
M18	B&K 4955	2863783
M19	B&K 4955	2792995
M20	B&K 4955	2806536

Table A.3: Model and serial numbers of the Microphones used in the setup.

The positions of the microphones are given below with (x,y,z)=(0,0,0) corresponding to the origin of the sphere created by mirroring the half-sphere around the floor plane y=0.

Microphone number	x	y	z
M1	-2.8000	0.0700	0
M2	1.3972	0.2100	-2.4192
M3	1.3888	0.3500	2.4052
M4	-1.3776	0.4900	2.3884
M5	-1.3636	0.6300	-2.3632
M6	2.6908	0.7700	0
M7	0	0.8960	2.6516
M8	-2.2484	1.0500	-1.2992
M9	2.1952	1.1900	-1.2684
M10	2.1336	1.3300	1.2320
M11	-2.0636	1.4700	1.1928
M12	0	1.6100	-2.2904
M13	2.1868	1.7500	0
M14	-1.0332	1.8900	1.7892
M15	-0.9632	2.0300	-1.6688
M16	0.8848	2.1700	-1.5316
M17	0.7924	2.3100	1.3692
M18	-1.3552	2.4500	0
M19	0	2.5900	-1.0640
M20	0.5376	2.7300	0.3108

Table A.4: Microphone positions specified in ISO 3745. In this project the orientation of the coordinate system is different so the y and z axis are swapped compared to the standard.

ADC number	Model	Serial number
A1	B&K 3050-B	3050-106160
A2	B&K 3050-B	3050-106157
A3	B&K 3050-B	3050-106168
A4	B&K 3050-B	3050-106159

Table A.5: Model and serial numbers of the ADCs used for the microphone array.

A.1.2 Connections

From	Comment	To	To Channel
HATS (9)	Left ear	ADC (5)	1
HATS (9)	Right ear	ADC (5)	2
Force transducer (1)	Via preamp (7)	ADC (5)	6
Accelerometer (2)	-	ADC (5)	5
M1-M6	Increasing order	A1	1-6
M7-M12	Increasing order	A2	1-6
M13-M18	Increasing order	A3	1-6
M19-M20	Increasing order	A4	1-6
Tone generator (6)	Via amplifier (8)	Shaker (3)	-

Table A.6: Equipment connections.

Below some photos of the setup are shown:

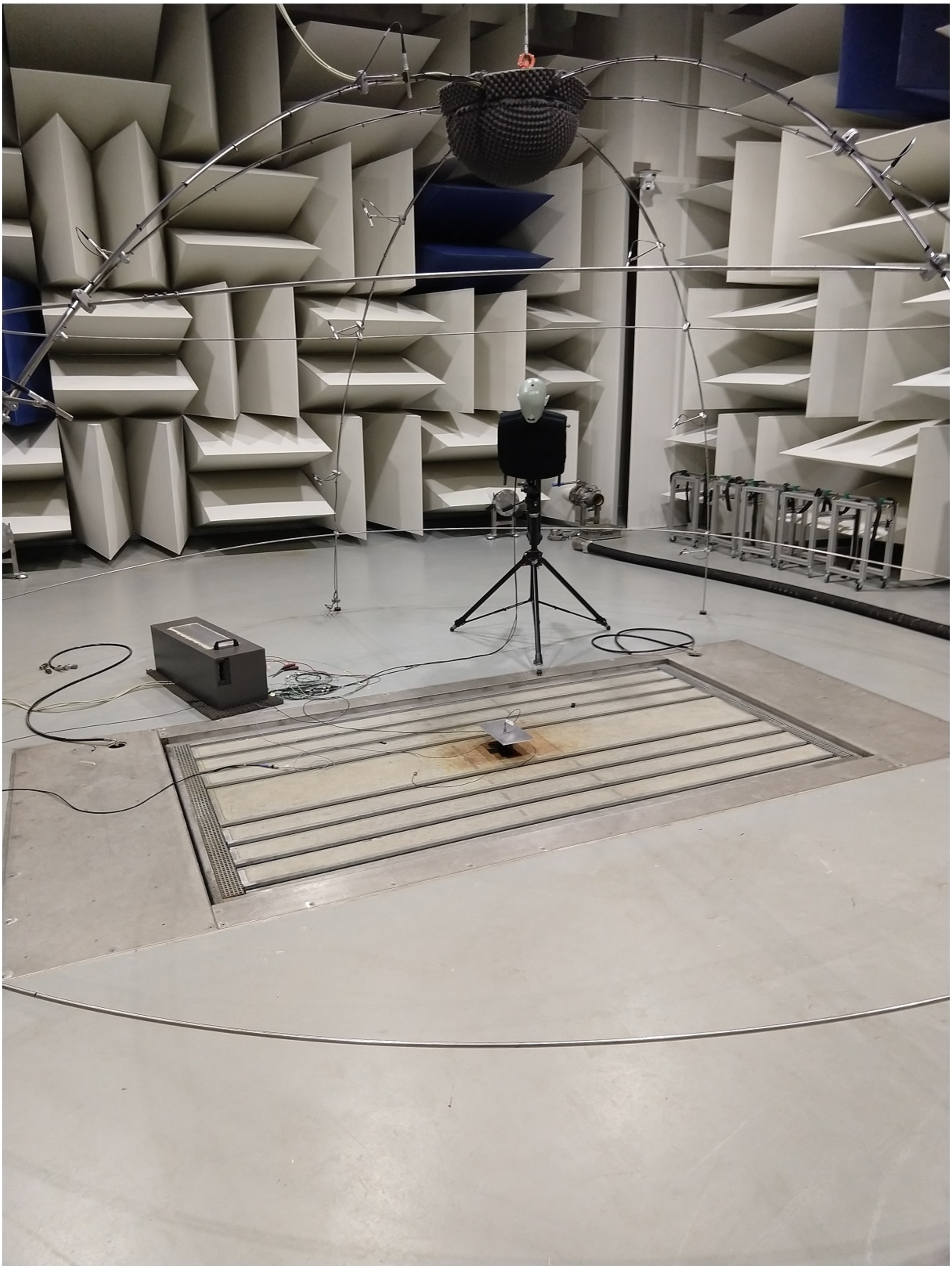

Figure A.3: Plate setup seen from front with HATS in position 2.

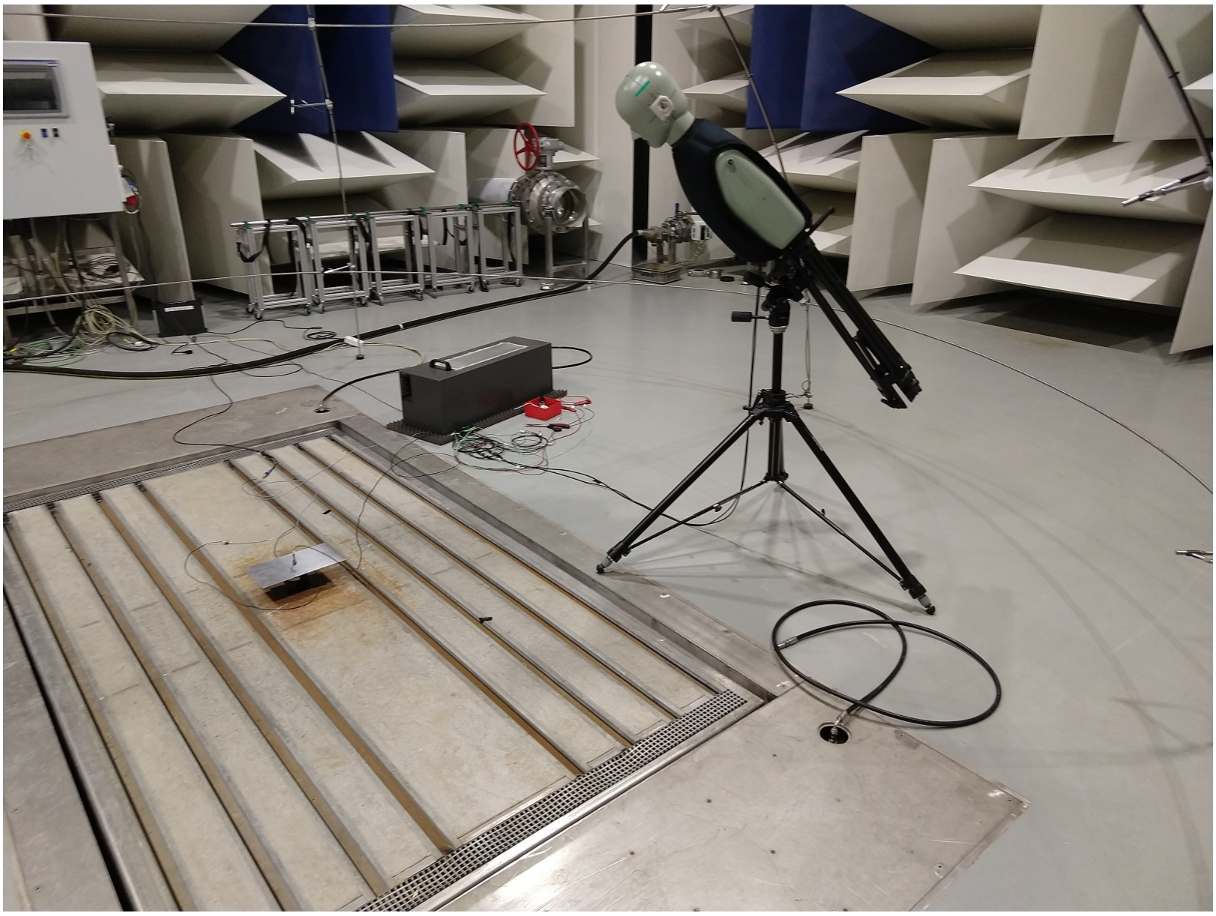

Figure A.4: Plate setup seen from side with HATS in position 2.

A.1.3 Settings

One advantage with B&K Pulse LabShop 22 is that most equipment is recognized (by serial number) and the program takes care of charge signals and level adjustments automatically. This plus the fact that this measurement system is close to identical to the standard setup at Grundfos makes setup in Pulse simple. The only item that require special care is the force transducer (1) which has to be manually found in the list of available equipment. The fact that this the power sphere and HATS are part of the standard measurement system at Grundfos means that calibrations are carried out for the system regularly so the existing calibration values are used.

Item number	Setting
(6)	Tone generator noise 1 Vpp
(M1-M20) / (A1-A4)	Sample rate microphones 65.536 kHz
(9)/(5)	sample rate HATS microphones 65.536 kHz
(2)/(5)	Sample rate accelerometer 65.536 kHz
(1)/(5)	Sample rate force transducer 65.536 kHz

Table A.7: Settings for equipment.

A.1.4 Procedure

The procedure uses an interface specific to Grundfos, which is not documented further here.

- Start the tone generator and adjust the power amplifier to 2 o'clock. (A mark exist on this specific power amplifier.)
- Start the measurement.
- When measurement is done press 'calculate'.
- Press 'Report' to get the sound power level and save the data.

A.1.5 Results

The results are obtained by exporting the auto spectra from Pulse. What Pulse does to create the data is averaging frames over time, similar to Welch's method [Welch, 1967]. The runtime is 1 minute and a window length of 6400 samples and an overlap of 75% is used. The windowing filter is a Hamming filter. For the HATS measurement a downsampled version of the recording (fs 12.8 kHz) is used for averaging as memory is an issue in Pulse. The force transducer and accelerometer signals are also downsampled to 12.8 kHz as they are unlikely to yield useful data at high frequencies. The first 10 seconds of the time signal is stored from the HATS, accelerometer, force transducer and M10, M15 and M20. This allows for post processing data afterwards. The time signal from M20 is displayed below.

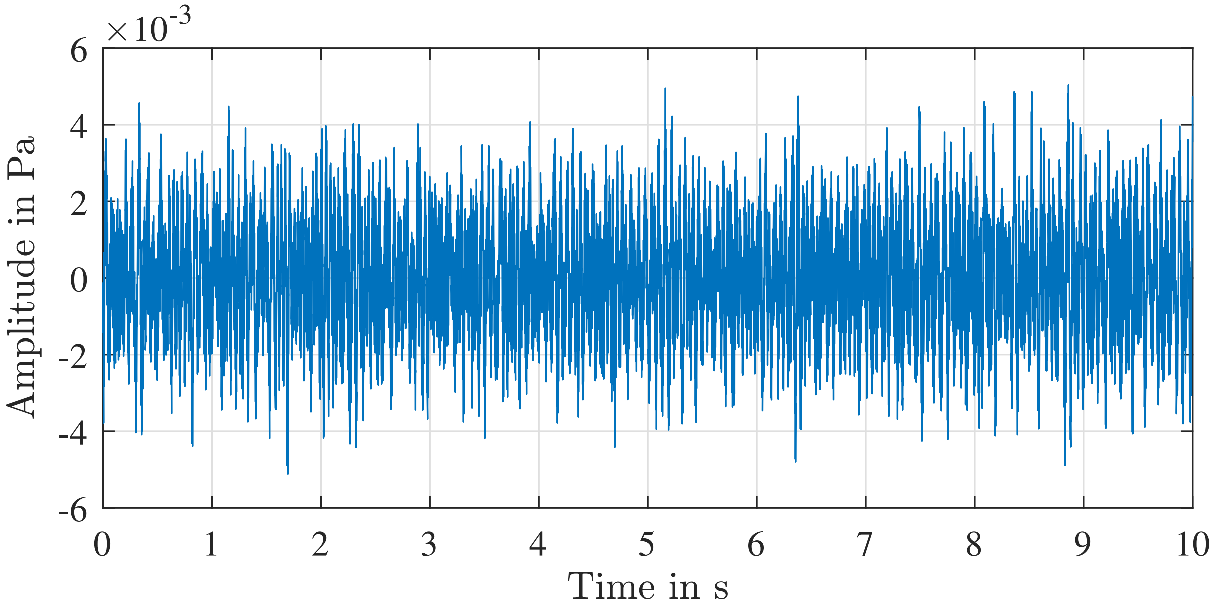

Figure A.5: The time signal at the M20 microphone position.

In figure A.6 the responses from the 20 microphones are shown and the resonant behaviour of the plate is clearly visible.

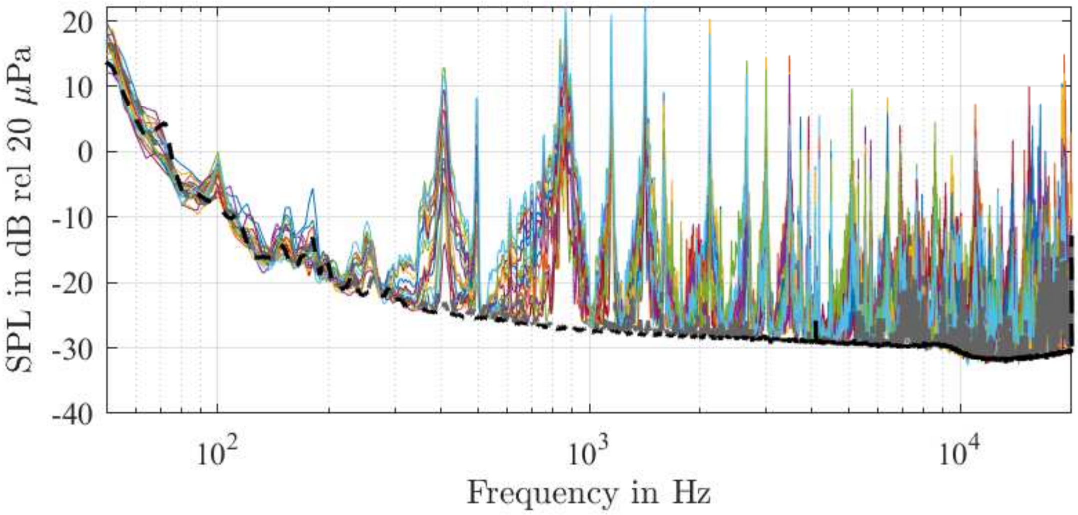

Figure A.6: The sound pressure level at the 20 microphone positions. Background noise at M10(– –) and noise from shaker without plate at M10 (– –).

In figure A.7 the responses from the left and right ear of the HATS in position 1 are shown.

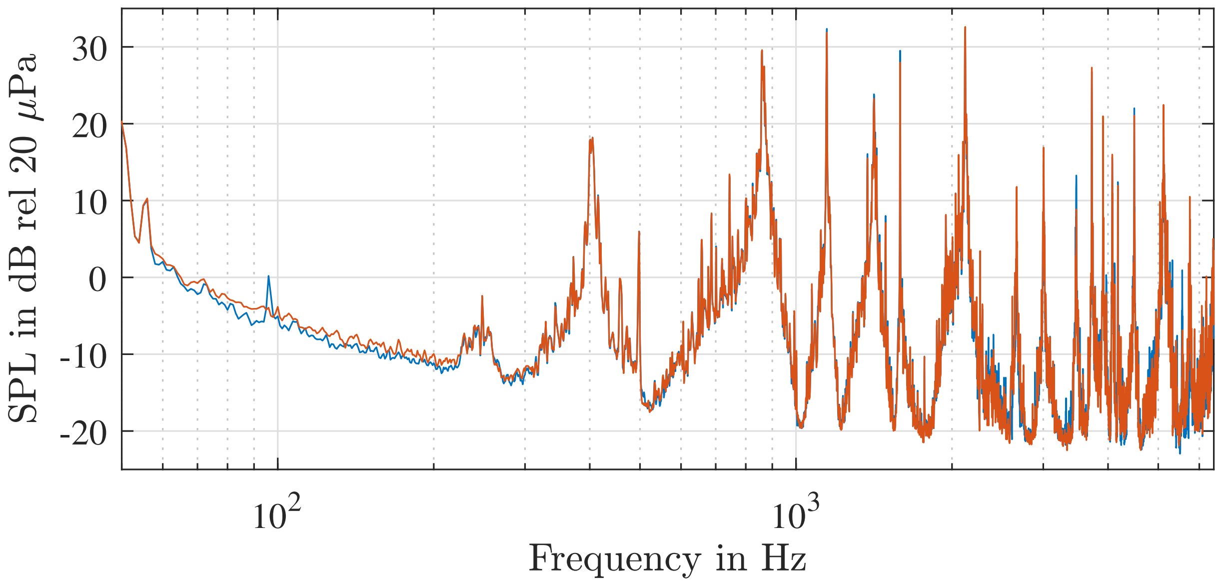

Figure A.7: The sound pressure level at the HATS left (—) and right (—) ear in position 1.

In figure A.8 the responses from the left and right ear of the HATS in position 2 are shown.

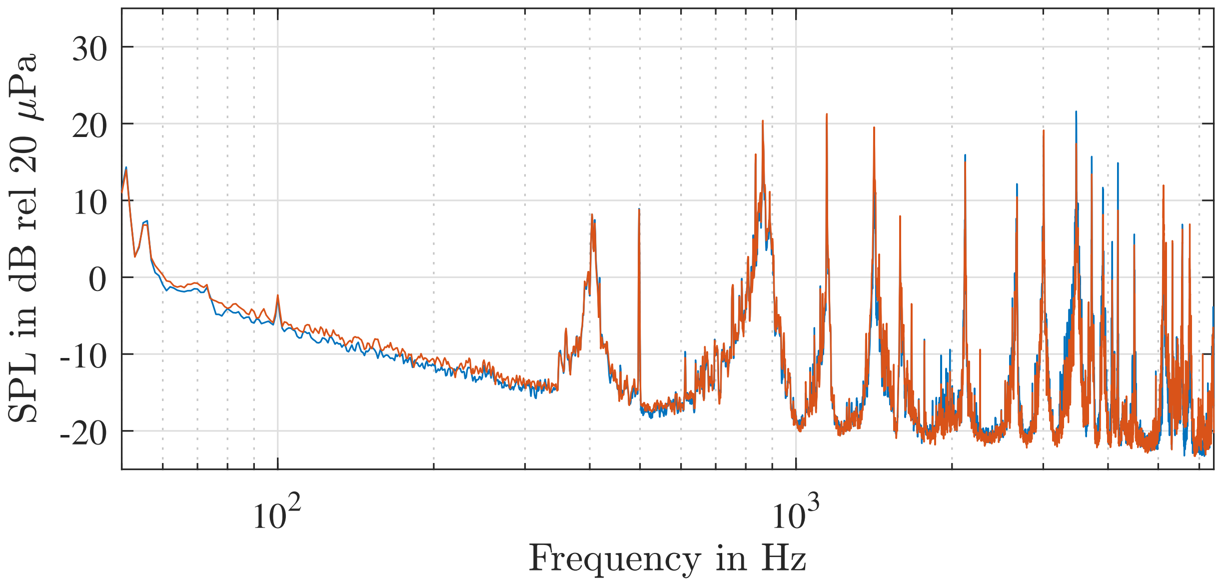

Figure A.8: The sound pressure level at the HATS left (—) and right (—) ear in position 2.

in order to calculate the input impedance of the plate the time signal from the accelerometer and force transducer can be used. A Fourier transform of the un-averaged time signals from the accelerometer and force transducer are plotted below.

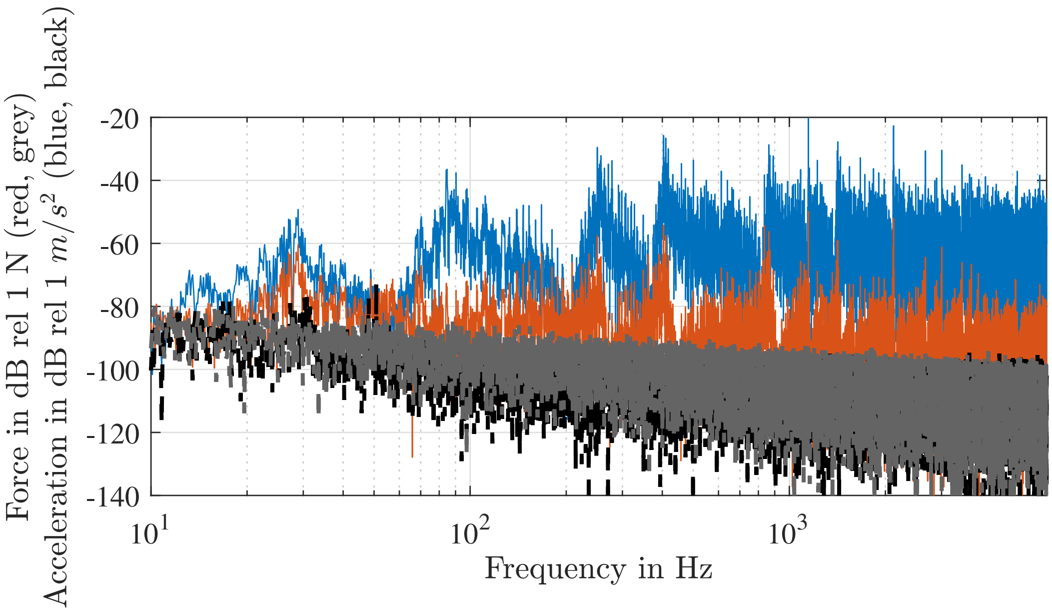

Figure A.9: The acceleration (—) and force (—) magnitude in the input point. Accelerometer noise floor (– –) and force transducer noise floor (– –).

It is clear from figure A.9 that the SNR in the force measurement is not sufficient to raise it over the noise floor. The accelerometer signal is also noisy. Therefore the result of calculating the input impedance as $Z(\omega)_{in} = \frac{Force(\omega)\cdot j\omega}{Acceleration(\omega)}$ is noisy as shown in figure A.10.

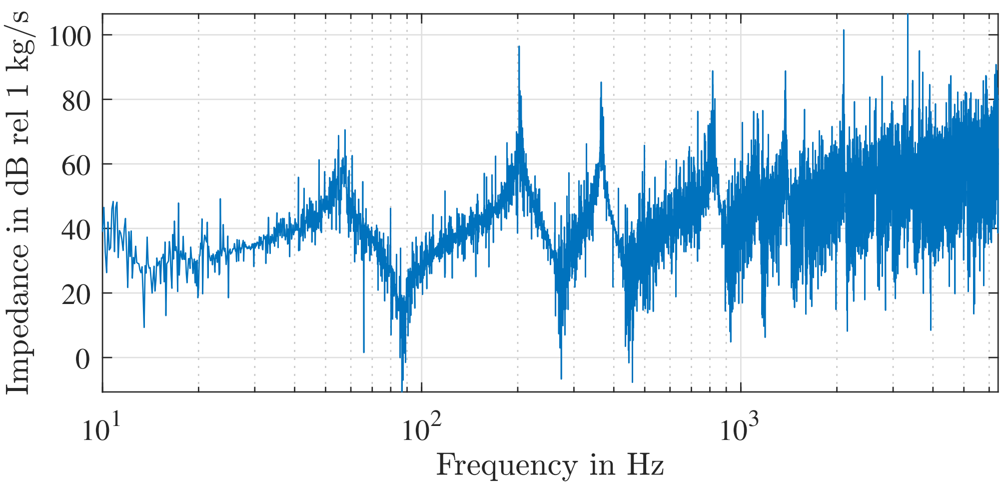

Figure A.10: The input impedance of the plate in the centre position.

In the middle position of the plate the displacement is small, especially at higher frequencies, resulting in a low SNR the measurement of acceleration. This means that the impedance cannot be calculated for all frequencies from an un-averaged signal. To solve this more sensitive equipment with a lower noise floor could be used, but the B&K 4514 is already a rather big and sensitive accelerometer and a more sensitive force transducer is not available. Instead the averaged acceleration and input force are calculated at the cost of frequency resolution. The averaging is done using Welch's method with a Hanning window with a size of 16384 samples and an overlap of 75%. Here no downsampling is performed before the averaging - but the plot is still limited to 6.4 kHz. The results from averaging the acceleration and force is shown in figure A.11.

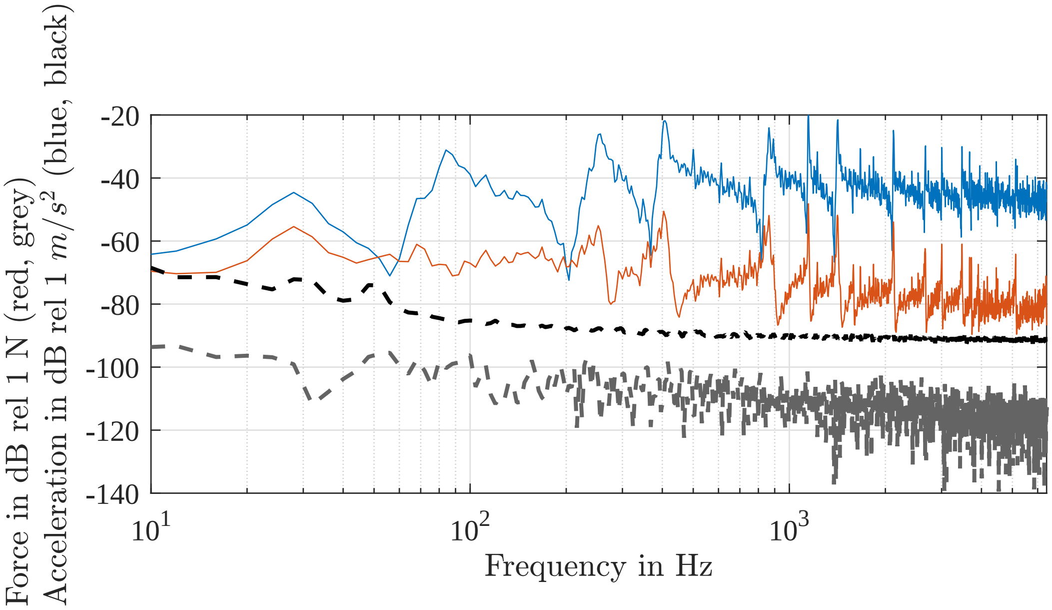

Figure A.11: The averaged acceleration (—) and force (—) magnitude in the input point. Accelerometer noise floor (– –) and force transducer noise floor (– –).

In order to calculate the averaged input impedance the input impedance is calculated for each frame using the complex force and acceleration spectra. Then the calculated impedances from all frames are averaged before plotting.

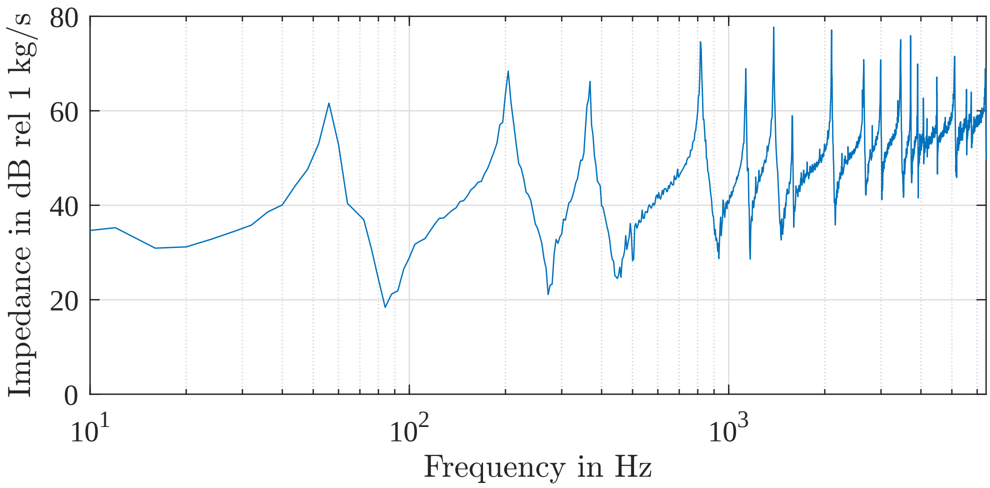

Figure A.12: The averaged input impedance.

Based on figure A.12 is is noted that the measured input impedance increase with frequency. This is in contradiction with the fact that the input impedance of an isotropic plate should be $8\sqrt{E\rho h}$ [Cremer et al., 2005], which is independent of frequency. In the setup the input impedance is not only that of a plate but includes the mass of the top of the force transducer and accelerometer. Removing these from the impedance does however not make the input impedance independent of frequency as expected. The influence of the additional components is removed by subtracting the impedance of a mass of M=11.7 grammes ($j\omega M$) from the impedance in each frame.

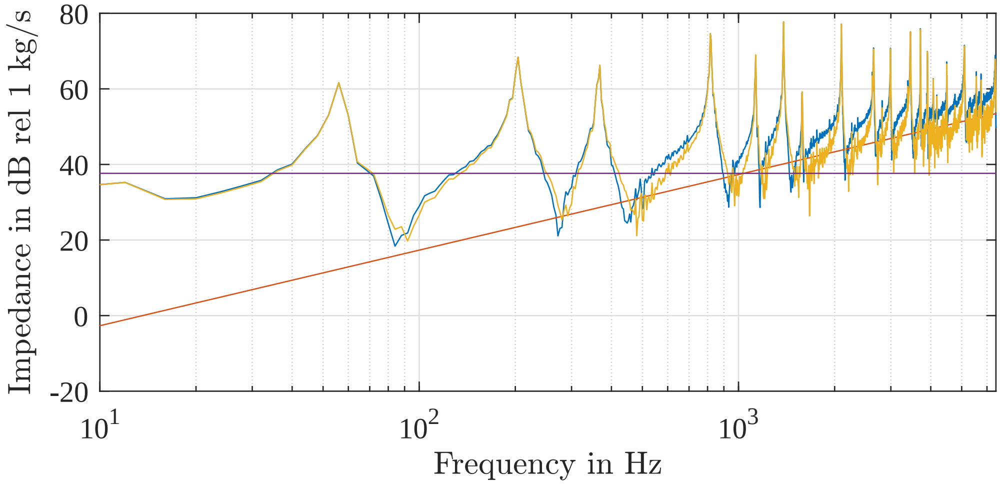

Figure A.13: The averaged input impedance - corrected for the mass loading. Measured input impedance (—). Impedance of mass 11.7 grammes (—). Input impedance of plate alone (—). Theoretical input impedance of an infinite plate (—).

The input impedance of a finite plate should in average be that of an infinite plate of same material and thickness. Therefore the yellow line should be centred around the purple line. This seems to hold at low and mid frequencies, but at higher frequencies the measured result deviates from theory. It is possible that the force transducer is used above its operating range. This is examined further in subsection 12.2.3.

Removing the influence of the mass from the input impedance although elegant does not change the physical setup, where the plate is loaded by this additional mass. For this reason figure A.12 is used to determine the resonances of the system including the mass load. The resonance frequencies on the yellow line in figure A.13 are comparable to the an analytical solution, where no mass loading is included.

From figure A.12 it can be seen that resonances occur at frequencies below those that are clearly visible in the audio spectra. It is established that resonances exist at 87 Hz and 276 Hz for the plate disregarding the measurement system. If the measurement system is to be included in the considerations the frequencies with highest displacement are better found directly from figure A.11 as the frequencies of highest acceleration. This would be 256 Hz and the frequency below this is not really clear but probably a bit lower than the 87 Hz found above. Anyhow the frequencies are so low compared to plate dimensions that it is not an efficient radiator of sound. By combining the resonance frequencies determined through the input impedance and those determined by audio a full picture of the plates vibrational frequencies is available in the audio range.

A.2 | Vibration measurement

The second part of the appendix seeks to determine the mode shapes of the plate. In order to examine these a simple approach is used. Sugar is poured on the vibrating plate to reveal nodal lines - where the sugar will settle.

During the course of the project many different frequencies have been examined at different times. Only some are actually of interest but all results are included for completeness.

A.2.1 Setup

The setup is a simplified version of the one used above. All remaining equipment is the same as above. The plate is mounted as in figure A.1 with the accelerometer (2) and force transducer (1) disconnected from the ADC.

A.2.2 Connections

The tone generator is connected via the power amplifier (8) to the shaker (3) as in table A.6

A.2.3 Settings

Item number	Setting
(6)	Tone generator sine 1 Vpp

Table A.8: Settings for equipment.

A.2.4 procedure

The selection of frequencies of interest is based on the impedance and audio measurement 87 Hz, 256 Hz, 400 Hz and 496 Hz. In between some frequencies based on an early, with wrong material parameters, analytical solution are included. These images serve the purpose of proving the point that the non doubly symmetric modes will not be excited and the nearest symmetrical mode will dominate the vibration instead. Also 57 Hz is included as sound is recorded at that frequency in the HATS positions and it was seen as an eigenfrequency in some preliminary FEM works.

The following is repeated for all frequencies of interest:

- Sugar is poured on the plate while the shaker is turned off.
- The tone generator is set to vibrate sinusoidally at a specific frequency - i.e. forced vibration.
- The gain on the power amplifier is increased until the sugar moves - or just before the clipping limit (light on power amplifier).
- When the sugar settles at nodal lines and the lines are stationary the shaker is stopped. (In case the sugar is not moving at the clipping limit the shaker is also stopped.)
- A picture is taken and the procedure is repeated for the next frequency.

A.2.5 Results

Mode shapes from vibration experiment are shown below. For easier overview blue lines indicate where sugar is collected. No blue lines indicate that no clear pattern is recognized. The post-its were added after the shaker was stopped to keep track of frequency. The pictures are taken at different times so the background does vary - the mounting of the plate and the setups are the same.

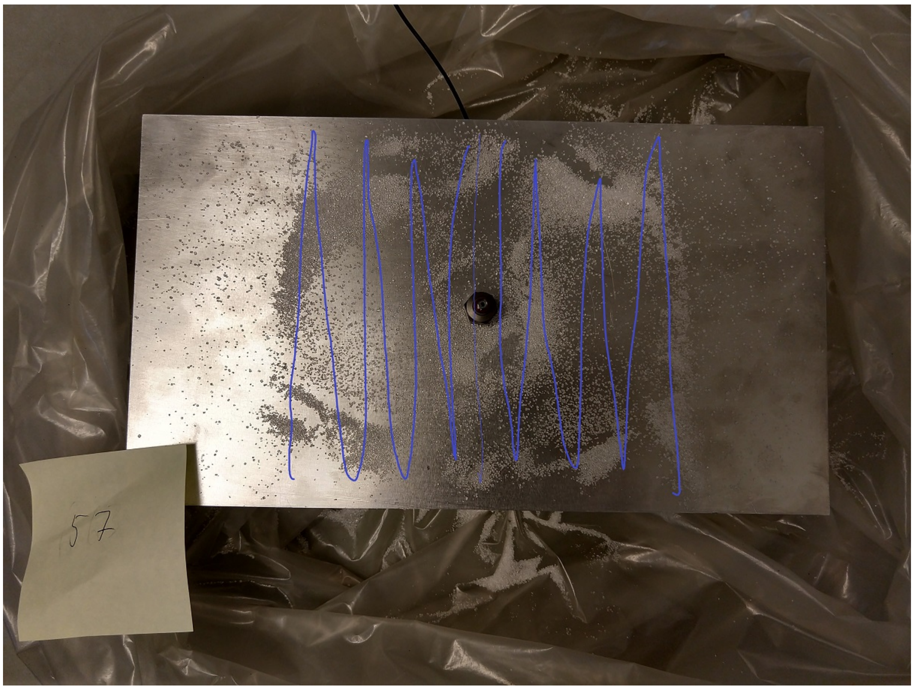

Figure A.14: Mode shape at 57 Hz. (Additional resonance.)

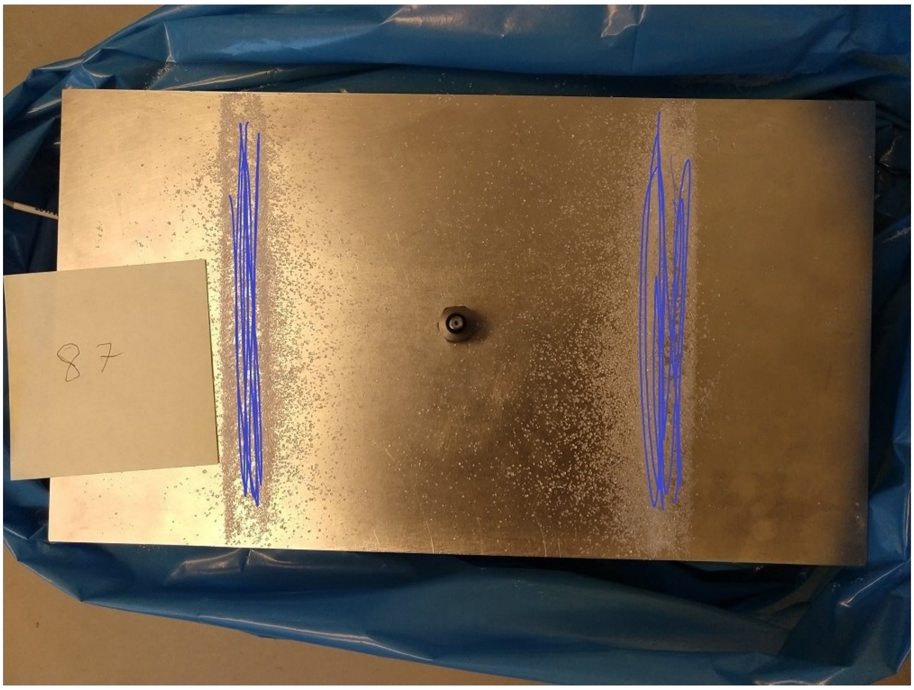

Figure A.15: Mode shape at 87 Hz. (Expected resonance.)

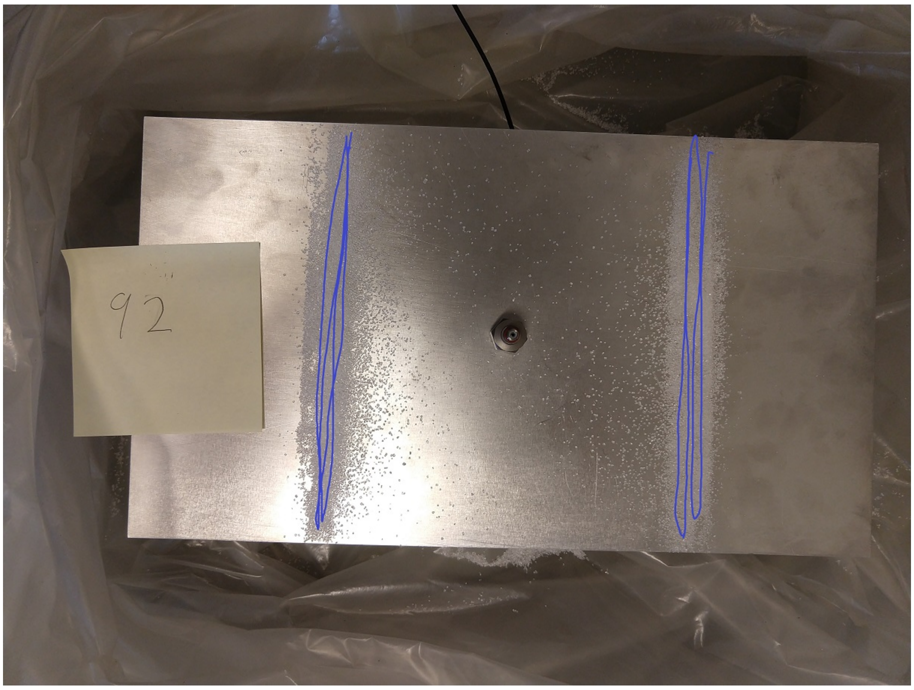

Figure A.16: Mode shape at 92 Hz. (Vibration dominated by 87 Hz mode shape.)

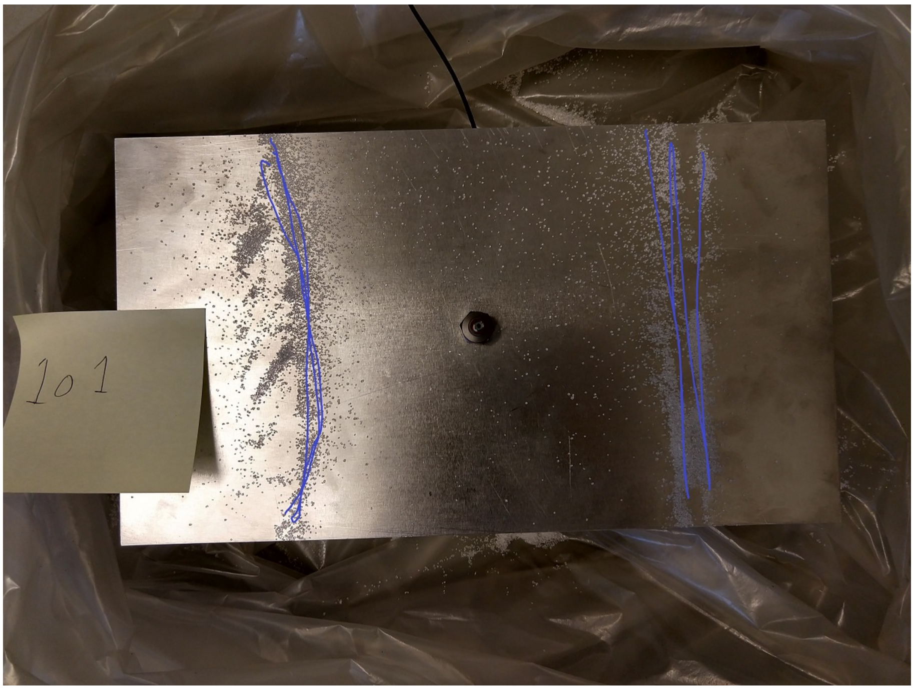

Figure A.17: Mode shape at 101 Hz. (Vibration dominated by 87 Hz mode shape.)

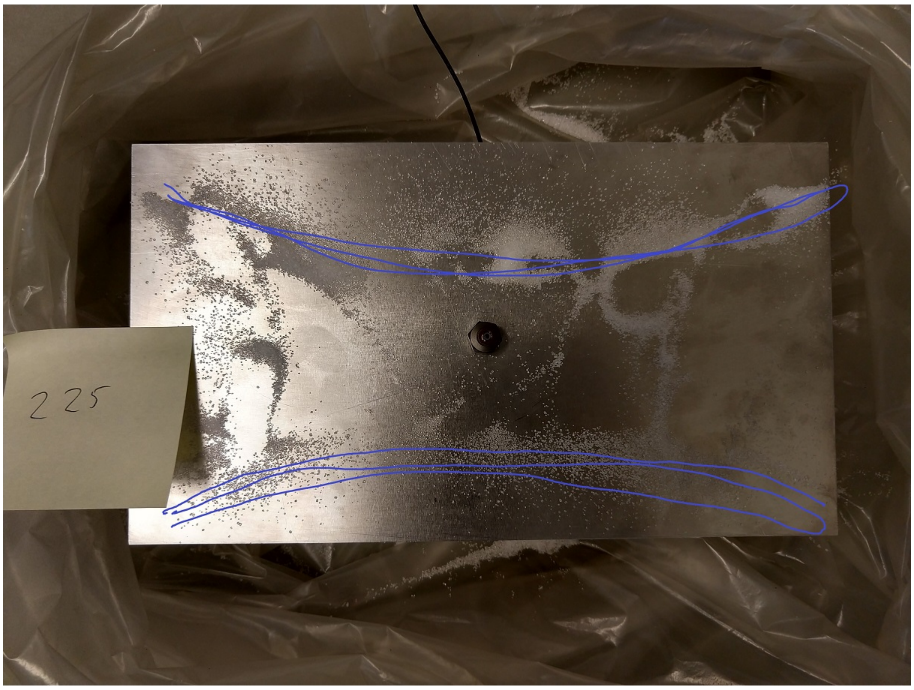

Figure A.18: Mode shape at 225 Hz. (Vibration dominated by 256 Hz mode shape.)

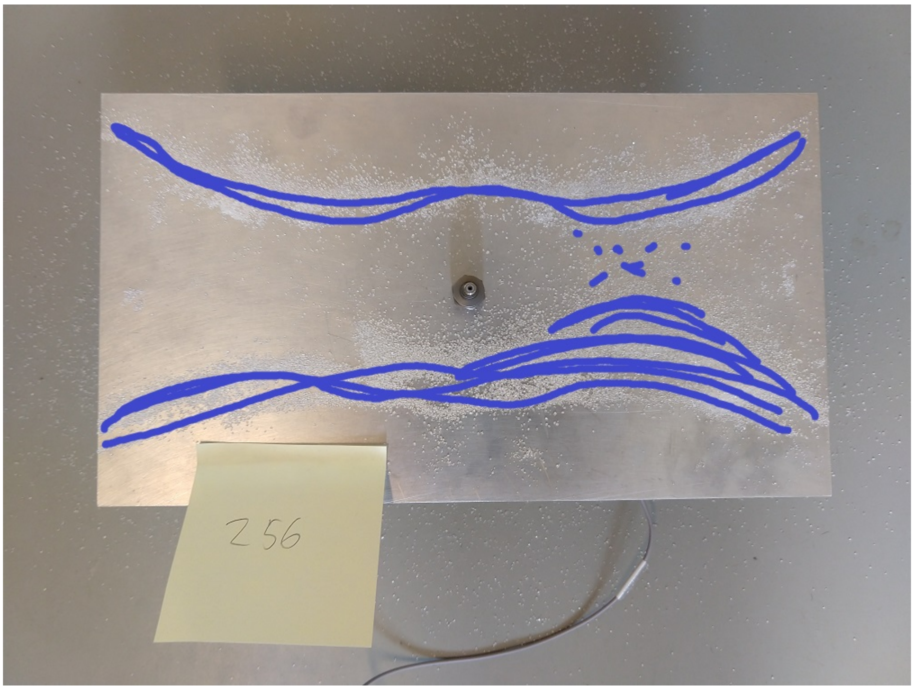

Figure A.19: Mode shape at 256 Hz. (Expected resonance.)

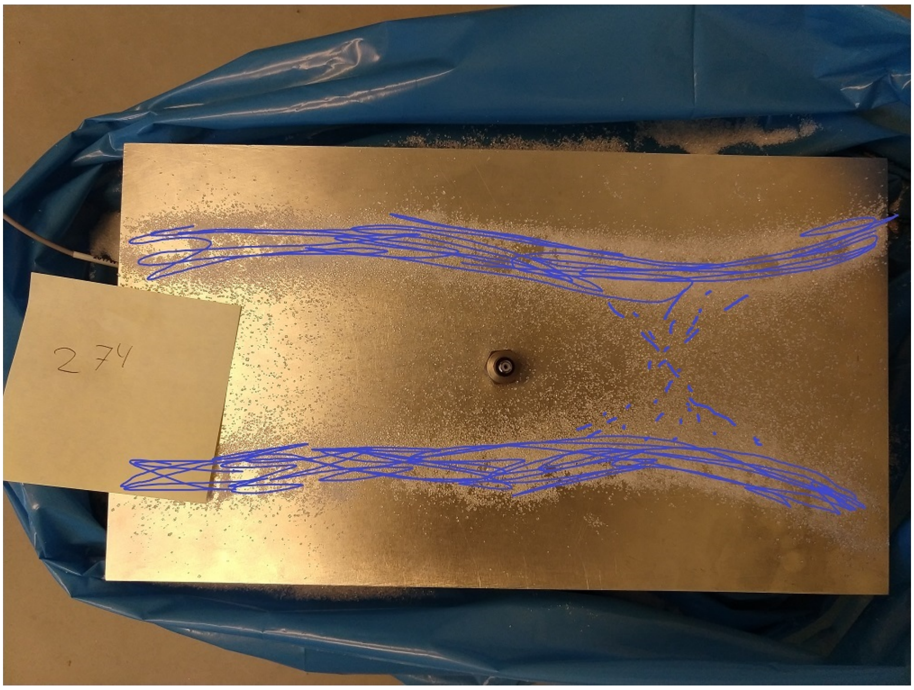

Figure A.20: Mode shape at 274 Hz. (Vibration dominated by 256 Hz mode shape.)

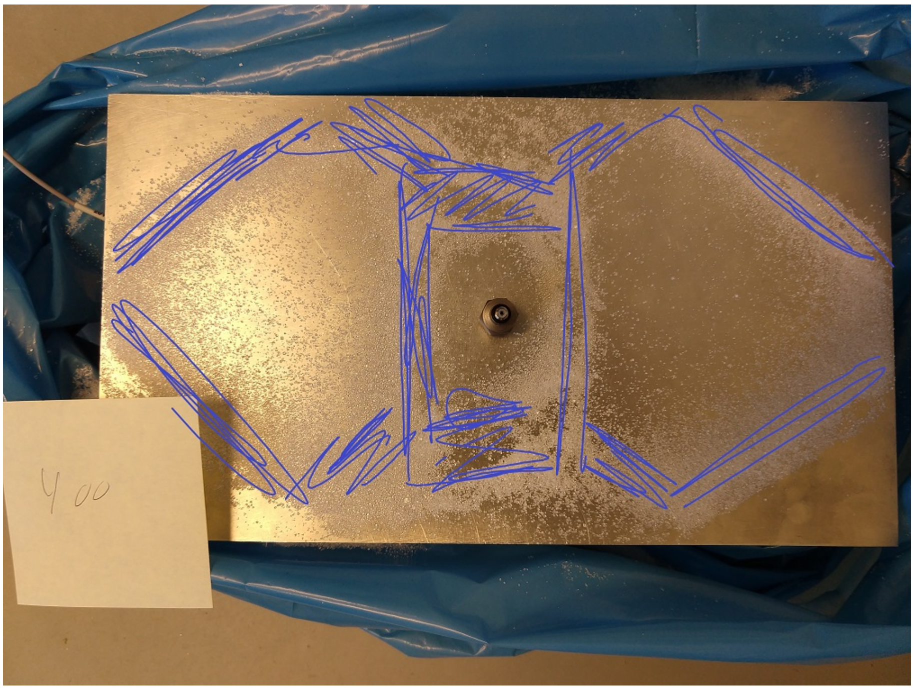

Figure A.21: Mode shape at 400 Hz. (Expected resonance.)

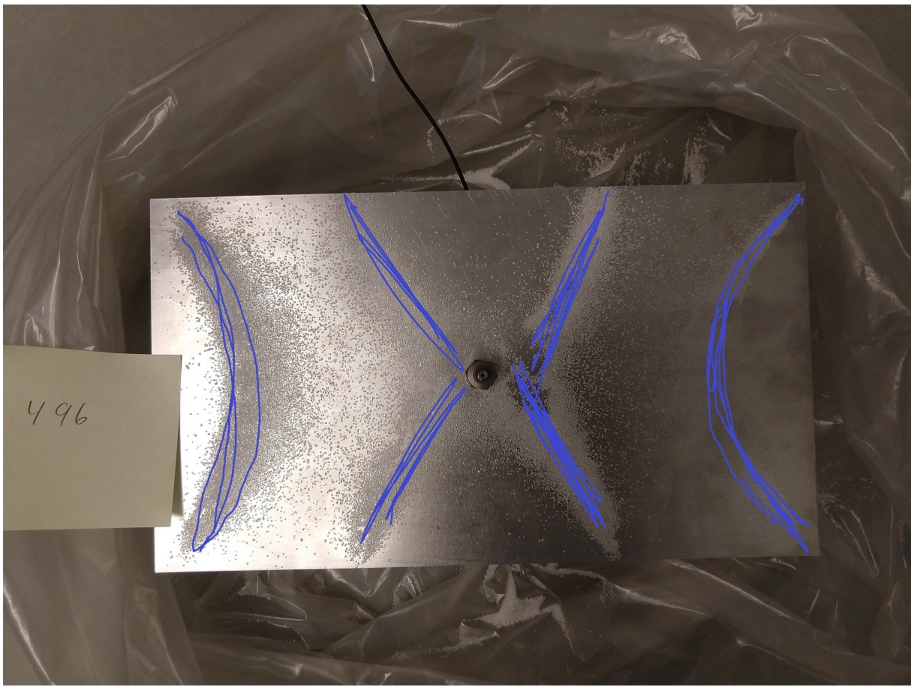

Figure A.22: Mode shape at 496 Hz. (Expected resonance.)

The mode shapes on the plate have been determined at the frequencies of interest. It is noted that the mode shapes at multiple frequencies might look similar. This is because non-symmetric mode shapes cannot be excited in the middle of the plate. Instead a neighbouring eigenfrequency with a doubly symmetric mode shape determines the mode shape .

A.2.6 Results part 2

At a later stage it turned out that the original choice of sugar as material and the resulting upper frequency limit of the experiment of 500 Hz was inadequate. Substituting the sugar with fine salt it was possible to extend this limit up to 1588 Hz. Only the frequencies where sound is radiated are considered, namely 864 Hz, 1148 Hz, 1416 Hz and 1588 Hz. On this second set of experiments the plate was turned 180 degrees by mistake, so the pictures have been rotated 180 degrees to make results comparable - resulting in the post-its being upside down.

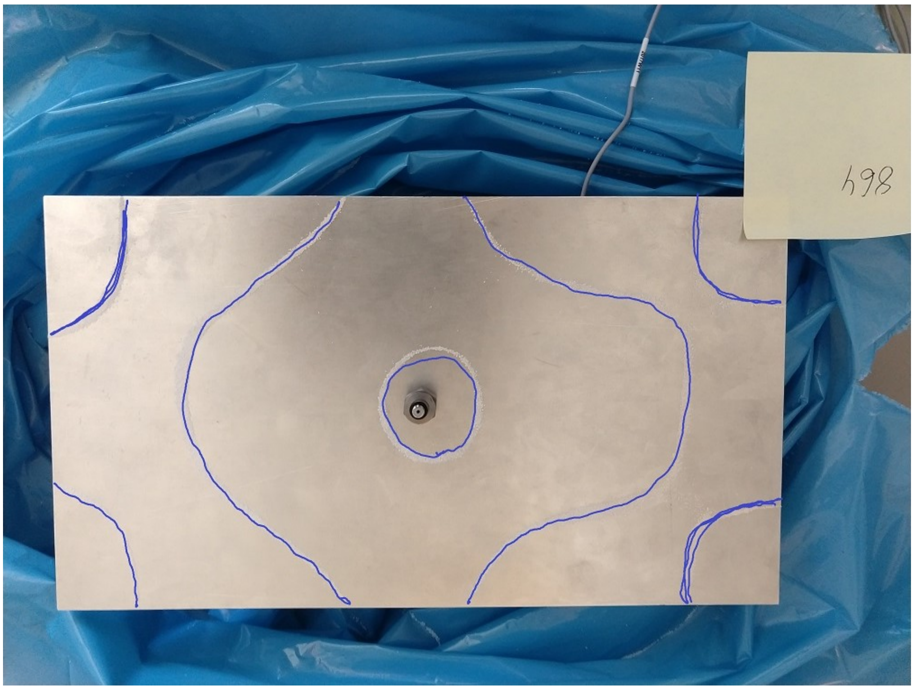

Figure A.23: Mode shape at 864 Hz.

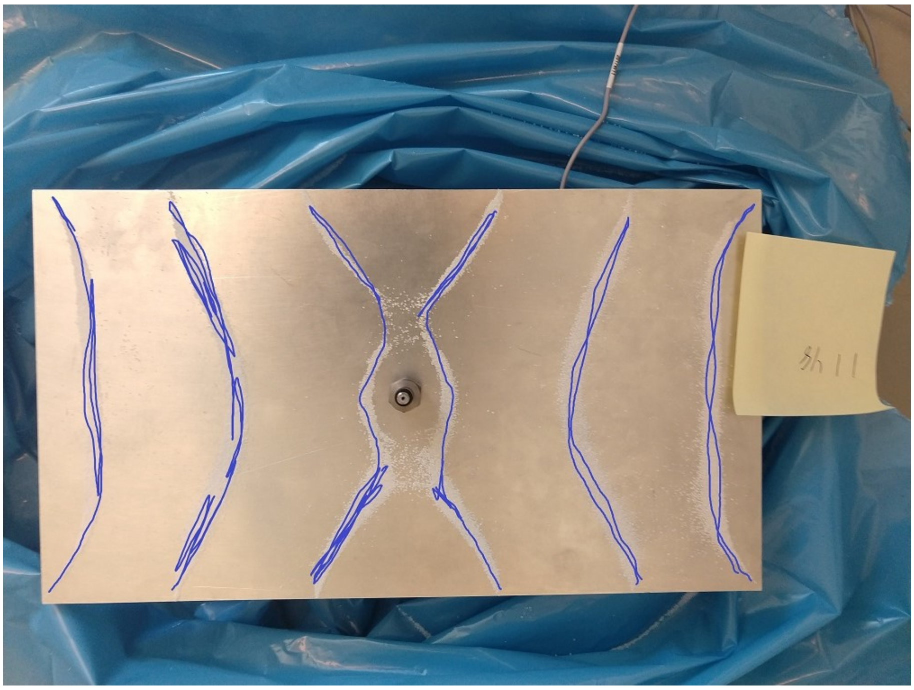

Figure A.24: Mode shape at 1148 Hz.

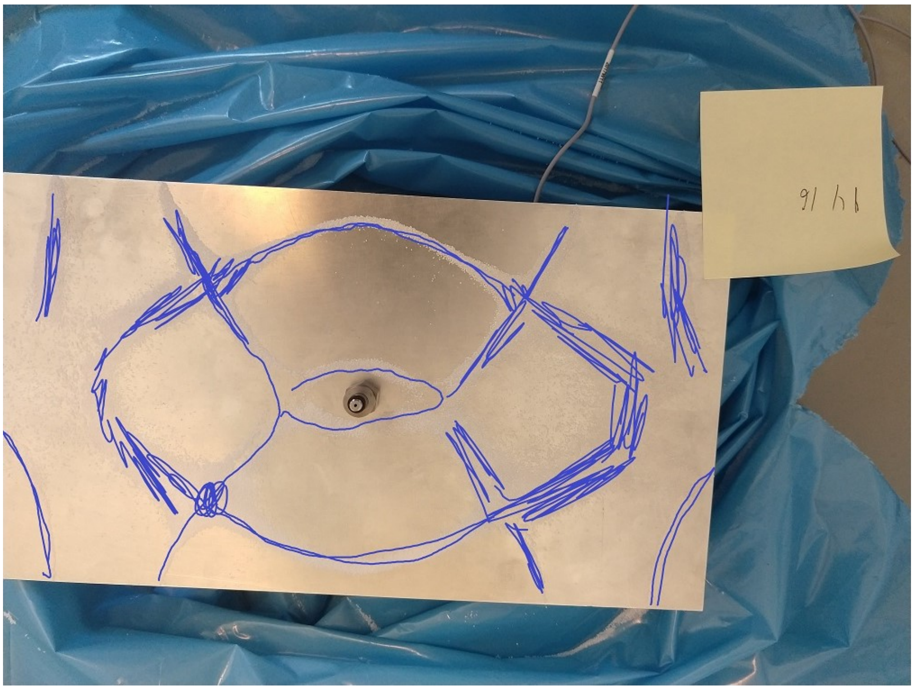

Figure A.25: Mode shape at 1416 Hz.

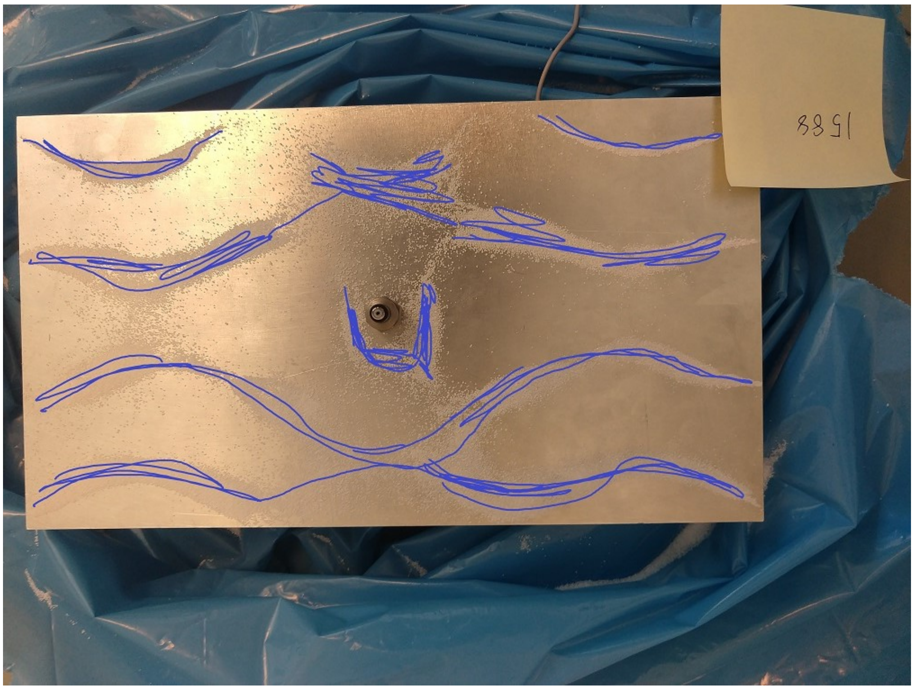

Figure A.26: Mode shape at 1588 Hz.

This concludes the section on determining mode shapes. The mode shapes of the first 8 doubly symmetric modes have been determined.

A.3 | In situation HRTF measurement

In this section the HRTF for the HATS is measured in situation in the hemi-anechoic room at Grundfos using a loudspeaker.

Note: the results from this experiment are not useful due to low SNR. The experiment should be re-performed using more suitable equipment namely a better sweep generator than the tone generator, a better power amplifier than the one intended for the shaker as well as some means of controlling the power input to the loudspeakers or less fragile loudspeakers. For the purpose of this project and a more general case than auralization of the measurement room at Grundfos the HRTF database acquired in Appendix B is seen as a better alternative.

A.3.1 Setup

In order to measure the in situation HRFT of the HATS basically the same setup as that given in section A.1 is used. The main difference is that a loudspeaker is used instead of the plate. Due to the size of available loudspeakers the position of the loudspeaker membrane is (0,0.25,0)m compared to the (0,0.097,0)m of the plate. This is unavoidable due to the enclosure of the loudspeaker and is not compensated for. Giving in an error in distance for both positions as well as in angle for position 2.

The loudspeaker is a single transducer mounted in a box. The transducer is a 4 inch Peerless SDS-P830855 mounted in a closed box with inner dimensions HxWxD = 0.147x0.0.147x0.152 m. It has a maximum power handling of 30 W and no crossover is used.

To measure the sound pressure and HATS response in Position 1 and Position 2 in addition to the items given in table A.2 the following equipment is used.

Function	Model	Serial number
Microphone	B&K 4189	2117848
Pre amplifier	B&K 2671	2143356
Calibrator	B&K 4231	2459857
Loudspeaker in box	NaN	NaN

Table A.9: Model and serial numbers of the additional items used in the setup.

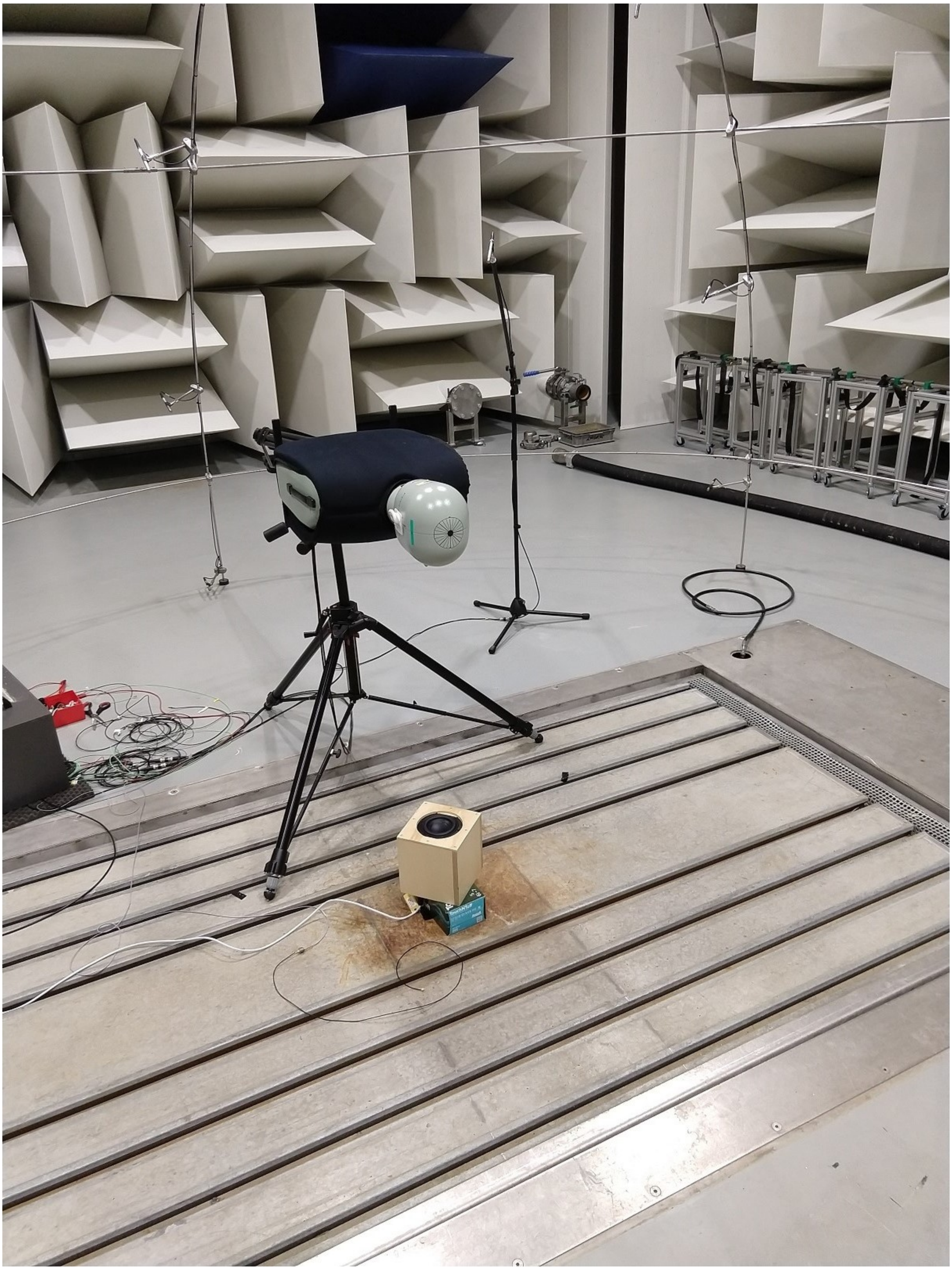

Figure A.27: The setup used for measuring in situation HRTF. Here the HATS is in position 1 and the microphone in position 2. The HATS was naturally removed when measuring the reference in Position 2.

A.3.2 Connections

The connections are identical to those used in table A.6 except the shaker and plate are replaced with the loudspeaker and the force transducer and the accelerometer are disconnected. Instead an additional microphone is connected together with a loopback.

From	Comment	To	To Channel
B&K 4189	Via preamp B&K 2671	ADC (5)	5
Tone generator (6)	Via amplifier (8)	loudspeaker	-
Tone generator (6)	Via amplifier (8)	ADC (5)	6

Table A.10: Equipment connections.

A.3.3 Settings

All settings are left as in section A.1 with the exception that the volume on the power amplifier is set to 10 o'clock instead of 2 o'clock.

The additional microphone and the loopback are sampled at 65.536 Hz like the other microphones. The additional microphone is calibrated using B&K 4231 (calibration value 1.018) since it unlike the other microphones is not part of the standard setup, which is calibrated regularly.

The tone generator is set to create a logarithmic sine sweep from 100 Hz to 20 kHz over 5 seconds with a level of 1 Vpp.

A.3.4 Procedure

- The tone generator is set to send a single sweep on a manual trigger.
- The measurement system is started.
- The sweep is triggered.
- The measurement system records stores the first 10 seconds whereof five should contain the sweep. This is confirmed by listening to the recorded signal in Pulse.

The above is repeated 4 times with the microphone and the HATS in the 2 positions

A.3.5 Results

Method for calculating transfer functions

In order to calculate the HRTF the transfer frequency response from the HATS ears have to deconvolved with the reference microphone. This is done using a method described by [Müller and Massarani, 2001]. The method is called non-cyclic deconvolution and it's schematic overview is shown in figure A.28

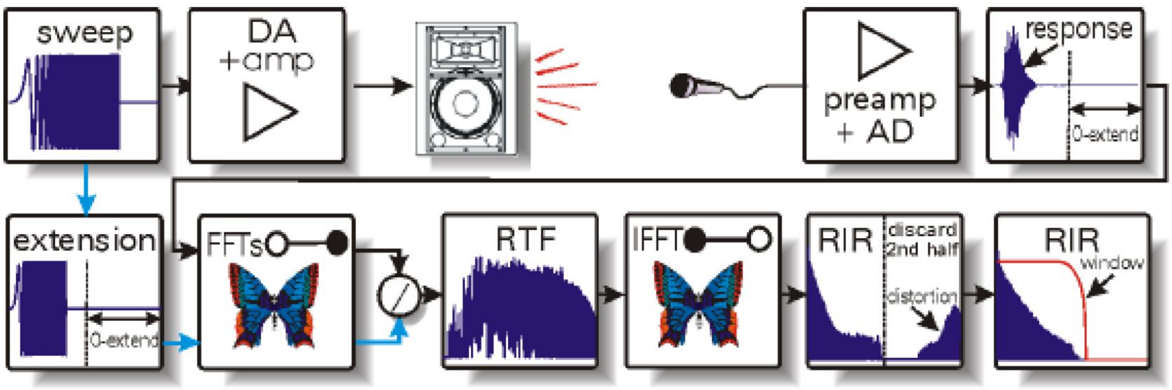

Figure A.28: Non-cyclic deconvolution as given in [Müller and Massarani, 2001].

The usage of a tone generator as source has some drawbacks. Firstly the sweep and recording is started manually and separately, which means that the delay before the sweep starts in the recording differs between measurements. So in order to calculate the HRTFs first the fact that the timing of the sweep is not controlled has to be accounted for. This is done by deconvolving the recordings with the sampled loopback signal instead of a digital copy of the sweep. This yields an impulse response for the loudspeaker in the measurement position, where the reference or HATS microphone is placed.

The second issue with the tone generator is that it generates a constant tone at the sweep start frequency until the sweep is started. This means that the sound before and after the sweep is a 100 Hz tone and not silence as intended in the paper. This should be resolved by using a computer controlled generator such as the B&K 3060A. The issues caused by this was however realized after the measurements were performed, setup removed and the room in use for other measurements.

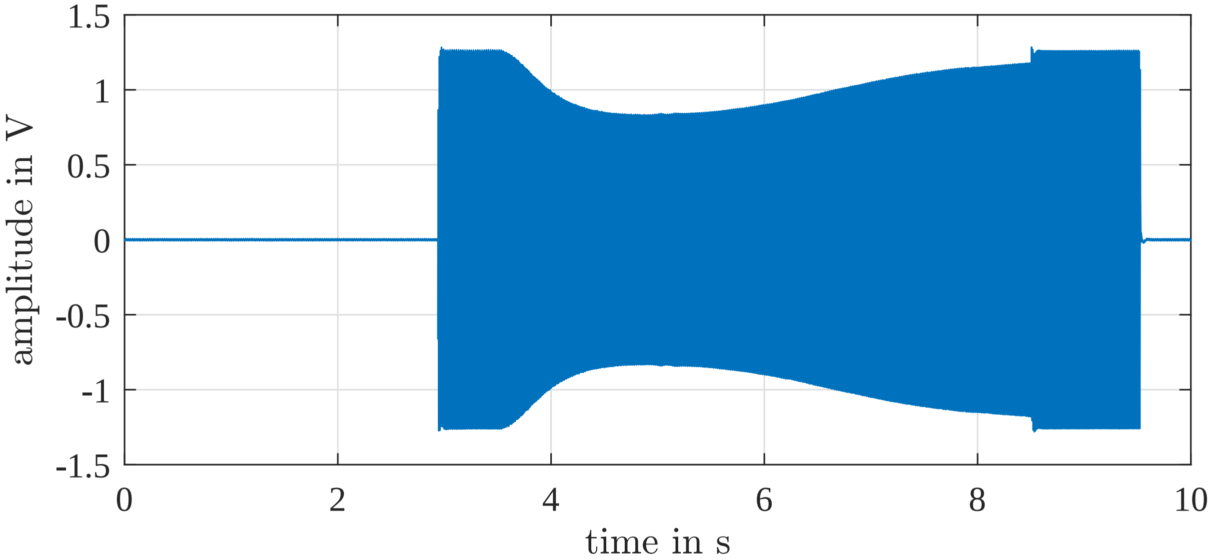

Figure A.29: The loopback signal in time domain. The 100 Hz tone before and after the sweep are seen as the 'flat' 2.5 Vpp part. Furthermore spikes at onset and offset of the signal are seen.

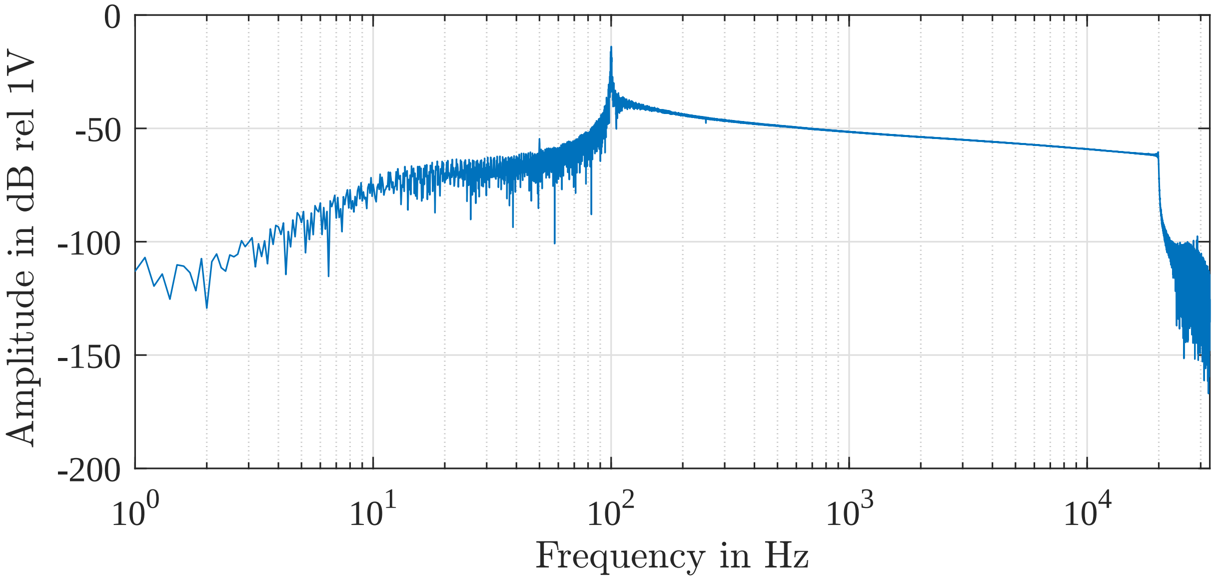

Figure A.30: The loopback signal in frequency domain.

In theory the deconvolution method should work with any stimuli, so the 100 Hz start and stop should just be seen as part of the reference signal and be deconvolved. However the results will later show overtones of 100 Hz which could be caused by this or possibly 50 Hz humming.

The Third issue is that the sweep does not cover all frequencies in the sampled range as no safety crossover is mounted before the loudspeaker. This is solved by only plotting the valid frequency area 100 Hz to 20 kHz.

Data acquired

Below the recordings from the microphones are given in position 1 and position 2 in frequency domain.

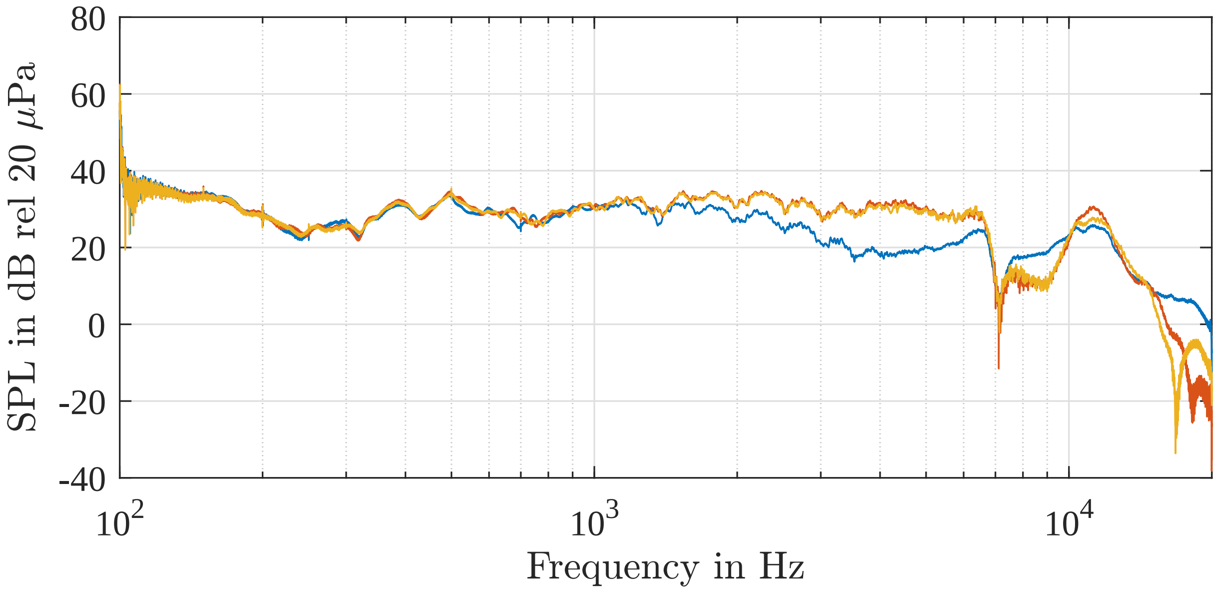

Figure A.31: The SPL at the different microphones in position 1. Reference microphone (—), HATS left ear (—) and HATS right ear (—).

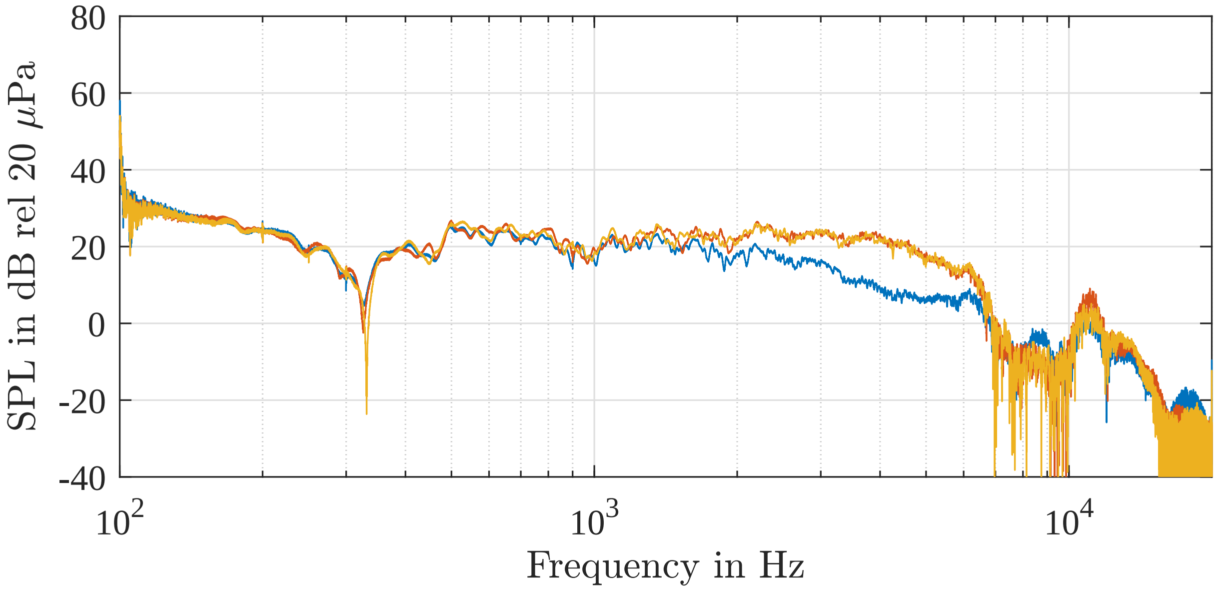

Figure A.32: The SPL at the different microphones in position 2. Reference microphone(—), HATS left ear (—) and HATS right ear (—).

Calculated results

The frequency response of the loudspeaker in position 1 and position 2.

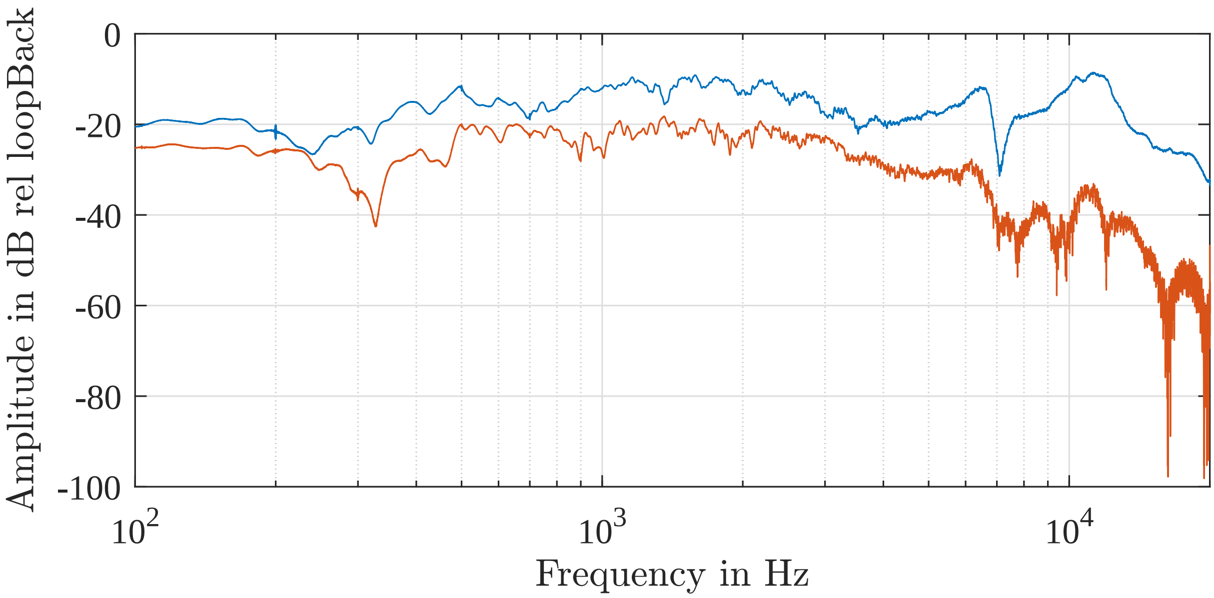

Figure A.33: The response of the loudspeaker in position 1 (—) and position 2 (—).

The signal generated by the loudspeaker is not flat especially not in position 2 which is at an off angle to the loudspeaker. Since the measured signals in the positions are used as reference this is not a problem as long as the level is above the noise floor. Unfortunately that is not the case. Deconvolving the individual ear responses with the reference yield the HRTF at that position. The deconvolution is performed as a spectral division of the complex frequency response at the ear microphone with the complex frequency response from the reference microphone.

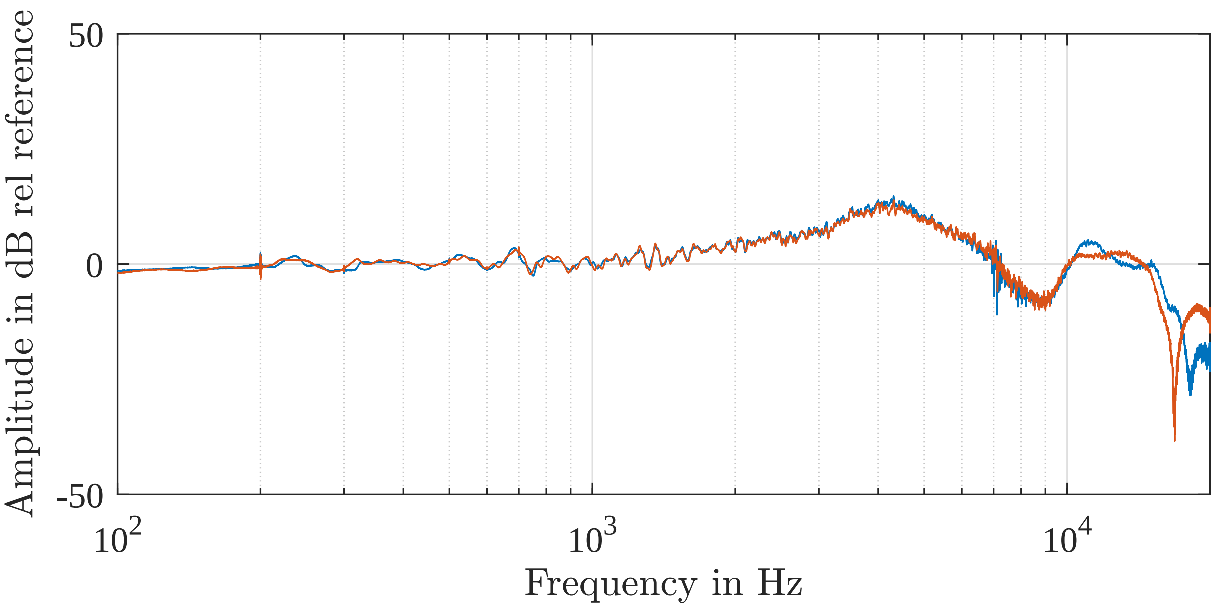

Figure A.34: The HRTF of the HATS in position 1 left ear (—) and right ear (—).

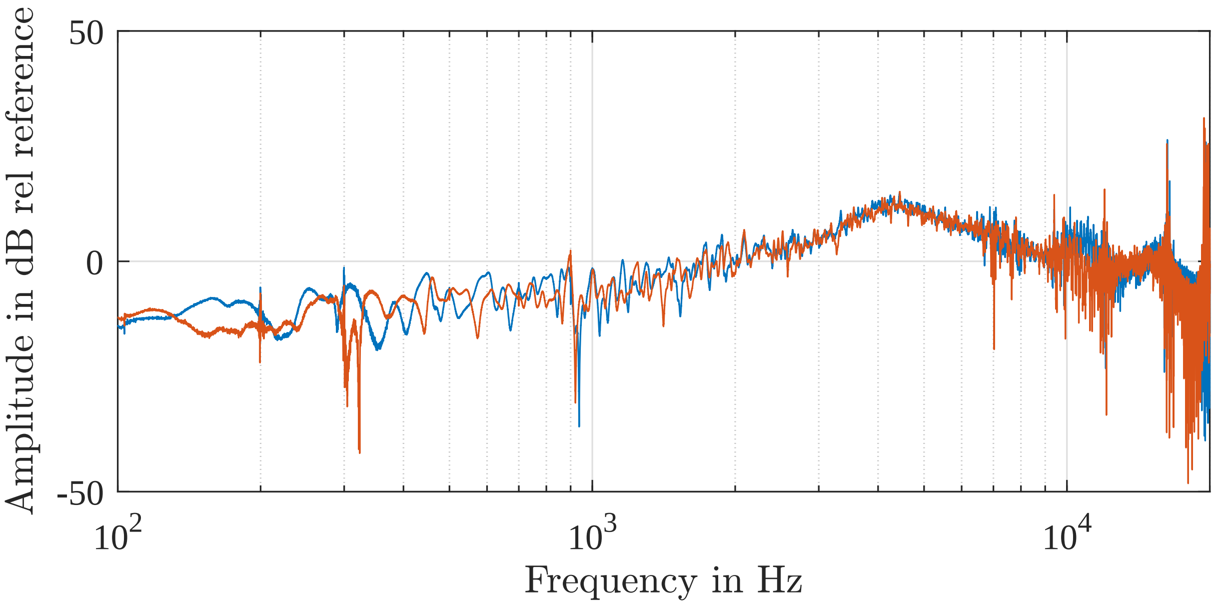

Figure A.35: The HRTF of the HATS in position 2 left ear (—) and right ear (—).

The HRTFs for the HATS have been determined in the two positions where recordings were performed in section A.1.

As discussed in the introduction to the measurement the SNR is very low. The recordings are made at level of about 30 dBSPL. The inherent noise in the microphones is 6.5 dB(A) [Brüel & Kjær, no date c]. The background noise in the room is 5.5 dB(A) according to the certification. The experiment should be re-performed but that is not done seeing as the HRTFs are measured in anechoic conditions in Appendix B instead.

B | Measuring HRTF

Another student at Aalborg University was measuring head related transfer functions (HRTF) on human subjects during the same time as as I did my thesis. Therefore a complete setup for measuring HRTF was available. The setup was fully automated and is described below together with the results. For a fully comprehensive walk-through the reader is referred to the master's thesis written by Sigurd Van Hauen [Hauen, 2018].

B.1 | Setup

The setup consists of 11 loudspeakers positioned on an arc at a distance of 1.7 meters from the reference position. The loudspeakers cover elevation angles from $-40°$ to $-40°$ in $8°$ intervals. The vertical rotation is made using a turntable where turns are made from direct front ($0°$) in $1°$ intervals to the back of the HATS is turned towards the loudspeakers ($180°$). The data for the other side is created as a mirror, since the HATS is fully symmetric.

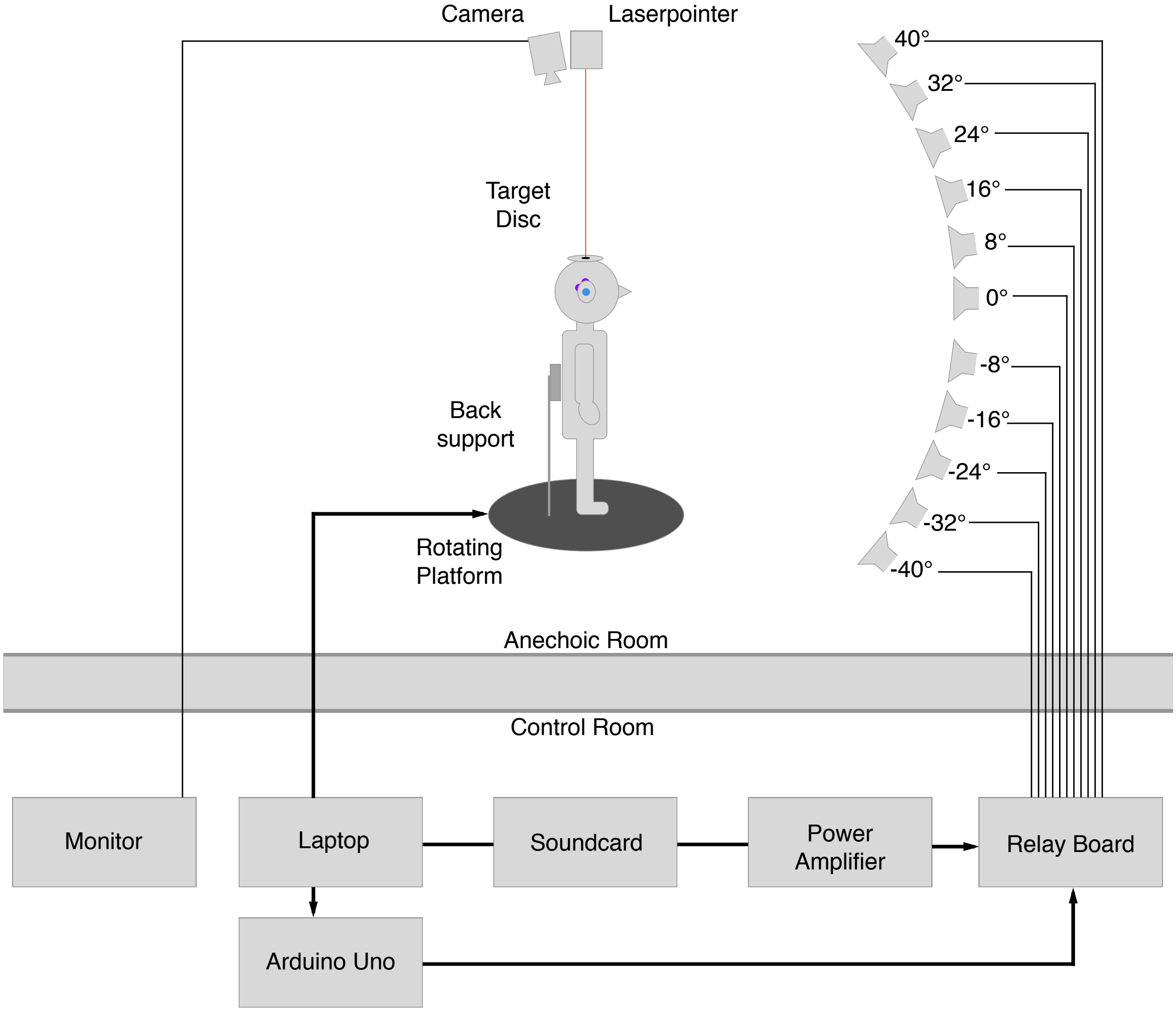

Figure B.1: Schematic of setup from [Hauen, 2018]. The blue and purple dots represent a hearing aid used in the original project. The target disc is built into the HATS.

Figure B.1 shows the setup as it is used in [Hauen, 2018]. In this context a few differences exist. The major difference is that the person with blue and purple hearing aid with a back support is replaced with the HATS on it's stand. When human subjects are tested the camera and monitor is used to make sure the participant is not moving, in the setup with a HATS it is redundant. Instead the cross lasers used for building the setup came in handy as they were used to position the HATS accurately. On the note of accuracy; the setup is made to be accurate compared to how stationary people can be expected to be for prolonged periods of time, about 20 minutes. Obviously the HATS is superior to humans when the challenge is standing still, so the slight misalignments due to the setup that were irrelevant before might be influence the results.

Another difference from the setup used by [Hauen, 2018] is that he uses small microphones mounted in peoples ears. In this project the internal microphones of the HATS are used. These internal microphones are connected to the same sound card as that which drives the power amplifier. The 48V phantom power built in to the sound card is used to supply the microphones.

For the reference measurement a pressure field measurement microphone is used. The microphone is placed vertically with 90° incidence from the 0° elevation loudspeaker. At the time this was thought as best compromise between all sources - at a later stage it has been realized that 90° incidence could have been achieved for all sources by mounting the microphone horizontally and turning the microphone to be orthogonal to the plane of the sources. The error due to this is in the order of 4 dB [Brüel & Kjær, no date e] in the range 15 kHz to 20 kHz for the outermost source angles. The microphone is connected via a pre-amplifier and a measurement amplifier with polarization voltage to the soundcard.

Figure B.2: Picture of the HATS in the measurement system.

B.2 | Equipment

Item	Description	AAU-no.
1	Macbook Pro (medio 2012) running MATLAB 2017b	NaN
2	B&K HATS 4100D	NaN
3	RME Fireface UFX II Sound card	108227
4	Pioneer A-656 Power Amplifier	08698
5	11 x M10MD39-08 in ball mount	NaN
6	Outline Rotational table	NaN
7	12 channel Relay Board	NaN
8	Arduino uno	NaN
9	GRAS 26ak pre-amp	52665
10	B&K microphone 4134	61447
11	B&K Charge Amplifier 2636	08717

Table B.1: Equipment used in HRTF measurement setup.

B.3 | Settings

The measurement system uses a sampling rate of 48 kHz and an MLS signal as stimuli. The MLS signal is generated with 3 cycles, one for exciting the system and the following two for pre-averages. The order of the used MLS signal is 12 resulting in a length $L = 4095$, the lowest frequency in the signal being $fs/L = 11.7$ Hz and the upper frequency being $fs/2 - fs/(2L) = 23994.1$ Hz [Vanderkooy, 1994].

B.4 | Procedure

Before the measurements can be performed the setup is calibrated. The reference microphone is calibrated using a calibrator and the sensitivity is put into the measurement script. For the HATS measurement the calibration values used at Grundfos are used.

B.4.1 Reference measurement

The reference measurement is made using the reference microphone in the future centre position of the HATS. This point is found as the point where all four laser lines meet. The reference measurement is made once for each loudspeaker for a total of 11 measurements using an automated script described in [Hauen, 2018]. The script is set to only measure at 0° to avoid that the turntable turns.

B.4.2 HATS measurement

The procedure for the HATS measurement is similar to that of the reference measurement. The HATS is positioned using the lasers and the script is started. This time the script is set to measure at 0°, 1°, 2° ... 180°.

B.5 | Results

B.5.1 Raw data

The recorded SPL level at the reference position is shown in figure B.3 with the level from the HATS ear microphones on top.

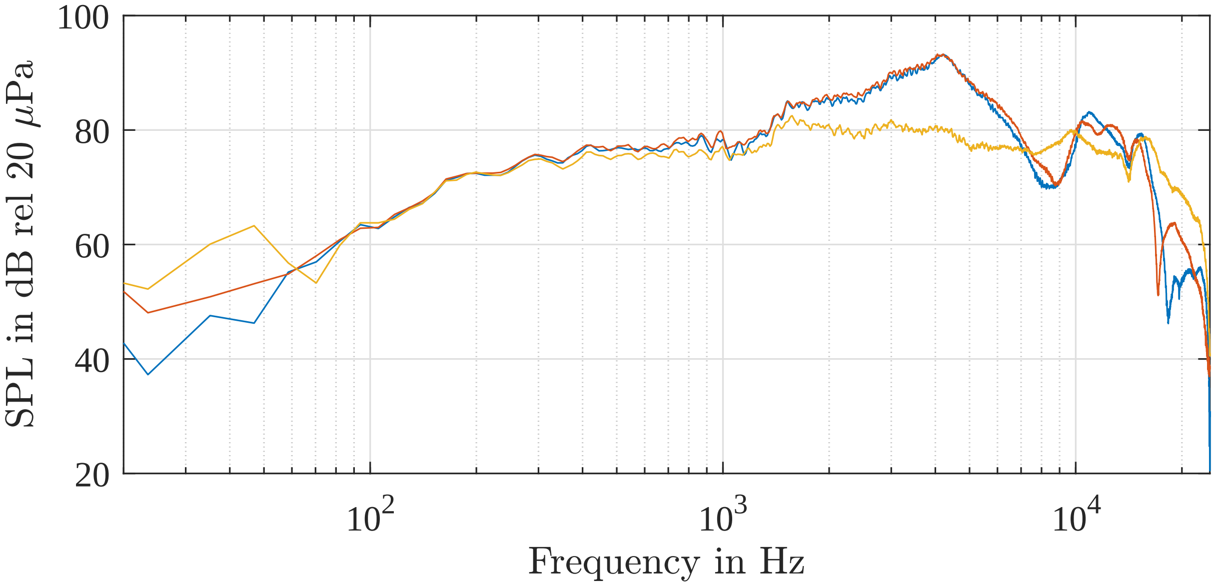

Figure B.3: The SPL measured at the reference position (—) and the HATS left ear (—) and right ear (—).

The response is also plotted in time domain figure B.4. The impulse response from the reference microphone is flipped as the phase is inverted by the microphone as described by [Brüel & Kjær, 1996] 'phase of the output voltage is opposite to that of the sound pressure'.

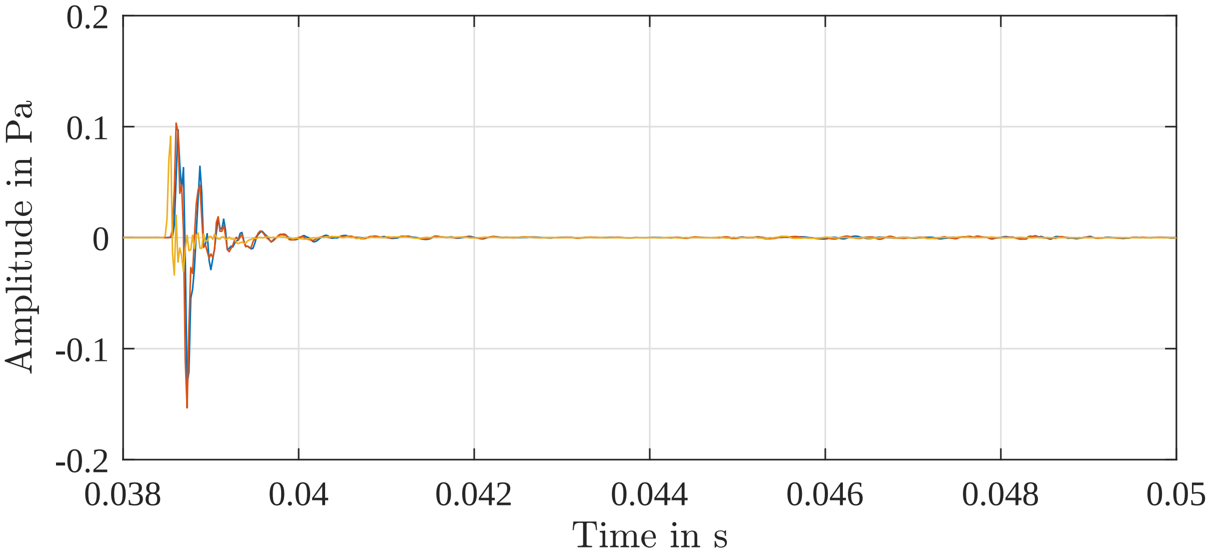

Figure B.4: The SPL measured at the reference position (—) and the HATS left ear (—) and right ear (—).

Removing reflections from setup

From figure B.3 a very fluctuating frequency response is seen, this is due to a comb filter caused by reflections from the setup. These reflections are removed by time gating with a Hanning filter with an order of 512 on both reference and HATS impulse responses. The window is kept stationary in time even though the impulses move slightly due to different delays with position.

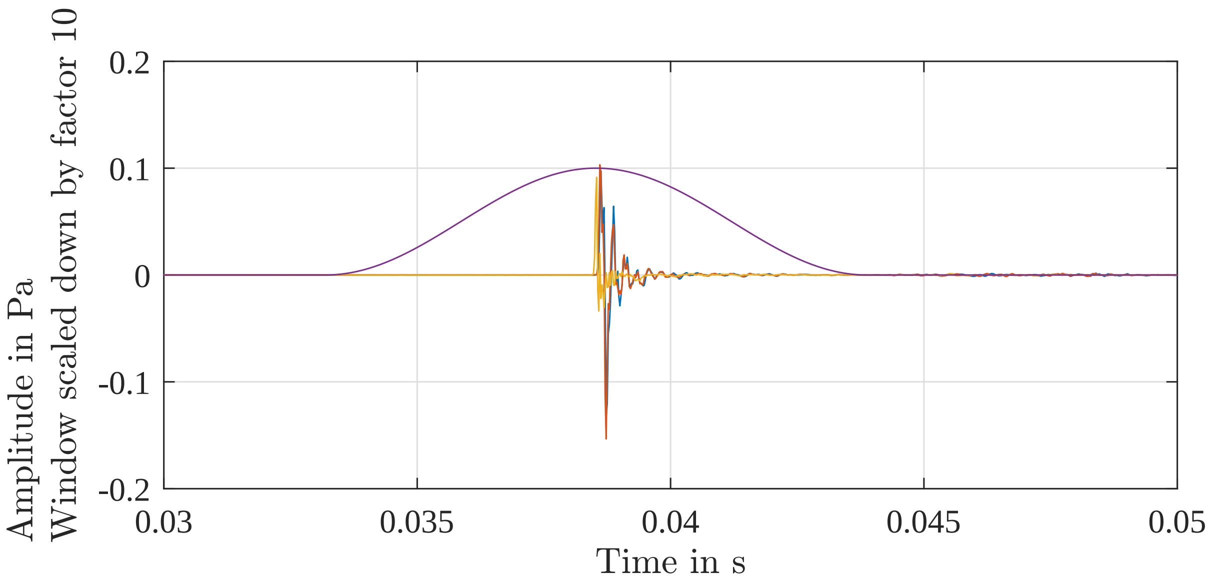

Figure B.5: The SPL measured at the reference position (—) and the HATS left ear (—) and right ear (—). The Hanning window (—) is scaled down by a factor 10 for easier viewing.

In figure B.5 the window is scaled down by a factor 10, it's true amplitude is 1. In the unedited impulse responses the reflections can be seen as small ripples in the impulse response even after it has decayed fully - starting from $\approx$ 45 ms. Having removed the reflections from setup the frequency response is much smother as seen in figure B.6

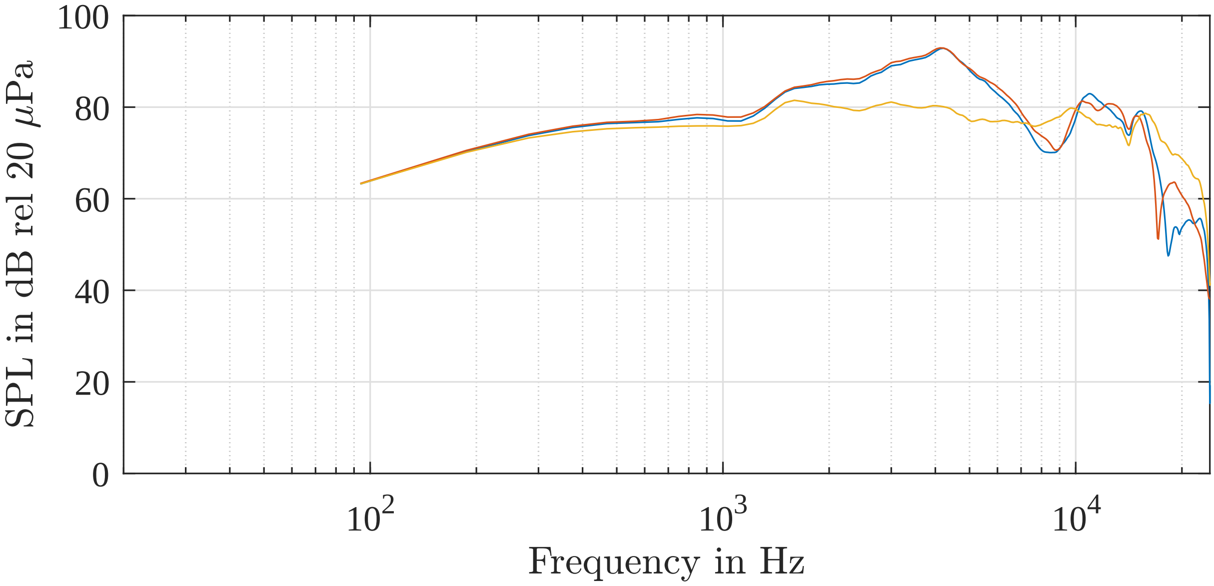

Figure B.6: The SPL measured at the reference position (—), the HATS left ear (—) and right ear (—). Time gating has been performed to remove reflections from the setup.

B.5.2 Data Treatment

The HRTF is calculated as a spectral division of the ear signals with the reference signal. The resulting frequency response is inverse Fourier transformed to acquire the impulse response. Since the deconvolution is done cyclically the onset of the impulse response might be in the end of the frame, instead of in negative time, where it should have been (corresponding to the sound arriving at an ear before it arrives at the reference position). This is solved by shifting the response cyclically 28 samples to the right. This will allow the impulse to arrive at the time corresponding sound propagating 20 cm before the reference to be wrapped around.

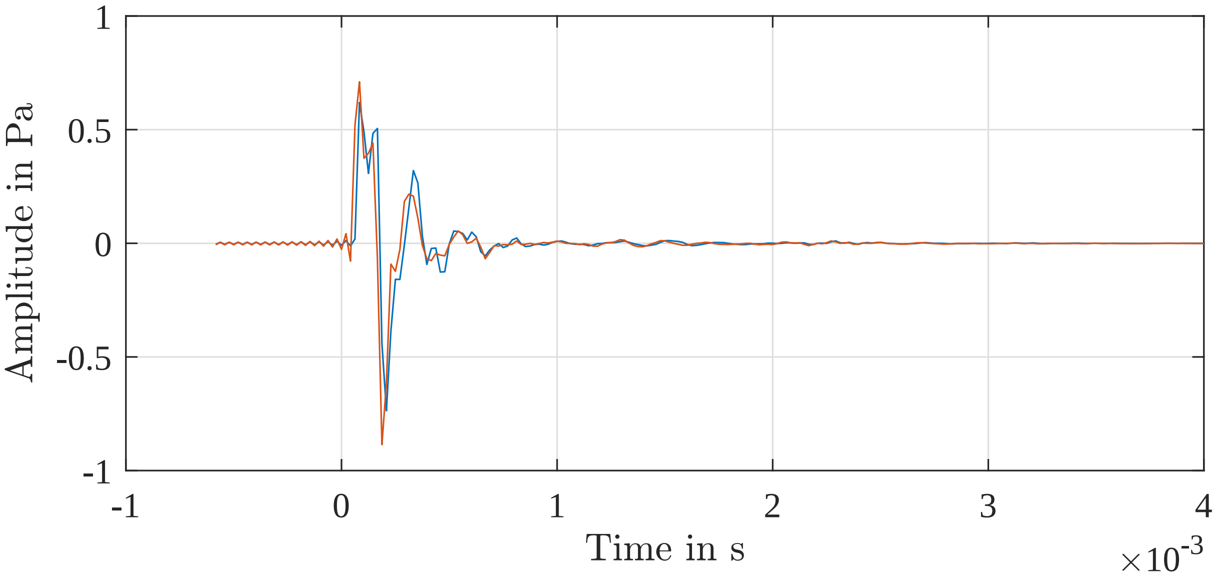

Figure B.7: The The HRTF of the HATS facing forwards left ear (—) and right ear (—).

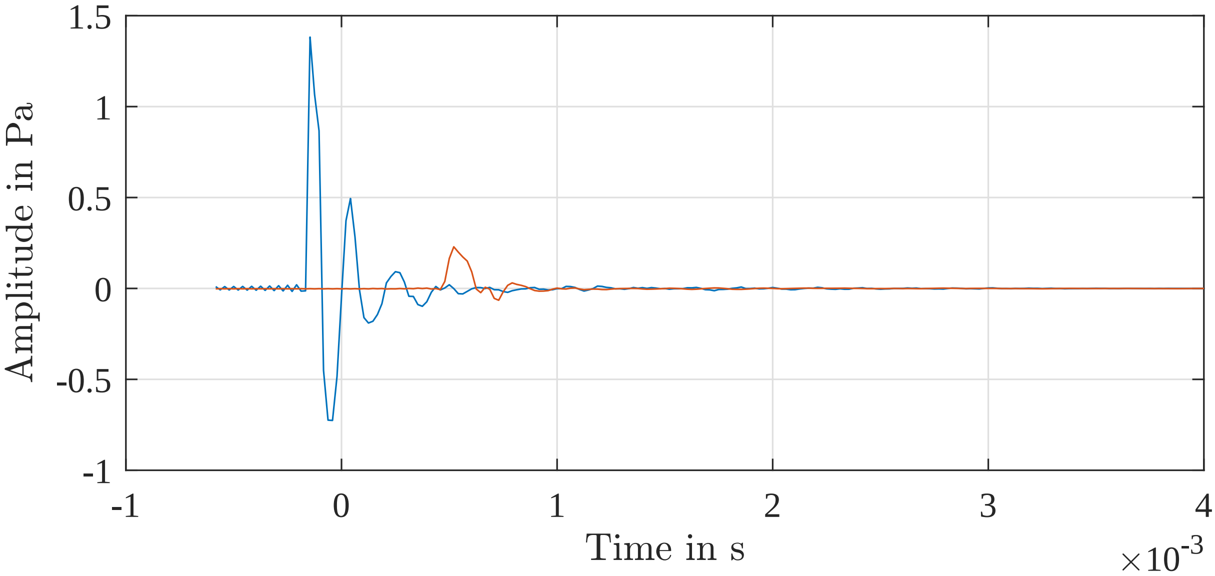

Figure B.8: The The HRTF of the HATS turned 90° clockwise, left ear (—) and right ear (—).

A few phenomena are observed, first pre-ringing is treated. The pre-ringing is not present in the impulse responses in figure B.5 but appears after the cyclic deconvolution. This is most likely due to the fact that different channels are used for the three different measurements, so the division includes some artefacts from the non identical anti aliasing filters. The preringing is removed using a 4th order Buttorworth IIR low pass filter at 23 kHz created by the matlab command 'butter()'. figure B.9 and figure B.10 shows figure B.7 and figure B.8 again after the filtering.

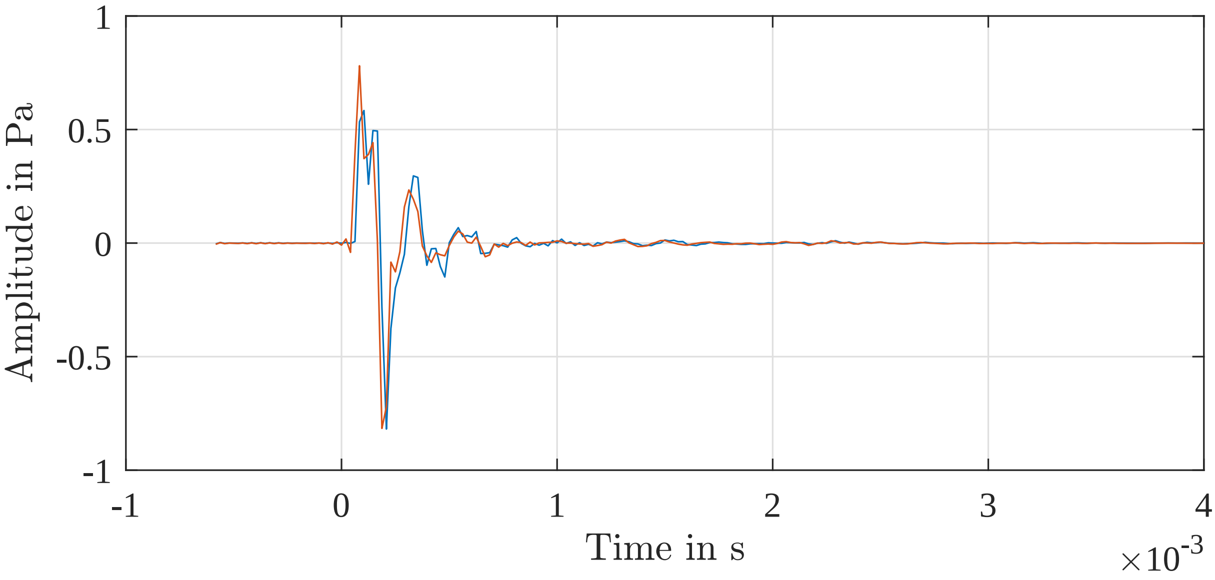

Figure B.9: The The HRTF filtered for pre-ringing of the HATS facing forwards left ear (—) and right ear (—).

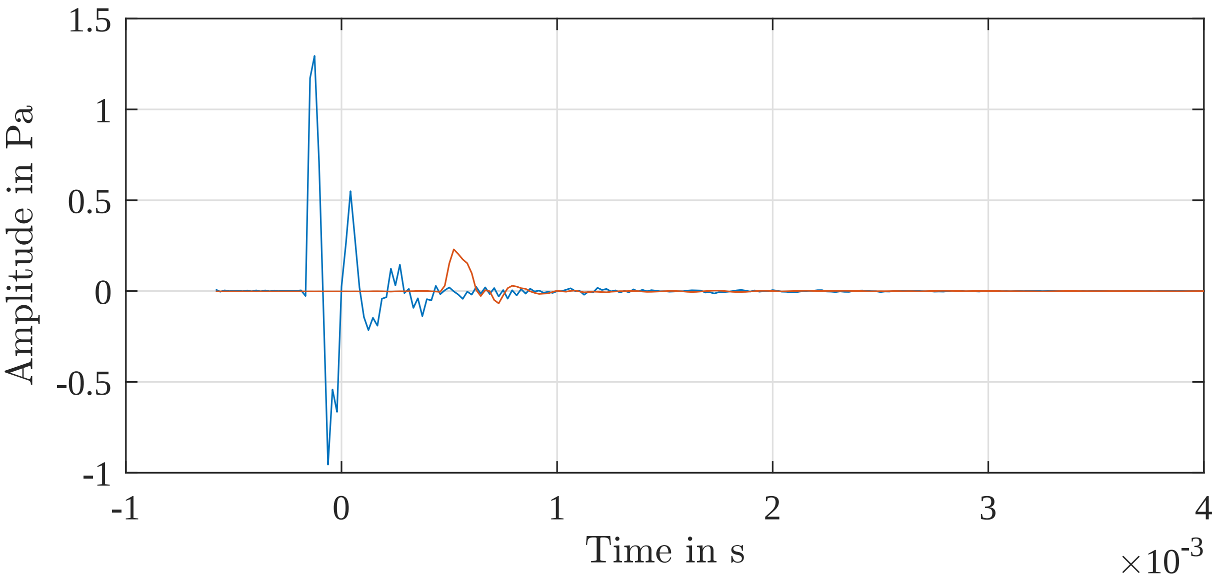

Figure B.10: The The HRTF of the HATS turned 90° clockwise and filtered for pre-ringing, left ear (—) and right ear (—).

The second phenomena appears when taking the Fourier transform of the HRTF. The phenomena is that some DC offset is present, and as it is known that the HRTF should converge to 0 dB at DC as the dummy is infinitely small compared to the wavelength of 0 Hz. For some positions however the gain it is rather significant and as such should be removed by as suggested by [Hammershøi and Møller, 2005]. in order to show the low frequency phenomena the FFT length used is 2^{16}, which means that the 512 samples long impulse responses are zero padded to that length.

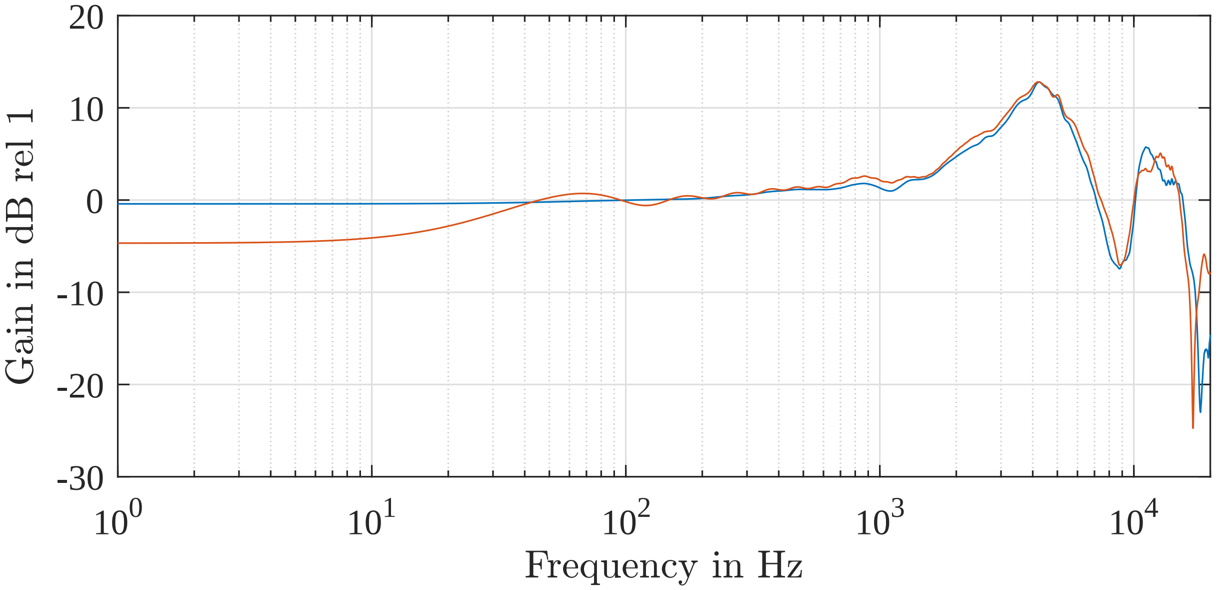

Figure B.11: The The HRTF of the HATS facing forwards left ear (—) and right ear (—).

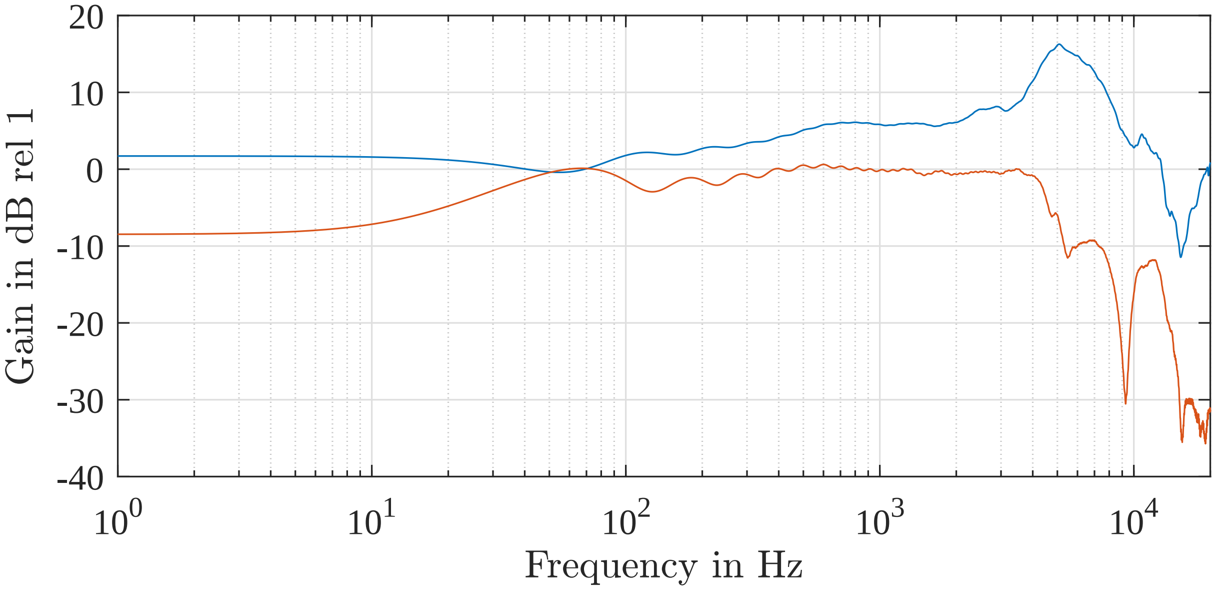

Figure B.12: The The HRTF of the HATS turned 90° clockwise, left ear (—) and right ear (—).

From figure B.11 and figure B.12 it is clear that the 512 sample long impulse response has a DC offset. The method proposed in [Hammershøi and Møller, 2005] is to simply set the DC component to unity in the frequency domain before the inverse Fourier transform. This method removes the DC component as desired.

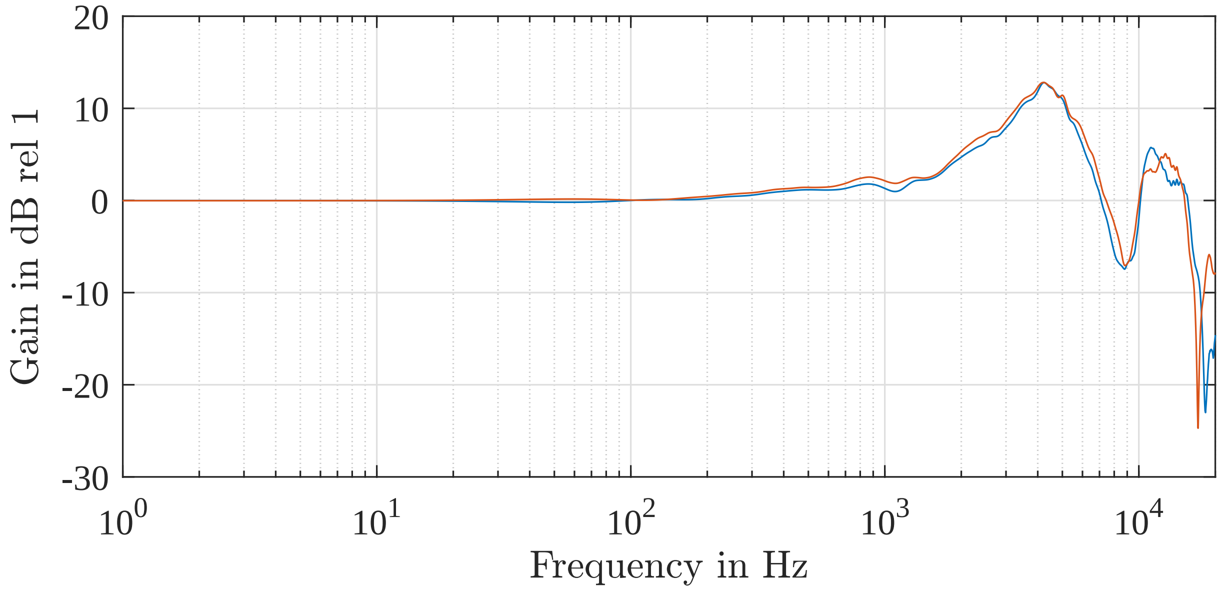

Figure B.13: The The HRTF of the HATS facing forwards left ear (—) and right ear (—).

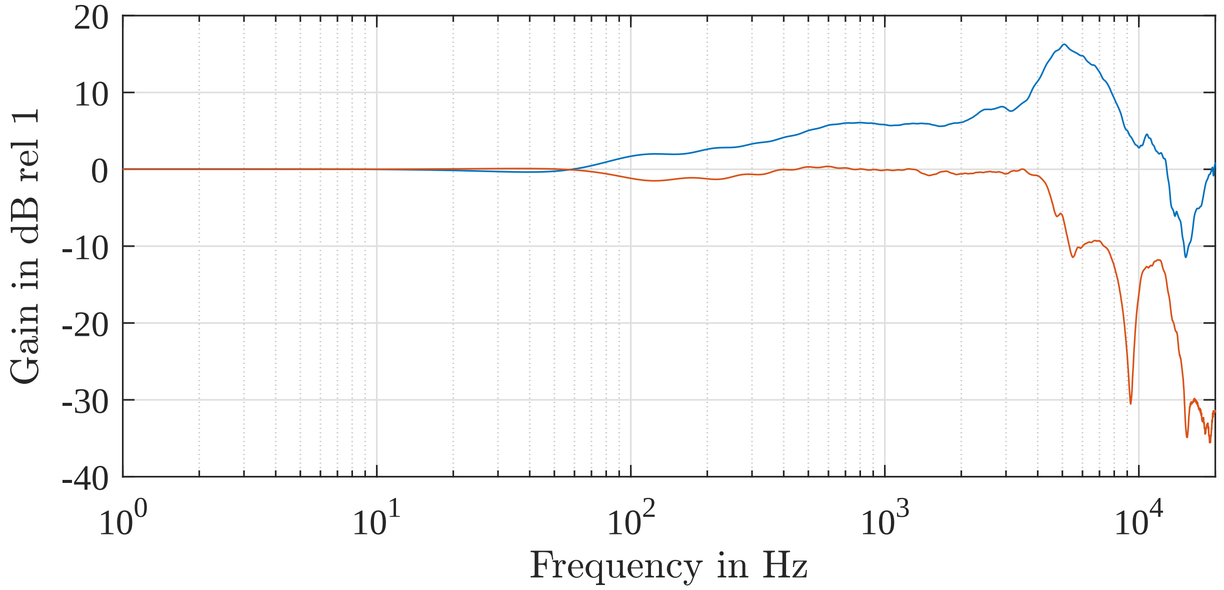

Figure B.14: The The HRTF of the HATS turned 90° clockwise, left ear (—) and right ear (—).

B.6 | Summary

The HRTF of the dummy head has been determined at 1° intervals from 0° to 180° at 11 elevations from −40° to 40°. The data can be mirrored by swapping the ears to yield a full circle.

C | Headphone transfer function

This appendix describes the setup required to acquire the frequency response of a pair of headphones. This is required since headphones are not normally tuned to have a flat frequency response, which is required when making a binaural playback system. This is because the filtering with a HRTF describes the sound pressure as it would be at the ear-drum. It is that sound pressure that the headphone should reproduce, without an additional frequency response of the headphone itself.

Ideally the headphone transfer function should be individually measured, meaning that it should be measured directly on the intended listener. Preferably even on the same mounting, so that the headphones are not moved before the binaural representation. Here the procedure is shown on a HATS, the HATS used when measuring the HRTFs.

C.1 | Setup

A list of equipment is given in table C.1 and the setup is illustrated in figure C.1. In addition to the setup depicted in figure C.1 a setup consisting of a loopback connecting the sound card output and input channels is used.

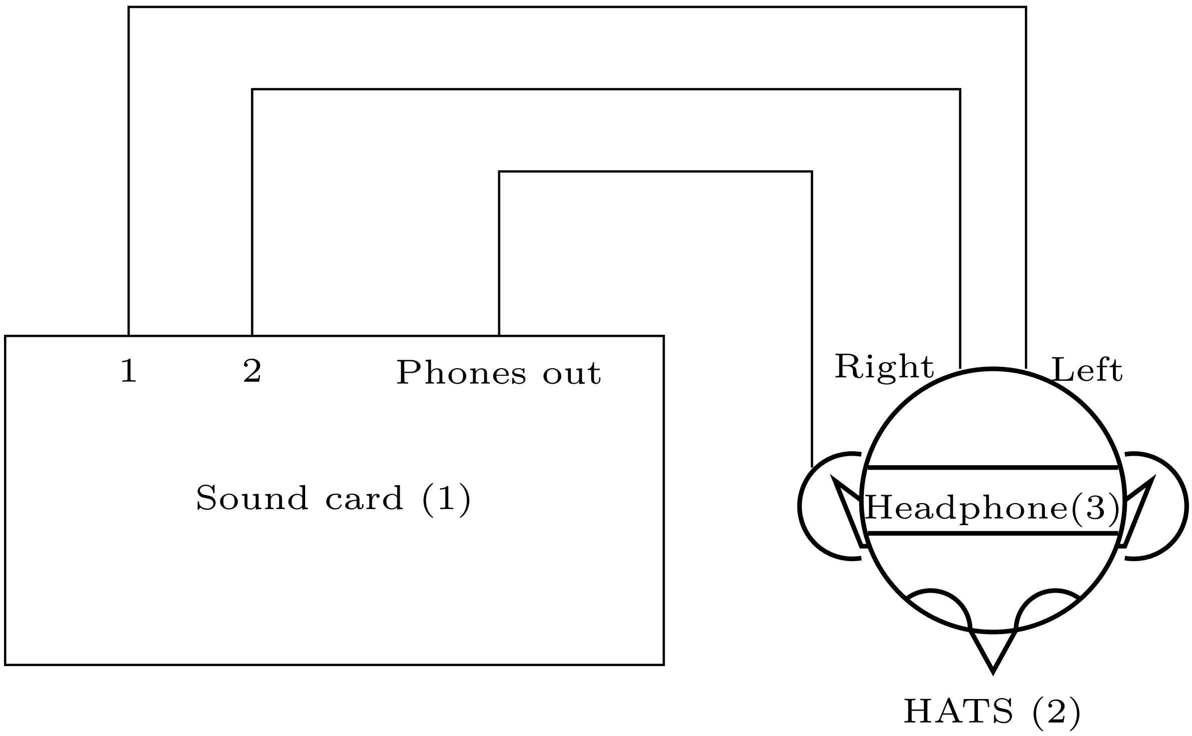

Figure C.1: Experimental setup for measuring a headphone frequency response.

Figure C.2: Picture of experimental setup for measuring a headphone frequency response.

C.2 | Equipment

Function	Model	Serial number	Number in setup
Sound card	Steinberg UR242	EEV001310	1
HATS	B&K 4100D	2209464	2
Headphone	Beyerdynamic T90	09637	3
Jack cable	Jack stereo -> 2 jack mono	-	-
2x adaptor	XLR male -> BNC female	-	-

Table C.1: Model and serial numbers of the items used in the setup. The headphone can naturally be interchanged with any other headphone one might want to use.

From	From channel	To	To channel
Sound card (1)	Phones out	Sound card (1)	1 & 2

Table C.2: Equipment connections when measuring loopback. Left channel (white) is connected to channel 1.

From	From channel	To	To Channel
Sound card (1)	Phones out	Headphone (3)	-
HATS (2)	Left microphone	Sound card (1)	1
HATS (2)	Right microphone	Sound card (1)	2

Table C.3: Equipment connections when measuring Headphone.

C.3 | Settings

Item number	Setting
(1)	Sample rate sound card 48 kHz
(1)	Input 1 ’Pad’ on
(1)	Input 2 ’Pad’ on

Table C.4: Settings for equipment connections. (’Pad’ is an attenuator.)

C.4 | Procedure

The setup is not calibrated to work at absolute sound pressure levels since only the 'shape' of the magnitude response is to be corrected and the sensitivity is irrelevant. The loopback will naturally have a much higher amplitude than the microphone signal, so the gain settings should be adjusted to make the loopback use most of the ADC range. In the case of the Here it is chosen to set the phones out to 12 O'clock and the input gain to 10 O'clock.

The measurement script 'HeadphoneTransfer.m' controls the playback and recording of sweeps. The following steps are required to perform the experiment

1. Connect the loopback as described in table C.2.
2. Run the script 'HeadphoneTransfer.m' and press 'g' when prompted to do so.
3. When the script displays a message in the command window with instructions for connecting the HATS follow these:
   (a) Disconnect the loopback
   (b) Connect the HATS as described in table C.3 using the XLR to BNC connectors.
   (c) Turn on the 48 V phantom power.
   (d) Press 'g' to continue measurement.
4. When the script is done turn off the 48 V phantom power before disconnecting the HATS.

C.5 | Results

The recordings of the loopback as well as the microphone signals are shown below.

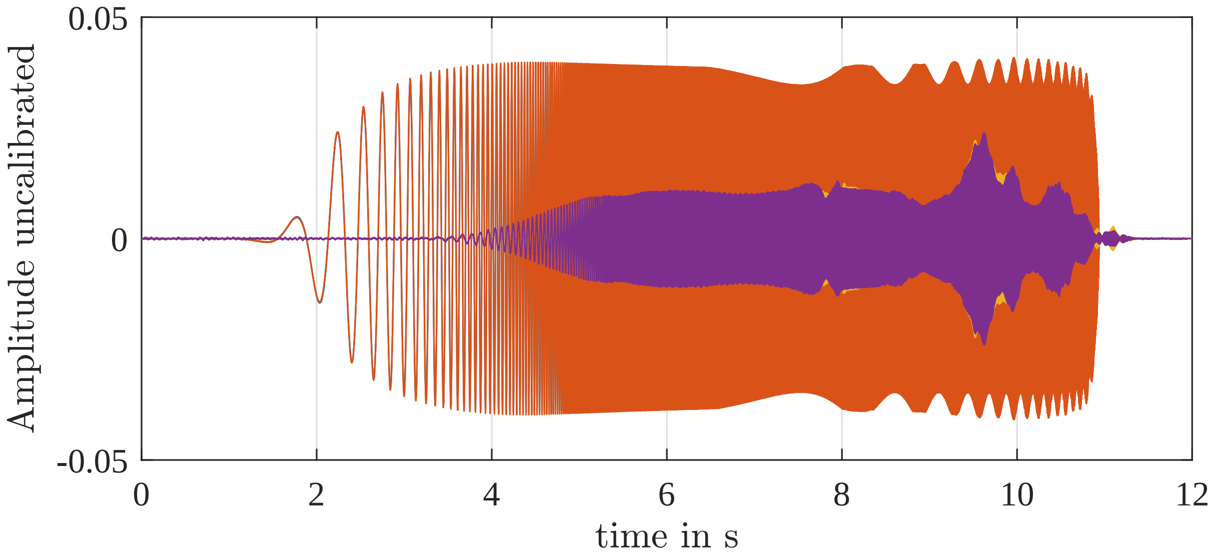

Figure C.3: Time domain plot of the loopback signal in channel left (—) and right (—) - they coincide. The recording at the HATS left ear (—) and right ear (—) - they also almost coincide.

The four recordings are also shown in frequency domain below.

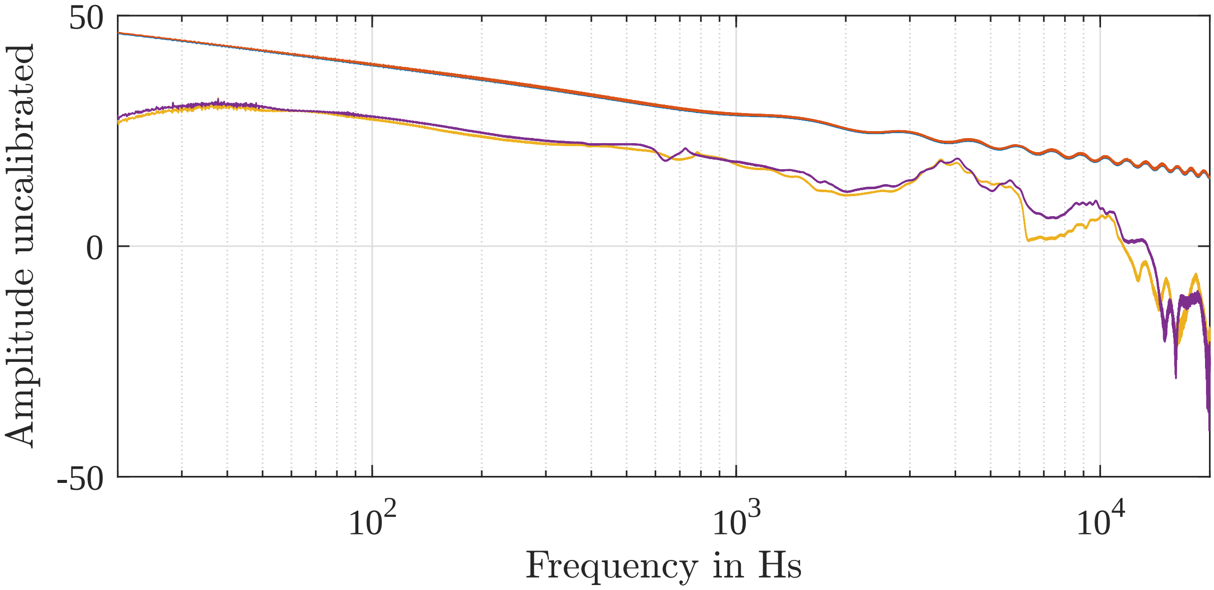

Figure C.4: Frequency domain plot of the loopback signal in channel left (—) and right (—) - they coincide. The recording at the HATS left ear (—) and right ear (—).

The transfer function is calculated as shown in figure 11.3. This is done in the script 'PostProcess.m'

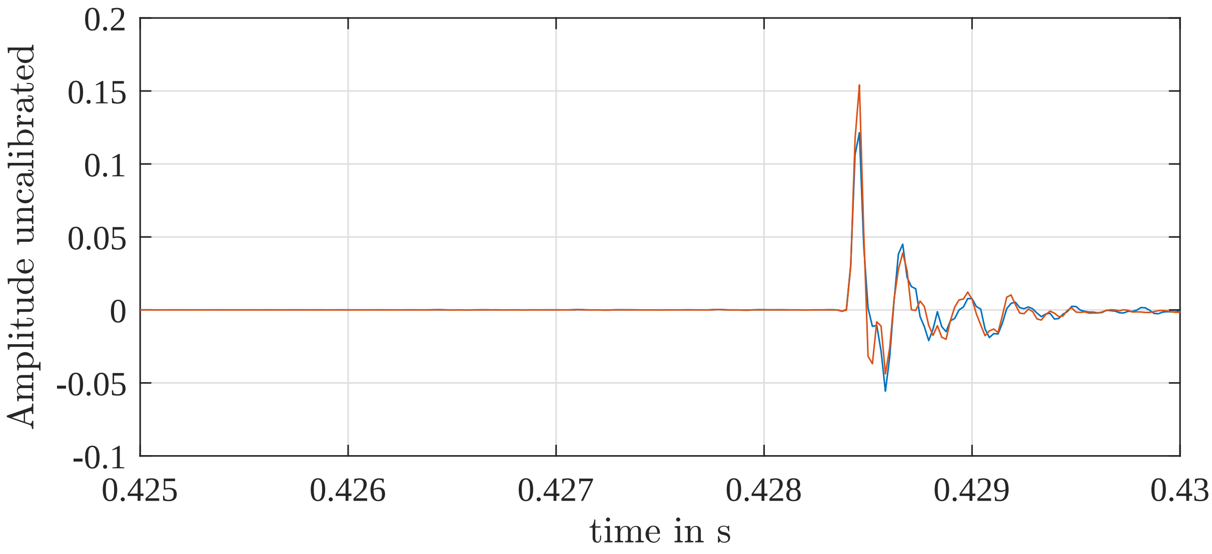

Figure C.5: Impulse response of left channel (—) and right channel (—).

And again in frequency domain.

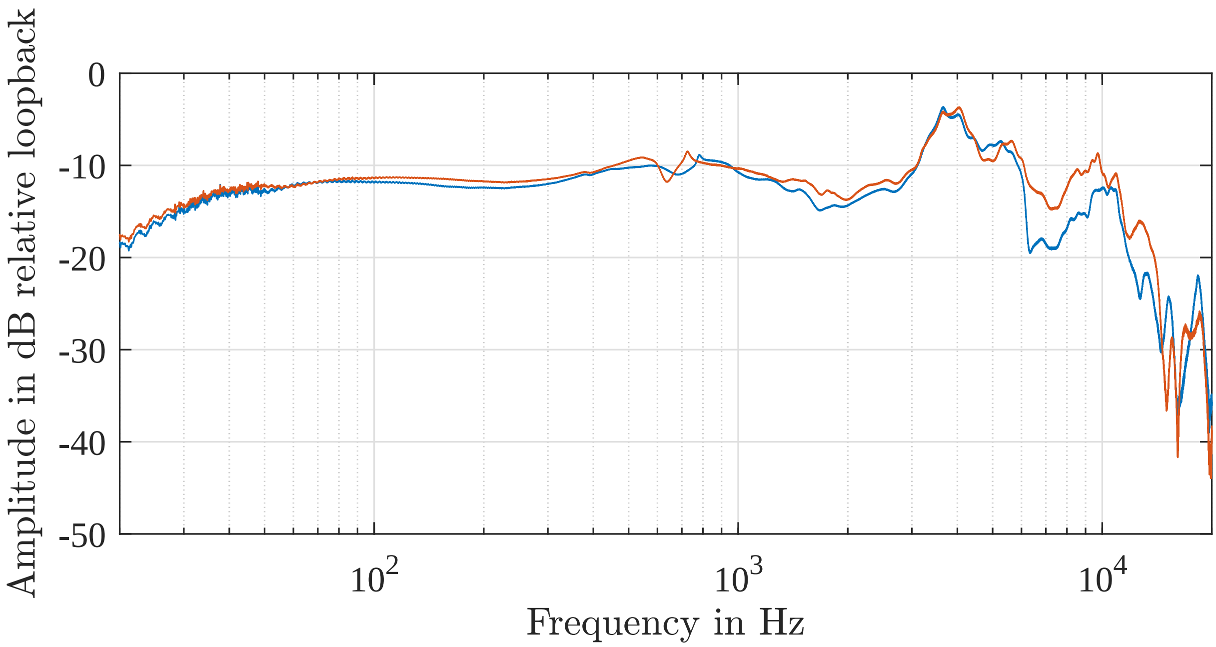

Figure C.6: Frequency response of left channel (—) and right channel (—).

C.6 | Summary

It is clear from figure C.6 that assuming a this pair of headphones to be 'flat' would introduce errors of more than 10 dB in the range 100 Hz to 10 kHz. The deviations between the two channels at low and very high frequency is likely due to mounting. In a setup where a binaural representation is given an average of multiple measurements, where the headphone is removed and remounted between measurements, would be beneficial. That being said the two drivers cannot be completely identical so some variation between the channels is to be expected.

D | Gorman superposition

Here The structure of the code finding the eigenfrequencies is given in Listing D.1. This is followed by an outline og the code determining mode shapes is given in Listing D.2.

```
K=number of terms
searchRange=lowLim:step:upLim % Define serchrange
for TrialEigenvalue=searchRange %loop over all trial eigenvalues
    for M=1:K % Loop over number of terms building block 1
        for N=1:K % Loop over number of terms
            if N==1
                A(M,M)= %Fill upper left diagonal
            end
            A(N+K,M)= %Fill upper right quadrant
        end
    end
    for N=1:K % Loop over number of terms building block 2
        for M=1:K % Loop over number of terms
            if M==1
            A(N+K,N+K)= %Fill lower right diagonal
            end
        A(N+K,M)= %Fill lower left quadrant
        end
    end
    % Calculate the determinant of the trial eigenvalue
    Y(TrialEigenvalue)=det(A)
end
```

Listing D.1: Pseudocode of the standard Gorman Superposition algorithm determining eigenvalues.

```
% in this code Y and A are used as the Y and A corresponding to those calculated for the trial eigenvalue above. W contains the amplitude of derformation at the position (L,j).
K=number of terms
Nxx=numberOfSamplingPoints per direction
for L=1:Nxx
for j=1:Nxx
for M=1:K %first building block
W(L,j)=W(L,j)+term M's contribution
end
for N=1:K %second building block
W(L,j)=W(L,j)+term N's contribution
end
end
end
3Dplot(W) %Display the modehshape
```

Listing D.2: Pseudocode of the standard Gorman Superposition algorithm determining mode shapes.

E | Parameter sensitivity study

E.1 | Design goal parameter sensitivity study

As the simulated results are dependent on many variables it is desired to examine which parameters cause significant changes to the eigenfrequencies or mode shapes. Due to time constraint only the more complex setup 'complete simplified' is considered and not '11.7g'. The parameter study is done by varying the following parameters for the setup 'complete simplified' in figure 13.5b within reasonable amounts.

E.2 | Original parameters

- Thickness = 1.5 mm
- Length = 299.3 mm
- Width = 169.3 mm
- Young's modulus 71 GPa
- Centre hole Ø = 4.8 mm
- Centre hole location L=149.9 mm, W=84.4 mm
- Spring stiffness shaker 2000 N/m

E.3 | Variations

1. Plate thickness $\pm 0.1 mm$
2. Plate length $\pm 1 mm$
3. Plate width $\pm 1 mm$
4. Young's modulus 69 GPa to 75 GPa
5. Centre hole location $+1 mm$
6. Spring stiffness shaker 1000 N/m, 3000 N/m, 5000 N/m, 10000 N/m, 15000 N/m and 20000 N/m.

Variations in length and width of the plate are made on with half the variation on either side of the plate, to not change the asymmetry due to the centre hole placement. The diameter of the centre hole is not varied but kept at the measured 4.8 mm. The centre hole location is varied once to be as offset from the true plate centre as possible. The new centre hole is at L=150.9 mm, W=83.4 mm and the spring and mass connected to the centre are moved to the same amount to keep them normal to the centre hole.

E.4 | Results

Reference	1 +0.1 mm	1 -0.1 mm	2 +1 mm	2 -1 mm	3 +1 mm	3 -1 mm	4 69 GPa	4 75 GPa	5 +1 mm
81 Hz	87 Hz	75 Hz	81 Hz	82 Hz	81 Hz	81 Hz	80 Hz	83 Hz	81 Hz
245 Hz	263 Hz	227 Hz	245 Hz	245 Hz	243 Hz	248 Hz	242 Hz	252 Hz	244/247 Hz †
482 Hz	513 Hz	449 Hz	479 Hz	484 Hz	480 Hz	482 Hz	474 Hz	495 Hz	481 Hz
415 Hz	444 Hz	385 Hz	413 Hz	415 Hz	412 Hz	417 Hz	408 Hz	426 Hz	414 Hz
860 Hz	911 Hz	793 Hz	849 Hz	855 Hz	848 Hz	856 Hz	840 Hz	876 Hz	853 Hz
1166 Hz	1227 Hz	1072 Hz	1143 Hz	1156 Hz	1147 Hz	1152 Hz	1133 Hz	1181 Hz	1150 Hz
1624 Hz	1691 Hz	1480 Hz	1584 Hz	1587 Hz	1569 Hz	1602 Hz	1563 Hz	1630 Hz	1586 Hz
1440 Hz	1498 Hz	1309 Hz	1399 Hz	1408 Hz	1395 Hz	1412 Hz	1384 Hz	1442 Hz	1404 Hz

Table E.1: Eigenfrequencies in plate parameter sensitivity study for parameters 1 through 5. The complete simplified setup from chapter 13 is used as reference and parameters are varied within limits. The columns should be read as 'parameter number variation'.

† Splits the mode in two deformed mode shapes similar to figure 13.6d.

The parameter that the simulation is the most sensitive towards is the thickness of the plate. This is expected as the plate thickness is used in the power of three in the equation for bending stiffness of a place as shown in subsection 8.1.3 and [Cremer et al., 2005]. Secondly the Young's Modulus, which also affects the bending stiffness, has large influence on the eigenfrequencies.

The variations in length and width move the eigenfrequencies slightly, but much less than the other parameters. Moving the centre hole mainly changes mode shapes and the eigenfrequency of the higher order modes.

Reference	1000 N/m	3000 N/m	5000 N/m	10000 N/m	15000 N/m	20000 N/m
81 Hz	80 Hz	82 Hz	83 Hz	86 Hz	89 Hz	92 Hz
245 Hz	245 Hz	245 Hz	246 Hz	247 Hz	248 Hz	250 Hz
482 Hz	483 Hz	483 Hz	483 Hz	483 Hz	483 Hz	483 Hz
415 Hz	415 Hz	415 Hz	415 Hz	416 Hz	416 Hz	417 Hz
860 Hz	859 Hz	860 Hz	860 Hz	860 Hz	860 Hz	860 Hz
1166 Hz	1166 Hz	1166 Hz	1166 Hz	1166 Hz	1166 Hz	1166 Hz
1624 Hz	1624 Hz	1624 Hz	1624 Hz	1624 Hz	1624 Hz	1624 Hz
1440 Hz	1440 Hz	1440 Hz	1440 Hz	1440 Hz	1440 Hz	1440 Hz

Table E.2: Eigenfrequencies after variation of parameter 6 spring stiffness.

Fromtable E.2 it is clear that most eigenfrequencies are not sensitive to the value of the spring. The first mode is the most sensitive and the second mode the second most sensitive. Choosing the spring stiffness to be 10 kN/m would result in the average error in percent to drop from 3% to 2% with the largest error in percent dropping from 7% to 4%. It is likely that the stiffness of the shakers suspension has changed over time. A factor 5 change however is unlikely, this could be examined further by measurement but the relatively small possible gain in accuracy is not deemed worth the time and effort. Therefore the specified 2 kN/m is retained in the simulation.

E.5 | Summary parameter sensitivity study

The parameter to which the simulation is the most sensitive is the plate thickness. Fortunately this parameter is quite well defined as the plate is rolled with an accuracy much better than the callipers used in determining thickness. The Young's modulus also influence the results drastically - this parameter is part of the defining material properties and as such the specifications should be somewhat accurate. The upper limit, 75 GPa, is from 'High Pressure Die Cast' aluminium which has a higher Young's Module than other variants of aluminium. It was determined in section 13.3 that the inclusion of a spring drastically affects results, however the eigenfrequencies do not seem to be sensitive to the exact value of it.

F | Sound generation implementation

This appendix contains pseudocode for the Matlab algorithm which takes the vibration of faces as input and computes the sound pressure at a receiving position.

F.1 | Pseudocode for sound generation script

In the actual code data is structured in matrices with time in the rows and frequency in columns. This is done since the GPU does matrix multiplications much faster than for loops. This vectorization is omitted from the pseudo code for readability.

```
1  %Loop over all faces.
2  for i=1:length(faces)
3  %Determine location of centre of face
4  OrigPos=mean([Loc1 Loc2 Loc3])
5  %Determine displacement of involed nodes as function of time
6  meanDIsplacement=mean([Dis1 Dis2 Dis3]);
7  %Determine position of centre as function of time
8  PosTime=OrigPos+meanDIsplacement;
9  %Determine propagation distance
10 PropVector=PosTime-ReceiverPos;
11 d=vecnorm(PropVector,2); % takes the norm2 of the 3 dimensional vector
12 PropDelay=d/343; % calculates the excact propagation time in seconds
13 %Convert to phase delay for individual frequencies
14 %(how many periods propagation takes)
15 PhaseDelayProp=2*pi*freq*PropDelays;
16 %Calculate propagation amplitude as described by O'brian
17 PropAmpl=FaceArea/d*cos(AngleToReciver);
18
19 %Determine displacement and phase amplitude as a function of frequency.
20 %Should be velocity hence the w weight
21 DispAmpl=mean([displ disp2 disp3],2).*(2*pi*freq);
22 %Should all be turned 90 due to j above, but turning all is pointless
23 DispPhase=mean([phas1 phas2 phas3],2);
24
25 %Generate face contribution
26 Received=Received+(rho*c*DispAmpl*PropAmpl...
27 *sin(2*pi*freq*t+PhaseDelayProp+DispPhase);
28 end
```

Listing F.1: Pseudo code of sound propagation. In line 23 the rotation of all phases is ignored as it is identical for all frequencies.

In line 4 through 17 in Listing F.1 the time varying propagation delay and decay is determined. An intuitive way of describing the difference between the propagation proposed by [O'Brien et al., 2001a] and the one in Listing F.1 is that [O'Brien et al., 2001a] generates sound at the sender and then adds propagation. In Listing F.1 the sound is generated at the receiver accounting for the propagation. On top of this steps are taken to allow for a time dependant propagation distance as the matrix 'PhaseDelayProp' contains the propagation delay in number of cycles at all frequencies as a function of time.

Having calculated and summed the parameter 'Received' in Listing F.1 the simulated sound at the desired position has been calculated not accounting for the dipole characteristics of the plate and the floor reflection. These two phenomena are added in post processing as filters in chapter 15.

F.2 | GPU calculation considerations

In order to run the supplied script Matlab 2018a with the Parallel Computing Toolbox installed is required. The script is set up to run on a Nvidia 1070 as described in the Preface and as such 8 GB of memory and an Nvidia GPU is required. To avoid overfilling the GPU memory the sound generation is split in parts of one second. In case the reader has less GPU memory available the 'endtime' parameter can be decreased resulting in the calculation to work on shorter time frames. No drastic speed-up is observed for varying the length of the time frames, probably as any considered frame length is much larger than the number of computations the GPU can do per cycle resulting in small overhead.

```
stattime=0;
endtime=1;
t_frame=stattime:1/fs:endtime-1/fs;
Frames=10;

for i=1:Frames
% Sets the t vector to run in next frame
t=(i-1)*endtime+t_frame;
%Pass Data to coputation algorithm
Soundgen=GPUFaceVibration(faces, nodes, frequencies, displacement,
    dispPhase,t,receiverPos);
SoundBuf=[SoundBuf Soundgen]; %Store the result of this frame
t2=[t2 t]; %Store the time vector of this frame
end
```

Listing F.2: Pseudo code of GPU control.

F.2.1 Computation times

On the note of the GPU calculation the computation times for the different parts of the algorithms are listed. The reader is reminded that the computation times are from two different computers as mentioned in the Preface. The FEM computation times are from a HP laptop and the auralization computation time is from a desktop with a GPU.

- Modal analysis for complete simplified $\approx$ 250 modes from 20 Hz to 20 kHz - 4 min.

- Harmonic analysis for the above including 150 extra points - 17 min.
- Harmonic analysis as above including APDL script Listing 8.3 - 33 min.
- The auralization algorithm for a single frame of one second - 40 min.

So in total the computational load of the algorithm is quite cumbersome, yet not unreasonable. It should be noted that the ANSYS pre-computation can be reused if a new listening position is desired. Comparison with the works by [O'Brien et al., 2001a] is pointless as they work on a maximum of 727 nodes resulting in a total computation time per second of about 17 hours using a 350 MHz processor.

G | ANSYS analysis systems

Different types of analysis are available in ANSYS and are called 'analysis systems'. They include among many others modal analysis, random vibration, harmonic response and transient structural. The before mentioned analysis systems are the ones deemed possibly relevant for this project and a brief description of each and their possible use in this project is given below.

G.1 | Modal

A modal study is equivalent to what was done in section 5.3 where the eigenfrequencies and mode shapes of a structure were determined. The choices to make when setting up a modal analysis are very simple. You need an object, which has to be meshed properly and have correct boundary conditions. Then you need to select how many modes to find and press run. The runtime for such an analysis is also quite small, less than 1 minute for the first 40 mode shapes of the plate.

The modal analysis can be used on its own or be used as the foundation for further analysis. The idea is to utilize the fact that most of an undamped resonant structures vibration happens at the eigenfrequencies, allowing modal decomposition to be uses. Basically after finding the eigenfrequencies the solver ignores all other frequencies in the following analysis yielding a large speed-up at the expense of slightly smaller accuracy. The solutions from the individual modes can then be added by superposition for a complete system response. Increasing the number of modes included in the modal analysis extends the upper frequency limit of the following analysis.

A comparison has been made to examine if the results obtained with FEM in ANSYS[1] are comparable to those obtained using SOLIDWORKS in section 5.3. The plate dimensions, mesh size and analysis type were kept identical to the fine meshing used previously. The choices of mesh type and the mesh creation were in both cases left for the program to choose.

[1]This test and all that follow were made in ANSYS Workbench 19.0

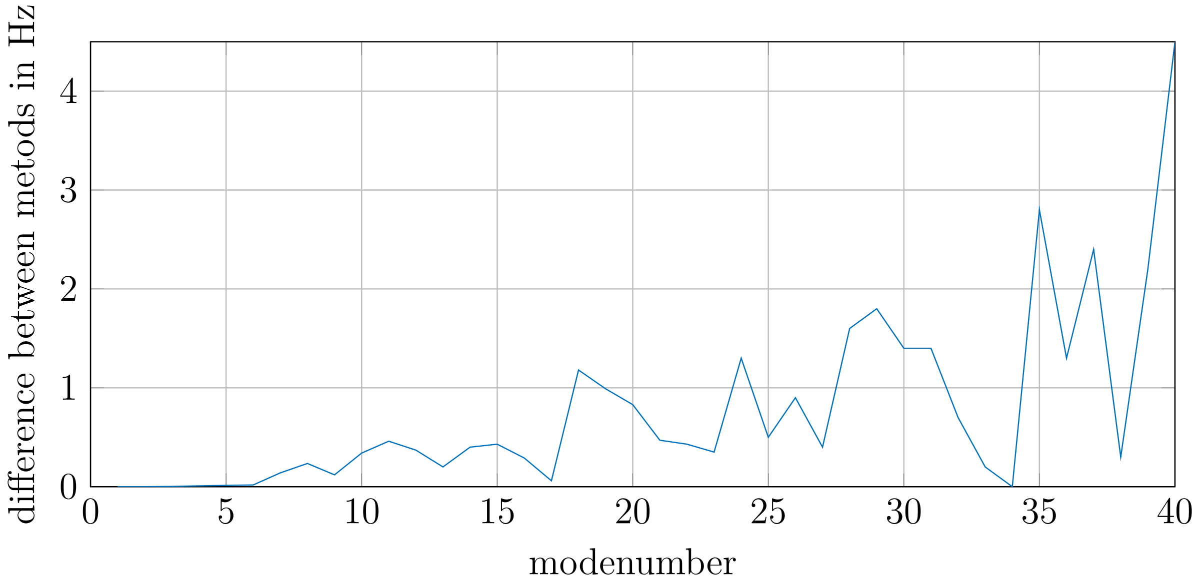

Figure G.1: Difference between eigenfrequencies found in SOLIDWORKS and ANSYS.

Keeping in mind that the frequencies for mode numbers above 35 are above 2 kHz, it is clear that the difference between the two solutions is negligible so modal analysis in ANSYS and SOLIDWORKS can be interchanged - at least in the case of a thin plate. Having shown this the meshing is refined to the degree required to adequately model frequencies of 20 kHz. Using the rule of 6 elements per wavelength [Schmiechen, 1997]. This requirement is with regards to the wavelength in the solid medium, however it should also be fulfilled for the wavelength in air to make the sound generation accurate. Therefore the element size is chosen as the smallest of the two requirements thereby fulfilling both. The element size required due to the material is calculated using eq. 8.2 and dividing by 6:

$$\frac{1}{6}\lambda_{plate} = \frac{1}{6}\frac{2\pi\sqrt[4]{\frac{B}{m'}}}{\sqrt{\omega}} = \frac{1}{6}\frac{2\pi\sqrt[4]{\frac{7.5\cdot 10^{10}N/m^2\cdot(0.0015m)^3\cdot 0.1693m/12}{2770kg/m^3\cdot 0.0015m}}}{\sqrt{20000Hz\cdot 2\cdot pi}} = 2.86mm \tag{G.1}$$

The element size required due to air is $\lambda_{air} = \frac{c}{6f_{max}} = \frac{343m/s}{6*20000Hz} = 2.85mm$. The two values are almost identical but the requirement in air is dominating with a maximum element size of 2.85mm. This new meshing results in a total of 84456 nodes for the plate. On a side note, the fact that the wavelength on the plate is longer than that on the medium means that 20 kHz is below the critical frequency - so sound radiation should only be generated at the edges as discussed later in subsection 9.1.3.

G.2 | Modal -> Random

The random vibration analysis system allows a random acceleration with a chosen PSD to be applied to the structure. Up until this point only a completely free plate has been discussed. This however does not resemble the real world and therefore ANSYS does not allow the random vibration to be put into a free floating structure. If it did the entire structure would move to infinity. Instead a simply supported boundary is defined, where the random acceleration can be applied. In order to mimic the setup that later will be used for the measurement part it was chosen to split the plate into four equally sized rectangular parts. The four plates are then rigidly connected at the surfaces where they meet in pairs and the single vertical edge where they all meet is defined as simply supported[2]. The random excitation is defined in the direction normal to the plate. This plate which is split in four pieces is used for all the following simulations in this chapter.

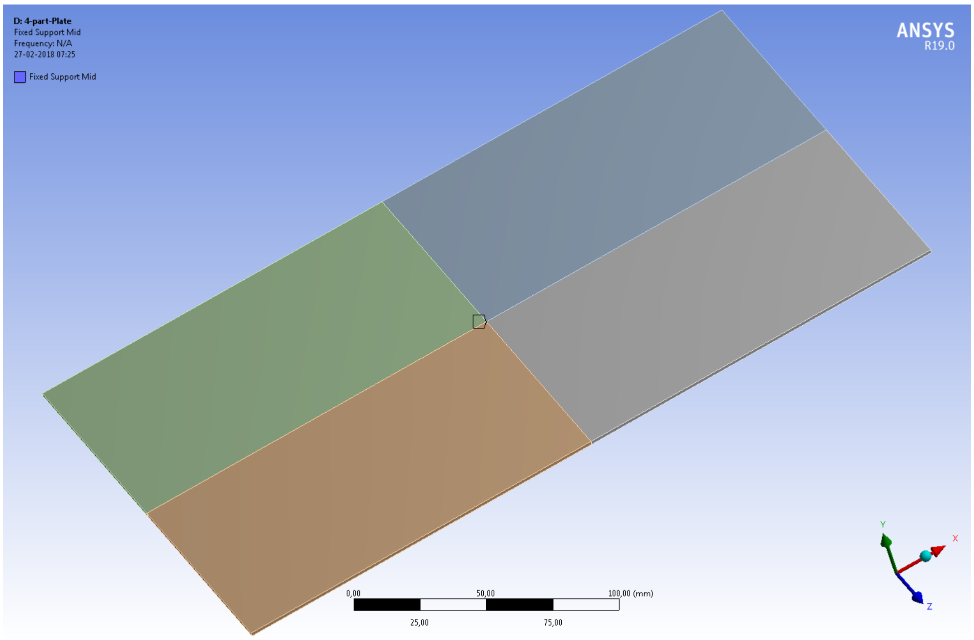

Figure G.2: The plate split in four parts and simply supported in the middle.

For the random vibration analysis system a modal pre-computation is a prerequisite. The result obtained is a maximum deformation of all vertices including the contribution from each mode in terms of amplitude. Phase relations are not available. The runtime for the calculation was <1 minute. The PSD of the input acceleration was setup as follows.

	Frequency / Hz	Acceleration / mm/s^2
1	50	5.00E+06
2	20000	5.00E+06

Table G.1: Input PSD in y-direction for random vibration analysis. ANSYS makes linear interpolation to determine the level between the points.

[2]Called fixed support in ANSYS

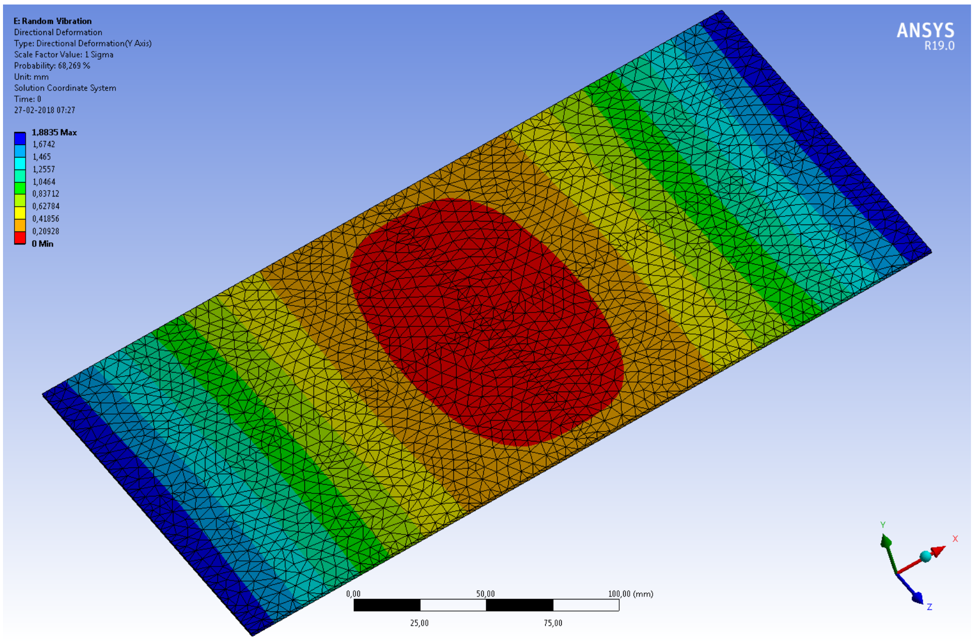

Figure G.3: The maximum displacement from random vibration analysis. All mode contributions are summed in the application, but individual contribution ratios can be extracted.

The storage requirement for the data from the random vibration is very small as only the node positions and the mode shapes of the structure has to be stored plus a weighting and the eigenfrequency, which is negligible in terms of storage space.

$$Storage = NoNodes \cdot NoDimension \cdot \frac{bit}{single}(1 + NoModeShapes) \tag{G.2}$$

$$= 84456 nodes \cdot 3 dimensions \cdot 32 \frac{bit}{single} \cdot (1 + 40) \tag{G.3}$$

$$= 3.32 \cdot 10^8 bit = 39MB \tag{G.4}$$

G.3 | Modal -> Harmonic

The harmonic response analysis system is setup in a very similar way as the random vibration system. However instead of a PSD defining random vibration a sweep is used to calculate the response at individual frequencies. The sweep can be linear or logarithmic and the number of desired points over a frequency range is specified. It is possible to increase the point density around the eigenfrequencies, ensuring that all modes are included.

The output from the calculation is, as with the random vibration, a 'max total deformation' at all points with the individual mode contributions are known. Here however the phase information is included. The runtime for the calculation was 1 minute. The input was setup as an acceleration in y-direction (normal to the plate) with magnitude of $5.00 \cdot 10^3 m/s^2$.

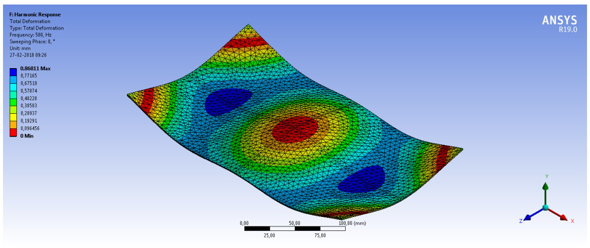

(a) Result for harmonic analysis at 500 Hz.

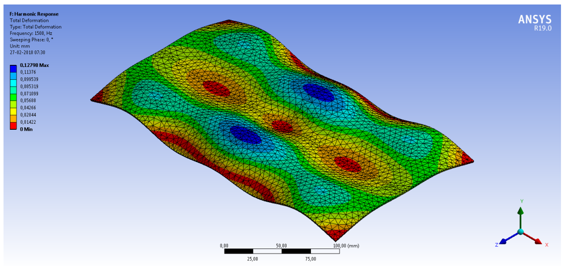

(b) Result for harmonic analysis at 1500 Hz.

Figure G.4: The output from harmonic analysis.

It is worth noting that the plate shape can be extracted between modes by interpolation. This is useful in the case of forced vibration where the vibration pattern will be determined by the nearest modes.

The storage requirement from this type of analysis is that for each node the amplitude, phase and position in 3 dimensions has to be stored. For 4000 points on the frequency axis this will yield.

$$
\begin{aligned}
Storage &= NoNodes \cdot NoDimension \cdot \frac{bit}{single}(1 + 2NoFrequencies) && \text{(G.5)}\\
&= 84456nodes \cdot 3dimensions \cdot 32\frac{bit}{single} \cdot (1 + 2 \cdot 4000) && \text{(G.6)}\\
&= 6.48 \cdot 10^{10} bit = 7724MB && \text{(G.7)}
\end{aligned}
$$

G.4 | Pure transient

As a different approach to the modal decomposition based approaches above a time domain solver can be used. The transient structural analysis system allows for a discretized solution at sampled times. The main application for this analysis system is drop tests, where it is of interest to find maximum stress or large deformation which might not be linear. The maximum stress or deformation will be achieved very quickly after impact, so short analysis times are normal; typically micro seconds. The drop test scope of this analysis system makes it not suitable for simulating stationary conditions as the harmonic response or random vibration did. Instead it can be used to find the result of an impact in the centre of the plate. After the impact the response can be sampled for minimum one period of the lowest frequency of interest. If damping is to be considered this will increase drastically as the decay would have to be sampled as well. This will yield an impulse response at all nodes of the structure, which is accurate both in terms of amplitude and phase. The solver does not assume anything about modes and does not assume linearity of the material making this analysis system very versatile. The drawback is the computation time, which was 71 minutes for the simulation of 0.02 seconds. A further drawback is the need to store the position of each node at each time-step. Assuming that the coordinates are stored at single precision accuracy the solution of the plate will result in a storage requirement of

$$Storage = NoNodes \cdot NoDimension \cdot 32\frac{bit}{single} \cdot TimeFrame \cdot fs \tag{G.8}$$
$$= 84456nodes \cdot 3dimensions \cdot 32\frac{bit}{single} \cdot 0.02second \cdot 48000Hz \tag{G.9}$$
$$= 7.78 \cdot 10^9 bit = 972.5MB \tag{G.10}$$

The input acceleration was applied as a impulse acceleration in a single time frame. The setup of the impact can be seen in table G.2

Step	Time / s	X / mm/s²	Y / mm/s²	Z / mm/s²
1	0	0	0	0
1	2.08E-05	0	5.00E+06	0
2	4.17E-05	0	0	0
3	1.04E-04	0	0	0
3	0.02	0	0	0

Table G.2: Input acceleration (direction components) during the different time frames.

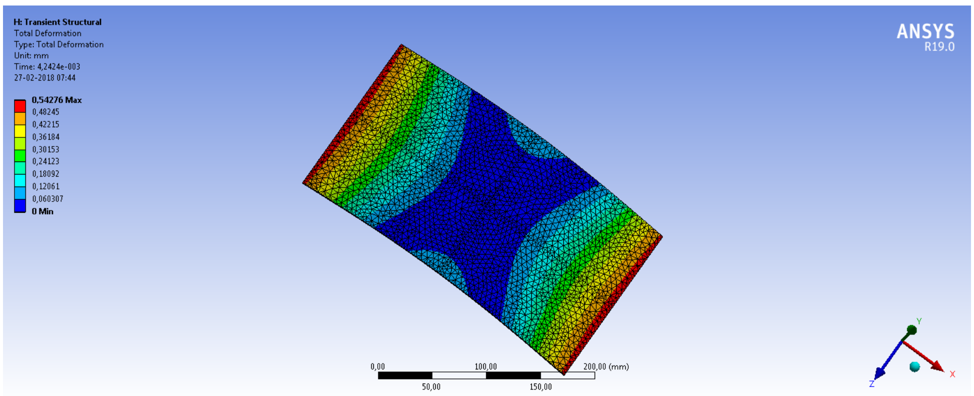

Figure G.5: The maximum displacement from transient structural analysis. The snippet is made at the peak of mode 1, which has the largest contribution to deformation.

G.5 | Modal -> Transient

In order to overcome the computation time of the transient structural analysis system the simulation can be based on the results of a modal study. This significantly decreases the computation time to 9 minutes if the first 40 modes are included. Non linear behaviour is not supported by this analysis system. A study has been made to show the convergence of the calculated maximum displacement to a reference found using the pure transient structural analysis system.

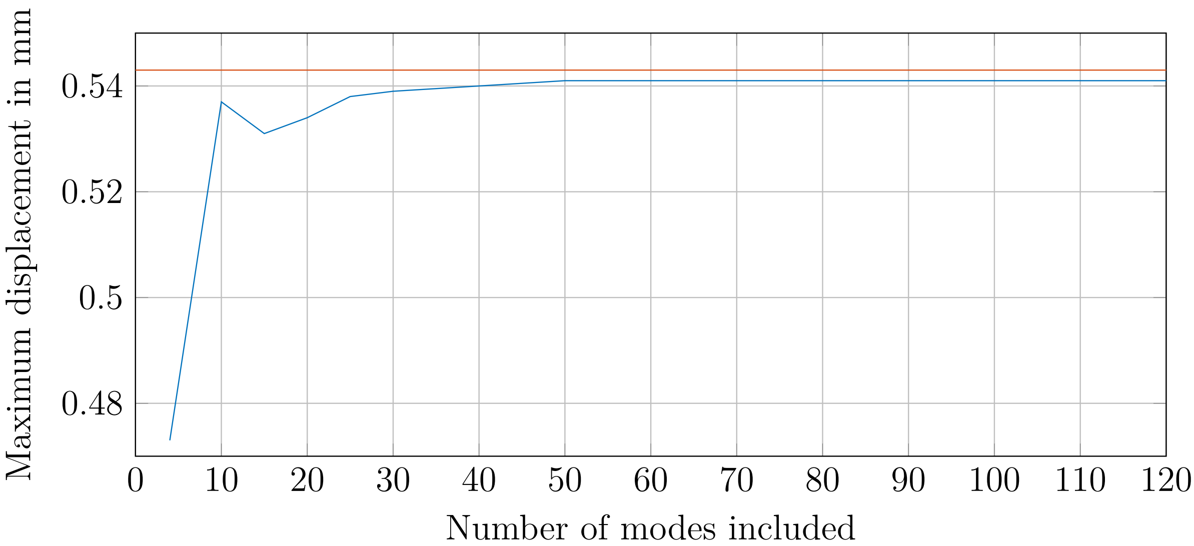

Figure G.6: The convergence of the modal transient analysis toward the full transient solution. Modal transient analysis (—), full transient (—). The offset at the end is likely to be caused by some non linear deformation which is only included in the full transient analysis.

It should be noted that even if the maximum displacement converges rapidly this does not guarantee the accuracy of the displacement in terms of auralization. This is because higher frequencies are radiated as sound much more efficiently than low frequencies. So even a small displacement at high frequency can play a large role in the sound radiation. Therefore the modal analysis has to be performed for the entire frequency range of interest as for all the other systems based on the modal approach.

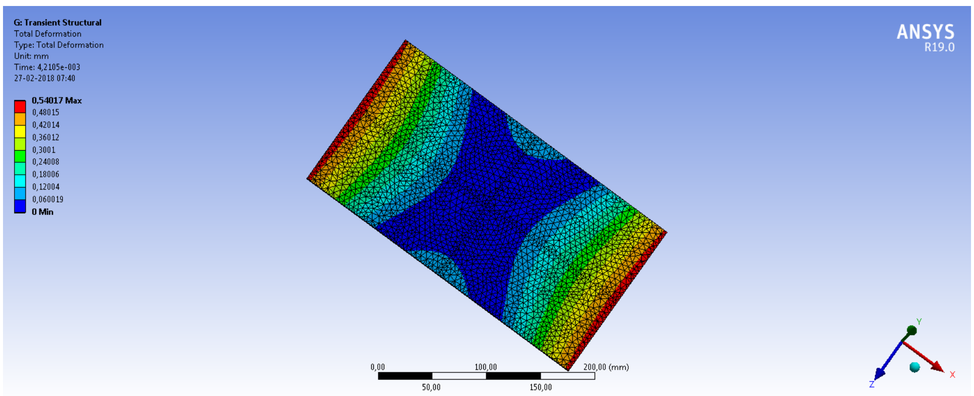

Figure G.7: The maximum displacement from transient structural analysis based on a modal response analysis of 40 modes. The snippet is made at same timestep as figure G.5.

Visually no difference can be established between figure G.5 and figure G.7, not even when running the animations. In terms of storage the requirement will be the same.